2009

# Effective Width of Gusset Plate with Single or Double Bolts in Tension

Hassan Abbasi
*University of Windsor*

# Effective Width of Gusset Plate with Single or Double Bolts in Tension

**By**

**Hassan Abbasi**

A Thesis
Submitted to the Faculty of Graduate Studies
through
the Department of Civil and Environmental Engineering
in Partial Fulfillment of the Requirements for
the Degree of Master of Applied Science at the
University of Windsor

Windsor, Ontario, Canada

2009

# Effective Width of Gusset Plate with Single or Double Bolts in Tension

By

Hassan Abbasi

APPROVED BY:

---

N. Zamani, Outside Department Reader

Department of Mechanical, Automotive and Materials Engineering

---

M.K.S. Madugula, Department Reader

Department of Civil and Environmental Engineering

---

S. Das, Principle Advisor

Department of Civil and Environmental Engineering

---

J.B. Kennedy, Co-Advisor

Department of Civil and Environmental Engineering

---

B.B. Budkowska, Chair of Defense

Department of Civil and Environmental Engineering

May 15, 2009

## AUTHOR'S DECLARATION OF ORGINALITY

In hereby certify that I am the sole author of this thesis and that no part of this thesis has been published or submitted for publication.

I certify that, to the best of my knowledge, my thesis does not infringe upon anyone's copyright nor violate any proprietary rights and that any ideas, techniques, quotations, or any other material from the work of other people included in my thesis, published or otherwise, are fully acknowledged in accordance with the standard referring practices. Furthermore, to the extent that I have included copyrighted material that surpasses the bounds of fair dealing within permission from the copyright owner(s) to include such material(s) in my thesis and have included copies of such copyright clearances to my appendix.

I declare that this is a true copy of my thesis, including any final revisions, as approved by my thesis committee and the Graduate Studies office, and that this thesis has not been submitted for a higher degree to any other University or Institution.

**ABSTRACT**

In this study experimental and numerical investigation to determine the behaviour of gusset plate connections with one and two bolts under quasi-static monotonically increasing tension load was undertaken. The experiments on full-scale gusset plate connections were undertaken in the Structural Engineering Laboratory of the University of Windsor. The numerical modeling and analysis were undertaken using commercially available finite element code, ABAQUS. The results obtained from experimental and numerical methods agree well. The results of the study were also used to determine the strain distribution in the gusset plates connected with one and two bolts. The yield load of gusset plate specimens were used to determine the effective width of gusset plate. It was found that angle of load dispersion for gusset plate with two bolts ranges from 25º to 32º which is approximately half of angle (60º) suggested by Whitmore. It was also found that for gusset plate connections with one bolt, the concept of effective width is not applicable and dispersion of the connection is based on other factors.

## DEDICATION

To my parents

and my wife Mina

whose love and support

have made everything I do possible.

## ACKNOWLEDGMENTS

I would like to thank my advisor Dr. Sreekanta Das and my co-advisor Dr. John B. Kennedy who helped me in all stages of this research. I also appreciate the contribution of Dr. Murty Madugula and Dr. Nader Zamani for their guidance in this project. I am also thankful to Mr. Lucian Pop, Mr. Pat Seguin and Mr. Mat St. Louis for their help during experimental work.

**TABLE OF CONTENTS**

## LIST OF TABLES

**LIST OF FIGURES**

# 1. INTRODUCTION

## 1.1 General

Lateral load resisting systems for steel structures include concentrically braced frames (CBF), eccentrically braced frames (EBF), moment resisting frames (MRF), and shear walls. Of these, concentrically braced frames (CBF) are the most commonly used because of their structural efficiency. Another reason is the relative ease with which they may be designed, constructed and repaired (Redwood and Jain, 1992). The lateral load resisting system dissipates energy imparted to the structure by earthquake or strong winds during the life of a structure.

CBF consists of beam and columns for resisting gravity loads, braced with inclined lateral bracing members. It can assume different configurations such as diagonal bracing, cross bracing, and chevron bracing (see Figure 1.1). (Walbridge et al.1998). It is usual that a bracing member is connected to another structural member using a gusset plate.

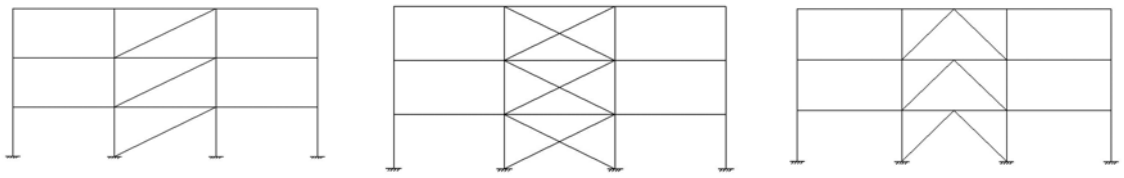

a) Diagonal Bracing b) X-Bracing c) Chevron Bracing

Figure 1. 1– Various configurations for concentric braced frames

The behaviour of gusset plate connection is complex which is simplified for the design purposes as recommended by various researchers. The earlier studies concentrated on the behaviour of gusset plates in the elastic stress limit (Whitmore,

1952). Recent research has focused on the inelastic behaviour of gusset plates loaded monotonically and cyclically in tension and compression (Jain et al., 1987; Cheng et al., 2000; Topkaya, 2003, and Walbridge et al., 2004).

The connections between two members in antenna tower structures are made by thin gusset plates with one or two bolts (Figure 1.2). Various standards and codes such as AISC and ANSI/TIA recommend design considerations for such gusset plate connections with several bolts. However, none of the existing standards/guidelines/codes make any recommendations on how to determine the effective plate width and design the gusset plate connections that use only one bolt. For, gusset plate connections with two bolts, the only recommendation available is in the ANSI/TIA (2006) and their recommendation on effective width calculation is a modified version of Whitmore model. Therefore, this study focused on the investigation of the behaviour of gusset plate connections with one or two bolts that are commonly used in antenna tower structures and to determine the effective plate width and stress distribution for such connections.

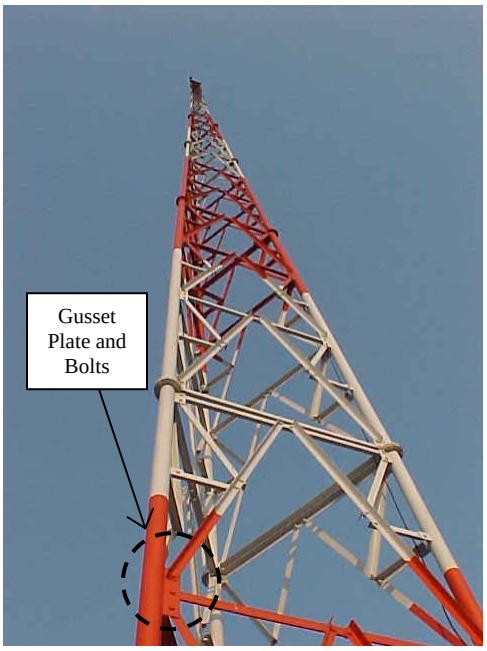


Figure 1. 2 – Gusset plate connection in antenna tower structure

## 1.2 Objectives

The primary objective is to determine the gusset plate width that is the width of the plate which is effective in transferring the load from one tension member to the other.

## 1.3 Methodology

The project includes both experimental and numerical study. The experimental investigation includes tests on gusset plate connections with one and two bolts and with three different plate widths. The numerical investigation includes finite element simulations and analyses for all the tests.

## 1.4 Scope

The scope of this research is as follow,

- Detailed literature review
- Experimental study as explained above
- Finite element modeling, analysis and validation

## 1.5 Organization of Thesis

The whole thesis is divided into seven chapters. Chapter 2 provides the detailed literature review on the gusset plate connections. Following two chapters (Chapters 3 and 4) provide the test method and test results obtained from the experimental study. Chapter 5 discusses the different methods for effective width calculation. Finally, Chapter 6 describes the finite element model of gusset plate with one bolt and two bolts connection and comparison of the results of experimental and finite element analysis.

# 2. LITERATURE REVIEW

## 2.1 Introduction

In this chapter, past work done on gusset plate connection is reviewed. Section 2.2 examines gusset plate research from an historical perspective, while section 2.3 reviews recent research into the ultimate load behaviour of gusset plates under both monotonic tensile and compressive loads. The other investigations of the behaviour of gusset plates under cyclic loads are considered in later section.

The most significant research on gusset plate connections began in the 1950's with the experimental work performed by Whitmore (1952). Following the 1950's more research on the behaviour of gusset plate connections was performed to gain a better understanding of the behaviour of gusset plate connections and develop simple guidelines for the design of gusset plates for monotonic and cyclic loading. A summary of this earlier work is presented in the following sections.

## 2.2 Elastic Behaviour of Gusset Plate

Whitmore (1952) studied the stress distribution in a gusset plate connection detail commonly found in Warren truss type bridges. The research was based on the results of an experimental investigation. Determination of location and magnitude of the peak stress in the gusset plate was the main objective of Whitmore's investigation. Also, a practical method for estimating this peak stress for use in structural design was developed.

The measurement of strains in quarter scale aluminum gusset plate models loaded in the elastic range was the primary objective of Whitmore's experimental investigation. Whitmore also studied stress distributions on Masonite and Bakelite gusset plate

models using stresscoats and photoelastic methods. It was found that the location of the peak stress in the gusset plate usually occurs near the last row of fasteners in the gusset-to-brace connection. Whitmore also determined that the direct, bending and shear stress distributions across critical sections of the gusset plate did not compare well with values determined using the previous popular beam method. The beam method did, however, provide a conservative estimate of the peak stress. Figure 2.1 shows the first and last row of bolts in gusset plate connections which is used for Whitmore's method.

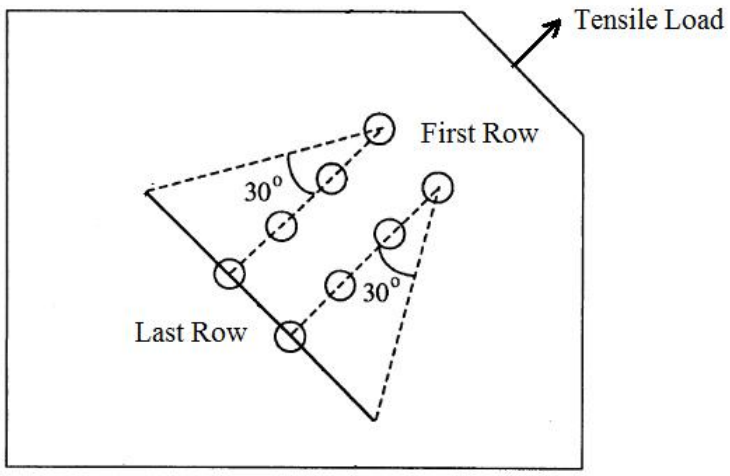


Figure 2. 1 - The first and last row of bolts in gusset plate connection

According to the results of this research, Whitmore suggested a method to predict the peak stress in a gusset plate for a given brace load. It is proposed that the peak stress could be calculated by taking the brace load and dividing it by an area equal to the plate thickness times "Whitmore Effective Width" (Figure 2.2). The Whitmore effective width is defined as the distance between two lines radiating outward at 30 degree angles from the first row of bolts in the gusset-to-brace connection along a line running through the last row of bolts (see Figure 2.2). The resulting stress agreed well with test results of Whitmore's experiments. However, it should be noted that this relationship to determine the peak stress was proposed for brace load in linear elastic range only.

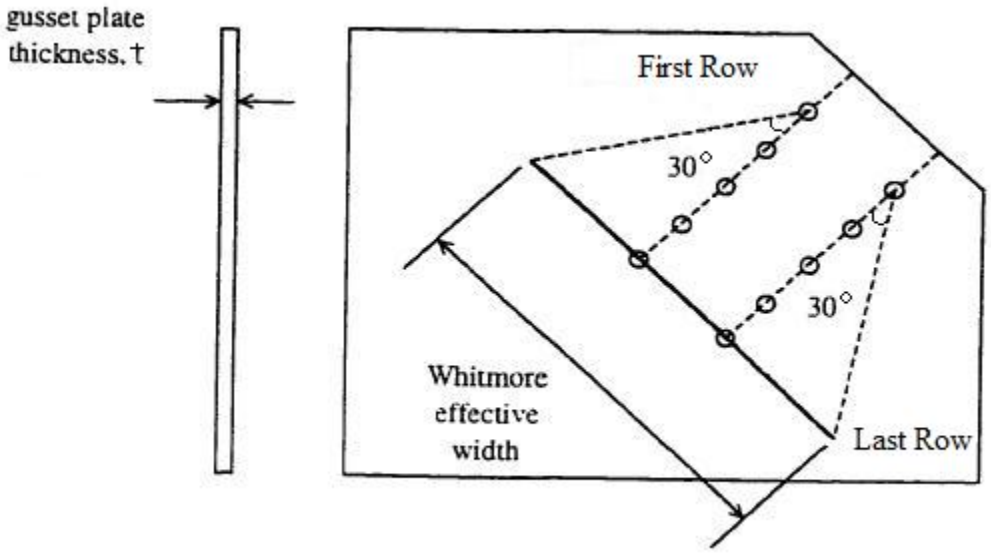


$$Peak \quad Stress = \frac{Brace \quad Load}{Whitmore\, Effective \quad Width \quad \times \quad t}$$

Figure 2. 2 – Explanation of Whitmore method for predicting peak stress in gusset plate (Whitmore, 1952)

Irvan (1957) performed a similar study with an aluminum model of a double gusset plate Pratt truss connection. Once again, his investigation indicated that stress distributions computed with the beam method did not agree well with the test results. Irvan suggested a method of determining the peak stress that was similar to the Whitmore's method.

Hardin (1958), Davis (1967), Varsarelyi (1971) also focused on the stress distribution in the gusset plates loaded in the elastic range. Hardin's experimental study confirmed Irvan's conclusions regarding the inability of beam method and supported Irvan's method for determining the magnitude of the peak stress in the gusset plate. Davis (1967) and Varsarelyi (1971) performed finite element investigations of the elastic stresses in gusset plates. In general, these investigations confirmed the conclusions made by Whitmore (1952), Irvan (1957) and Hardin (1958) based on experimental investigations regarding the stresses in gusset plates loaded in the elastic range.

## 2.3 Inelastic Behaviour of Gusset Plates

### 2.3.1 Monotonic Loading

Chakrabarti and Bjorhovde (1983) investigated the behaviour and strength of gusset plates further than the elastic range, in monotonic tension. Current design practices (including a yield criterion based on the Whitmore method) were evaluated using test results.

The test program involved six gusset plate specimens loaded in monotonic tension. Two gusset plate thickness of 9.6 mm (3/8 in.) and 3.2 mm (1/8 in.), with three brace angles of 30, 45 and 60 degrees were tested. Because of limitations of the testing equipment, only the 3.2 mm specimens were loaded to failure (Figure 2.4).

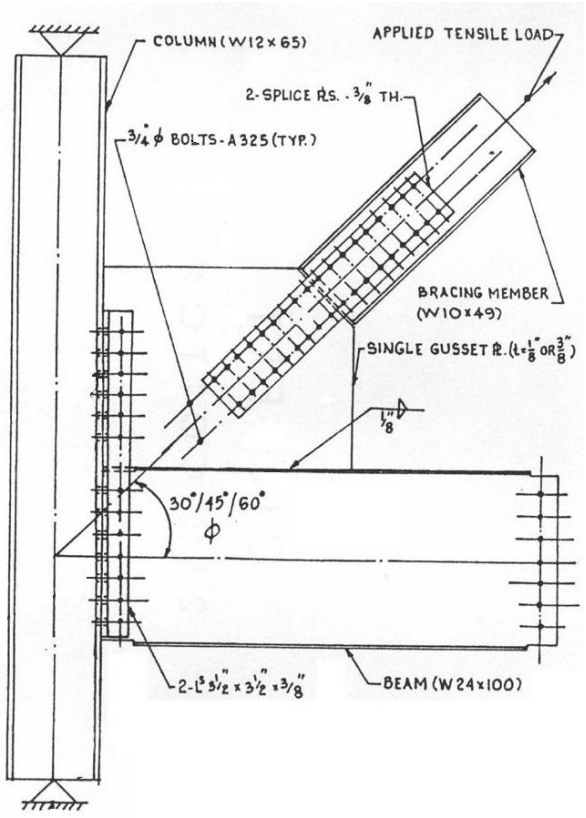


Figure 2. 3 – Overall geometry of gusset plate with 30, 45 and 60 degrees bracing angle (Chakrabarti and Bjorhovde, 1983)

It was found that the primary failure mode for the test specimens was tearing of the gusset plate across the last row of bolt holes in the gusset-to-brace connection. Tearing of the gusset-to-frame fasteners was found to occur in specimens where the Whitmore effective width intercepted the boundaries of the plate. It was also found that a yield criterion based on the Whitmore method (i.e. with yield occurring at the brace load that causes the Whitmore peak stress to exceed the yield strength of the material) was appropriate for the design of gusset plate connection used by them. Further study of the influence of plate boundaries, including the use of stiffeners along the free edges were recommended for future work. (Chakrabarti and Bjorhovde, 1983)

Hardash and Bjorhovde (1984) suggested an ultimate strength design procedure for gusset plates loaded in monotonic tension. A block shear model was proposed based on the results of tests on 42 gusset plate specimens tested at the University of Arizona, the University of Illinois and the University of Alberta. It was found that the ultimate strength can be taken as the sum of the ultimate tensile strength of the gusset plate between the bolts in the last row of bolts and the shear strength along the connection length. They proposed as the following equation to calculate the ultimate strength:

$$R_n = F_u S_{net} t + 1.15 F_{eff} L_t \tag{2.1}$$

Where, $F_u$ is the ultimate tensile strength of gusset plate material. $S_{net}$ is the net width of gusset-to-brace connection as shown in Figure 2.5., $L$ is the length of gusset-to-brace connection (see Figure 2.5), $t$ is the gusset plate thickness, and $F_{eff}$ is a uniform effective shear stress given as follows:

$$F_{eff} = (1 - C_l) F_y + C_l F_u \tag{2.2}$$

Where, $F_y$ is the yield strength of the gusset plate material and $C_l$ is given as following:

$$C_l = 0.95 - 0.047l \qquad \text{(with } l \text{ in inches)} \qquad (2.3)$$

The tensile tearing along the last row of bolt holes was found to be most common mode of failure in this test program.

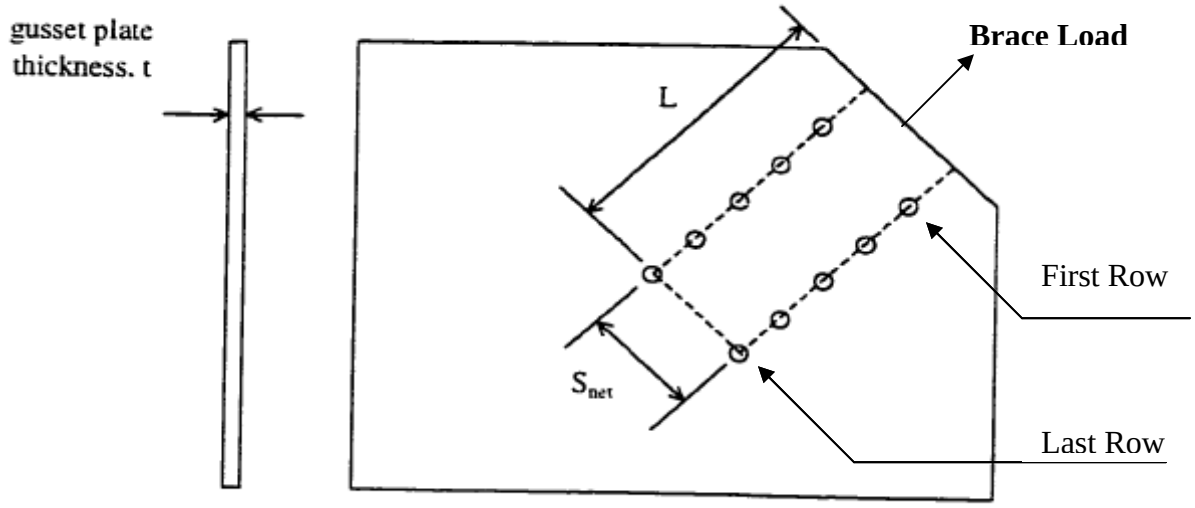


$$F_{eff} = (1 - C_l)F_y + C_l F_u$$

$$C_l = 0.95 - 0.047l$$

Brace load = $R_n = F_u S_{net} t + 1.15 F_{eff} L_t$

Figure 2. 4 – Explanation of block shear method for predicting tear-out strength of gusset plate (Hardash and Bjorhovde, 1984)

The following results were also found for these gusset plate connections:

1. All ultimate failure modes consist of a tensile tear across the last row of bolts, with various stages of shear yielding along outside lines of bolts. The extent of the latter depends on the connection length (L).

2. The governing block-shear model is shown to be the one incorporating tensile ultimate stress on the net effective shear stress acting on the gross area along the outside bolt lines.

3. The effective shear stress acting along the outside bolt lines can be assumed to be uniformly distributed, with the magnitude given as a function of the total connection length, and material yield and ultimate stress levels.

Thornton (1984) studied a steel gusset plate connection design example, demonstrating the application of an intuitive, lower bound solution method for determining the ultimate capacity of the connection in tension and in compression. A lower bound solution as one in which: (1) equilibrium is satisfied, and (2) all stresses are below yield. This definition was modified by adding that members must be strong enough to eliminate buckling.

Thornton (1984) investigated on the block shear method in his example to check the tear-out strength of gusset plate connection and suggested a lower bound method for determining compressive strength of the gusset plate. Thornton's proposed method for determining compressive strength defines a unit strip with a characteristic length equal to the largest of *L1*, *L2*, or *L3* (see Figure 2.6) and an effective length factor , k=0.65, from which the elastic buckling capacity of the unit strip is calculated. This capacity should be multiplied by the Whitmore effective width. According to the prediction by Thornton (1984) the model is expected to be conservative estimate of the compressive strength of the gusset plate. Thornton (1984) proposed that a shorter effective length (such as the average of lengths *L1*, *L2* and *L3*) might be more suitable for approximating the buckling strength of the gusset plate.

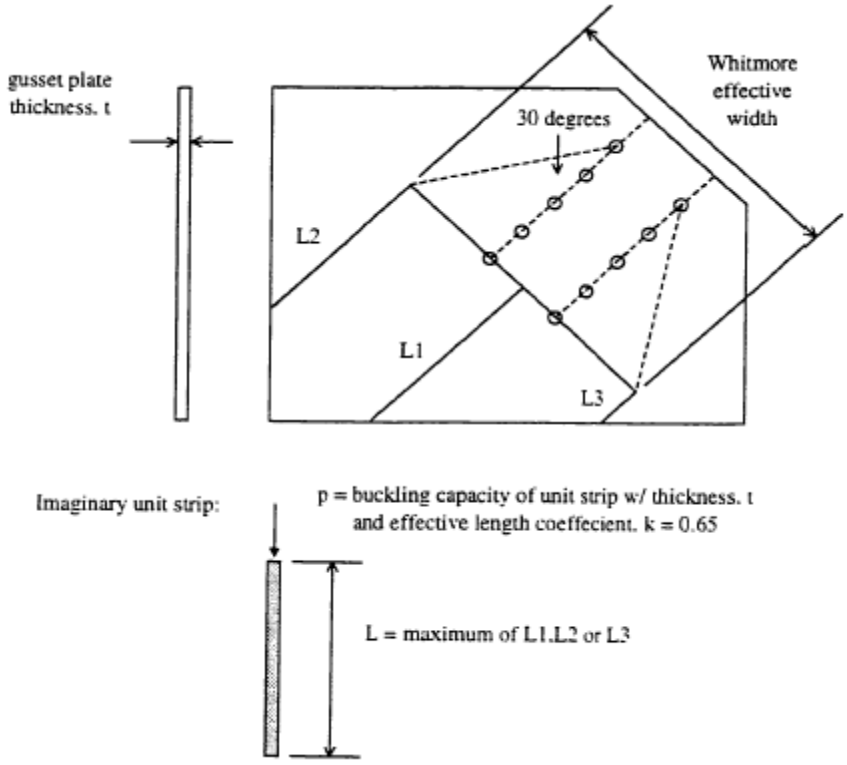


Brace load*= (p) × (Whitmore effective width)

* to cause buckling of gusset plate

Figure 2. 5 – Explanation of Thornton method for predicting buckling capacity of gusset plate (Thornton, 1984)

It is found that in high-rise structures where diagonal braces carry primarily lateral loads and are typically much smaller than the beams and columns, it may not be critical for the centerline of the diagonal brace to pass through the center of the beam-column connection. This means that under certain conditions gusset plate connections can be designed to be more compact (see Figure 2.7) (Thornton, 1984).

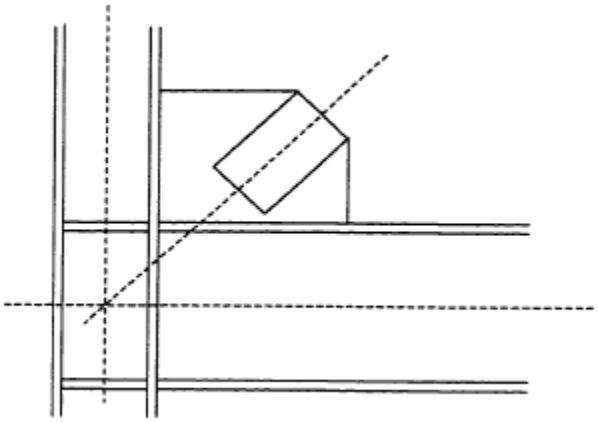

(a) Gusset plate connection detail with no in-plane connection eccentricity

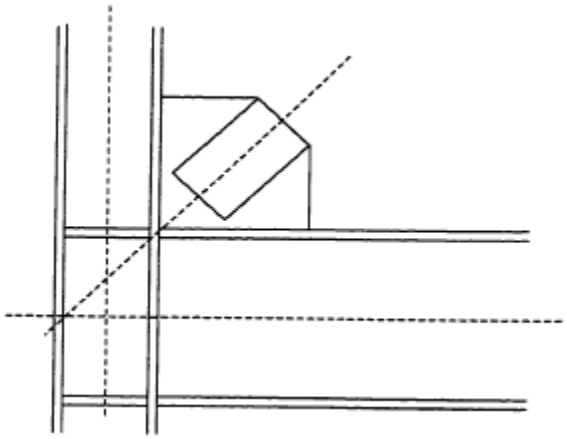

(b) Gusset plate connection detail with in-plane connection eccentricity

Figure 2. 6 – Explanation of in-plane connection eccentricity. (Thornton, 1984)

Williams and Richard (1986) carried out analytical and experimental work to develop design procedures for gusset plate connections in diagonal braced frames. Their research focused on the distribution of forces in the gusset-to-frame and gusset-to-brace fasteners (Figure 2.8). A finite element analysis of several concentrically braced frame (CBF) connections was performed to study these forces.

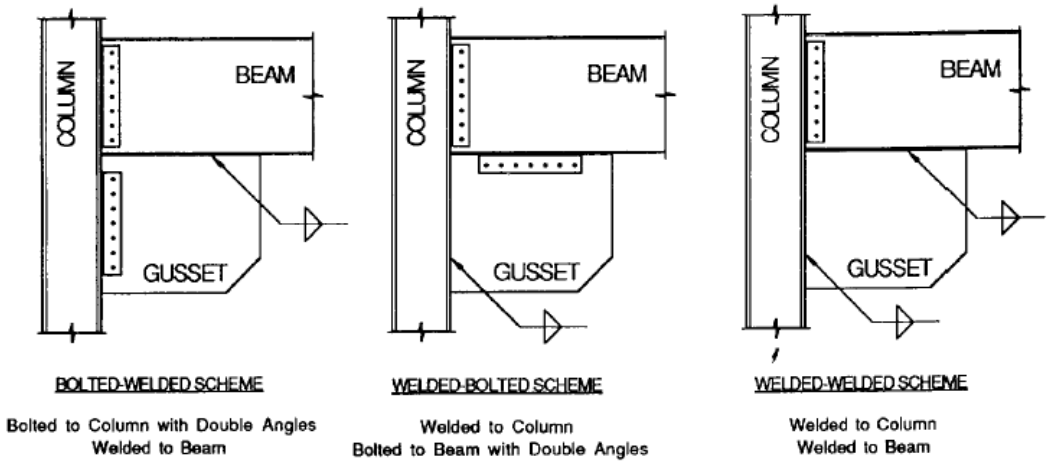


(a) Gusset-to-frame fastener connection

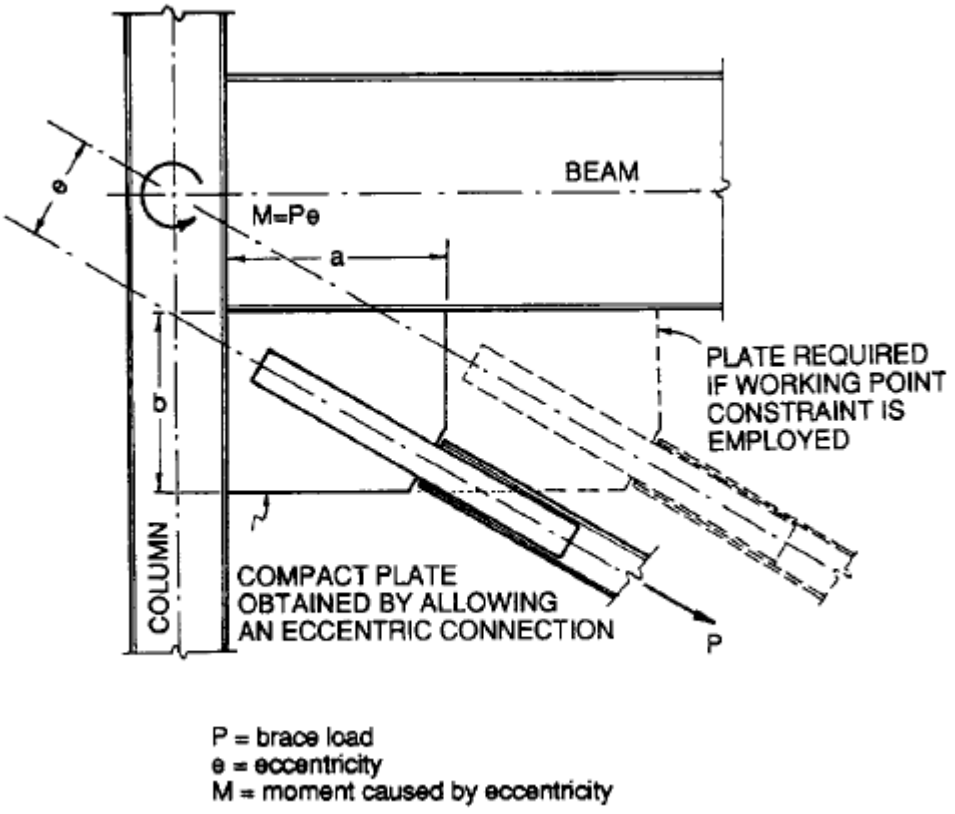


(b) Gusset-to-brace fastener connection

Figure 2. 7 - Gusset-to-frame and gusset-to-brace fasteners test specimen (Williams and Richard, 1986)

A procedure for developing two dimensional fastener elements was presented. The procedure involved the following steps:

(1) Isolate the fastener from the real structure.
(2) Design fastener tests to duplicate the forces and deformations that occur in the real structure.
(3) Perform fastener tests to obtain force-deformation data.
(4) Fit curves to the test data, and use the fitted curves as input parameters for nonlinear spring elements.

The nonlinear behaviour of the gusset plate material was studied in this investigation. In order to ensure that yielding was limited to the gusset plate and fastener, a linear elastic material model was developed for the framing members. They found that frame action had a significant effect on the gusset-to-frame force distribution. A comparison of models with the frame members and models without frame members showed that the frame needs to be included in the finite element models of this type.

Compressive versus tensile brace loads, brace configuration, beam and column properties, gusset-to-frame fastener type and brace eccentricity were the factors that were found to have little effect on fastener force distributions. Gusset plate length to width ratio, brace load and brace angle were the factors that were found to have a significant effect on fastener force distributions. It is found that gusset plates cause beam-to-column connections to act rigidly. Fastener force distributions were found to be more uniform in the more compact gusset plates, where small amounts of in-plane eccentricity were permitted (i.e. the centerline of the diagonal brace was not made to pass through the center of the beam-to-column connection). Fastener force design equations were suggested.

Williams and Richard (1986) also studied linear elastic buckling in their research. A method for estimating compressive capacity was proposed. The buckling load is

determined using Thornton's unit strip approach in conjunction with column design equations. This buckling load is then compared with the yield load predicted using the Whitmore effective width and the lesser of the two was taken as the compressive capacity of the gusset plate. It was suggested that as the gusset plate thickness is increased, gusset plate dimensions (length or width) be reduced, or gusset plate free edge stiffeners be incorporated in order to increase compressive capacity.

Gross (1990) presented findings from monotonic tests on three variations of a particular gusset plate connection detail. The tests were conducted to study the followings:

(1) The influence of framing members on the strength and behaviour of the gusset plate connection,
(2) The effect of in-plane connection eccentricity on the gusset plate capacity and on the forces transferred to the framing members, and
(3) The difference between a gusset plate connections made to the column flange as opposed to one made to the column web.

Gross (1990) presented that the yield load determined using the Whitmore method seemed to correspond well with the observed yield load. Gross's study was based on experimental investigation. Thornton's method for estimating the compressive strength of the gusset plate was found to be adequately conservative when an effective length factor, K, of 0.5 was used. It was also found that the compact specimens (with in-plane eccentricity) provide a higher buckling load than the less compact specimen (designed to have no in-plane eccentricity). The orientation of the column (i.e. gusset plate connected to column flange vs. gusset plate connected to column web) had little effect on the buckling load. Figure 2.9 shows the test configuration and connection detail of specimen which used in this study.

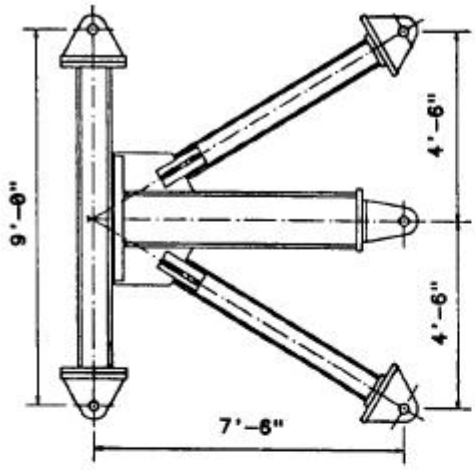


Test Configuration
(Specimen 1)

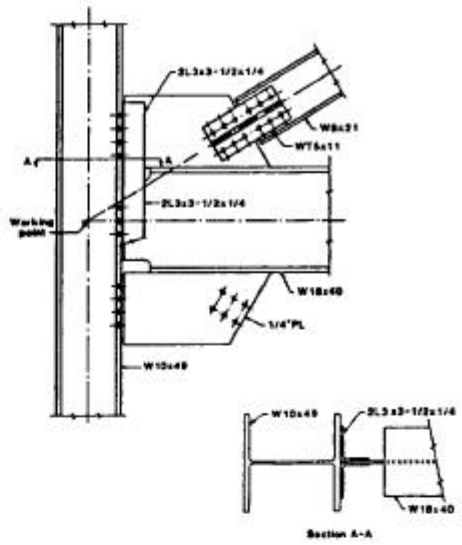


Connection Detail
for Specimen 1

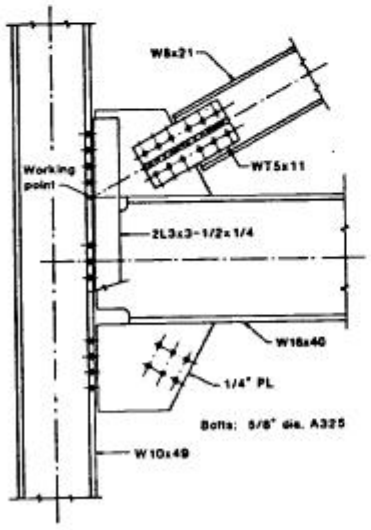


Connection Detail
for Specimen 2

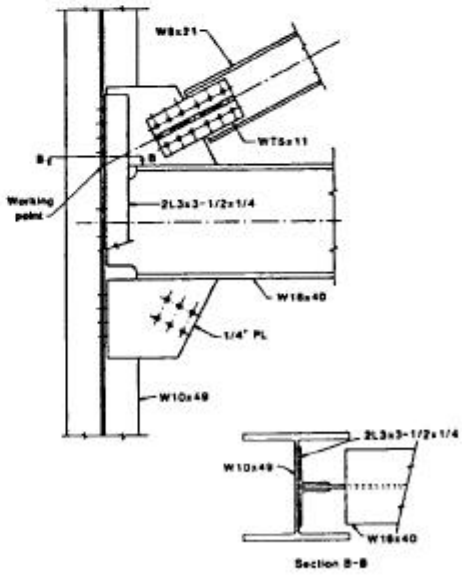


Connection Detail
for Specimen 3

Figure 2. 8 - Test configuration and connection detail of specimen (Gross, 1990)

Barth et al. (2001) focused on examining the effects of connection eccentricity and connection length on the ultimate capacity of bolted WT tension members. In particular, complementing prior experimental investigations by the authors and others, the main objective of their work was to develop robust finite element tools capable not only of estimating the failure loads but also to trace the entire load versus deflection path. The connecting bolts were assumed to be rigid and a surface-to-surface contact was used to fully transfer the load from the gusset plate to the web.

Tension members used in building construction are designed according to the American Institute of Steel Construction building specifications LRFD (2005) and ASD (1989). LRFD (2005) requires that the designer make three calculation checks to determine the capacity of a tension member: (i) yielding of the gross cross-sectional area; (ii) net section rupture of the critical cross-sectional area; and (iii) block shear. The lower of the three controls the allowable load capacity of a specified member.

Barth et al. (2001) investigated three modes of failure in their experimental study. The first failure mode, typically exhibited by the specimens having medium and large connection eccentricities, is caused by severe necking of the outside edge adjacent to the lead bolt hole, followed by the fracture of the outside edge. This failure mode is termed as *partial rupture* of the net section. The second failure mode was due to block shear failure as evidenced by the rupture of net tension area and either partial or full rupture of the gross shear area. The third mode of failure was due to full net section rupture of the web on either side of the lead bolt hole, which propagated through the rest of both the flange and web areas simultaneously.

Barth et al. (2001) studied a strain based failure criterion in which failure is assumed to have occurred once the maximum strain reached five times the initial yield strain to capture the failure load. Further, in the finite element model, the bolts were assumed to be rigid and the load is transferred from the gusset plate to the angle fully by the bearing of the bolts. Therefore, the longitudinal and the in-plane transverse

displacements of the nodes attached to the bearing surfaces, i.e. the surfaces on which the bolt surface bears against the hole surfaces, were coupled to one another.

They focused on predicting the failure capacities of tension members with medium to large connection eccentricities and varying connection lengths. The finite element methodology presented in their research is capable of not only predicting the failure capacities but also in tracing the entire load versus deflection path. The (partial) net section rupture failure mode of the specimens was accurately captured through the numerical simulations. The finite element model was used in conducting a detailed parametric investigation of the connection eccentricity and connection length on the failure capacities of WT sections with bolted end connections.

### 2.3.2 Cyclic Loading

Most of the research was carried out on the cyclic behaviour of the brace members in braced frame; however the amount of work that has been done to investigate the cyclic behaviour of gusset plate was quite small.

Jain et al. (1987) studied the effect of gusset plate bending stiffness and bracing member length on the cyclic behaviour of bracing members. The focus of their investigation was on the behaviour of the welded brace member. However some observations were also made on the interaction between the brace member and the gusset plate. Their investigation included 18 tests on different gusset plate-brace member combinations. In all cases the brace member was a 25.4 mm x 25.4 mm x 2.76 mm steel hollow structural section. Three different gusset plates were used and the length of the bracer member was varied. Figure 2.10 shows a typical gusset plate-brace member specimen tested by Jain et al. (1987).

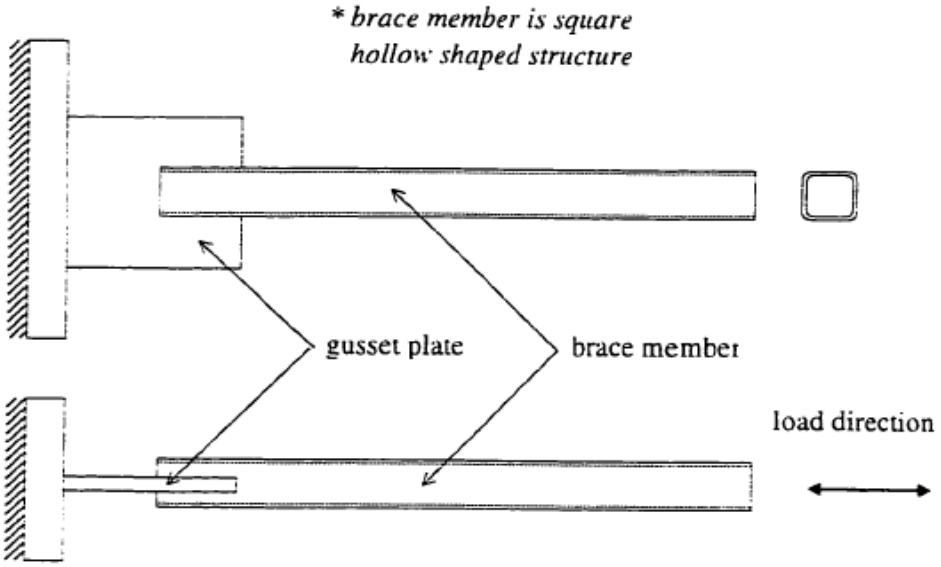


Figure 2. 9 – A typical test specimen from Jain et al., 1987.

All of the gusset plates were designed such that the yield strength was greater than the yield strength of the brace member. The flexural stiffness was computed for all gusset plates and brace members, and the ratio, *R*, of the gusset plate flexural stiffness to the brace member slenderness (*kl/r*). However, for a given brace member length, the effect of increasing the flexural stiffness of the gusset plate is to decrease the effective brace member slenderness, by decreasing the effective length factor, K. This has the same effect as reducing the brace member length, which results in an improvement in the cyclic behaviour of the brace member.

Astaneh et al. (1981) investigated the cyclic behaviour of brace members connected to gusset plates (Figure 2.11). The main contribution of their investigation was on brace member behaviour with single of multiple column of bolt. In-plane and out-of-plane buckling of the brace members was studied. Figure 2.10 shows a typical test specimen of Astaneh et al (1981). It is shown in this figure that the brace members were composed of back-to-back double angles tied with stitches. They stated their concerns regarding the current code design procedures. Practical design procedures for improving brace member ductility and energy dissipation characteristics were suggested.

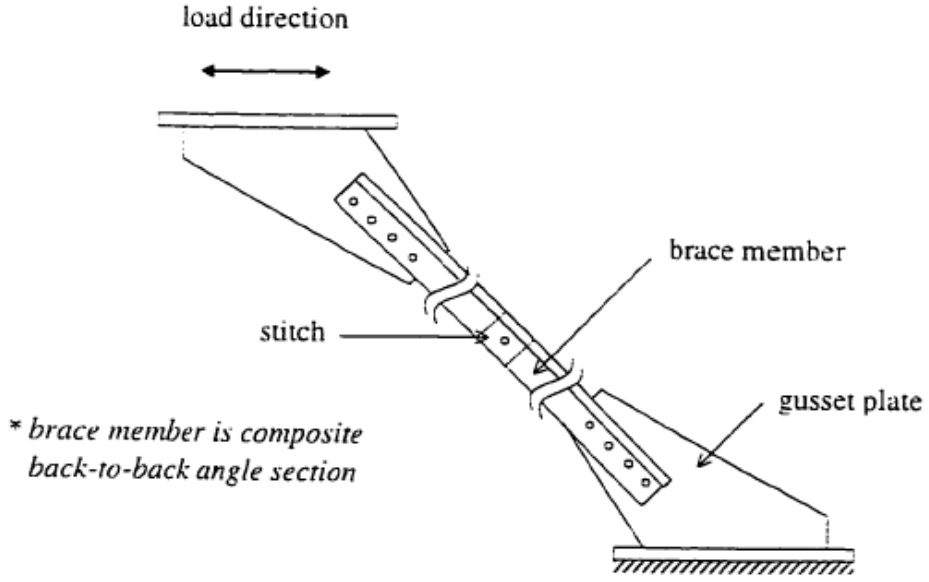


Figure 2. 10 – A typical test specimen from Astaneh et al., 1981.

Because of the importance of designing the gusset plates for brace members which buckle out-of-plane, Astaneh et al. (1981) allowed brace buckling to occur without tearing of the connection by providing the formation of plastic hinges. The test program included 16 specimens with gusset plates connected by bolts and fillet welds.

Cheng et al. (2000) investigated the effect of various parameters on the cyclic behaviour of gusset plate connections and the potential of a bracing system where the bracing member is designed as the strong element and the gusset plate is designed as the weak element. The focus of the investigation was using the test which is applied for monotonic and cyclic loading in previous and to compare the test result with finite element models. A three dimensional mesh was used to model the connection with the splice member placed on both sides of the gusset plate. The beam and column boundaries were fully restrained to simulate a rigid welded connection. The bolts were also modeled by rigid beam elements at the bolt locations. The comparison of test loads with analytical and design loads were made. This comparison showed that the Whitmore method provides a conservative estimate of the design load for the specimens, except for the type specimens which are more susceptible to the stability failure. The Thornton's (1984) method, however, provides conservative estimate for all the specimens. The test to predicted load ratio varied from 0.71 to 1.61 for the Whitmore method and from 1.31 to 1.87 for Thornton's method.

Cheng et al. (2000) conducted full-scale tests on bolted connections under both compressive and tensile monotonic and cyclic loading. Numerical investigations were carried out using the finite element method, incorporating the effect of material and geometry non-linearity and initial imperfections. Based on the monotonic compression test results, a modified Thornton method was proposed for proportioning the gusset plate to support compressive forces from brace members. In the modified Thornton method, a 45º dispersion angle was proposed to evaluate the effective width, instead of 30º, to account the load redistribution in the gusset plate.

They found from the cyclic tests, the tensile capacity of gusset plates under cyclic loading remained stable and the post-buckling compressive capacity tends to be stabilized after buckling. The addition of edge stiffeners was found to have little effect on the gusset plate buckling strength but significantly improve the post buckling compressive performance and hence, increase the energy absorbed by the gusset plate – brace member assembly in the compression cycle.

In general, hysteresis plots for the weak gusset – strong brace member models exhibited less pining and sustained higher post-buckling compressive loads than conventionally designed subassemblies. However, all the connections failed in tension in the gusset plate with a relatively small deformation. This may limit the use of the "weak gusset plate – strong brace member" concept in seismic applications. (Cheng et al., 2000)

Sheng et al. (2001) conducted a parametric study on the inelastic compressive behaviour and strength of gusset plate connections. Their specimens were built with four row and 2 columns of bolts as shown in Figure 2.12. Based on their study, general design guidelines were proposed. The finite element program, ABAQUS, was employed to perform an inelastic parametric study to examine the compressive strength and behaviour of gusset plate connections. The parameters studied included the length of longer unsupported edge of gusset plate, gusset plate shapes, types of connection between the splice member and the gusset plate, rotational restraint at the conjunction of bracing member and gusset plate, splice member types and stiffness, splice member length, and stiffeners. The results show that when the unsupported edge of a gusset plate is close to or exceeds $\frac{945}{\sqrt{f_y}}$ times its thickness, local buckling occurs along the unsupported edge and the ultimate load of the specimen is decreased significantly.

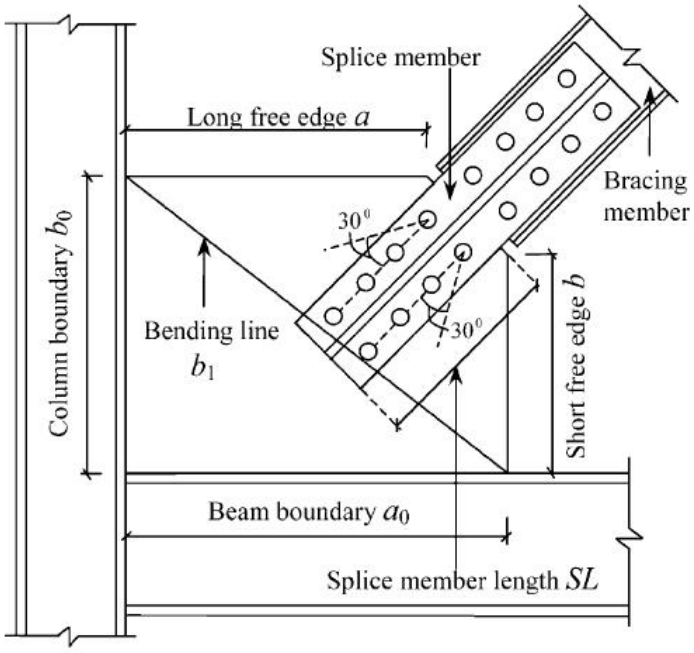


Figure 2. 11 - Typical gusset plate connection in braced steel frame (Sheng et al., 2001)

In addition, shape of the gusset plate according to a 30° load dispersion angle does not affect the ultimate loads of specimens significantly provided that the splice member is sufficiently extended beyond the bending line. The ultimate loads of specimens are increased by 10–20% when a welded connection is used to connect the splice member to the gusset plate instead of a bolted connection. (Sheng et al., 2001)

Providing infinite rotational restraint at the conjunction of bracing member and gusset plate increases significantly the ultimate loads of specimens. The types of splice member (tee-section or tubular section) do not affect the compressive strength of gusset plates so long as they provide high bending rigidity to the connection. This high bending rigidity ensures that full rotational restraint is provided to the gusset plate by the bracing member. (Sheng et al., 2001)

By increasing the splice member length, the ultimate loads of gusset plate connections increase significantly and the energy absorption behaviour of the

connections is also improved. Adding stiffeners along the centerline of the splice member or along both free edges of the gusset plate increases the ultimate load of the gusset plate significantly. In particular, stiffened gusset plates experience a slightly more stable post-buckling behaviour which may be important for earthquake loading where energy absorption is required. (Sheng et al., 2001)

By comparing the analytical ultimate loads with the Whitmore loads, Thornton loads, and modified Thornton loads, it was found that the Whitmore method is ineffective in estimating the ultimate loads of specimens. The Thornton method and modified Thornton method produced conservative estimates of the ultimate loads. To provide a better estimate of the compressive strength of gusset plate connections, a design method accompanied by some design charts for rectangular type gusset plates is recommended based on the theoretical inelastic plate buckling equation. It should be noted that the proposed design curves are based on the studies of the rectangular type gusset plates. In addition, single gusset plate connections of a 45° braced steel frame were used. The brace member was designed not to buckle and it was connected to the gusset plate by means of a bolted splice member connection. (Sheng et al., 2001)

Topkaya (2003) conducted a finite element parametric study on block shear failure of steel tension members with bolted connection. He conducted this study to develop simple block shear load capacity predication equations that are based on finite element analysis. In addition, the effects of eccentric loading were investigated. The angles and tee sections were modeled using 10-node tetrahedral elements which are capable of representing large deformation geometric and material nonlinearities. Based on numerical results to a theoretical model the equations were developed to predict the block shear load capacity of tension members. In this equation, it is assumed that the net tension plane reaches ultimate strength while the gross shear plane develops an effective shear stress which is represented as a percentage of yield stress. These equations quantify the value of effective shear stress based on geometric and material properties. Examination of analytical findings reveals that the effective

shear stress is mostly influenced by the ultimate-to-yield ratio and the connection length.

If the effective shear stress is based on both the ultimate-to-yield ratio and the connection length Eq. (2.4) could be found by regression analysis and rounding off the coefficients.

$$R_n = \left( 0.25 + 0.35\frac{F_u}{F_y} - \frac{Cl}{2800} \right) F_y A_{gv} + F_u A_{nt} \qquad (2.4)$$

Where, *Cl* is the connection length (distance from the center of the leading bolt hole to the end of the plate). The coefficient of determination ($r^2$) for the effective shear stress normalized by yield stress is 0.87 if the coefficients of Eq. (2.4) are used. The upper limit on effective shear stress is 0.6 Fu if Eq. (2.4) is used. In Eq. (2.4), Cl is expressed in millimeters and if another system of units is used, the coefficient for connection length should be adjusted accordingly.

A more simplified equation could be developed if the effective shear stress is based only on the ultimate-to-yield ratio. Regression analysis with rounding off the coefficients revealed that Eq. (2.5) could also be a simple alternative to Eq. (2.4).

$$R_n = \left( 0.20 + 0.35\frac{F_u}{F_y} \right) F_y A_{gv} + F_u A_{nt} \qquad (2.5)$$

The coefficient of determination ($r^2$) for the effective shear stress normalized by yield stress is 0.81 if the coefficients of Eq. (2.5) are used.

A careful examination of the data revealed that an equation in which effective shear stress is based solely on the ultimate strength could be developed. Two different ultimate strength values were used in the parametric study. For the 720 analyses cases the effective shear stress is normalized by ultimate strength and the data points are

presented in Fig. 11. According to this figure the effective shear stress values fall within a band that is bounded by 40–55% of ultimate strength averaging a value of 48%. Based on this observation a very simple prediction equation was developed and is presented in Eq. (2.6).

$$R_n = 0.48F_u A_{gv} + F_u A_{nt} \quad (2.6)$$

All the equations derived so far were for cases where loading was centric. As explained before out-of-plane eccentricity has no significant effect on the block shear capacity. On the other hand, in-plane eccentricity might cause a small reduction in the values. Therefore, for cases where in-plane eccentricity is present designers might reduce the block shear load capacity by 10% for longer connections.

A comprehensive analytical study on block shear failure of steel tension members was presented. A finite element analysis methodology was developed to predict the block shear failure load capacities. Specimens tested by three independent research teams were modeled and analyzed with this method. Finite element analysis was found to predict the failure loads of test specimens with acceptable accuracy.

A parametric study was conducted to identify the important parameters that influence the block shear response. Simple block shear load capacity prediction equations were developed based on the analysis results and their quality is assessed by making comparisons with experimental findings.
The following can be concluded from this study:

- Block shear load capacity is mostly influenced by the ultimate-to-yield ratio, connection length and boundary conditions.
- Presence of in-plane eccentricity can reduce the block shear load capacity by 10% for longer connections.
- Presence of out-of-plane eccentricity does not significantly affect the response.

- The developed equations provide load capacity estimates with acceptable accuracy.

Huns et al. (2004) studied tension and shear block failure of bolted gusset plates. Many Laboratory experiments were conducted to study tension and shear block failure of gusset plates. Two connection configurations were investigated, namely,

(i) Long and narrow connection

(ii) Short and wide connection.

The test results were obtained in the form of load versus deformation curves for each test specimen. Furthermore, a detailed photographic record of the failure process was collected for each of the four tests that were unloaded periodically. They used a preliminary finite element analysis based on a 9.6 mm gusset plate tested before. Load was applied to half of each bolt hole edge surface to simulate bearing of the bolts. All the nodes that would have been under the splice plate that connected a brace member to the gusset plate were restrained in the out-of-plane direction and were free to move in the plane of the plate.

A mesh refinement study was conducted to determine the correct mesh size to use in the analysis. The mesh was gradually refined, and a convergence check was conducted using the major principal strains on the tension portion of the failure surface. Because of material yielding, a high strain concentration was observed near the bolt holes, necessitating a very small mesh size. Once convergence of strains was achieved, a comparison of the finite element analysis results with the test results was performed to validate the finite element model.

Huns et al. (2004) found the following results Based on the finite element analysis and test results:

1. There exists confusion about the failure progression, and failure models such as the one presented in the AISC (1999) design specification predict failure

modes that are inconsistent with experimental observations. To some extent, the models used in the current design standards fail to capture the observed failure mode for tension and shear block failure.

2. A simple analysis technique, consisting of removing elements as fracture progresses, was developed to model ductile rupture. Tension and shear rupture criteria were proposed to model the tension and shear failures. The finite element model was validated by comparing analysis results with results from gusset plate tests. The validated finite element procedure was then used to expand the database of test results to include a larger number of long connections, larger pitch distance, and larger gauge distance.

3. The finite element analyses conducted in their investigation indicate that tension fracture always occurs prior to shear rupture. Furthermore, except for unusually long and narrow connections, the full capacity of the connection is reached by the time tension rupture takes place.

4. A reliability analysis was conducted on a database consisting of 128 test results and 5 finite element analysis results. Four models, two consisting of the design equations currently used in North American standards, an equation proposed by Hardash and Bjorhovde (1984), and an equation that was shown by Driver et al. (2004) to predict quite well the tension and shear block capacity of various connection types, were evaluated. A comparison of predicted capacities and test results indicated that the two equations provided a generally good prediction of the test results, whereas the equations in the two design standards under-predicted the capacities by a significant margin.

Walbridge et al. (2004) investigated on the monotonic and cyclic behaviour of steel gusset plate connections is conducted using a nonlinear finite element model. The models include the effects of framing member stiffness, nonlinear material behaviour,

initial imperfections, and bolt slip, are formulated and validated by comparison with test results.

ABAQUS shell element S4R was used to model the gusset plate and the T-shaped splice members. Two different material models were investigated: an elasto-plastic model and an isotropic strain-hardening model. The bolts were modelled as rigid links between the gusset plate and the splice members. The displacement and rotation of the nodes along the connected edges of the gusset plate were fully restrained, thereby simulating rigid framing members. The models were loaded by displacing the nodes along the loaded edge of each splice member.

The following procedure was adopted to develop the model:

1. A study of inelastic tensile gusset plate behaviour was performed to investigate the effects of mesh refinement, strain hardening, and framing member stiffness. The modelled gusset plates were all loaded beyond their peak tensile capacities. Since tensile test results were not available, peak tensile loads from the cyclic tests conducted by Rabinovitch and Cheng (1993) were used for validation purposes at this stage.

2. Initial imperfections were subsequently incorporated into the model developed in step (1). The modified model was then used to investigate gusset plate response under monotonic compressive loading with different imperfection shapes and magnitudes. The results of this investigation were compared with some of the test results of Yam and Cheng (1993).

3. Finally, the finite element model developed in step (2) was used to simulate gusset plate behaviour under cyclic loading. At this stage, a fastener model was developed to model the bolt slip that was observed for some of the specimens tested by Rabinovitch and Cheng (1993).

Walbridge et al. (2004) found that the effect of strain hardening on the load versus displacement behaviour in monotonic tension was an increase in the ultimate tensile capacity (Fig. 2.13). It was found, however, that the elasto-plastic material model resulted in a better prediction of the test specimen behaviour. The reasons that the models with strain hardening tended to overestimate the ultimate load are believed to be twofold.

- Firstly, bolt holes were not incorporated in the gusset plate model. The resulting excess material along the yield surface of the gusset plate (assuming a block shear failure mode) is believed to explain to a large extent the difference between the test results and the predictions of the gusset plate model with strain hardening.
- Another possible explanation is that no attempt was made to model local phenomena affecting the gusset plate behaviour near the bolt holes, such as the tearing observed in some of the tests (Rabinovitch and Cheng 1993).

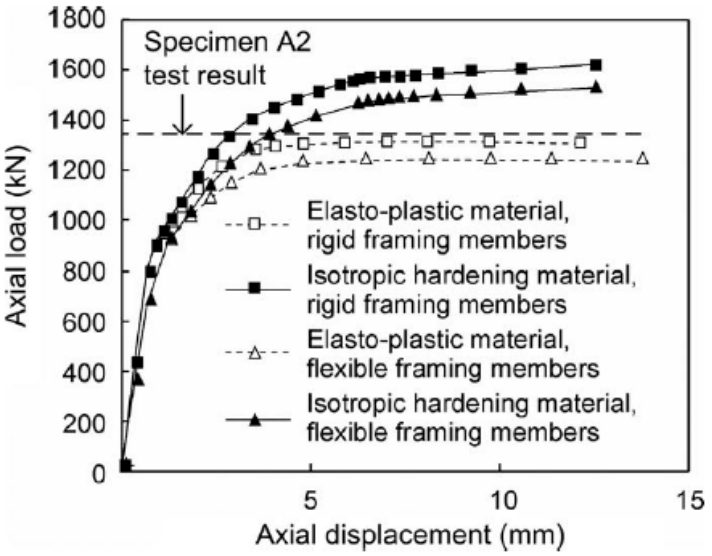


Figure 2. 12 – Effect of material model and boundary conditions on monotonic tension behaviour - Rabinovitch and Cheng (1993)

A parametric study conducted to examine the effects of the load sequence and the interaction between the gusset plate and the brace member under cyclic loading. The following conclusions can be drawn from this parametric study:

- Load sequence does not have a significant effect on the cyclic behaviour of the gusset plate – brace member subassemblies.
- Limiting the capacity in tension either by brace member yielding or by gusset plate yielding does not result in a significant change in behaviour over the displacement range studied.
- Buckling of the gusset plate results in only a small reduction in capacity and a very stable cyclic behaviour.

- Failure in compression by buckling of the gusset plate rather than buckling of the brace member results in better energy absorption characteristics.
- Although all plate thickness display good behaviour, the thicker gusset plate shows fuller hysteresis loops.
- Monotonic load versus displacement plots tended to delineate the cyclic load versus displacement hysteresis envelope.
- In general, hysteresis plots for the weak gusset plate – strong brace member models exhibited less pining and sustained higher post-buckling compressive loads than the conventionally designed subassemblies.

## 2.4 Other Studies under Compression Load

This section presents the results of three experimental investigations conducted at the University of Alberta to study the behaviour of gusset plate connection. The buckling behaviour of the thin corner gusset plates loaded monotonically in compression is studied by Hu and Cheng (1987). Yam and Cheng (1993) performed a similar research with thicker gusset plate specimens that showed inelastic behaviour prior to buckling. Rabinovitch and Cheng (1993) extended the Yam and Cheng (1993) test program to comprise the effect of cyclic loading on the behaviour of corner gusset plates. Some of the results from investigations of Yam and Cheng (1993) and Rabinovitch and Cheng (1993) were used to validate the finite element model improved for this research. The following sections are the summary of these researches.

### 2.4.1 Hu and Cheng (1987)

Hu and Cheng (1987) focused on the effects of plate thickness, geometry, boundary conditions, eccentricity and reinforcement in the buckling behaviour of gusset plate connections loaded monotonically in compression. This test program incorporated 14 tests on six thin gusset plate specimens. Two types of test were performed in this study; namely the free case and the fixed case. For the free case, the test frame was allowed to move out-of-plane while the diagonal bracing member was restrained from moving. For the fixed case, both the test frame and the diagonal bracing member were restrained from moving out-of-plane. Figure 2.14 shows the schematic of test setup used by Hu and Cheng (1987).

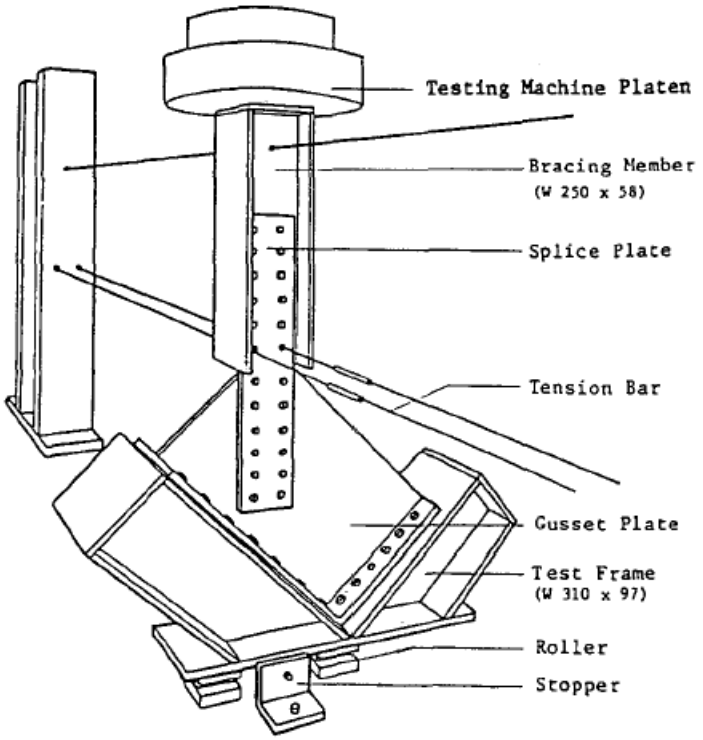


Figure 2. 13 – Schematic test setup by Hu and Cheng (1987).

They found that thin gusset plates tended to buckle at a load much lower than the yield load predicted using the Whitmore effective width. In general, either sway or local buckling modes were observed depending on the out-of-plane brace resistant conditions.

Figure 2.15 shows a typical finite element mesh of the gusset plate. The splice plates were placed on both sides of the gusset plate and a three-dimensional mesh was used to model the connection. The rigid welded connection was simulated which shown the restraints of beam and column boundaries. The infinite rotational restraint granted by the bracing member along the element x-axis at the conjunction of bracing member and gusset plate. As it is shown in Figure 2.14, the load applied as pressure on the splicing member and transfer form splice member to the gusset plate at the bolt locations.

The constraint equations were used at the bolt locations in order to simulate a rigid line tied across the splice plates and the gusset plate. The in-plane displacements were

participated at these locations and the connection rotated about the centerline of the gusset plate during buckling.

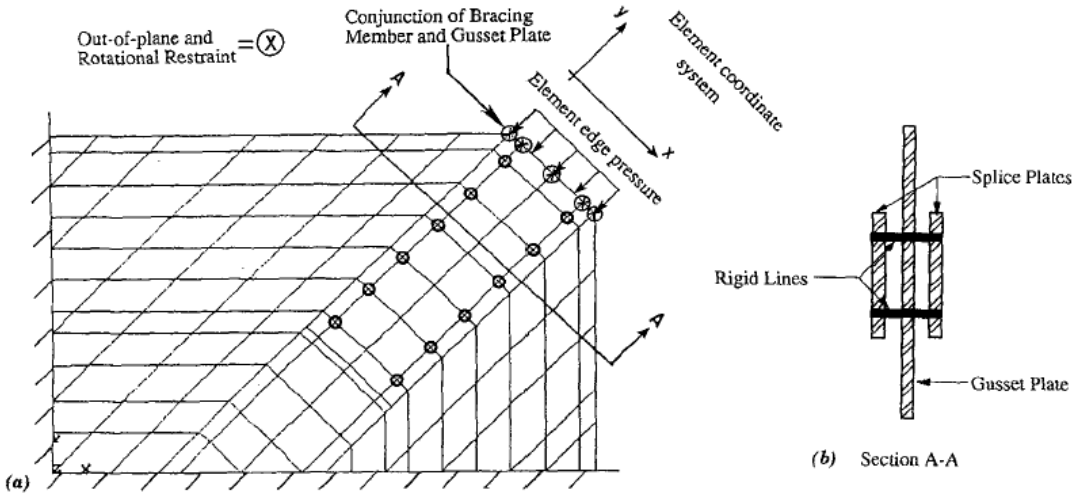


Figure 2. 14 – Finite element model of gusset plate and splice member
(Hu and Cheng, 1987)

A parametric study was afterwards performed using the finite element method. The parametric study showed that an increase in the stiffness of the gusset-to-brace splice plate should result in an increase in the buckling strength of the gusset plate up to a splice plate thickness of two to four times the gusset plate thickness. The gusset plate connections of this type must be designed in order that the distance between the end of the splice plate and the gusset-to-frame boundaries is reserved to a minimum. It was recommended that the interaction between the gusset plate and the brace member must be studied.

### 2.4.2 Yam and Cheng (1993)

Yam and Cheng (1993) studied the results of a test program on compressive behaviour and ultimate strength of gusset plate connections. Gusset plate thickness and size, brace angle, out-of-plane brace restraint conditions, moments in the framing members and out-of-plane eccentricity of the brace load were the parameters studied

in this research. The specimens which tested by Yam and Cheng were stronger than those tested by Hu and Cheng. As a result, it is tended to show considerably more inelastic behaviour prior to buckling. The test frames used by Yam and Cheng with a typical specimen in place is shown in Figure 2.16.

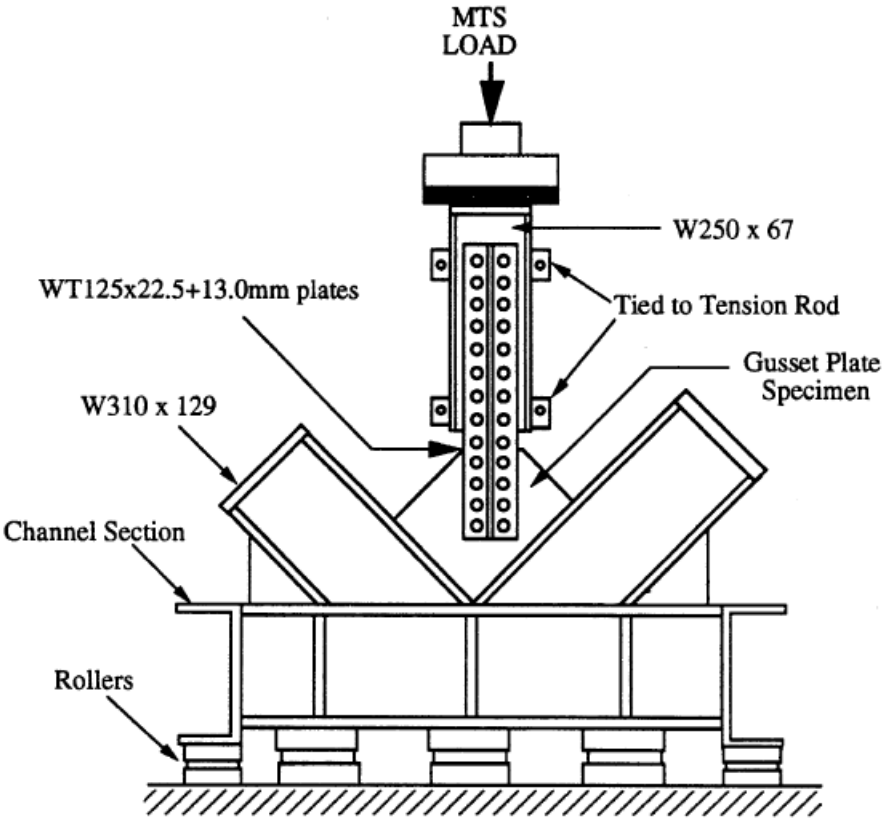


Figure 2. 15 – One of the test frames used by Yam and Cheng, 1993.

They found that the compressive capacity of the specimens which was tested was almost directly proportional to the thickness of the gusset plate. It was also found that the effect of the beam and column moments did have some effect on the measured strain distributions in the gusset plate. Yam and Cheng (1993) investigated that Thornton's method to give a conservative estimate of compressive capacity. It was recommended that a parametric study should be performed to determine "important design variables" in order that a reasonable design procedure may be improved. The test results for these specimens are presented in Table 2.1. Axial load versus out-of-plane displacement plots for these specimens are shown in Figure 2.17.

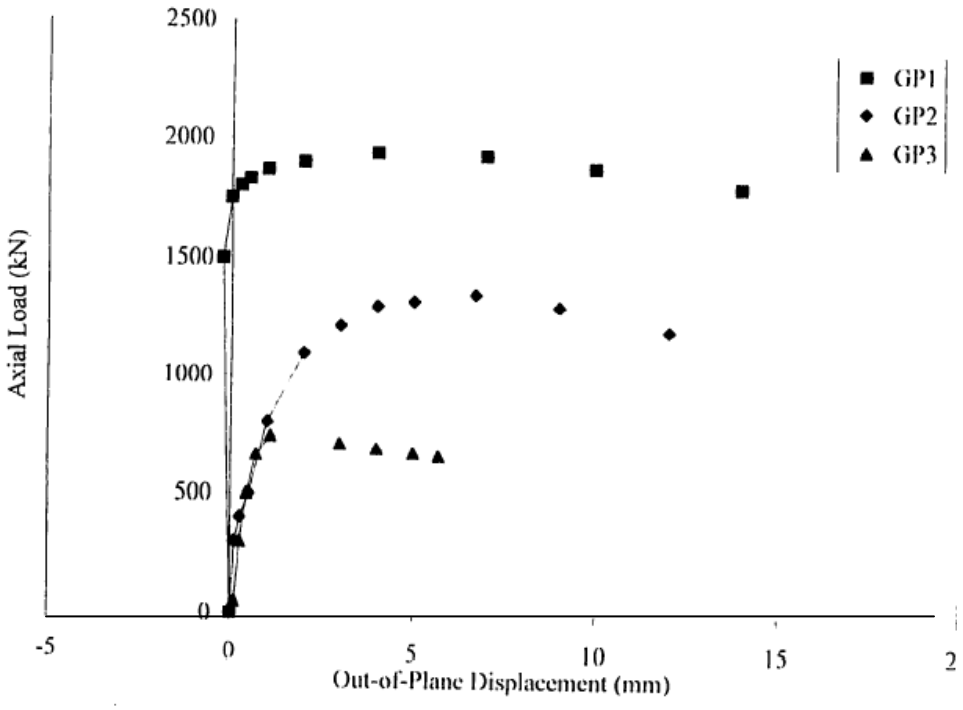


Figure 2. 16 – Axial load versus out-of-plane displacement plots for Yam and Cheng (1993) specimens.

Table 2. 1 – Summary of Yam and Cheng (1993) test results

| Specimen | Plate Size (mm) | Material Properties | | | Performance | |
|---|---|---|---|---|---|---|
| | | Modulus of Elasticity (MPa) | Yield Strength (MPa) | Ultimate Strength (MPa) | Ultimate Tensile Load (KN) | Ultimate Compressive Load (KN) |
| GP1 | 500 x 400 x 13.3 | 207600 | 295 | 501 | - | 1956 |
| GP2 | 500 x 400 x 9.8 | 210200 | 305 | 465 | - | 1356 |
| GP3 | 500 x 400 x 6.5 | 196000 | 275 | 467 | - | 742 |

### 2.4.3 Rabinovitch and Cheng (1993)

Rabinovitch and Cheng (1993) performed an experimental study to understand the cyclic behaviour of steel gusset plate connections. The effect of gusset plate thickness, geometry, edge stiffeners, and bolt slip were studied. The modeling of a CBF connection for which the gusset plate was designed to buckle before the brace member was proposed in test frame used by Rabinovitch and Cheng. The assembly of the beam, column and gusset plate was free to slide out-of-plane while the brace member was restrained. It was supposed that the brace provided infinite rotational resistant (i.e. the brace was assumed to have a much greater bending stiffness than the gusset plate). This meant that all of the energy introduced by the cyclic load dissipated by yielding and buckling of the gusset plate.

The forces of beam and column which would be present in an actual frame were ignored. The test frame used by Rabinovitch and Cheng with a typical specimen in place was shown in Figure 2.18. The numbers of five full-scale specimens were tested in this research.

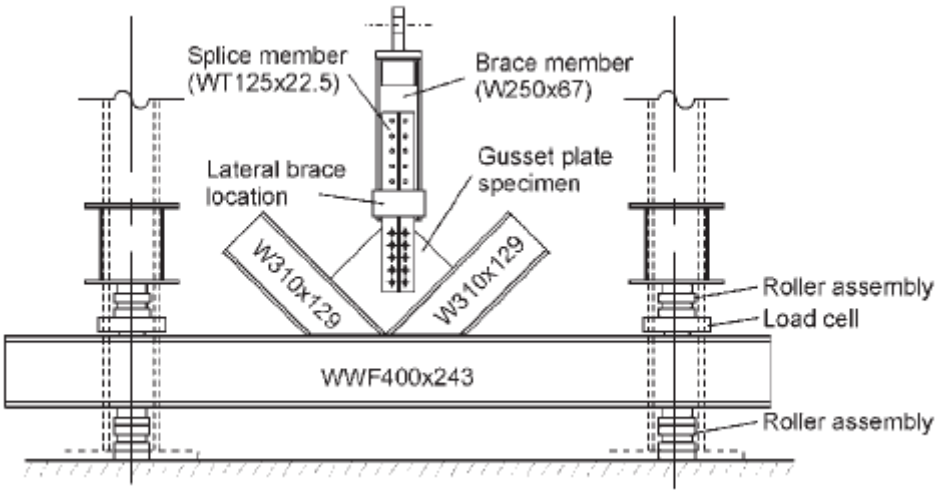


Figure 2. 17 – Test frame used by Rabinovitch and Cheng, 1993.

They found that cyclic loading causes the compressive strength of the gusset plate to drop to a stable post-buckling level, but has little effect on the tensile strength. The addition of edge stiffeners was shown to considerably improve the post buckling

compressive strength and the energy dissipation characterises of the gusset plates tested. A parametric study was recommended to improve edge stiffener design. The validation of the finite element model and test results by Rabinovitch and Cheng are presented in Table 2.2. The axial load vs. axial deflection hysteresis graphs for theses specimens are presented in Figures 2.19.

Table 2. 2 – Summary of Rabinovitch and Cheng (1993) test results

| Specimen | Plate Size (mm) | Material Properties | | | Performance | |
|---|---|---|---|---|---|---|
| | | Modulus of Elasticity (MPa) | Yield Strength (MPa) | Ultimate Strength (MPa) | Ultimate Tensile Load (kN) | Ultimate Compressive Load (kN) |
| A1 | 550 × 450 × 9.32 | 206,000 | 449 | 537 | 1794 | 1682 |
| A2 | 550 × 450 × 6.18 | 206,000 | 443 | 530 | 1340 | 1128 |
| A3 | 550 × 450 × 9.32 | 206,000 | 449 | 537 | 1884 | 2004 |
| A4 | 550 × 450 × 6.18 | 206,000 | 443 | 530 | 1265 | 1149 |

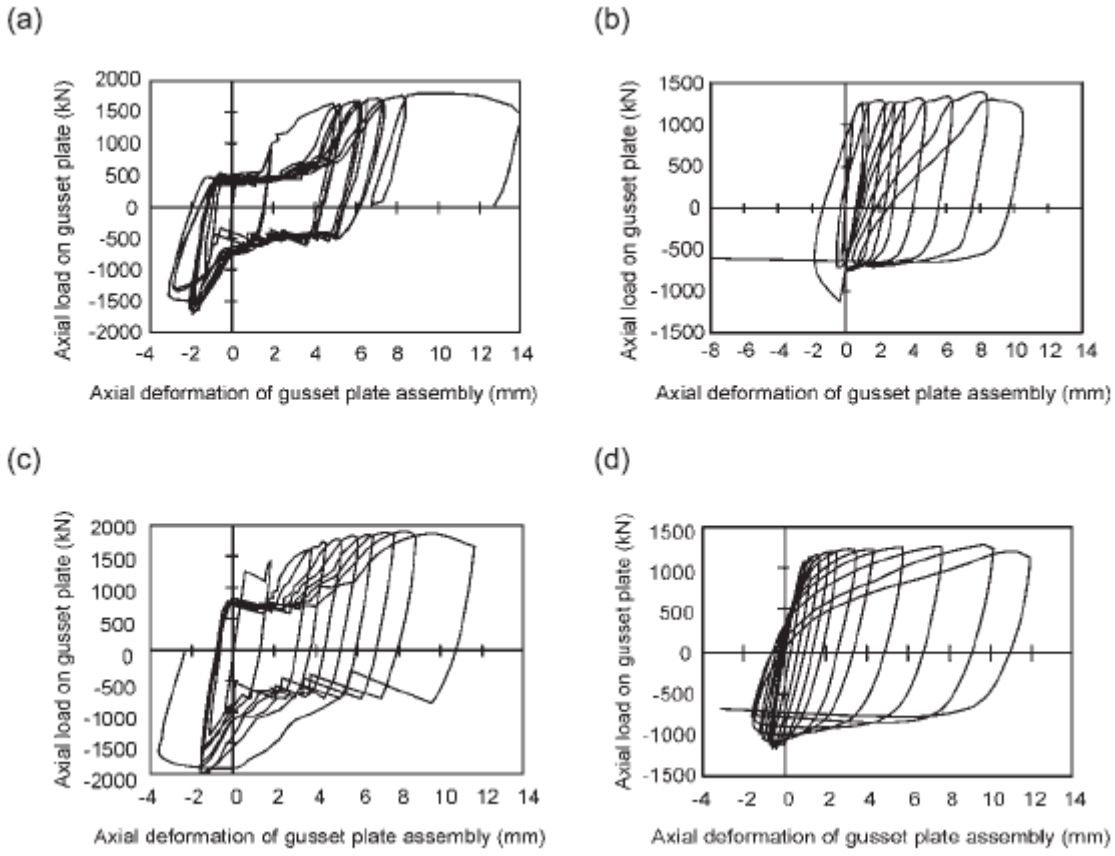


Figure 2. 18 – Axial load vs. axial displacement hysteresis plots for Rabinovitch and Cheng (1993) specimens.

## 2.5 Current Design Practice

Concentrically braced frames (CBF) are typically designed to dissipate energy revealed to the structure through yielding or buckling of the brace members. The remaining members and connections are able to carry the forces in the structure at the load level that causes the brace members to yield or buckle. Thus, gusset plates in CBF are designed to resist a tensile load equivalent to the load required to yield the lateral bracing in tension. The plate thickness selection is done based on this basis. The number of bolts required in the connection determined with in-plane dimensions of the gusset plate.

Clauses related to the design of gusset plate connections in CAN/CSA-S16.1 – Limit States Design of Steel Structures (2006) were for the most part performance oriented rather than prescriptive in nature. Some clauses in CAN/CSA-S16.1 (2006) concerned about gusset plate as follows:

1) Clause 13.4.3 recommends that the tensile resistance of a gusset plate should be determined using the CAN/CSA-S16.1 (2006) block shear formulas. Hardash and Bjorhovde (1984) suggested a variation of the block shear formulas.
2) Clause 27.4.4.1 recommends that eccentricities in bracing connections should be minimized, although, Thornton (1984) showed that is not essential to eliminate eccentricity all together.
3) Clause 27.4.4.2 recommends minimum strength for brace connections in tension. In zones with heavy seismic activity (velocity and acceleration related seismic zones of 3 or higher), the minimum strength is governed by capacity design. In lighter seismic zones, this criterion is relaxed somewhat.
4) Clause 27.4.4.3 recommends that gusset plates be detailed such a manner as to avoid brittle fracture when the brace member buckles, either in-plane or out-of-plane. Astaneh, Goel and Hanson (1981), Rabinovitch and Cheng (1993) suggest that these recommendations may not apply for corner gusset plates.

The detailing corner gusset plates in accordance with these recommendations may actually hinder their performance.

CAN/CSA-S16.1 (2006) recommends that seismic design of structures be done in accordance with the National Building Code of Canada (NBCC, 2005). CAN/CSA-S16.1 (2006) provides criteria for classify CBF's into three ductility categories: ductile, nominally ductile, or a third category for which no special provisions are made for ductility. These categories affect the design seismic loads assessed in accordance with the National Building Code of Canada.

The CAN/CSA-S16.1 (2006) also makes the assumption that the tension face of the fracture surface possesses sufficient ductility to enable the stress on the net shear surface to reach its ultimate value before rupture on the net tension face. Thus, the load at which block shear failure occurs is taken as the ultimate tensile strength times the net area in tension plus 0.60 times the ultimate tensile strength (i.e., approximately shear ultimate) times the net area in shear. This is expressed as:

$$P_u = \sigma_u A_{nt} + (0.6\sigma_u) A_{nv} \qquad (2.7)$$

Where, $\sigma_u$, is tensile ultimate strength, $A_{nt}$, net area subjected to tension and $A_{nv}$, net area subjected to shear.

The National Building Code of Canada (NBCC, 2005), section 4.1.9 gives guidelines for seismic design of structures. The assessment of the lateral design loads for the seismic design of structures was presented in this section. The magnitude of these lateral loads depends on, among other things, the ductility of the structure and the earthquake zone in which the structure is located. Redwood and Jain (1992) discussed about how this building code and others handle the seismic design of CBF's.

Several clauses in CAN/CSA-S37.01 (2001) – Antenna, Towers, and Antenna-Supporting Structures could be considered as following:

1) Clause 6.5.1 recommended that acceptable materials and product standard for bolts are ASTM standards A307, A325, A325M, and A394, and CSA standard B33.4.
2) Clause 6.5.2 recommended that the resistance factor for bolted connections shall be taken as 0.9 and 0.8 for members and bolts, respectively.
3) Clause 6.5.4 recommended that clause 21, 22 and 23 of CSA standard CAN/CSA-S16.1 shall apply expect that:
    a. Bearing-type connections may be used for connections subject to stress reversal; and
    b. Where bolts are in shear, nuts shall be prevented from working loose by pretensioning of the bolts, the use of jam or lock nuts, luck washers, or other methods acceptable to the engineer.

The AISC (2005) rules assume that shear yield and shear ultimate stress can be represented using the Von Mises criterion. The design rules are as follows:

$$\text{If} \quad \sigma_u A_{nt} \geq (0.6\sigma_u) A_{nv} \quad \textit{then} \quad P_u = \sigma_u A_{nt} + (0.6\sigma_y) A_{gv} \tag{2.8}$$

$$\text{and if} \quad (0.6\sigma_u) A_{nv} > \sigma_u A_{nt} \quad \textit{then} \quad P_u = (0.6\sigma_u) A_{nv} + \sigma_y A_{gt} \tag{2.9}$$

where, $\sigma_u$, is tensile ultimate strength, $\sigma_y$, is tensile ultimate strength, $A_{nt}$, net area subjected to tension, $A_{nv}$, net area subjected to shear, $A_{gv}$, gross area subjected to shear and $A_{gt}$, gross area subjected to tension.

Equation (2.8) indicate that if the ultimate tensile resistance is greater than the ultimate shear resistance, then the block shear resistance is the sum of the tensile resistance (on the net section) and the shear yield resistance (on the gross shear area). Conversely, if the ultimate shear resistance is greater than the ultimate tensile resistance Equation (2.9), then the block shear resistance is the sum of the ultimate shear resistance (net shear area) and the tension yield force (gross cross-section).

The rules presented in Eurocode 3 – ENV 1993-1-1 (1992) are based on the fundamental assumption that this mode of failure "consists of tensile rupture along the line of fastener holes on the tension face of the hole group, accompanied by gross section yielding in shear at the row of fastener holes along the shear face of the hole group". Eurocode uses a shear yield stress equal to $\frac{\sigma_y}{\sqrt{3}}$, and thus the block shear capacity of a gusset plate or tension member can be expressed as follows:

$$P_u = \sigma_u A_{nt} + (\frac{\sigma_y}{\sqrt{3}}) A_{gv} \qquad (2.10)$$

Equation (2.10) is not specifically given in Eurocode, but it can be deduced easily from the description of the mode of failure. A more detailed procedure is presented for block shear rupture in beam webs. For the common case, the procedure is as follows:

$$P_u = \frac{\sigma_y}{\sqrt{3}} A_{v,eff} \qquad (2.11)$$

Where, $A_{v,eff}$ is the effective shear area, taken as the product of the web thickness, t, and the effective length in shear, $L_{v,eff}$ . The effective shear area regards for both yielding along the gross shear area and tension rupture along the net tension area. For the coped beam illustrated in (Figure 2.20(b)) the following equation could use.

$$L_{v,eff} = L_v + L_1 + (a_2 - kd_{o.t}) \frac{\sigma_u}{\sigma_y} \qquad (2.12)$$

Where, the first two terms on the right hand side of the equation represent the gross shear length, as shown in (Figure 2.20(b)), and the third term represents the net tension area. The dimension $a_2$ is also illustrated in (Figure 2.20(b)), $d_{o.t}$ is the bolt

hole diameter and the constant k is taken as 0.5 for one line of bolts and 2.5 for two lines of bolts.

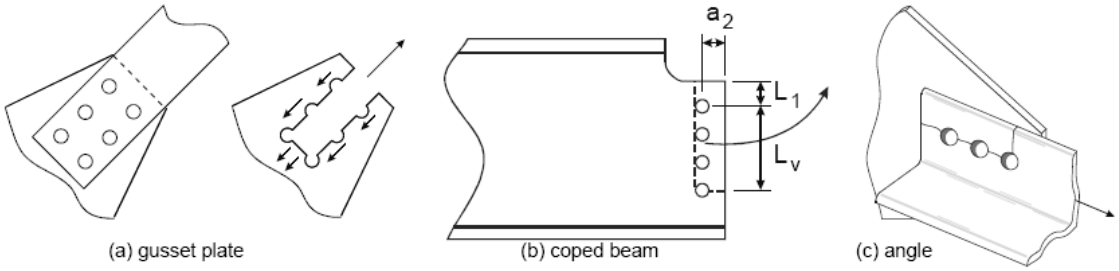


Figure 2. 19 – Examples of block shear

The procedure adopted by the Architectural Institute of Japan, Standard for limit state design of structures (1990) is the most conservative of the provisions reviewed. It uses the net areas on both the shear and tension planes. The block shear capacity is taken as least of: (1) shear yield on net shear area plus tensile ultimate on net tension area or (2) shear ultimate on net shear area plus tensile yield on net tension area. The shear yield is taken as $\frac{\sigma_y}{\sqrt{3}}$ and the shear ultimate as $\frac{\sigma_u}{\sqrt{3}}$. This can be written as:

$$P_u = \sigma_u A_{nt} + (\frac{\sigma_y}{\sqrt{3}})A_{nv} < \quad \sigma_y A_{nt} + (\frac{\sigma_u}{\sqrt{3}})A_{nv} \tag{2.13}$$

## 2.6 Summary

The following items are presented as a summary of this chapter:

1. The primary investigation on elastic behaviour of gusset plate was done by Whitmore (1952). The research was based on experimental program and a practical method for estimation the peak stress in gusset plates presented. It is proposed that the peak stress could be calculated by taking the brace load and dividing it by an area equal to the plate thickness times "Whitmore Effective Width". The Whitmore effective width is defined as the distance between two lines radiating outward at 30 degree angles from the first row of bolts in the gusset-to-brace connection along a line running through the last row of bolts.

2. Irvan (1957) suggested a method of determining the peak stress that was similar to the Whitmore's method.

3. Hardin (1958) investigated on experimental study which confirmed Irvan's conclusions regarding the inability of beam method and supported Irvan's method for determining the magnitude of the peak stress in the gusset plate.

4. Davis (1967) and Varsarelyi (1971) performed finite element investigations of the elastic stresses in gusset plates. In general, these investigations confirmed the conclusions made by Whitmore (1952), Irvan (1957) and Hardin (1958) based on experimental investigations regarding the stresses in gusset plates loaded in the elastic range.

5. Chakrabarti and Bjorhovde (1983) investigated the behaviour and strength of gusset plates further than the elastic range, in monotonic tension. Current design practices (including a yield criterion based on the Whitmore method) were evaluated using test results.

6. Hardash and Bjorhovde (1984) suggested an ultimate strength design procedure for gusset plates loaded in monotonic tension. A block shear model was proposed based on the results of tests on 42 gusset plate specimens tested at the University of Arizona, the University of Illinois and the University of Alberta. It was found that the ultimate strength can be taken as the sum of the ultimate tensile strength of the gusset plate between the bolts in the last row of bolts and the shear strength along the connection length.

7. Thornton (1984) studied on a steel gusset plate connection design example, demonstrating the application of an intuitive, lower bound solution method for determining the ultimate capacity of the connection in tension and in compression. The investigation was on the block shear method in his example to check the tear-out strength of gusset plate connection and suggested a lower bound method for determining compressive strength of the gusset plate.

8. Williams and Richard (1986) carried out analytical and experimental work to develop design procedures for gusset plate connections in diagonal braced frames. Their research focused on the distribution of forces in the gusset-to-frame and gusset-to-brace fasteners. They also studied linear elastic buckling in their research and a method for estimating compressive capacity was proposed.

9. Gross (1990) presented findings from monotonic tests on three variations of a particular gusset plate connection detail. This study showed that the yield load determined using the Whitmore method seemed to correspond well with the observed yield load.

10. Barth et al. (2001) focused on examining the effects of connection eccentricity and connection length on the ultimate capacity of bolted WT tension members. The main objective of their work was to develop robust finite

element tools capable not only of estimating the failure loads but also to trace the entire load versus deflection path.

11. Jain et al. (1987) studied the effect of gusset plate bending stiffness and bracing member length on the cyclic behaviour of bracing members. The focus of their investigation was on the behaviour of the welded brace member.

12. Astaneh et al. (1981) investigated the cyclic behaviour of brace members connected to gusset plates. The main contribution of their investigation was on brace member behaviour with single of multiple column of bolt. In-plane and out-of-plane buckling of the brace members was studied.

13. Cheng et al. (2000) investigated the effect of various parameters on the cyclic behaviour of gusset plate connections and the potential of a bracing system where the bracing member is designed as the strong element and the gusset plate is designed as the weak element. The focus of the investigation was using the test which is applied for monotonic and cyclic loading in previous and to compare the test result with finite element models.

14. Sheng et al. (2001) conducted a parametric study on the inelastic compressive behaviour and strength of gusset plate connections. The finite element analysis was performed to present an inelastic parametric study to examine the compressive strength and behaviour of gusset plate connections.

15. Topkaya (2003) conducted a finite element parametric study on block shear failure of steel tension members with bolted connection. He conducted this study to develop simple block shear load capacity predication equations that are based on finite element analysis. In addition, the effects of eccentric loading were investigated.

16. Huns et al. (2004) studied tension and shear block failure of bolted gusset plates. Many Laboratory experiments were conducted to study tension and shear block failure of gusset plates. Two connection configurations were investigated which called long and narrow connection and short and wide connection. A finite element analysis was conducted and a comparison of the finite element analysis results with the test results was performed to validate the finite element model.

17. Walbridge et al. (2004) investigated on the monotonic and cyclic behaviour of steel gusset plate connections is conducted using a nonlinear finite element model. The models include the effects of framing member stiffness, nonlinear material behaviour, initial imperfections, and bolt slip, are formulated and validated by comparison with test results. A parametric study conducted to examine the effects of the load sequence and the interaction between the gusset plate and the brace member under cyclic loading.

18. Hu and Cheng (1987) focused on the effects of plate thickness, geometry, boundary conditions, eccentricity and reinforcement in the buckling behaviour of gusset plate connections loaded monotonically in compression. A parametric study was afterwards performed using the finite element method. The parametric study showed that an increase in the stiffness of the gusset-to-brace splice plate should result in an increase in the buckling strength of the gusset plate up to a splice plate thickness of two to four times the gusset plate thickness.

19. Yam and Cheng (1993) studied the results of a test program on compressive behaviour and ultimate strength of gusset plate connections. They found that the compressive capacity of the specimens which was tested was almost directly proportional to the thickness of the gusset plate. It was also found that the effect of the beam and column moments did have some effect on the measured strain distributions in the gusset plate.

20. Rabinovitch and Cheng (1993) performed an experimental study to understand the cyclic behaviour of steel gusset plate connections. The effect of gusset plate thickness, geometry, edge stiffeners, and bolt slip were studied. They found that cyclic loading causes the compressive strength of the gusset plate to drop to a stable post-buckling level, but has little effect on the tensile strength.

21. The design of gusset plate connections is presented in CAN/CSA-S16.1 (2006) – Limit States Design of Steel Structures (2000). CAN/CSA-S16.1 (2006) recommends that seismic design of structures be done in accordance with the National Building Code of Canada (NBCC, 2005). CAN/CSA-S16.1 (2006) provides criteria for classify CBF's into three ductility categories: ductile, nominally ductile, or a third category for which no special provisions are made for ductility.

22. CAN/CSA-S37.01 (2001) – Antenna, Towers, and Antenna-Supporting Structures has recommendation about acceptable materials, product standard for bolts, bolts connection, bearing-type connections and bolts in shear.

23. The AISC (2005) rules assume that shear yield and shear ultimate stress can be represented using the Von Mises criterion. It is indicated that if the ultimate tensile resistance is greater than the ultimate shear resistance, then the block shear resistance is the sum of the tensile resistance (on the net section) and the shear yield resistance (on the gross shear area). Conversely, if the ultimate shear resistance is greater than the ultimate tensile resistance, then the block shear resistance is the sum of the ultimate shear resistance (net shear area) and the tension yield force (gross cross-section).

24. Eurocode 3 – ENV 1993-1-1 (1992) are based on the fundamental assumption that this mode of failure "consists of tensile rupture along the line of fastener

holes on the tension face of the hole group, accompanied by gross section yielding in shear at the row of fastener holes along the shear face of the hole group".

25. The Architectural Institute of Japan, Standard for limit state design of structures (1990) is the most conservative of the provisions reviewed. It uses the net areas on both the shear and tension planes. The block shear capacity is taken as least of shear yield on net shear area plus tensile ultimate on net tension area or shear ultimate on net shear area plus tensile yield on net tension area.

# 3. EXPERIMENTAL PROGRAM

## 3.1 Introduction

The design of a bracing should consider the bracing members, gusset plate connections and framing members. The variation of the load which is applied to a bracing system could be affected in the stability of gusset plate connection. In this research, the load applied to gusset plate though a tension member (i.e. angle) which is connected to plate with one or two bolts. The ultimate tension strength of gusset plate could be evaluated using CAN/CSA-S16.1 (2006). The ultimate load applied to a few gusset plate connections was based on the limitation of experimental setup and its failure such as jack capacity, or failure in the plate connection and mostly dependent on failure in the plate connection. The experimental parameters were one or two bolts, widths of plate, thickness of plate, far end as fixed or pinned condition. This chapter describes the experimental program including instrumentation, test setup and test procedure used in this study.

## 3.2 Instrumentation

The following equipments and instruments were used for the experimental program.

- Hydraulically operated universal loading jack
- Universal flat load cell
- Strain gauges
- Data acquisition system
- LVDT

### 3.2.1 Hydraulically Operated Universal Loading Jack

The hydraulic loading jack is powered by pressurized hydraulic fluid, which is typically oil. The hydraulic jack consists of a cylinder barrel, in which a piston connected to a piston rod moves up and down. The barrel is closed on each end by the cylinder bottom (also called the cap end) and by the jack head where the piston rod comes out of the cylinder. The piston has sliding rings and seals. The piston divides the inside of the cylinder in two chambers, the bottom chamber (cap end) and the piston rod side (rod end) chamber. The hydraulic pressure acts on the piston to do linear work and motion.

A hydraulic cylinder is the actuator or "motor" side of this system. The "generator" side of the hydraulic system is the hydraulic pump which brings a fixed or regulated flow of oil into the system. The piston rod also has mounting attachments to connect the cylinder to the object or machine component that it is pushing.

By pumping hydraulic oil to the bottom side of the hydraulic cylinder, the piston rod starts moving upward. The piston pushes the oil in the other chamber back to the reservoir. If the oil pressure in the piston rod chamber is zero, the force on the piston rod equals the pressure in the cylinder times the piston area. Figure 3.1 and 3.2 show a hydraulic pump and hydraulic loading jack which were used in plate test. A 10 gallon capacity hydraulic pump made by ENERPAC Company and a 900 kN (200 kips) capacity universal loading jack made by ENERPAC Company were used in this study.


Figure 3. 1 - Hydraulic pump connecting to loading jack


Figure 3. 2– Hydraulically operated universal loading Jack

### 3.2.2 Universal Flat Load Cell

A load cell is an electronic device that is used to convert a force into an electrical signal. This conversion is indirect and happens in two stages. Through a mechanical arrangement, the force being sensed deforms a strain gauge. The strain gauge converts the deformation (strain) to electrical signals. A load cell usually consists of four strain gauges in a “Wheatstone” bridge configuration. Load cells of one or two strain gauges are also available. The electrical signal output is typically in the order of a few “Millivolts” and requires amplification by an instrumentation amplifier before it can be used. The output of the transducer is plugged into an algorithm to calculate the force applied to the transducer.

Every load cell is subject to "ringing" when subjected to abrupt load changes. This stems from the spring-like behaviour of load cells. In order to measure the loads, they have to deform. As such, a load cell of finite stiffness must have spring-like behaviour, exhibiting vibrations at its natural frequency. An oscillating data pattern can be the result of ringing. Ringing can be suppressed in a limited fashion by passive means. Alternatively, a control system can use an actuator to actively damp out the ringing of a load cell. This method offers better performance at a cost of significant increase in complexity. The figure 3.3 shows universal flat load cells which were used in plate tests. The capacity of load cells were 450 kN (100kips) and 900 kN (200 kips) in compression and tension which made by STRAINSERT and INTERFACE company, respectively.


(a) Load cell 450 kN (100 kips) (b) Load cell 900 kN (200 kips)

Figure 3. 3 - Universal flat load cell 100 and 200 kips (STRAINSERT and INTERFACE Company)

### 3.2.3 Strain Gauge

A strain gauge (alternatively: strain gauge) is a device used to measure the strain of an object. Invented by Edward E. Simmons and Arthur C. Ruge in 1938, the most common type of strain gauge consists of an insulating flexible backing which supports a metallic foil pattern. The gauge is attached to the object by a suitable adhesive, such as "superglue". As the object is deformed, the foil is deformed, causing its electrical resistance to change. This resistance change, usually measured using a Wheatstone bridge, is related to the strain by the quantity known as the "*gauge factor*".

The gauge factor *GF* is defined as:

$$GF = \frac{\Delta R / R_G}{\varepsilon} \tag{3.1}$$

Where, $R_G$ is the resistance of the undeformed gauge, $\Delta R$ is the change in resistance caused by strain, and $\varepsilon$ is strain.

For metallic foil gauges, the gauge factor is usually a little over 2. For a single active gauge and three dummy resistors, the output *v* from the bridge is:

$$\upsilon = \frac{BV \cdot GF \cdot \varepsilon}{4} \tag{3.2}$$

where *BV* is the bridge excitation voltage.

Foil gauges typically have active areas of about 2-10 $mm^2$ in size. With careful installation, the correct gauge, and the correct adhesive, strains up to at least 10% can be measured. The figure 3.4 shows the strain gauge sensitive pattern during the tension and compression load. In this study strain gauge of 5 mm gauge length, 120 ohm resistance made by KYOWA Company was used measuring local strains.

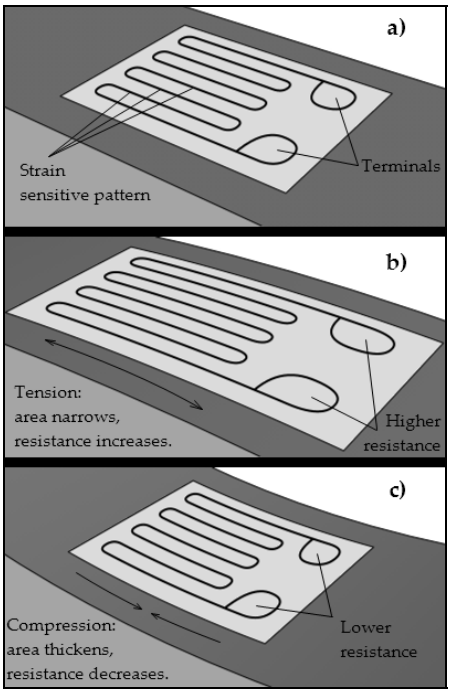


Figure 3. 4- Strain gauge in tension and compression (Wikipedia, 2006)

### 3.2.4 Data Acquisition System

Data acquisition system is an instrument to generate data that can be manipulated by a computer. Sometimes abbreviated as DAQ or DAS, data acquisition typically involves acquisition of signals and waveforms and processing the signals to obtain desired information. The components of data acquisition systems include appropriate sensors that convert any measurement parameter to an electrical signal, which is acquired by data acquisition hardware.

Acquired data are displayed, analyzed, and stored on a computer, either using vendor supplied software, or custom displays and control can be developed using various general purpose programming languages such as BASIC, C, FORTRAN, Java, Lisp, Pascal. Specialised programming languages used for data acquisition include, EPICS used to build large scale data acquisition systems, LabVIEW, which offers a graphical programming environment optimized for data acquisition and MATLAB provides a programming language but also built-in graphical tools and libraries for data

acquisition and analysis. Figures 3.5 and 3.6 show the data acquisition system (DATASCAN 7210) and computer connections which were used for the current experimental study. The maximum scanning rate that can be achieved by this DAS is one sample per second.

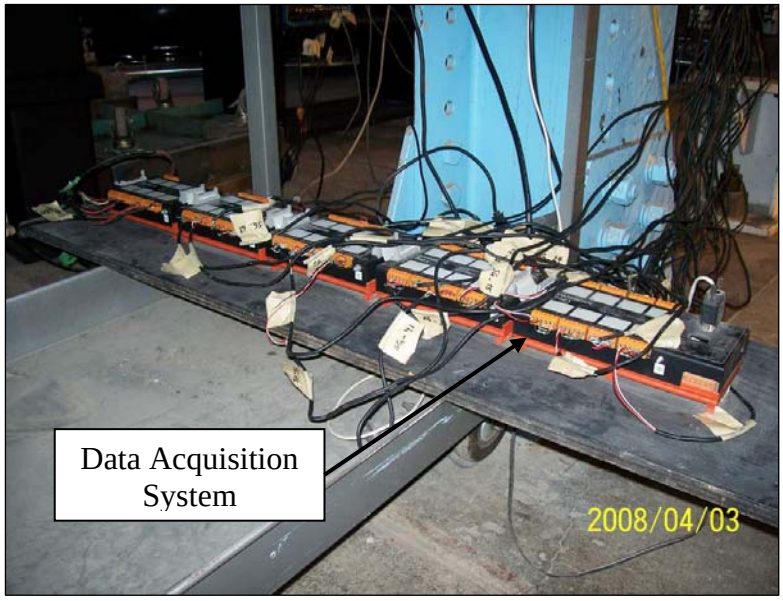


Figure 3. 5- Data Acquisition System


Figure 3. 6– Computer and data acquisition system in test condition

The data acquisition system was made ready before applying any load. The data acquisition system used DATLITE software to append the output data for the different instruments which were used in the test program. Some of the data were in millivolts, millimetre or other units which the user sets the program for that. All the required channels were set to one instrument and calibrated in order to record the correct data using offset and scale factor.

### 3.2.5 LVDT

The linear variable differential transformer (LVDT) is a type of electrical transducer used for measuring linear displacement. The transformer has three solenoidal coils placed end-to-end around a tube. The centre coil is the primary, and the two outer coils are the secondaries. A cylindrical ferromagnetic core, attached to the object whose position is to be measured, slides along the axis of the tube.

An alternating current is driven through the primary, causing a voltage to be induced in each secondary proportional to its mutual inductance with the primary. The frequency is usually in the range 1 to 10 KHz.

As the core moves, these mutual inductances change, causing the voltages induced in the secondaries to change. The coils are connected in reverse series, so that the output voltage is the difference between the two secondary voltages. When the core is in its central position, equidistant between the two secondaries, equal but opposite voltages are induced in these two coils, so the output voltage is zero.

The voltage in one coil increases when the core is displaced in one direction. The other decreases, causing the output voltage to increase from zero to a maximum. This voltage is in phase with the primary voltage. When the core moves in the other direction, the output voltage also increases from zero to a maximum, but its phase is opposite to that of the primary. The magnitude of the output voltage is proportional to the distance moved by the core (up to its limit of travel), which is why the device is described as "linear". The phase of the voltage indicates the direction of the

displacement. Figure 3.7 shows the LVDT with spring core being used in the plate test. The 150 mm (6 in) travel LVDTs were used. A few of them were free core type and remaining was spring loaded type. The numbers of the LVDT in each test varied from 1 to 4 depending on the test number. However, at least 3 LVDTs were used for every test except Specimen GP-01. The total travel of LVDT used in this study was between 100 to 150 mm (4 to 6 in). There were also two kinds of LVDT spring loaded and free core and they were used in this investigation.


Figure 3. 7- Typical LVDT (Spring Core) used in this study

The calibration for each LVDT was done before the load test was performed. The LVDTs were used to determine the in-plane deformation of plate. The positions of LVDTs were secured in order to prevent from falling down or slipping during the test. The LVDTs which were used in specimen GP-01 to GP-05 were located on plate surface. (See Figure 3.8)


Figure 3. 8- LVDT Locations in Plate for Specimen GP-05

As a result, as soon as the plate buckled out-of-plane the readings of the LVDT were affected and in many cases, the LVDT either stopped working or the LVDT core slipped off. Therefore, for the next seven specimens (GP-06 to GP-12) the locations of the LVDTs were changed from plate surface to the brackets which were connected to the bottom steel base and plate attached to the load cell. As a result, the LVDTs were not connected to the plate surface for these specimens. Hence, the local buckling of the plate did not affect the LVDT readings for tests GP-06 to GP-12. Figure 3.9 and 3.10 shows the LVDT locations and the brackets which were used in plate test for specimens GP-06 to GP-12.


Figure 3. 9- LVDT 1 and 2 Locations in Plate

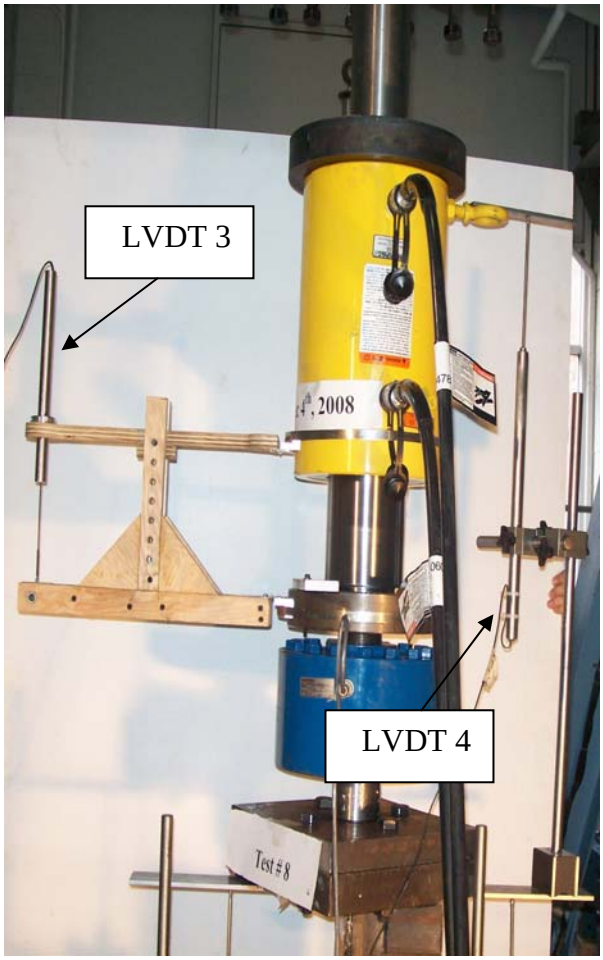


Figure 3. 10 - LVDT 3 and LVDT4

### 3.3 Test Specimens and Test Setup

Figure 3.11 shows the typical schematic test setup with load cell connection to angle and LVDT locations on plate surface which was the case for GP-06 to GP-12. The LVDTs were not connected to gusset plate surface in specimen GP-06 to GP-12 and it is shown in Figure 3.12.

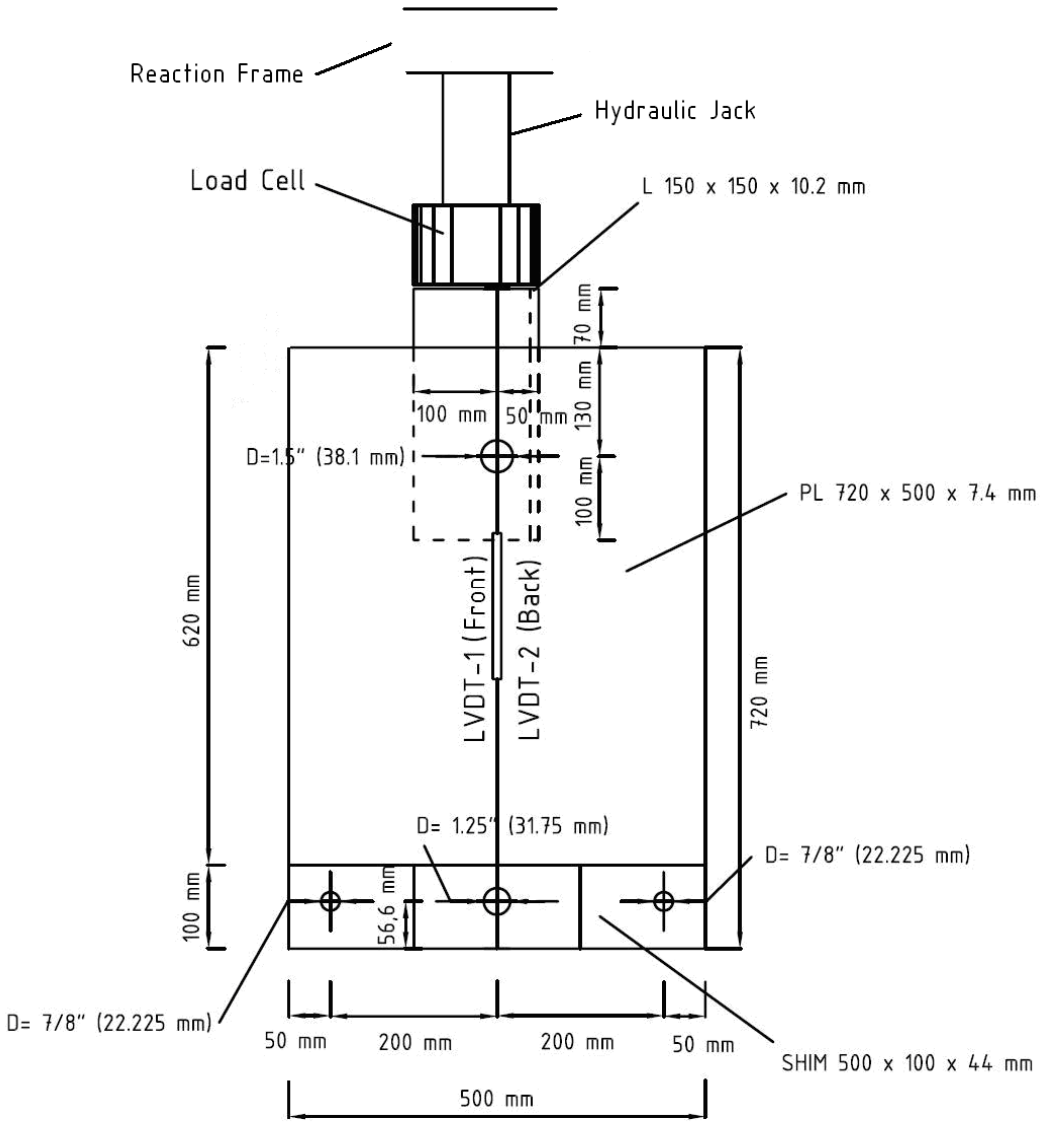


Figure 3. 11 - Typical Test Setup with Load Cell and LVDT for GP-06 to GP-12

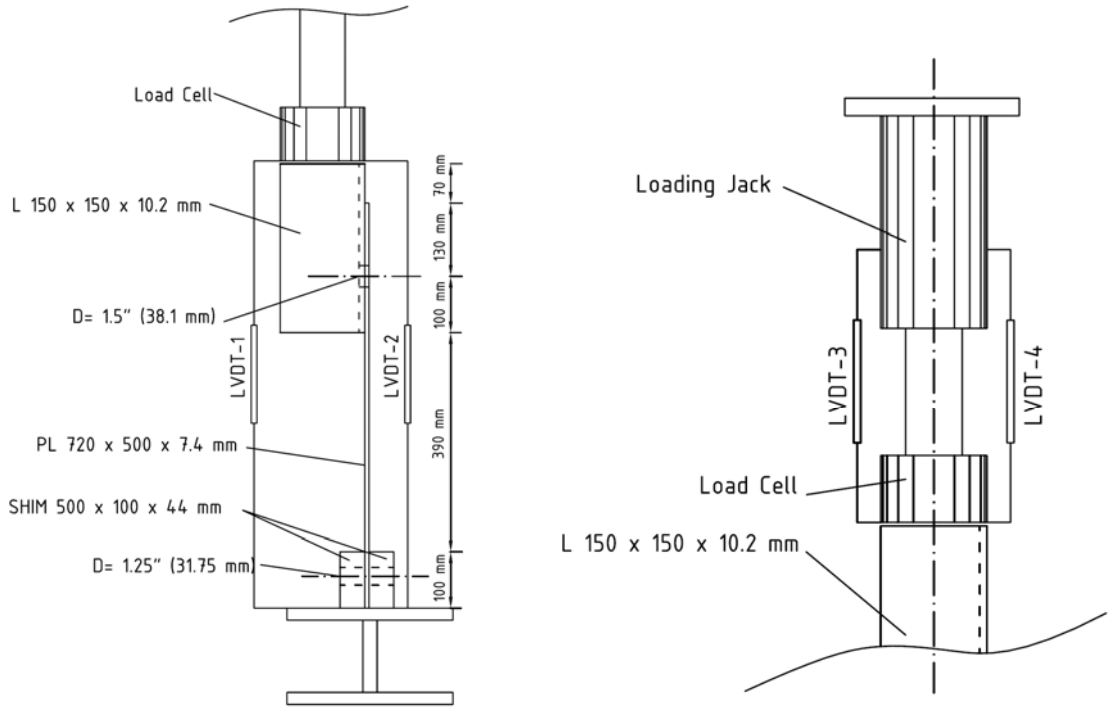


(a) Position of LVDTs attached to angle

(b) Position of LVDTs attached to jack

Figure 3. 12 - Typical position of LVDT in GP-06 to GP-12 (side view)

The test matrix as shown in Table 3.1 indicates details of the changes in experimental factors such as: plate size, plate thickness, far-end boundary condition, number of bolt and number of LVDT. The tests were conducted to obtain the strain data and load-deformation behaviour. First four tests (Specimen GP-01 to GP-04) were conducted by Mrs. Halima Dewanbabee and the remaining tests were conducted by the author in the Structural Engineering Lab of the University of Windsor. Due to the improper installation of strain gauges on plate surface, the results of strain gauge plot were unacceptable for specimen GP-03. The specimens GP-09 to GP-11 were used to compare the effect of two bolts versus one bolt connection.

Table 3. 1 – Test matrix with detailed data of tests

| Specimen No. | Length (mm) | Width (mm) | Thickness (mm) | No. of Bolt | Bolt Size & Grade | Boundary Condition | No of LVDT |
|---|---|---|---|---|---|---|---|
| GP-01* | 600 | 300 | 12.8 | 1 | 28.6 mm, SAE-G5 (ASTM -A325) | Hinged | 1 |
| GP-02* | 350 | 300 | 6.4 | 1 | 28.6 mm, SAE-G5 (ASTM -A325) | Hinged | 3 |
| GP-03* | 250 | 300 | 6.4 | 1 | 28.6 mm, SAE-G5 (ASTM -A325) | Fixed | 3 |
| GP-04* | 710 | 305 | 6.4 | 1 | 28.6 mm, SAE-G5 (ASTM -A325) | Fixed | 4 |
| GP-05 | 850 | 500 | 7.0 | 1 | 38.1 mm, SAE-G8 (ASTM-A354 Grade BD) | Hinged | 4 |
| GP-06 | 720 | 500 | 7.0 | 1 | 38.1 mm, SAE-G8 (ASTM-A354 Grade BD) | Hinged | 4 |
| GP-07 | 720 | 500 | 7.0 | 1 | 38.1 mm, SAE-G8 (ASTM-A354 Grade BD) | Fixed | 3 |
| GP-08 | 590 | 500 | 7.0 | 1 | 38.1 mm, SAE-G8 (ASTM-A354 Grade BD) | Hinged | 4 |
| GP-12 | 490 | 200 | 6.5 | 1 | 38.1 mm, SAE-G8 (ASTM-A354 Grade BD) | Hinged | 4 |

* These tests were completed by Mrs. Halima Dewanbabee from August to November 2007.

* Specimen GP-01 was repeated once.

Table 3.1 – Test matrix with detailed data of tests (continued)

| Plate No. | Length (mm) | Width (mm) | Thickness (mm) | No. of Bolt | Bolt Size & Grade | Boundary Condition | No of LVDT |
|---|---|---|---|---|---|---|---|
| GP-09 | 640 | 500 | 6.9 | 2 | 38.1 mm, SAE-G8 (ASTM-A354 Grade BD) | Hinged | 4 |
| GP-10 | 620 | 500 | 6.9 | 2 | 38.1 mm, SAE-G8 (ASTM-A354 Grade BD) | Hinged | 4 |
| GP-11 | 635 | 500 | 6.9 | 2 | 38.1 mm, SAE-G8 (ASTM-A354 Grade BD) | Hinged | 4 |

The typical test setup with load cell, strain gauges and LVDTs is shown in Figure 3.13. The load cell was connected to the angle with a 65 mm thick plate and four 8 mm (5/16 in) diameter bolts of Grade 6. The location of each LVDT was secured by using four brackets which is welded to the top plate in load cell and shim. These brackets helped the LVDT to obtain the deformation data of the specimen without effect of gusset plate out-of-plane buckling. The strain gauges were connected to data acquisition system and the variation of the strain was determined during the test. There were also two LVDTs (LVDT-3 and LVDT-4) which were located between the loading jack and load cell in order to determine the total deformation of specimen.

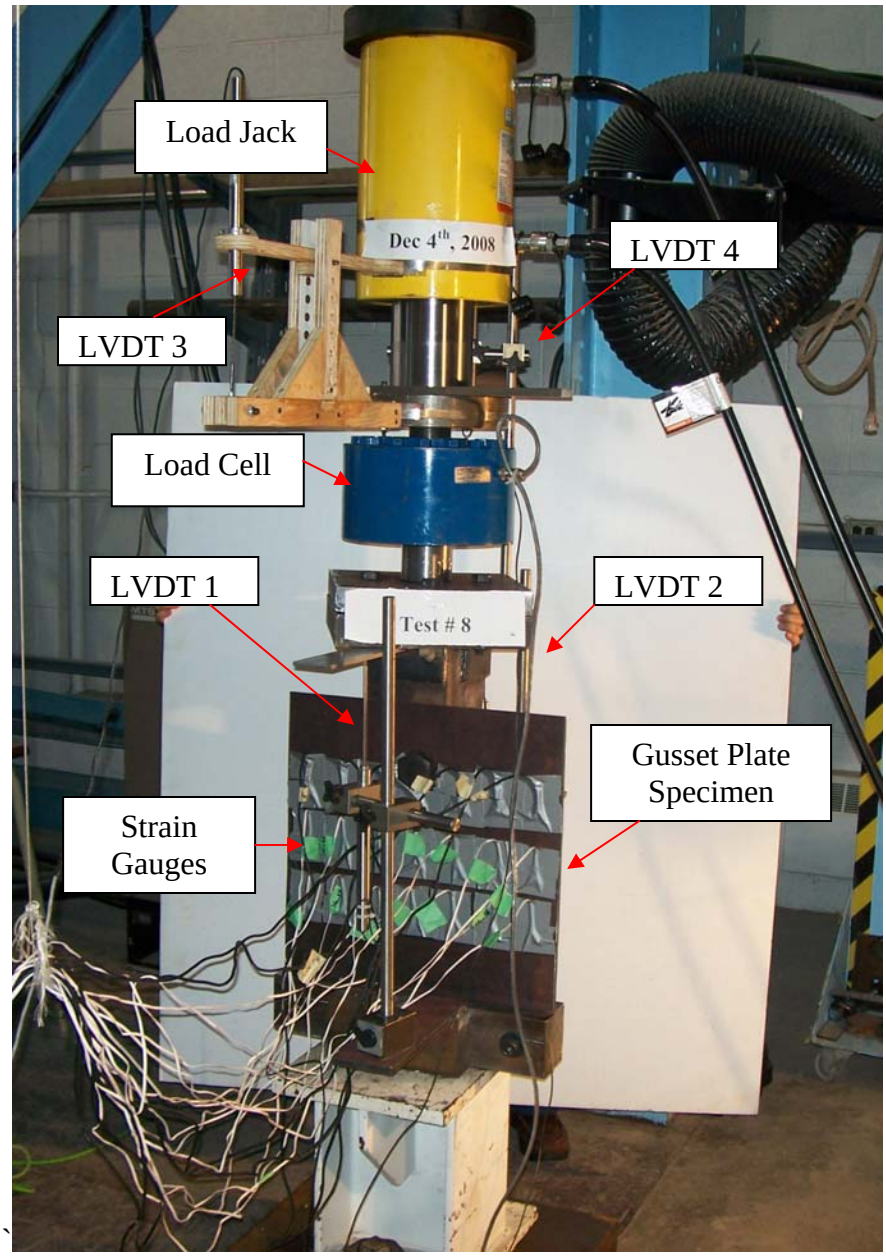


Figure 3. 13 - Typical Test Setup with Load Cell, Strain Gauge and LVDT (Specimen GP-06 to GP-12)

A 150 × 150 × 10.2 mm angle steel section was used as the brace member and bolted to the gusset plate in order to transfer the tension load for Specimens GP-02 to GP-12. For Specimen GP-01 smaller angle section (75 x 75 x 8.3 mm) was used. The lower end of gusset plate was then sandwiched between two shims of 44 mm thickness using 22.2 mm (7/8 in) bolts to simulate a pin condition for the far-end. The lower

end of gusset plate was welded to shim plates when a fixed far-end boundary condition was required. To prevent failure of the loading jack and deformation of frame, the loading jack was connected to the main load frame with 20 clamps as shown in Figure 3.14.


Figure 3. 14 – Loading jack connected to the load frame with 20 clamps.

### 3.3.1 Load Cell Calibration

The load cell calibration was completed before the test was performed. The load cell calibration was undertaken in another calibrated loading machine (TINIUS OLSEN) in compression and tension. Table 3.2 and Figure 3.15 show the tension load calibration table and graph for 900 kN load cell which used in the current study, respectively.

Table 3. 2 – Calibration sheet for 900 kN load cell

| Reading | Load (kN) | Load (kips) | Reading | Load (kN) | Load (kips) |
|---|---|---|---|---|---|
| 118 | 10 | 2.3 | 4223 | 230 | 51.8 |
| 280 | 20 | 4.5 | 4380 | 240 | 54.0 |
| 484 | 30 | 6.8 | 9438 | 510 | 114.8 |
| 675 | 40 | 9.0 | 9624 | 520 | 117.0 |
| 861 | 50 | 11.3 | 9811 | 530 | 119.3 |
| 1035 | 60 | 13.5 | 9997 | 540 | 121.5 |
| 1218 | 70 | 15.7 | 10184 | 550 | 123.8 |
| 1425 | 80 | 18.0 | 10371 | 560 | 126.0 |
| 1594 | 90 | 20.3 | 10557 | 570 | 128.3 |
| 1780 | 100 | 22.5 | 10744 | 580 | 130.5 |
| 1976 | 110 | 24.8 | 10930 | 590 | 132.8 |
| 2155 | 120 | 27.0 | 11117 | 600 | 135.0 |
| 2339 | 130 | 29.3 | 11303 | 610 | 137.3 |
| 2539 | 140 | 31.5 | 11490 | 620 | 139.5 |
| 2720 | 150 | 33.8 | 11677 | 630 | 141.8 |
| 2924 | 160 | 36.0 | 11863 | 640 | 144.0 |
| 3096 | 170 | 38.3 | 12050 | 650 | 146.3 |
| 3280 | 180 | 40.5 | 12236 | 660 | 148.5 |

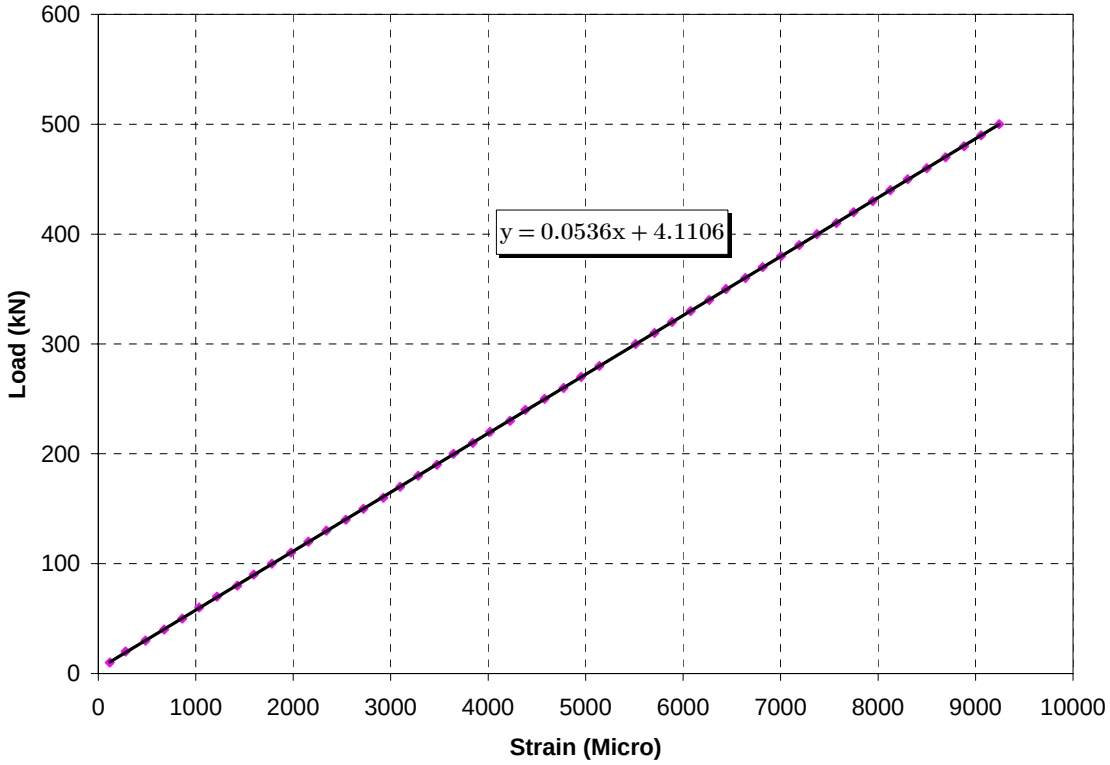


Figure 3. 15 – Calibration graph for 200 kip load cell in tension

### 3.3.2 Strain Gauge Installation

Strain gauge installation is one of the most important stages during the test. Before the strain gauge installation the desired area of the plate was ground for white metal finish and then cleaned and normalized with *"Isopropyl Alcohol"*, *"M-prep Conditioner A"* and *"M-prep Neutralizer 5A"*. Then the strain gauges were installed on the surface with glue which is special adhesive used for strain gauge on steel surface. The lead wires of strain gauge were connected to the long wires and sockets. These long wires were connected to data acquisition system for acquiring strain data. Figure 3.16 shows typical strain gauge layout in a plate specimen of 500 mm width and 720 mm length (Specimens GP-06 and GP-07). Table 3.3 indicate the details of strain gauges and LVDTs used in this study.

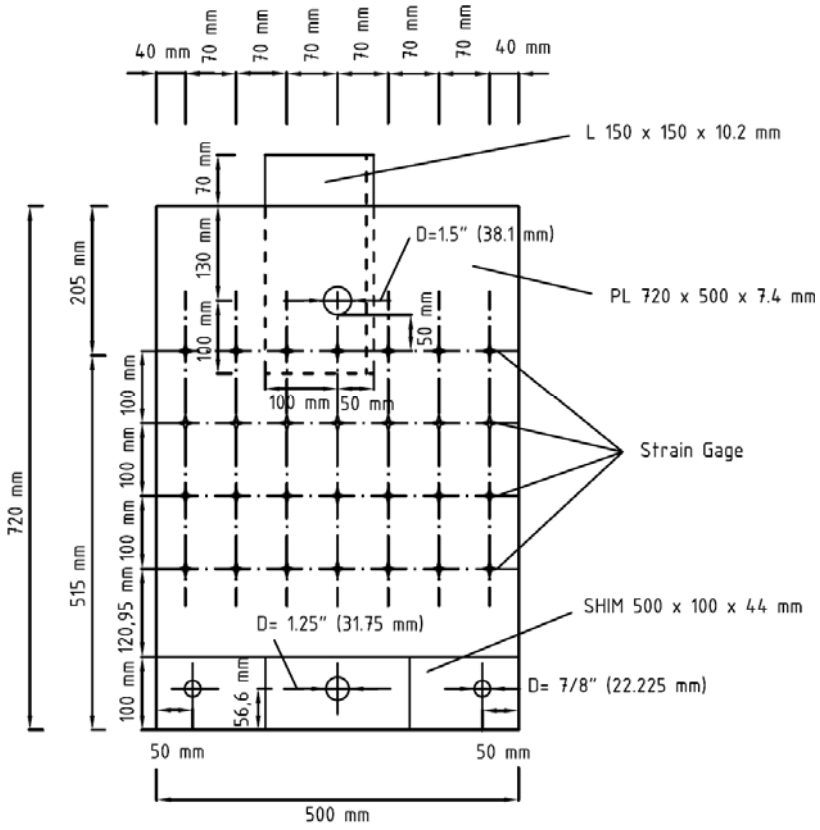


Figure 3. 16 - Strain Gauge Locations in Plate Test

Table 3. 3 – Details of LVDTs and strain gauges

| Test No. | Date | Plate Dimensions (mm) | No. of Strain Gauges | | No. of LVDT |
|---|---|---|---|---|---|
| | | | Rows | Columns | |
| 1* | Aug 2007 | 600 x 300 x 12.8 | 4 | 5 | (1) One at the back of plate |
| 2* | Sept 2007 | 350 x 300 x 6.4 | 3 | 5 | (3) One at left, One at right of front face and One at back face of plate |
| 3* | Oct 2007 | 250 x 300 x 6.4 | 3 | 5 | (3) One at left, One at right of front face and One at back face of plate |
| 4* | Nov 2007 | 610 x 310 x 6.4 | 3 | 5 | (4) One at left, One at right, One at middle of front face and One at back face of plate |
| 5 | Apr 2008 | 800 x 500 x 7.0 | 4 | 7 | (4) One at left, One at right, One at middle of front face of plate and One between jack and load cell |
| 6 | July 2008 | 720 x 500 x 7.0 | 4 | 7 | (4) One at front face, One at back face of plate, One at front and One at back of plate between jack and load cell |
| 7 | Nov 2008 | 720 x 500 x 7.0 | 4 | 7 | (3) One at front face, One at back face of plate and One at front of plate between jack and load cell |
| 8 | Dec 2008 | 590 x 500 x 7.0 | 3 | 7 | (4) One at front face, One at back face of plate, One at front and One in back of plate between jack and load cell |

* These tests were completed by Mrs. Halima Dewanbabee from August to November 2007.

Table 3.3 – Details of LVDTs and strain gauges (continued)

| Test No. | Date | Plate Dimensions (mm) | No. of Strain Gauge | | No. of LVDT |
|---|---|---|---|---|---|
| | | | Row | Column | |
| 9 | Dec 2008 | 640 x 500 x 6.9 | 4 | 7 | (4) One at front face, One at back face of plate, One at front and One in back of plate between jack and load cell |
| 10 | Dec 2008 | 620 x 500 x 6.9 | 4 | 7 | (4) One at front face, One at back face of plate, One at front and One in back of plate between jack and load cell |
| 11 | Feb 2009 | 635 x 500 x 6.9 | 2 | 7 | (4) One at front face, One at back face of plate, One at front and One in back of plate between jack and load cell |
| 12 | Feb 2009 | 490 x 200 x 6.5 | 2 | 5 | (4) One at front face, One at back face of plate, One at front and One in back of plate between jack and load cell |

### 3.3.3 Test Procedure

The test procedure was similar for all of the specimens. The following steps were used for test preparation and during the test:

Step 1: Grinding the plate surface in the location which the strain gauges were to be installed.

Step 2: Installing the strain gauge using glue and cover them with tape.

Step 3: Connecting lead wires of strain gauge to long wire and socket.

Step 4: Setting the plate in position.

Step 5: Fixing the far-end boundary condition such as fixed or hinged using bolts or welds.

Step 6: Attaching angle to load cell using plate and bolts.

Step 7: Connecting angle and plate with one or two bolts and nuts.

Step 8: Setting the LVDTs in place and check the core movement.

Step 9: Connecting strain gauge, load cell and LVDTs wires to data acquisition system in order to check the amount of voltage.

Step 10: Calibrate LVDTs in place using data acquisition system and standard cube.

Step 11: Applying tension load to angle through load cell.

The data acquisition was started to log the data from LVDTs, load cell and strain gauges in a computer file. The load was applied with large increments in the elastic range and after that the displacement increments were small in order to acquire the small variation of test parameters. The test was discontinued either when a failure in bolt or plate or angle section occurred or when failure occurred elsewhere in the test setup or when capacity of loading jack or load cell reached. The log number of the important stage of the test recorded in order to observe the special data from output results. A typical load-deformation plot obtained from specimen GP-06 is shown in Figure 3.17. The detailed discussion about all of the specimens is presented in Chapter 4.

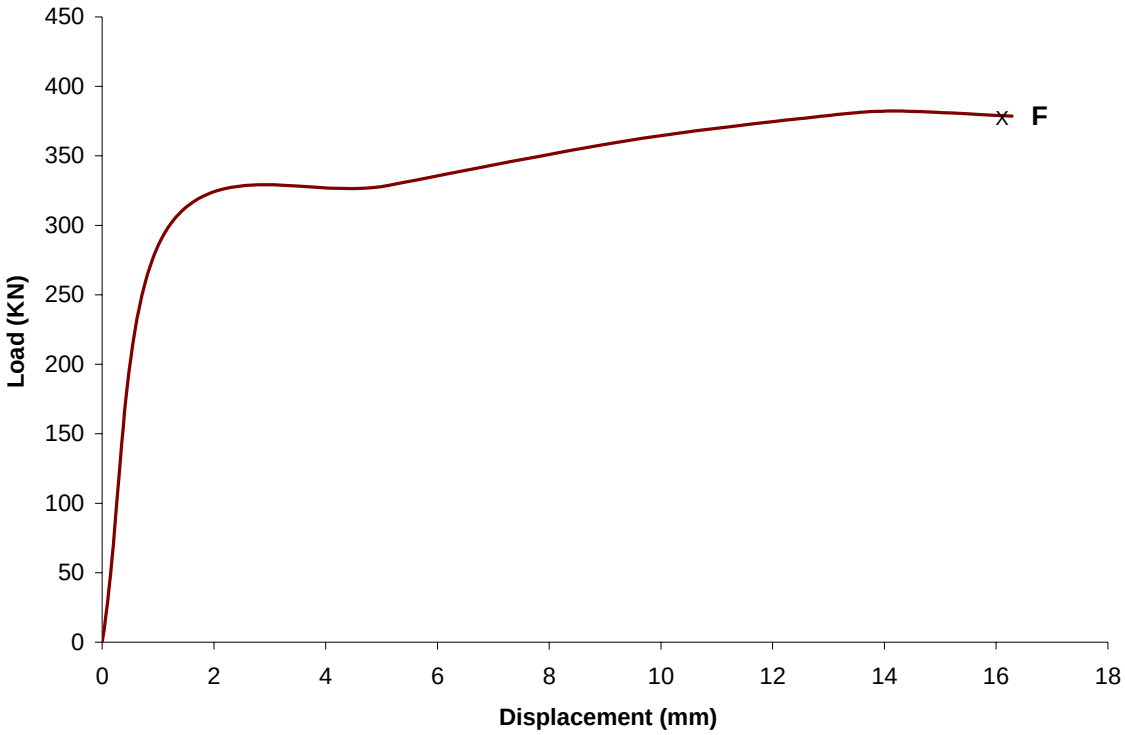


Figure 3. 17 – Typical load-deformation plot for specimen GP-06

## 3.4 Summary

The following items are presented as a summary of this chapter:

1. The tests with one and two bolts, different widths of plate, and different thickness of plate, far end as fixed and pinned condition were completed. The instruments for the experimental program such as hydraulically operated universal loading jack, universal flat load cell, strain gauges, data acquisition system and LVDT was used.

2. The hydraulic jack which was used in test had a side motor. The loading jack was connected to this motor or hydraulic pump in order to apply the tension load to load cell.

3. The capacity of load cells were 450 kN (100 kips) and 900 kN (200 kips) in compression and tension. These load cells were used in the test of specimens.

4. The surface of the plate was cleaned with alcohol, conditioner and neutralizer. Then, the strain gauges were attached to the plate surface using strain gauge adhesive.

5. The data accusation system (DATASCAN 7210) was used in order to record the variation of strain, displacement and load during the test of specimens.

6. Linear variable differential transformers (LVDT) were used for measuring linear displacement. The spring and free core type of LVDT was used for test of specimens.

7. The test setup of all specimens was similar and contains plate, angle, shim, load cell and bolts. These components were connected in order to transfer the applied load form angle to plate through one or two bolt connection.

8. The load cell calibration was undertaken in another calibrated loading machine (TINIUS OLSEN) in compression and tension and calibration data was prepared.

9. The test procedure is presented through several steps. The data acquisition was started to log the data of load cell and strain gauges in a file. The load was applied with large increments in the elastic range and after that the load increments were small in order to acquire the small variation of test parameters.

# 4. EXPERIMENTAL RESULTS

## 4.1 Introduction

In this chapter, the test results are presented. These results obtained from the strain gauges, load cell and LVDTs. The results are presented based on the different test condition shown in the "Test Matrix" (Table 4.1). The tests were conducted both in the elastic and inelastic ranges. This chapter focuses on the elastic and inelastic behaviour of a gusset plate with single or double bolts under tensile loading. In addition, the load versus deformation responses and the observed strain distributions of the specimens are presented.

## 4.2 Test Matrix

The test matrix, as presented in Table 4.1, shows details of the experimental parameters and instrument such as: plate width, plate length, plate thickness, far-end boundary condition, number of bolts, bolt size and grade, and number of LVDTs used. The information on bolt size and bolt grade is also presented in this table. The clear distance between the top bolt hole and top end of the plate was kept three times the diameter of the bolt hole or larger except for specimens GP-02, GP-03, GP-11 and GP-12 for which the distance was reduce to investigate the effect of this distance on failure mode. Actual distances are shown in the sketches for test specimens.

Table 4. 1 – Test matrix and failure modes

| Plate No. | Length (mm) | Width (mm) | Thick. (mm) | No. of Bolt | Bolt Size & Grade | Far-end Condition | No of LVDT | Test Results | Mode of Failure |
|---|---|---|---|---|---|---|---|---|---|
| GP-01* | 600 | 300 | 12.8 | 1 | 22 mm (7/8 in) SAE-G5 | Hinged | 1 | Good | Angle weld on top plate ruptured for first time and net section of angle occurred in repeat test |
| GP-02* | 350 | 300 | 6.4 | 1 | 28.6 mm (1 1/8 in) SAE-G5 | Hinged | 3 | Good | Bearing of the plate at the bottom |
| GP-03* | 350 | 300 | 6.4 | 1 | 28.6 mm (1 1/8 in) SAE-G5 | Fixed | 3 | Strain Gauges did not work | Load cell bolts failed in tension |
| **GP-04*** | **710** | **305** | **6.4** | **1** | **28.6 mm (1 1/8 in) SAE-G5** | **Fixed** | **4** | **Good** | **Shear failure of the bolt** |
| GP-05 | 850 | 500 | 7.0 | 1 | 38.1 mm (1.5 in) SAE-G8 | Hinged | 4 | Good | No Failure. Load cell capacity reached. |
| GP-06 | 720 | 500 | 7.0 | 1 | 38.1 mm (1.5 in) SAE-G8 | Hinged | 4 | Good | The top hole elongated and some tearing happened. |
| GP-07 | 720 | 500 | 7.0 | 1 | 38.1 mm (1.5 in) SAE-G8 | Fixed | 3 | Good | Failure at the bottom of the plate. Since weld ruptured at the far-end. |

Table 4.1 – Test matrix and failure modes (continued)

| Plate No. | Length (mm) | Width (mm) | Thick. (mm) | No. of Bolt | Bolt Size & Grade | Far-end Condition | No of LVDT | Test Results | Mode of Failure |
|---|---|---|---|---|---|---|---|---|---|
| **GP-08** | **590** | **500** | **7.0** | **1** | **38.1 mm (1.5 in) SAE-G8** | **Hinged** | **4** | **Good** | **Plate tearing occurred at top left side of the bolt hole.** |
| **GP-12** | **490** | **200** | **6.5** | **1** | **38.1 mm (1.5 in) SAE-G8** | **Hinged** | **4** | **Good** | **Plate tearing occurred at middle of the plate above top bolt hole.** |
| **GP-09** | **640** | **500** | **6.9** | **2** | **38.1 mm (1.5 in) SAE-G8** | **Hinged** | **4** | **Good** | **The top hole elongated and bearing failure happened.** |
| **GP-10** | **620** | **500** | **6.9** | **2** | **38.1 mm (1.5 in) SAE-G8** | **Hinged** | **4** | **Good** | **The top hole elongated and bearing failure happened.** |
| **GP-11** | **635** | **500** | **6.9** | **2** | **38.1 mm (1.5 in) SAE-G8** | **Hinged** | **4** | **Good** | **The top hole elongated and bearing failure happened.** |

Note: - SAE-G5 and SAE-G8 bolts are equivalent to ASTM-A325 and ASTM-A354 grade BD.

* These tests were completed by Mrs. Halima Dewanbabee from August to November 2007.

## 4.3 Tensile Test of Material (Coupon Test)

ASTM standard A370-08a (2008) procedure was used to determine the quasi-static mechanical properties of steel plate and steel angle. An INSTRON machine was used for the material test. A standard test specimen is gripped at both ends by suitable apparatus in a testing machine which slowly exerts an axial pull so that the steel is stretched until it ruptures. Results from the test were analyzed to provide the yield point, tensile strength, elongation and reduction of area of the sample metal. Metals including steel have a linear stress-strain relationship up to the yield point, as shown in the Figure 4.1.

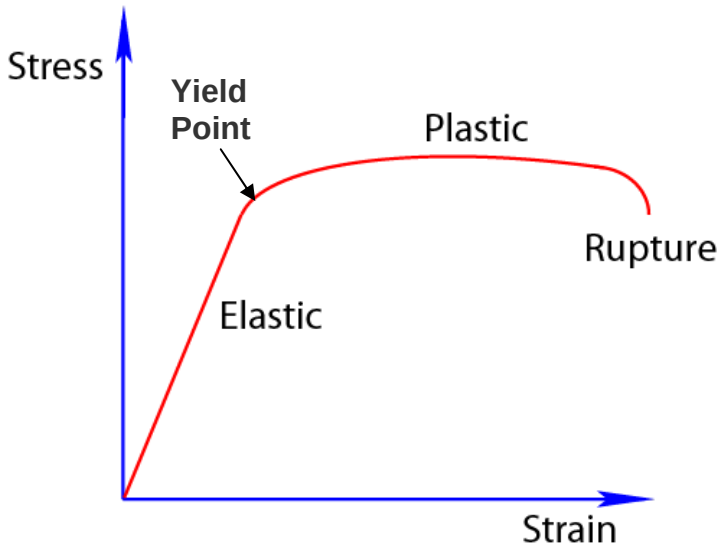


Figure 4. 1 - Typical stress vs. strain curve of structural steel

For most metals yield point is the elastic limit. The yield strength is defined as the "upper yield point" and the "lower yield point", or the 0.2% yield stress is defined for material with continuous yielding behaviour.

Below the elastic limit all deformation is recoverable, and the material will return to its initial shape when the load is removed. For stresses above the elastic limit the deformation is not recoverable, and the material will not return to its initial shape.

The yield strength is typically defined by the "0.2% offset strain" for metal which has no clear yield point. The yield strength at 0.2% offset is determined by finding the intersection of the stress-strain curve with a line parallel to the initial slope of the curve and which intercepts the abscissa at 0.2%. Figure 4.2 shows a stress versus strain curve of structural steel with 0.2% strain offset.

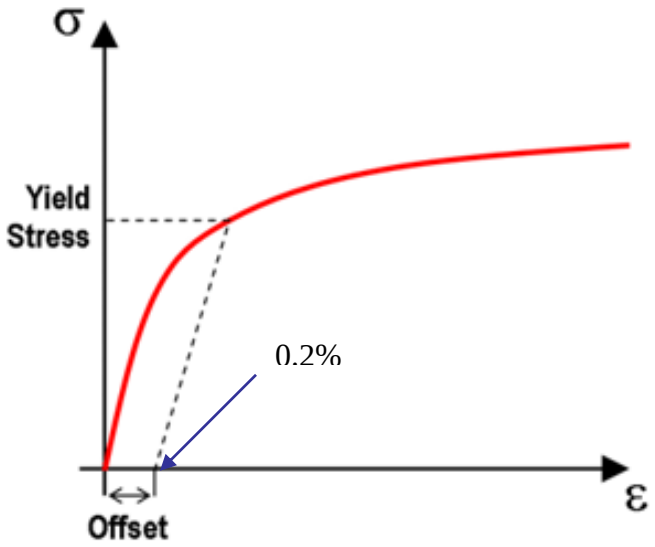


Figure 4. 2 - Stress vs. strain curve of structural steel with 0.2% strain offset

Three coupons were fabricated from each of the plate thickness utilized. All coupon tests were conducted in accordance with ASTM standard A370-08a (2008). A clip-on extensometer with 50.4 mm (2 in) gauge length was installed on one face of the specimen to obtain elongation. The specimens were loaded until the rupture or failure. The load and overall deformation curve was obtained for each specimen from the “INSTRON” loading machine output file. Figure 4.3 shows the typical coupon specimen before and after the test. Stress-strain curves of tension coupon specimens for various plates with different thickness are shown in Figure 4.4 to 4.7.


(a) Coupon specimen before test


(b) Coupon specimen after test

Figure 4. 3 - Typical tension coupon specimen (a) before and (b) after test

The values of the elastic modulus, the yield levels and the ultimate strength are listed in Table 4.2. These values were calculated using the data from the tensile tests on the test specimen coupons. The average material properties from all the tests were utilized in the analysis of the gusset plate test results.

Table 4. 2 – Material properties of plate coupon specimen with different thicknesses

| Coupon Specimen No. | Test Specimen No. | Plate Thickness (mm) | Modulus of Elasticity (GPa) | Yield Stress (MPa) | Ultimate Strength (MPa) |
|---|---|---|---|---|---|
| CT-001 | GP-02, GP-03, GP-04 | 6.4 | 217.8 | 389.9 | 516.4 |
| CT-002 | | 6.4 | 186.6 | 312.7 | 506.3 |
| CT-003 | | 6.4 | 210.8 | 374.0 | 519.0 |
| CT-01 | GP-05, GP-06, GP-07, GP-08 | 7.0 | 199.1 | 293.8 | 359.1 |
| CT-02 | | 7.0 | 200.6 | 411.2 | 525.2 |
| CT-03 | | 7.0 | 192.1 | 388.3 | 495.2 |
| CT-04 | GP-09, GP-10, GP-11 | 6.9 | 199.0 | 378.4 | 501.2 |
| CT-05 | | 6.9 | 207.7 | 369.1 | 503.2 |
| CT-09 | | 6.9 | 205.3 | 386.7 | 494.7 |
| CT-06 | GP-12 | 6.5 | 217.6 | 361.7 | 487.8 |
| CT-07 | | 6.5 | 212.5 | 362.3 | 490.5 |

Coupon test data for GP-01 was not good and therefore, it is not included in the thesis. It should be noted that the coupon tests for Specimen GP-12 was conducted with TINIUS-OLSUN machine in Deformable Bodies Lab where the extensometer is limited to 5 mm displacement and the gauge length is 50.4 mm (2 in) and therefore, no reading is available beyond stain of 0.1 and until the rupture strain. Therefore, the stress-strain curve between 0.1 and final strain in Figure 4.7 is interpolated based on experience from other coupon test data. The stress-strain curve of tension coupon test was also prepared based on the test data which was close to each other. Hence, the amount of data which had difference with two other tests was neglected in curves.

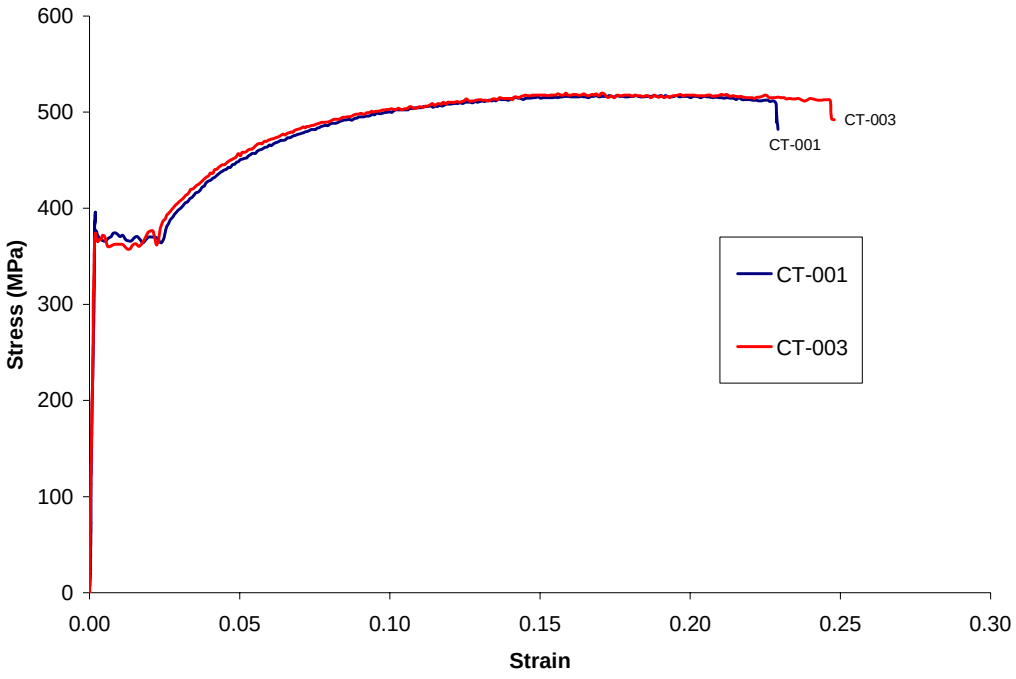


Figure 4. 4 - Typical stress vs. strain curve of tension coupon specimen for a plate with 6.4 mm thickness (Specimen GP-02, GP-03 and GP-04)

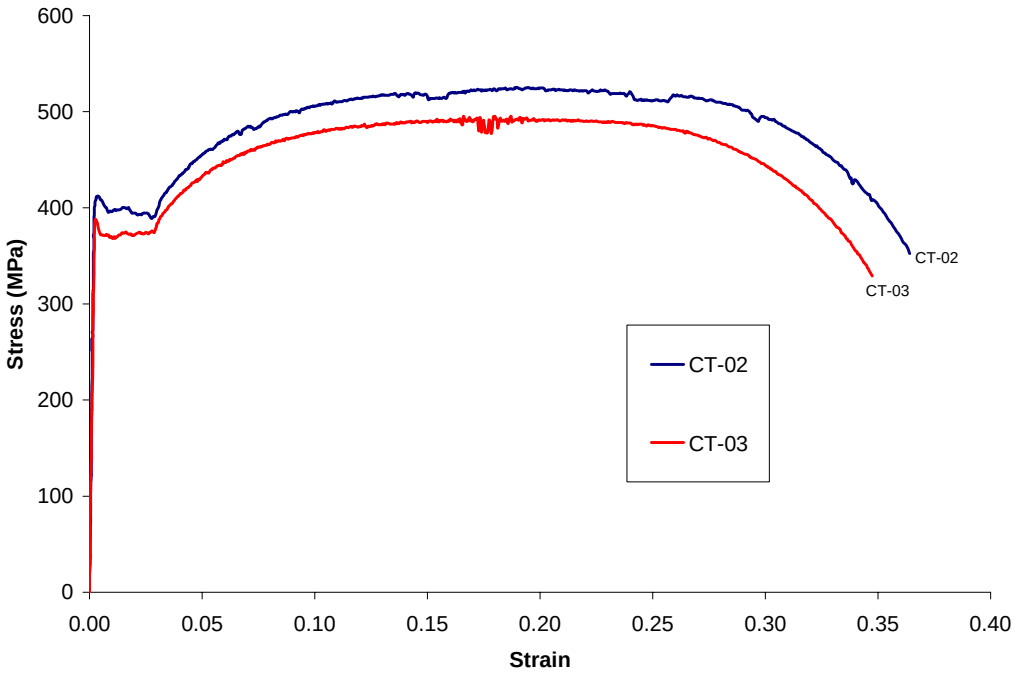


Figure 4. 5 - Typical stress vs. strain curve of tension coupon specimen for a plate with 7.0 mm thickness (Specimen GP-05, GP-06, GP-07, GP-08)

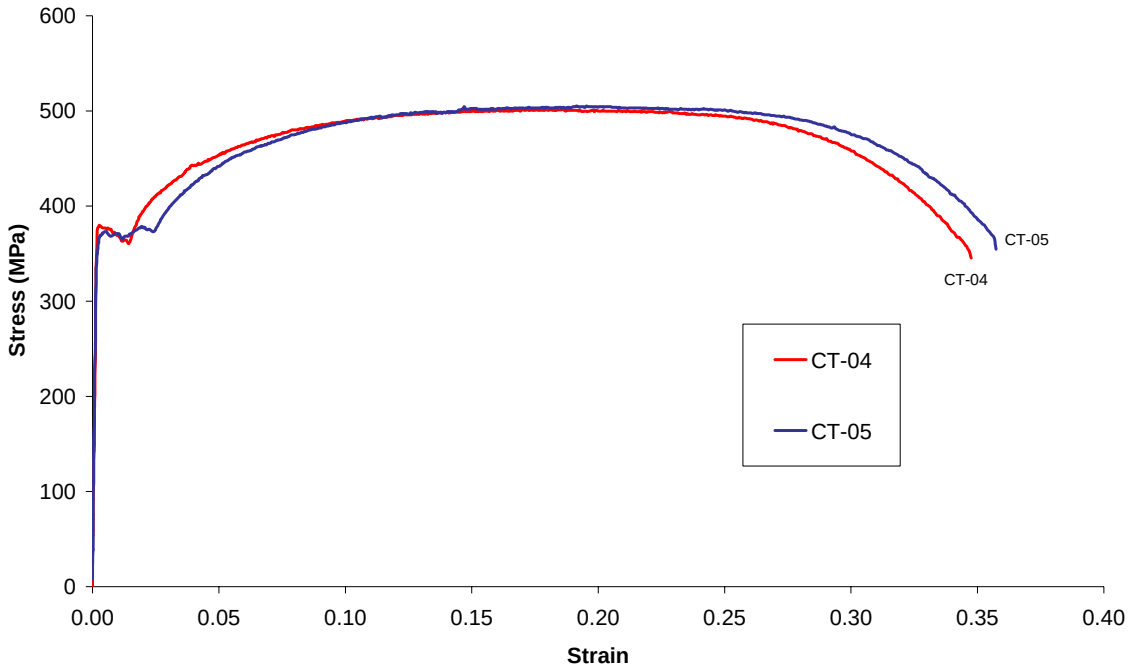


Figure 4. 6 - Typical stress vs. strain curve of tension coupon specimen for a plate with 6.9 mm thickness (Specimen GP-09, GP-10, GP-11)

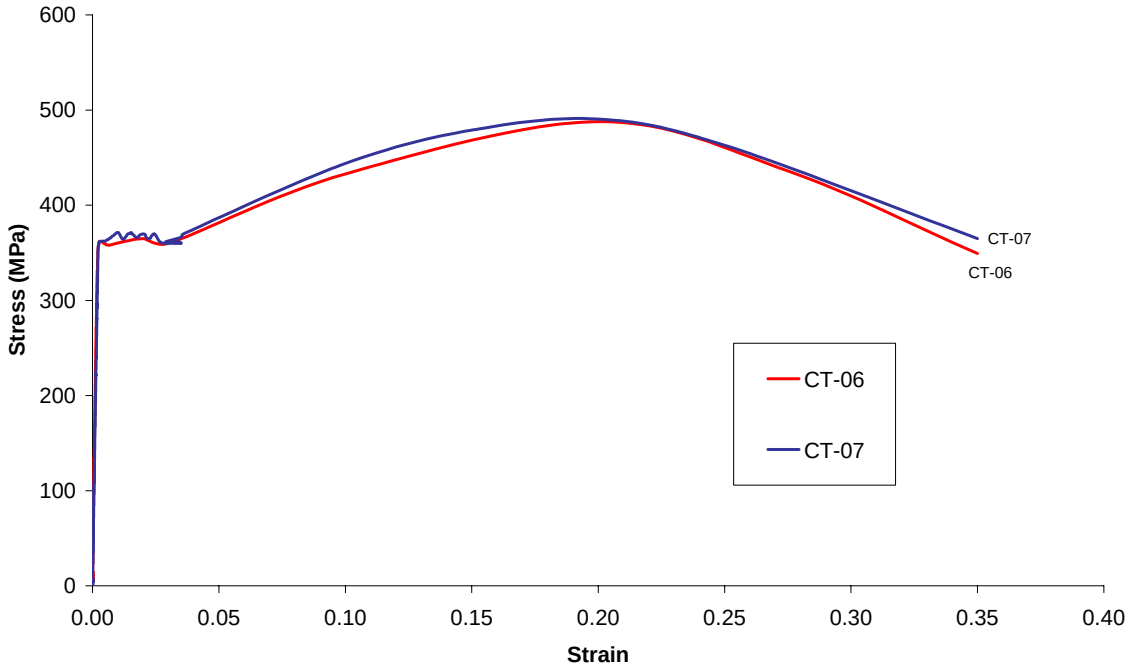


Figure 4. 7 - Typical stress vs. strain curve of tension coupon specimen for a plate with 6.5 mm thickness (Specimen GP-12)

## 4.4 Test Results

According to the test matrix which was discussed in the previous section, the yield load, ultimate tensile load and failure load achieved during testing are presented in Table 4.3. The ultimate load is defined as the maximum load level reached by a specimen throughout its loading history. The test results of each specimen are examined in Sections 4.4.1 through 4.4.10. The discussion of each specimen focuses on the physical response of the specimen during testing and then considers the load versus deformation response, the observed strain distribution within the specimen and the final deformed (failed) shape.

Multiple LVDTs were used for each specimen (except GP-01). However, only one LVDT was used for the global load-deformation plots. The way the LVDTs were mounted on or over the plate specimen measured the elongation occurring at the bottom hole as well. Therefore, this elongation was deducted from the total LVDT measurement for plotting the global load-deformation curves. The correction in LVDT deformations are shown ($\Delta_c$) in Table 4.3.

Table 4. 3 – Ultimate specimen capacity

| Specimen | Plate Size | Yield Load (kN) | Ultimate Load (kN) | Failure Load (kN) | Deformation Correction ($\Delta_c$) (mm) |
|---|---|---|---|---|---|
| GP-01* | 600 x 300 x 12.8 | 135.0 | 198.0 | 198.0 | 8.5 |
| GP-02* | 350 x 300 x 6.4 | 95.0 | 143.2 | 108.0 | 7.7 |
| GP-03* | 350 x 300 x 6.4 | 110.2 | 255.4 | 255.4 | 2.4 |
| GP-04* | 710 x 305 x 6.4 | 152.9 | 323.2 | 323.2 | 7.3 |
| GP-05 | 800 x 500 x 7.0 | 250.0 | 551.8 | 551.8 | --- |
| GP-06 | 720 x 500 x 7.0 | 296.7 | 378.5 | 378.5 | 11.3 |
| GP-07 | 720 x 500 x 7.0 | 250.0 | 349.5 | 264.0 | 13.3 |
| GP-08 | 590 x 500 x 7.0 | 316.6 | 422.6 | 422.6 | 27.2 |
| GP-09 | 640 x 500 x 6.9 | 278.0 | 549.3 | 549.3 | 7.9 |
| GP-10 | 620 x 500 x 6.9 | 270.0 | 612.4 | 612.4 | 9.3 |
| GP-11 | 635 x 500 x 6.9 | 291.5 | 566.0 | 566.0 | 9.3 |
| GP-12 | 490 x 200 x 6.5 | 230.3 | 304.7 | 257.8 | 7.9 |

* These tests were conducted by Mrs. Halima Dewanbabee for August to November 2007.

## 4.5 Specimen GP-01

Specimen GP-01 is a 12.8 mm thick gusset plate with 600 mm in length and 300 mm width. One 22 mm (0.85 in) diameter SAE-Grade 5 (ASTM-A325) high strength bolt with 62 mm length was used to connect the angle to the gusset plate. A 75 x 75 x 8.3 mm angle section was used in this test. The location of first row (row 4) of strain gauges was 60 mm below the center of hole. There were three other rows 100 mm each apart. Figure 4.8 shows the location of strain gauges and LVDT which were used for this specimen. One 100 mm (4 in) spring loaded LVDT was used on the back side (the face where angle was mounted on) of plate.

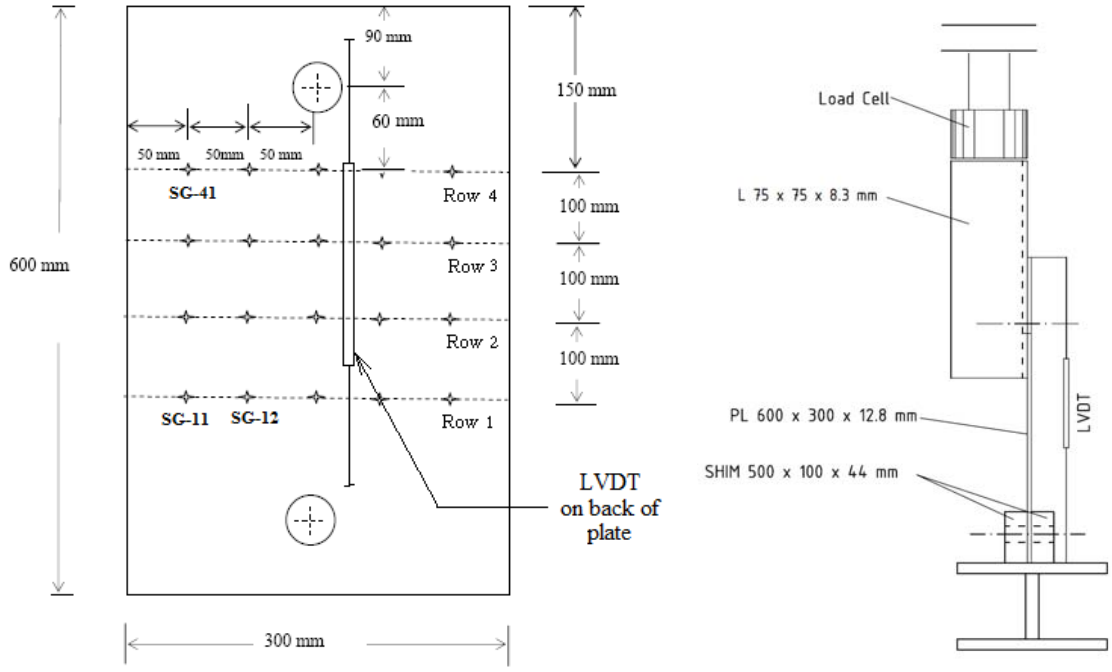


(a) Strain gauge location (b) LVDT(s) location

Figure 4. 8 – Locations of strain gauges and LVDT in Specimen GP-01

The test was repeated. At the first time, the failure (rupture) of the weld between angle and top loading plate occurred. The second test was done with the same angle and the angle experienced tension failure near the bolt connection. The plate remained in the elastic range until a load of 135 kN, after which plastic deformation began to occur. The elongation of the hole indicated that plastic deformation continued until ultimate rupture and tearing occurred. Due to the tension failure of angle in bolt-angle connection, the test was discontinued at load 198 kN (point F in Figure 4.9) but the tearing did not occur either in the plate or in the angle. Figure 4.10(c) shows the failure of this specimen. Figure 4.9 shows the load versus axial displacement response of first specimen GP-01. The displacement was recorded by the LVDT attached to the plate surface (see Figure 4.7).

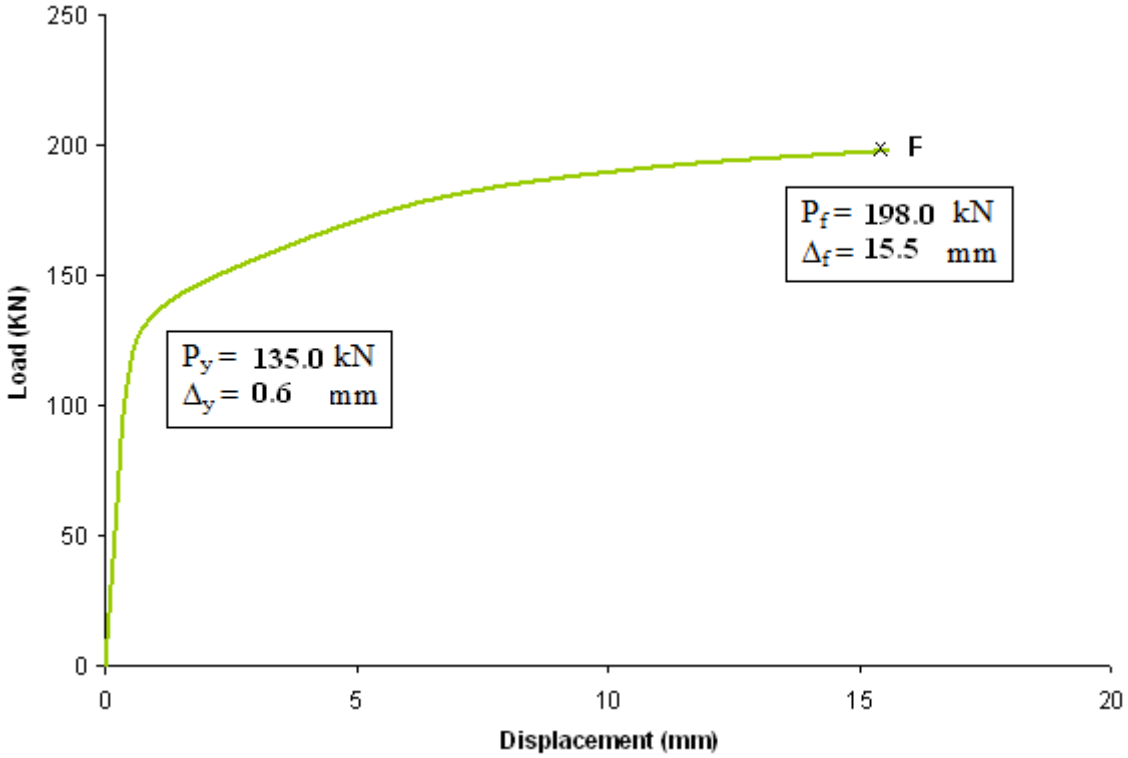


Figure 4. 9 – Load vs. axial displacement response of Specimen GP-01 (first test)

As it is shown in Figure 4.9, the specimen response under tension is reasonably stable. The load carrying capacity of the specimen increased as the deformation level

increased. The out-of-plane plate buckling of specimen was accompanied by the increase in axial deformation and drop in load carrying capacity.

After completion of the test, the failed gusset plate specimen was examined. The bolt hole in the connection elongated plastically due to the bearing of the bolts under loading. The test was discontinued when the rupture of weld between the top loading plate and the angle member and tension failure of angle occurred for first test and repeated test, respectively (Figure 4.10(b), Figure 4.10(c)).

(a) Test setup

(b) Rupture of weld in first test

(c) Tension failure of angle in repeat test

Figure 4. 10 – Rupture of weld between angle and top loading plate – Specimen GP-01

The angle member was assumed to deform elastically. A compatibility of specimen deformation was preserved at the top of the gusset plate. The displacement at the top

of the angle was assumed to be approximately equal to the in-plane displacement at the top of the gusset plate free edges.

During the loading of the specimen, strain gauges reading were recorded through data acquisition system. As soon as local yielding occurred in the plate and the stresses began to redistribute, the strain readings localized. Figures 4.11 to 4.14 show the strain distributions from 50 kN to 200 kN.

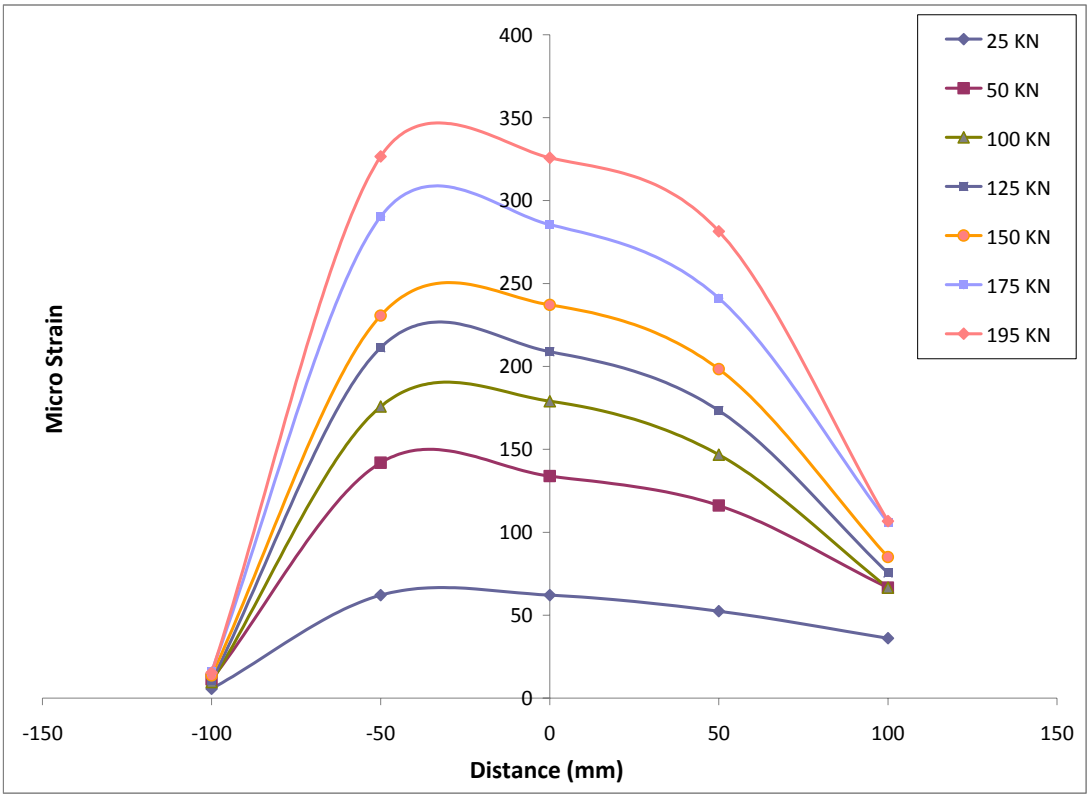


Figure 4. 11 – Strain values for (top) row 4 of specimen GP-01 at different loads

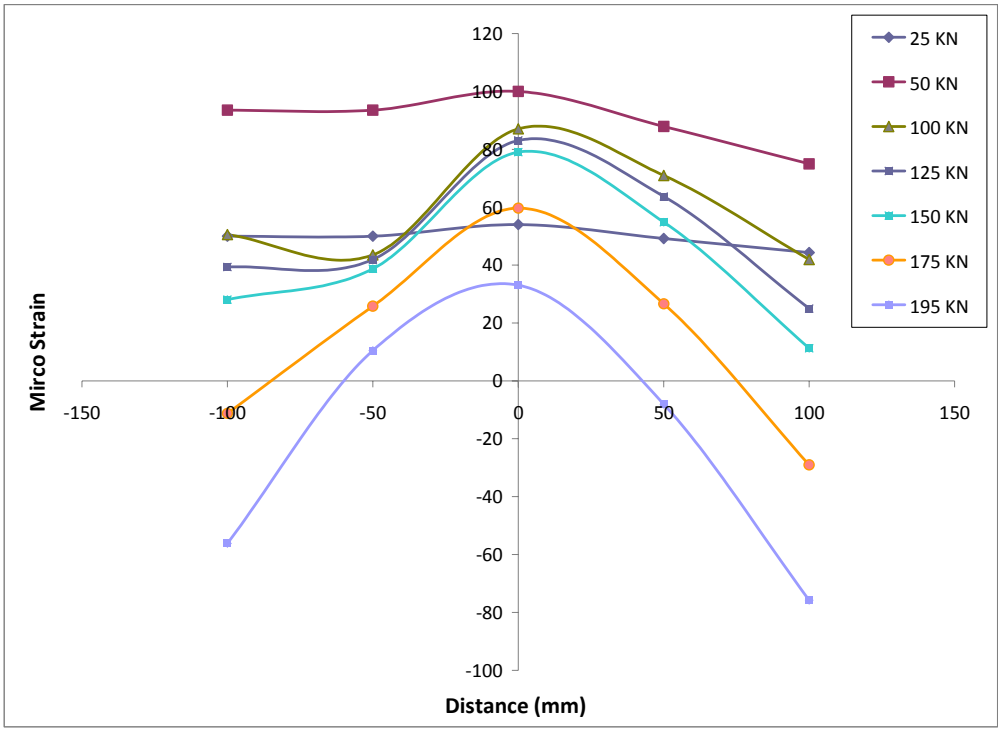


Figure 4. 12 – Strain values for (third) row 3 of specimen GP-01 at different loads

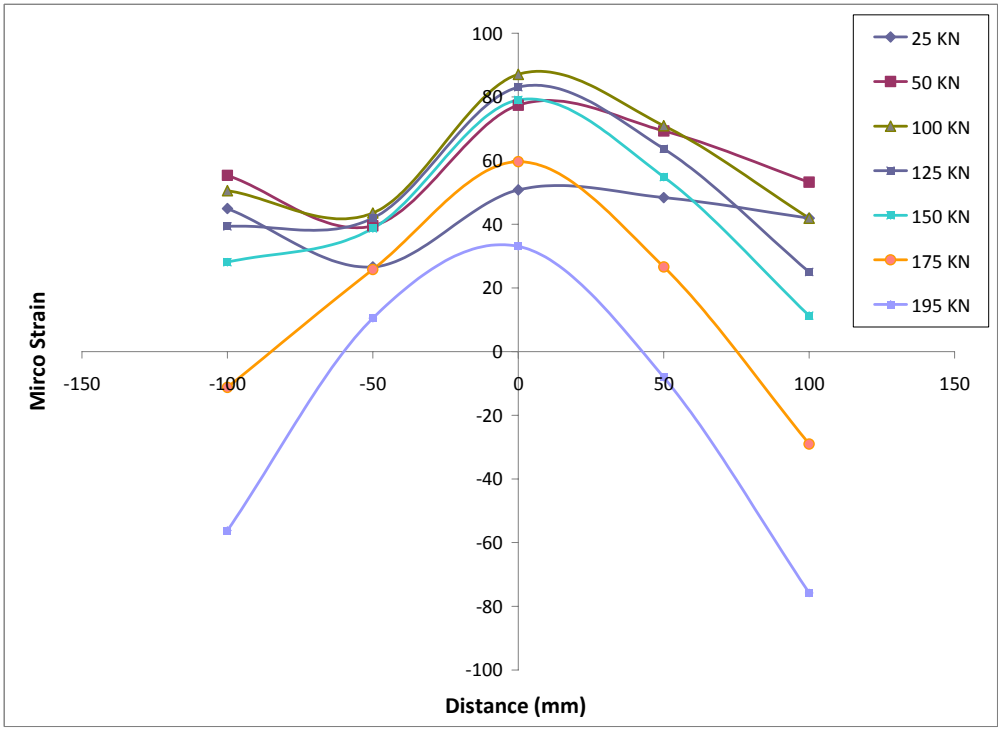


Figure 4. 13 – Strain values for (second) row 2 of specimen GP-01 at different loads

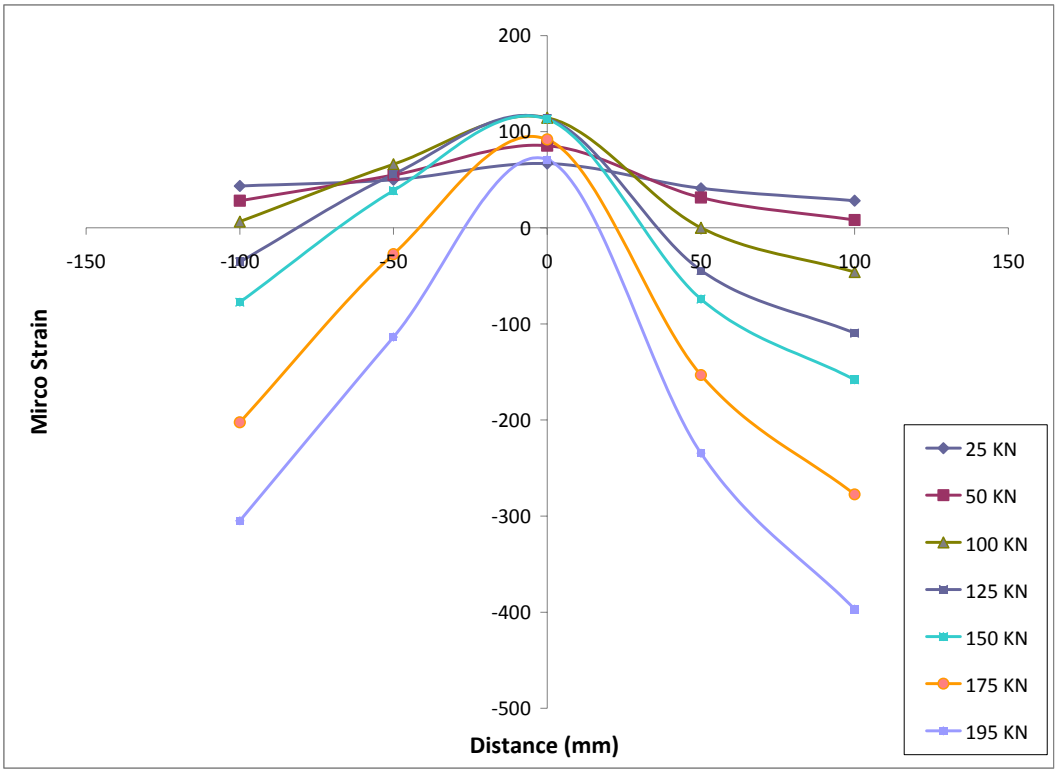


Figure 4. 14 – Strain values for (bottom) row 1 of specimen GP-01 at different loads

From Figures 4.11 through 4.14, it is observed that strain never exceeded yield strain value (at least 1600 micro strain). However, this is not to say that strain near the hole did not reach yield value. When the specimen load is increased beyond 135 kN level, strain level are changed. When the strain reading at the 195 kN load are analyzed, the strain level are generally slightly more than one and half times those recorded at the 135 KN level. Figures 4.15 to 4.18 show the strain gauge variation in the different rows of strain gauges on the plate surface. The strain values are in micro strain.

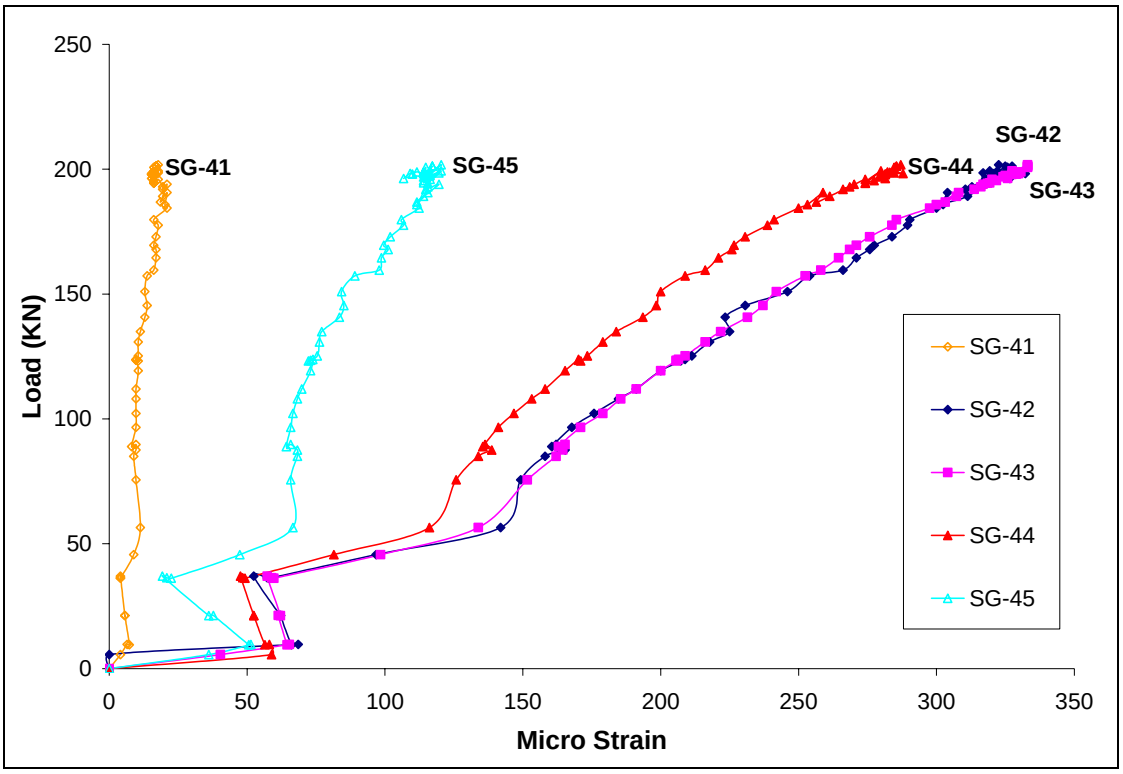


Figure 4. 15– Strain vs. load for (top) row 4 of specimen GP-01

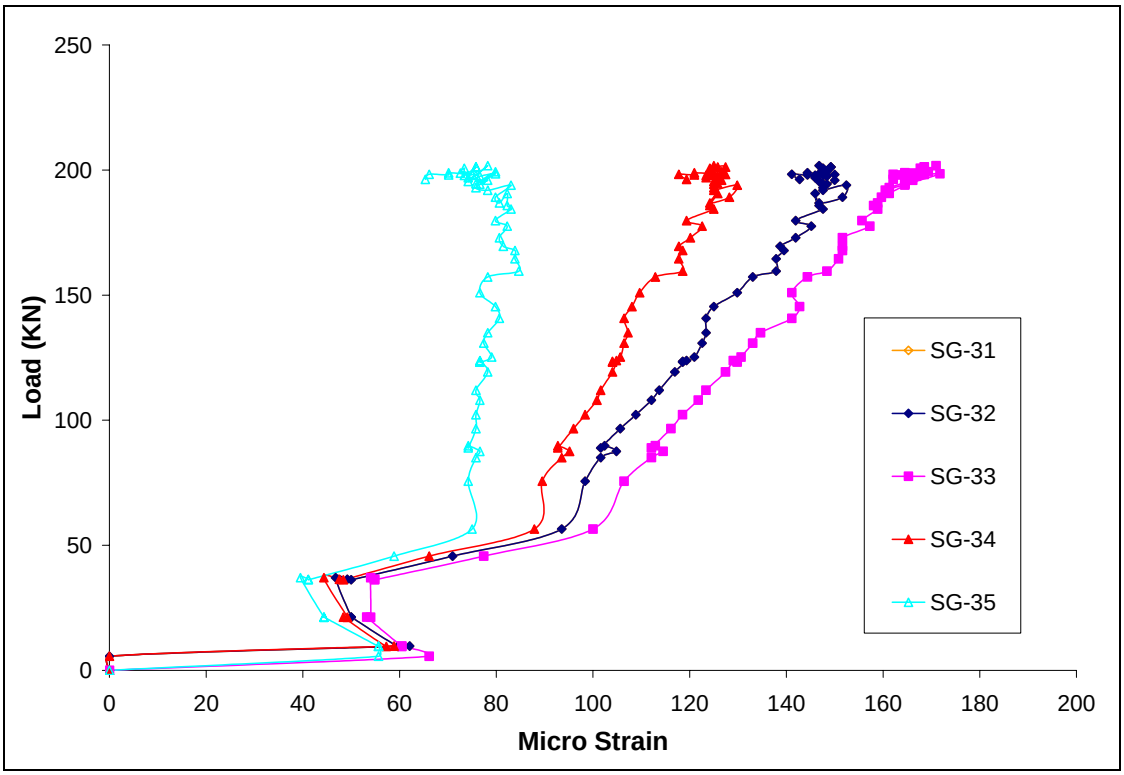


Figure 4. 16 – Strain vs. load for (third) row 3 of specimen GP-01

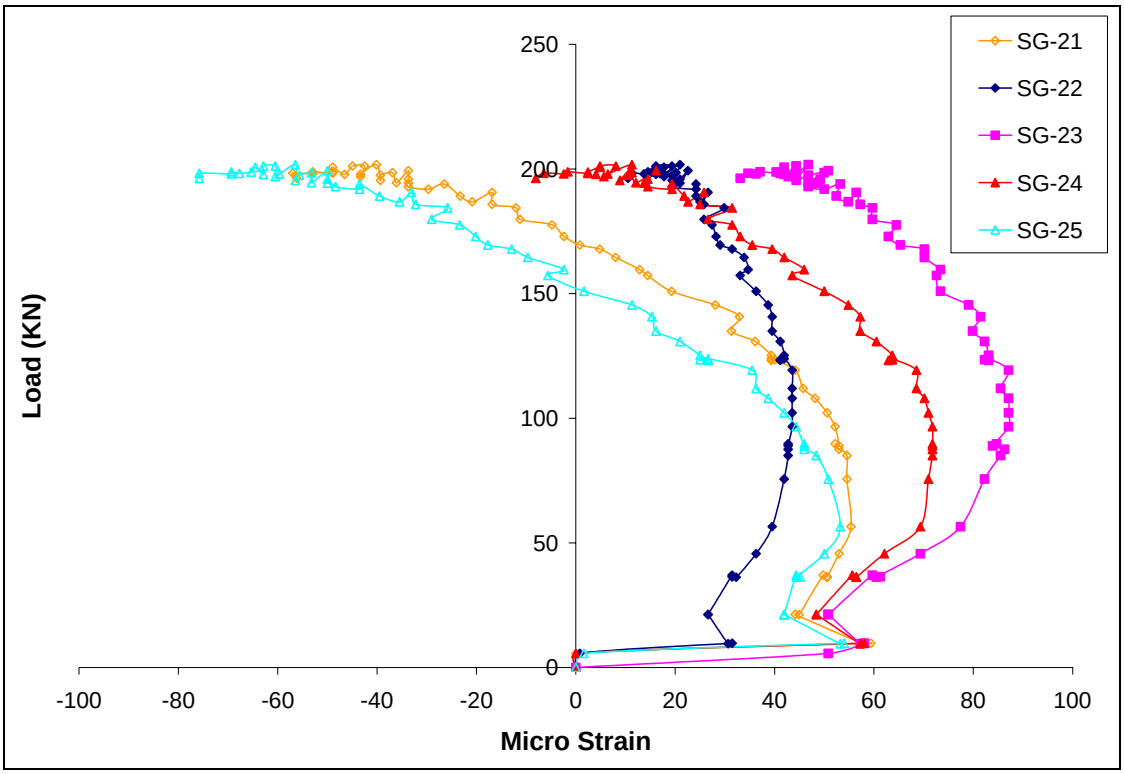


Figure 4. 17 – Strain vs. load for (second) row 2 of specimen GP-01

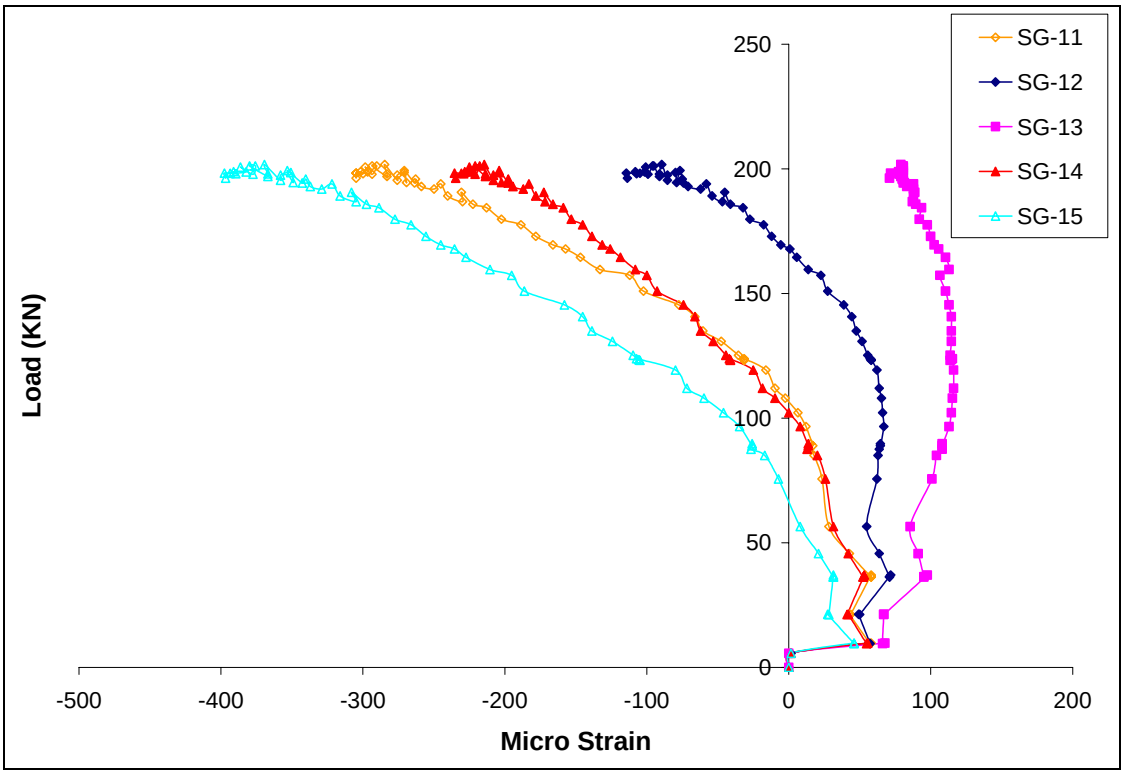


Figure 4. 18 – Strain vs. load for (bottom) row 1 of specimen GP-01

## 4.6 Specimen GP-02

Specimen GP-02 is the second gusset plate of 6.4 mm thickness with 350 mm in length and 300 mm wide. One 28.6 mm ($1\frac{1}{8}$ in) diameter SAE-Grade 5 (ASTM-A325) high strength bolt was used to connect the angle to the gusset plate. The diameter of top hole was 31 mm. It should be noted that in GP-01, bolt size and grade were 22 mm ($\frac{7}{8}$ in) and SAE Grade 5 (ASTM-A325). A 150 x 150 x 10.2 mm angle section was used in this test because tension failure occurred in repeat test, GP-01 which was built using smaller angle section (75 x 75 x 8.3 mm). The diameter of bolt was increased to ensure no shear failure occurred in the bolt. The location of first row of strain gauges was 60 mm below the hole (75 mm from center line of hole). The other two rows were installed at 40 mm centers. Figure 4.19 shows the location of strain gauge and LVDTs which were used for this specimen. There were two LVDTs (LVDT-1 and LVDT-2) located on the left and right side of the plate surface. One (the third) 100 mm (4 in) spring loaded LVDT (LVDT-3) was also used at the other side of plate on the angle.

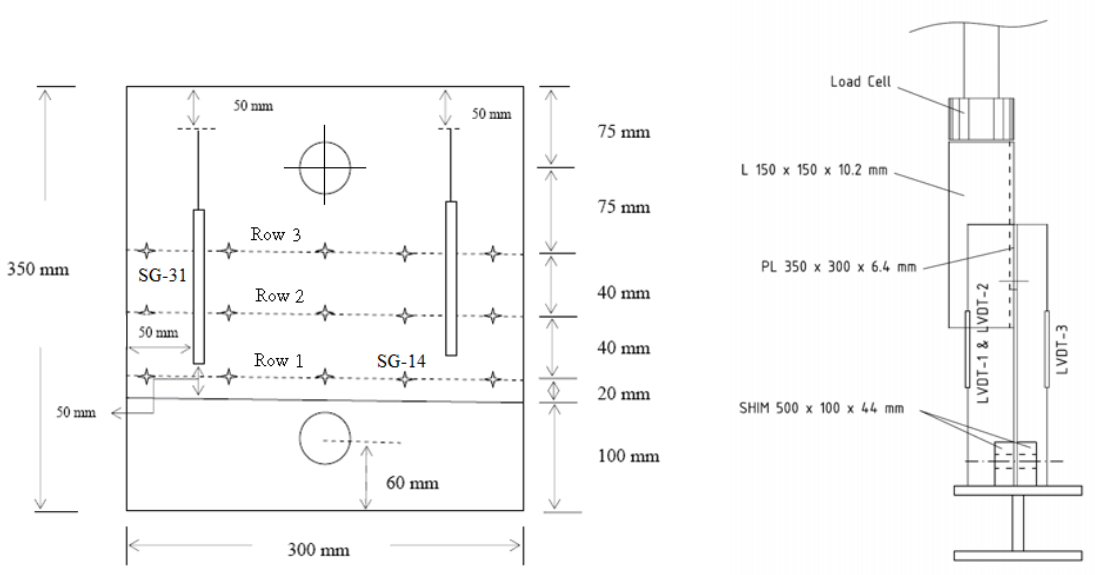


(a) Strain gauge locations (b) LVDT locations

Figure 4. 19 – Locations of strain gauges and LVDTs in Specimen GP-02

The plate remained in the elastic range until a load of 95 kN, after which plastic deformation began to occur. The elongation of the hole indicated that plastic deformation continued until ultimate rupture and tearing occurred. The maximum load capacity of the specimen was 143.2 kN. Due to the bearing (rupture) failure of plate at the bottom hole, the test was discontinued at load 108 kN (Point F in Figure 4.20). Figure 4.20 shows the load versus axial displacement response of specimen GP-02. The displacement was recorded by the LVDT (LVDT-3 in Figure 4.19) attached to the back face of the plate specimen between angle and bottom of the plate. The deformation of the gusset plate, the angle and the slip in angle to gusset plate connection was recorded as total displacement.

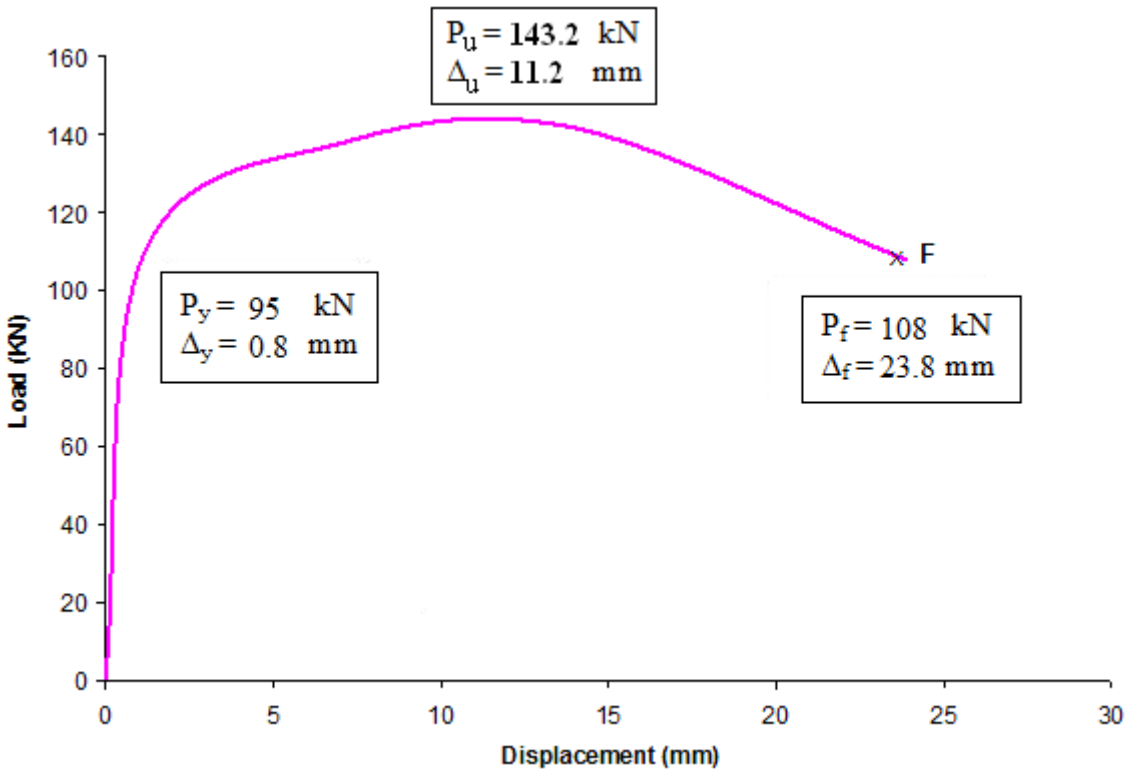


Figure 4. 20 – Load vs. axial displacement response of Specimen GP-02 (LVDT-3 output)

As it is shown in Figure 4.21, the specimen response under tension is reasonably stable. The load carrying capacity of the specimen increased as the deformation level

increased. The out-of-plane plate bending of specimen was accompanied by the increase in axial deformation and drop in load carrying capacity.

After completion of the test, the gusset plate was examined. It was observed that the specimen failed in tension due to a bearing failure of the plate material at the bottom (Figure 4.21(c)). The failed plate in bolt connection at top hole is shown in Figure 4.21(b). The top bolt hole in the connection elongated plastically due to the bearing of the bolts under loading. The test was discontinued because of plate tearing occurred at the bottom hole (Figure 4.21(c)).


(a) Test setup

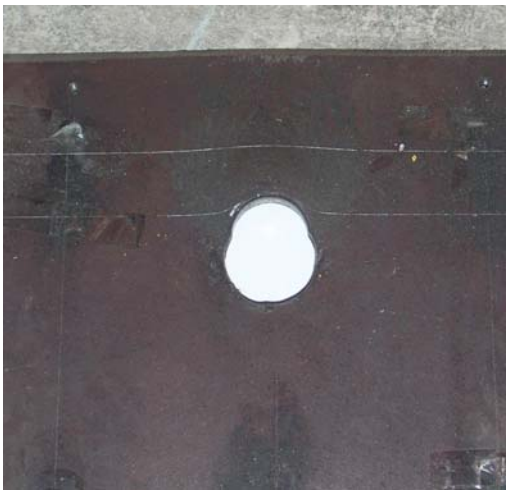

(b) Top hole elongation

(c) Bottom hole tearing


(d) LVDTs location on plate

Figure 4. 21 – Plate bearing failure at the bottom in bolted connection – Specimen GP-02

The angle member was assumed to deform elastically. A compatibility of specimen deformation was preserved at the top of the gusset plate. The displacement of the top of the angle was assumed to be approximately equal to the in-plane displacement at the top of the gusset plate free edges. Since the angle is relatively rigid compared to the gusset plate, this assumption appears to be valid.

During the loading of the specimen, strain gauge reading was recorded through data acquisition system. As soon as local yielding occurred in the plate and the stresses began to redistribute, the strains localized. Figures 4.22 to 4.24 show the strain distributions from 25 kN to 145N.

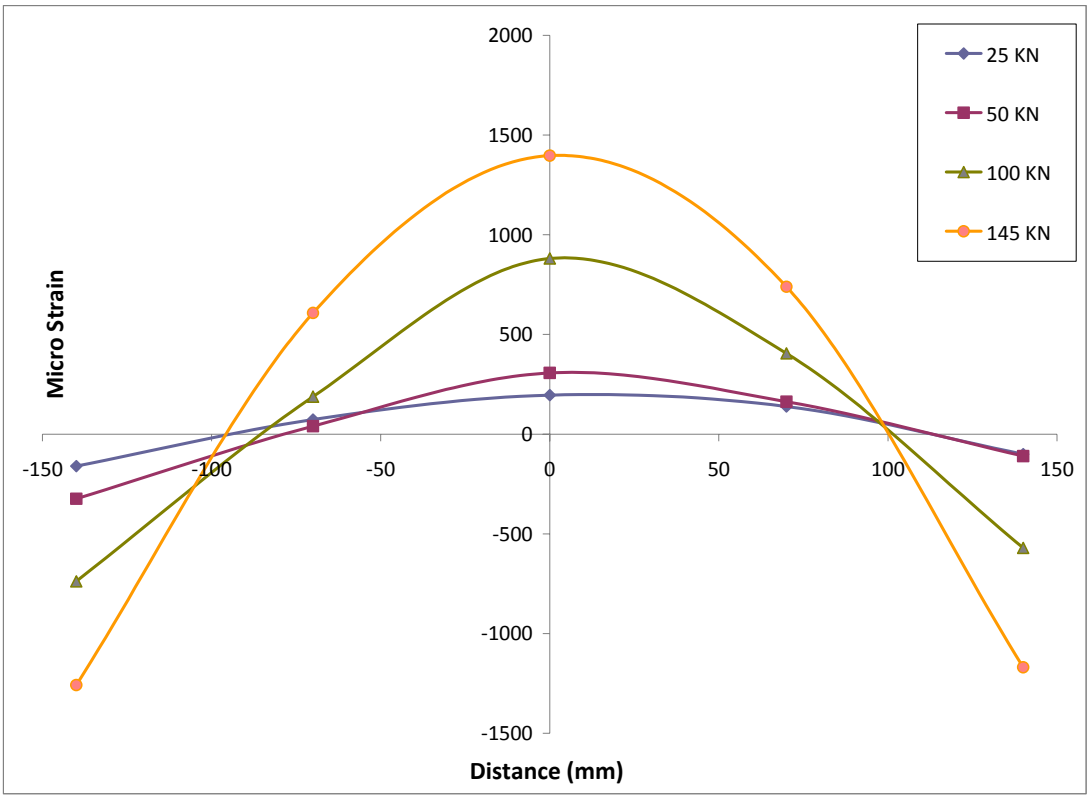


Figure 4. 22 – Strain values for (top) row 3 of specimen GP-02 at different loads

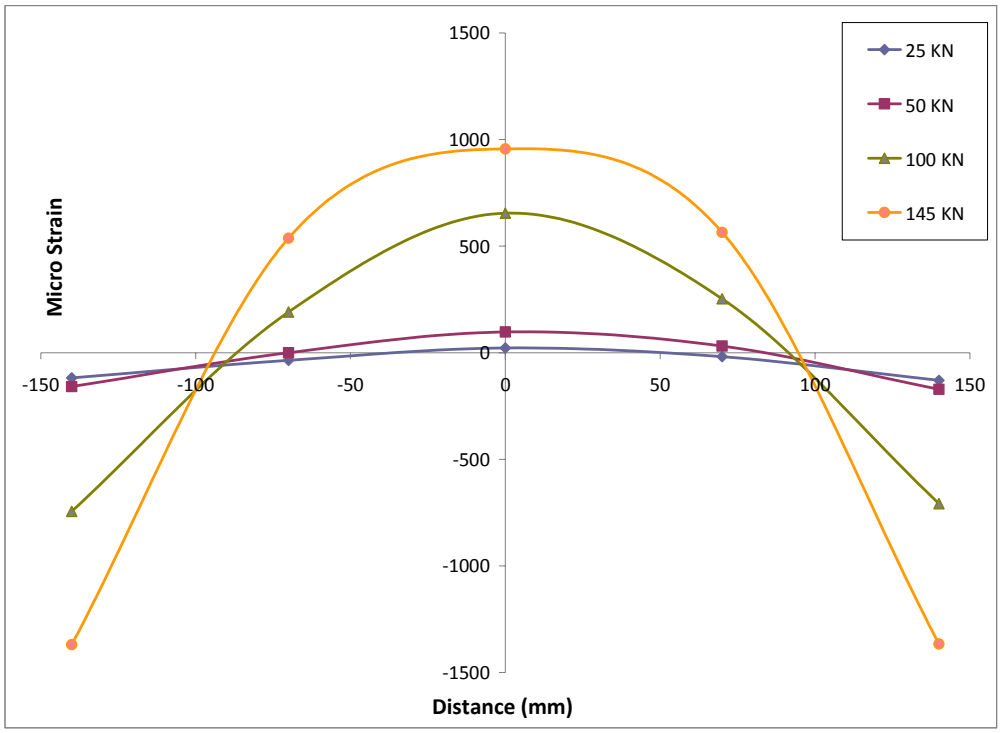


Figure 4. 23 – Strain values for (middle) row 2 of specimen GP-02 at different loads

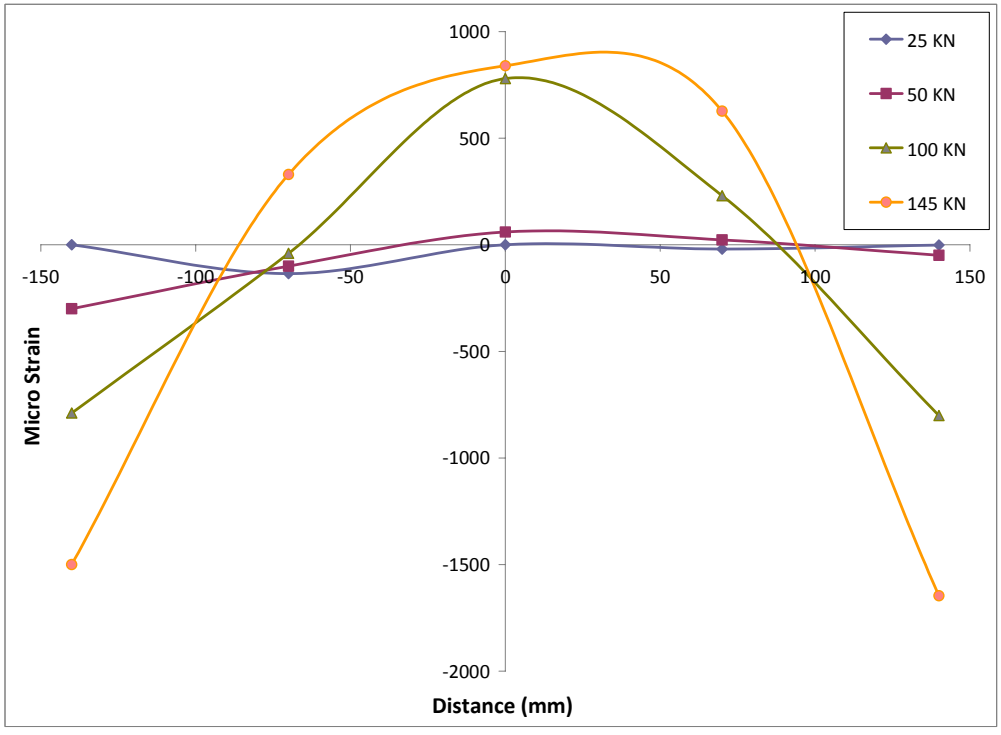


Figure 4. 24 – Strain values for (bottom) row 1 of specimen GP-02 at different loads

When the specimen load is increased beyond 95 kN level, strain levels were changed. When the strain readings at the 150 kN load are analyzed, the strain level are generally slightly more than three times those recorded at the 95 kN level. Figures 4.25 to 4.27 show the strain gauge variation in the different rows of strain gauges on the plate surface. The strain values are shown in microstrain. Again, for this specimen as well, the maximum strain recorded was about 1400 micro strain which is lower than yield strain. This does not mean that no yielding occurred at near the bolt hole.

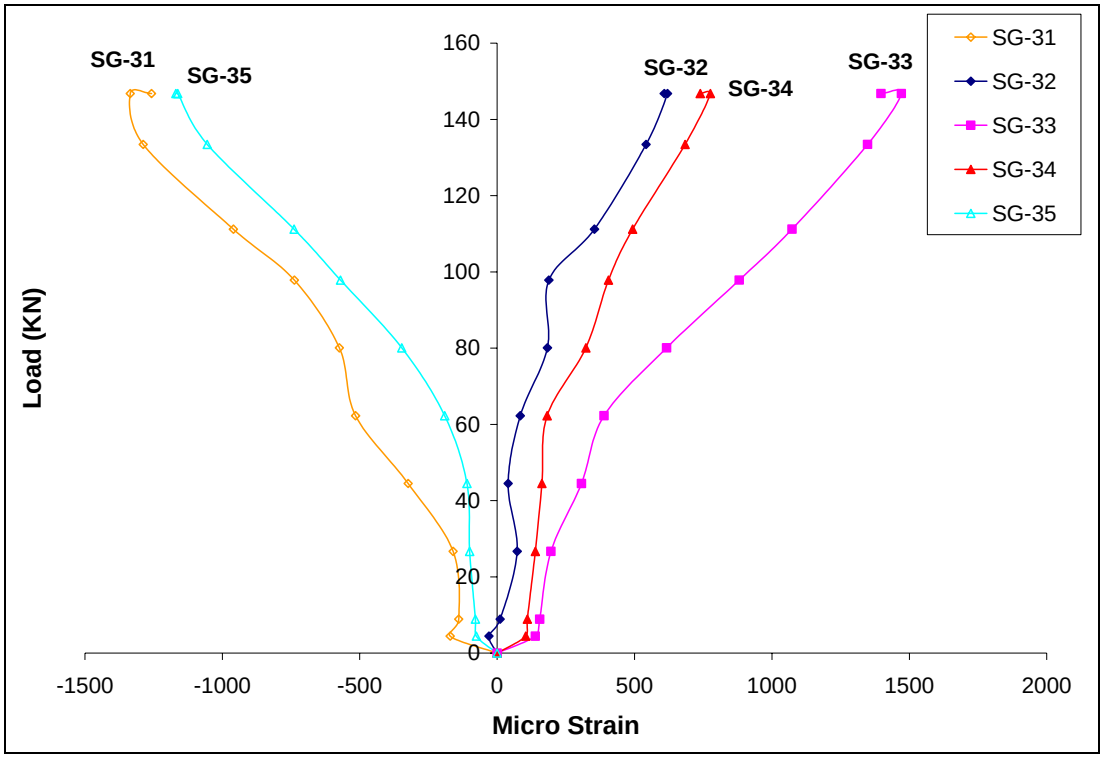


Figure 4. 25 – Strain vs. load for (top) row 3 of specimen GP-02

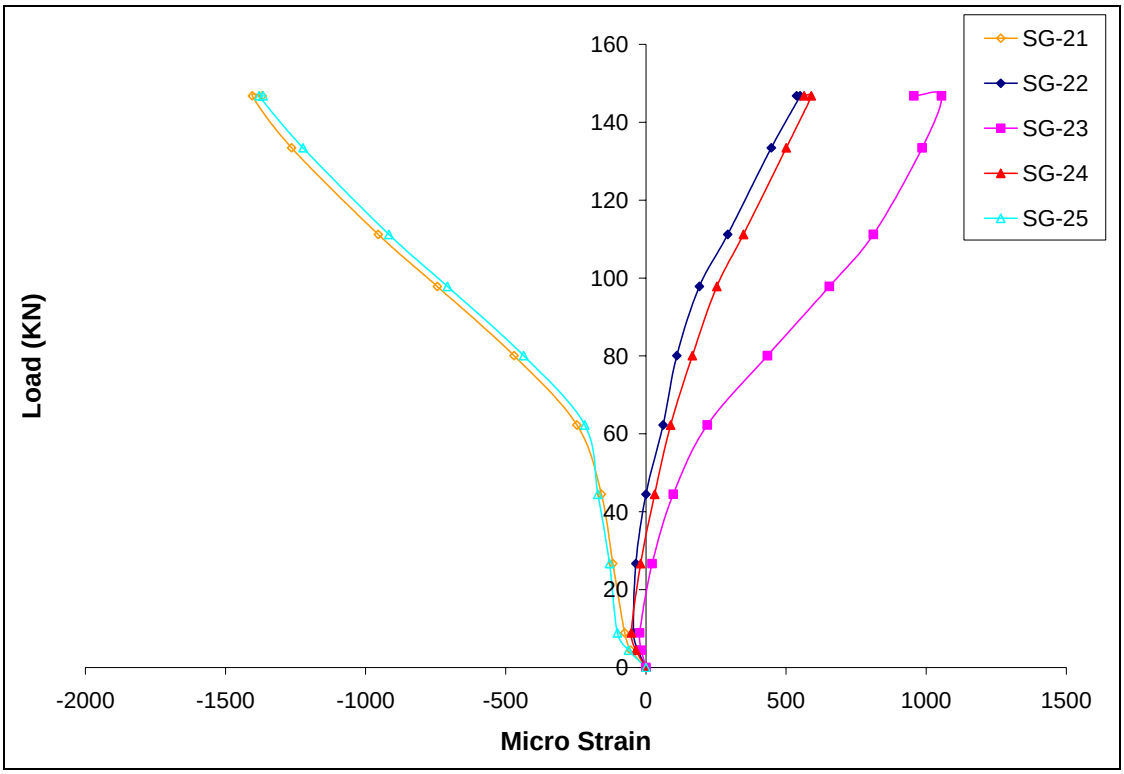


Figure 4. 26 – Strain vs. load for (middle) row 2 of specimen GP-02

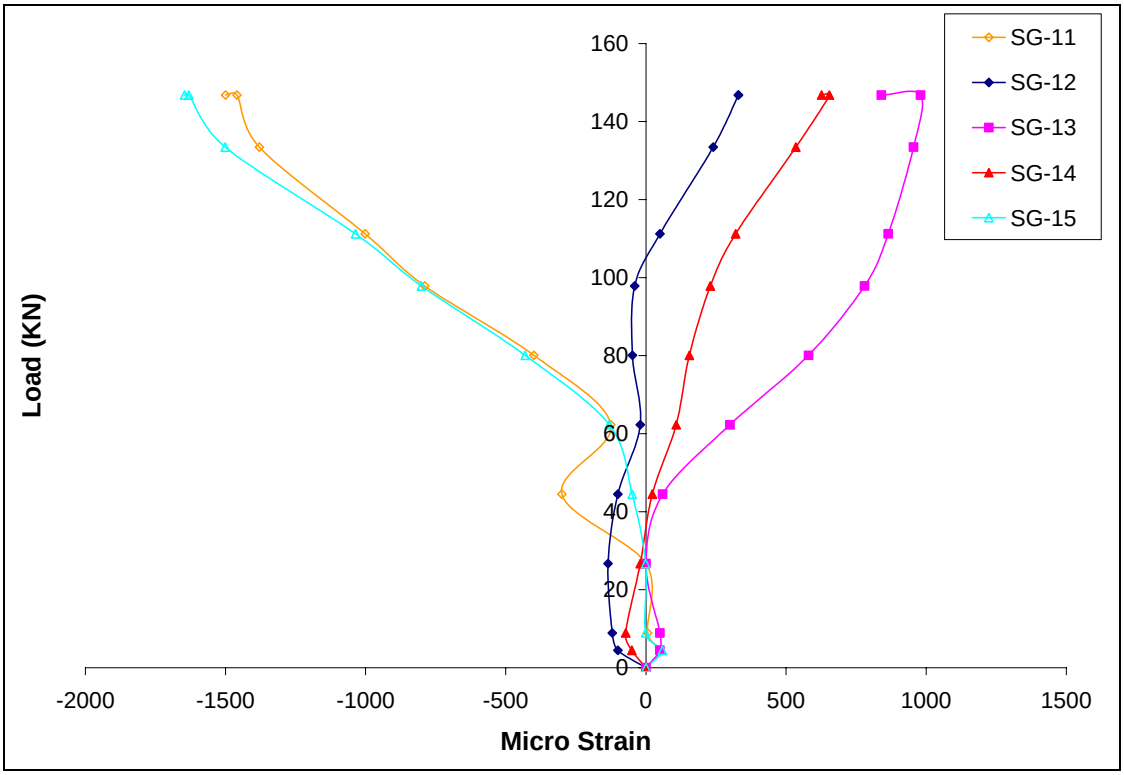


Figure 4. 27 – Strain vs. load for (bottom) row 1 of specimen GP-02

## 4.7 Specimen GP-03

Specimen GP-03 is a gusset plate of 6.4 mm thickness with 350 mm length and 300 mm width. One 28.6 mm ($1\frac{1}{8}$ in) diameter SAE-Grade 5 (ASTM-A325) high strength bolt was used to connect the angle to the gusset plate. The diameter of hole was 31 mm. A 150 x 150 x 10.2 mm angle section was used in this test. The locations of first row of strain gauges were very close to the edge of hole (4.5 mm below the hole). The other two rows were installed at 62.5 mm centers. Figure 4.28 shows the location of strain gauge and LVDTs which were used for this specimen. There were two LVDTs (LVDT-1 and LVDT-2) located on the left and right side of the plate surface at the front face. There was also one more 100 mm (4 in) spring loaded LVDT (LVDT-3) on the back face of the plate where angle was mounted.

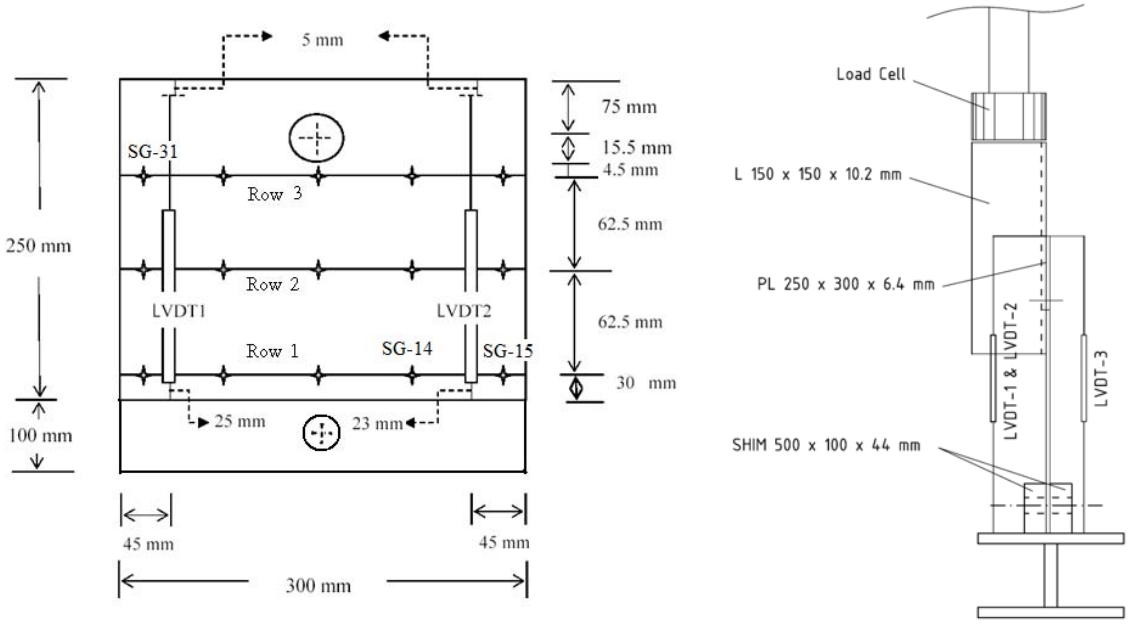


(a) Strain gauge locations (b) LVDT locations

Figure 4. 28 – Locations of strain gauges and LVDTs in Specimen GP-03

The plate remained in the elastic range until a load of 110 kN, after which plastic deformation began to occur. The elongation of the hole indicated that the plastic

deformation continued until ultimate rupture and tearing occurs. Due to the failure of bolts in load cell, the test was discontinued and the tearing did not occur in the plate. Figure 4.29 shows the load versus axial displacement response of specimen GP-03. The displacement was recorded by the LVDTs attached to the plate surface. The deformation of the gusset plate, the angle and the slip in the angle to gusset plate connection was recorded as total displacement. The maximum (ultimate) load recorded for this specimen was 255.4 kN (Table 4.3).

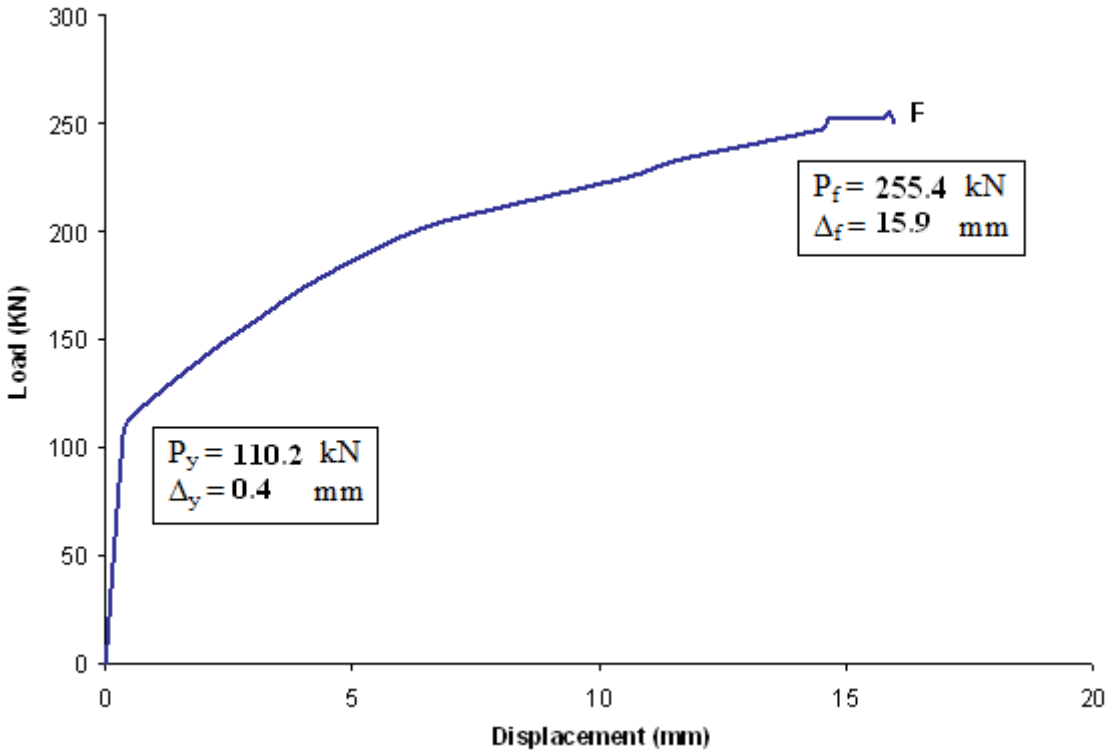


Figure 4. 29 – Load vs. axial displacement response of the gusset plate assembly - Specimen GP-03 (LVDT-3 output)

As it is shown in Figure 4.29, the specimen response under tension is reasonably stable. The load carrying capacity of the specimen increased as the deformation level increased. The out-of-plane plate bending of specimen was accompanied by the increase in axial deformation and drop in load carrying capacity.

After completion of the test, the gusset plate was examined. It was observed that the load went up to 255 kN then dropped down to 250 kN at failure of the four bolts in the load cell. The failed bolts of load cell are shown in Figure 4.30(c). The bolt hole in the connection elongated plastically due to the bearing of the bolts under loading. The test was discontinued because of failure of bolts in the load cell.


(a) Test setup

(b) LVDT location on angle


(c) Failed bolts of load cell

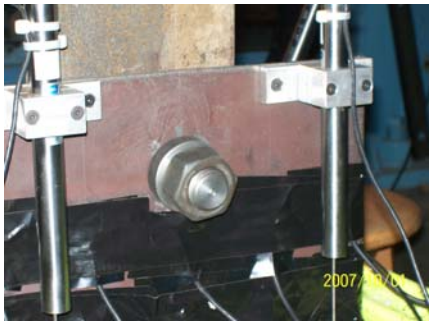

(d) Top hole connection

Figure 4. 30 – Failure of the four bolts in the load cell – Specimen GP-03

The angle was assumed to deform elastically. A compatibility of specimen deformation was preserved at the top of the gusset plate. The displacement of the top of the angle was assumed to be approximately equal to the in-plane displacement at

the top of the gusset plate free edges. Since the angle is relatively rigid compared to the gusset plate, this assumption appears to be valid.

During the loading of the specimen, strain gauges reading were recorded through data acquisition system. Due to the inappropriate installation of strain gauges in the plate surface, the output results of strain gauges were unacceptable.

## 4.8 Specimen GP-04

Specimen GP-04 is a gusset plate of 6.4 mm thickness with 710 mm length and 305 mm width. One 28.6 mm ($1\frac{1}{8}$ in) diameter SAE-Grade 5 (ASTM-A325) high strength bolt was used to connect the angle to the gusset plate. The diameter of hole was 31 mm. A 150 x 150 x 10.2 mm angle section was used in this test. For subsequent tests, the diameter of bolt diameter was increased to 1.5 in and Grade was increased to SAE Grade 8. The location of first row of strain gauges was very close to edge of top hole (5 mm below the bolt hole or 19.3 mm from center of hole). The other two rows were installed at 100 mm each apart. Figure 4.31 shows the location of strain gauges and LVDTs which were used for this specimen. There were three LVDT (LVDT-1, LVDT-2 and LVDT-4) were located at the left, middle and right side of the front plate surface. There was also one more 100 mm (4 in) spring loaded LVDT (LVDT-3) on the back face of the plate where angle section was mounted. The capacity of the universal load cell in test was 450 kN (100 kips).

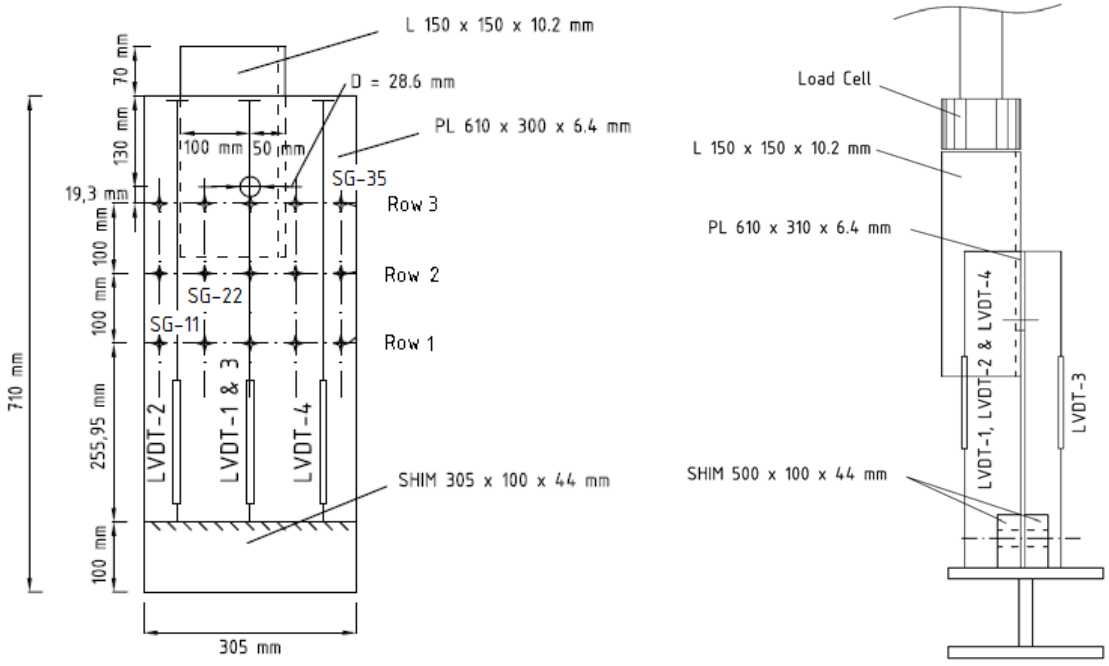


(a) Strain gauge location (b) LVDT(s) location

Figure 4. 31 – Locations of strain gauges and LVDTs in specimen GP-04

The plate remained in elastic range until a load of about 200 kN and after that the plastic deformation started and the elongation of the hole indicate that the plastic deformation in the plate occurred. Because of the shear failure of the bolt, the test was discontinued. Figure 4.32 shows the load versus axial displacement response of specimen GP-04 through its loading. The displacement was recorded by the LVDTs attached to the plate surface. The deformation of the gusset plate, the angle and the slip in the angle to gusset plate connection was recorded as total displacement. The maximum load was 323.2 kN (Table 4.3). The final length of top hole was 42.7 mm.

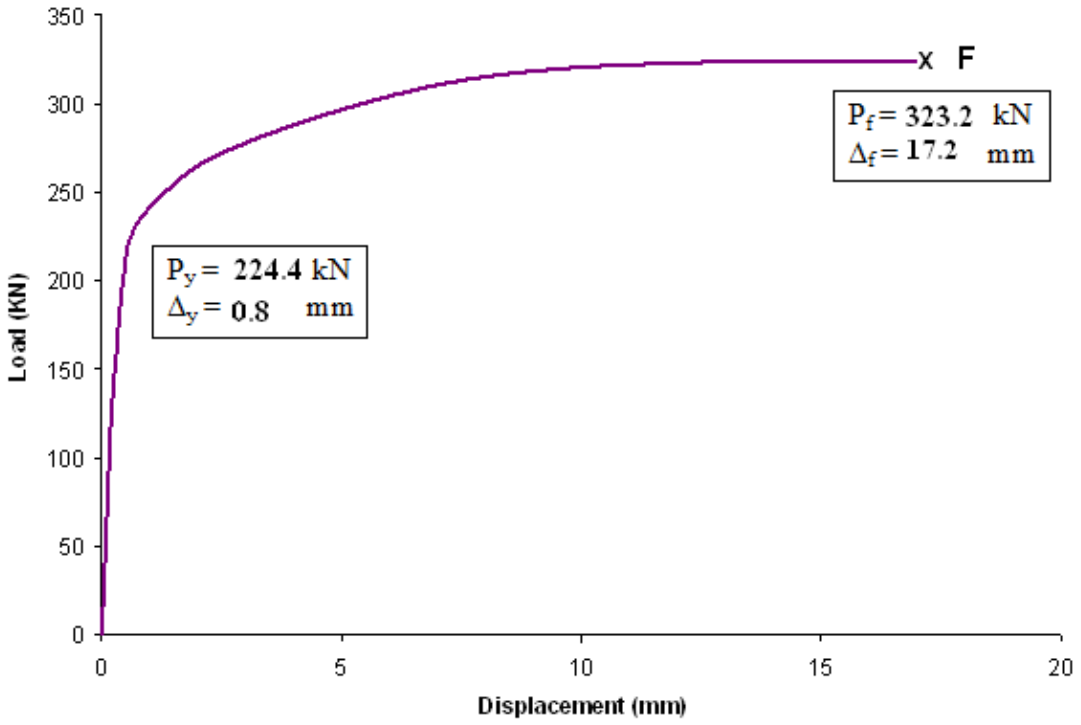


Figure 4. 32 – Load vs. axial displacement response of Specimen GP-04 (LVDT-3 output)

As it is shown in Figure 4.32, the specimen response under tension is reasonably stable. The load carrying capacity of the specimen increased as the deformation level increased. The out-of-plane plate bending of specimen was accompanied by the increase in axial deformation and drop in load carrying capacity.

After the completion of the test, the failed gusset plate specimen was examined. It was observed that the specimen failed in tension due a bearing failure of the plate material between the bolt holes of the connection. The failed plate material and bolt are shown in Figure 4.33(d). The bolt hole in the connection deformed due to the bearing of the bolts under load. The test was discontinued because of the bolt shear (Figure 4.33(c)).

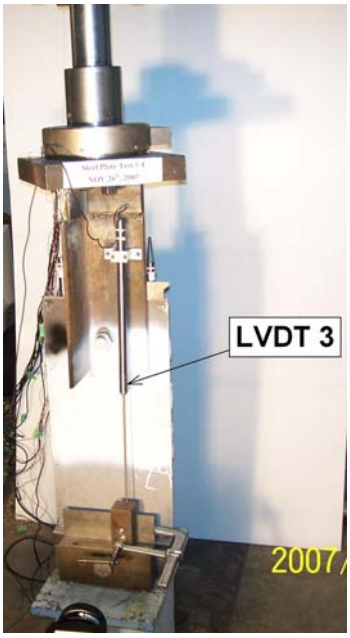


(a) Test setup

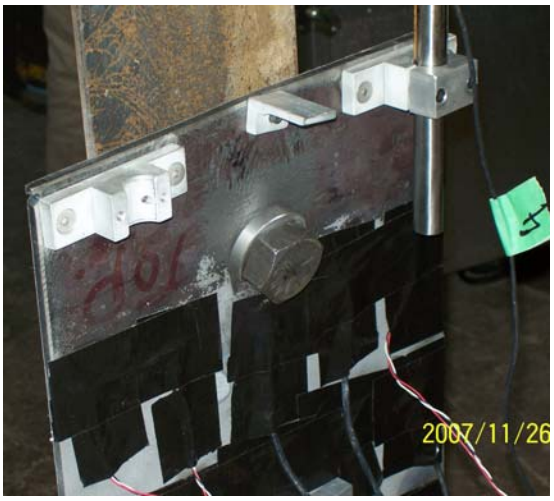


(b) LVDT location on plate


(c) Failed bolt

(d) Bearing failure of plate

Figure 4. 33 – Plate and angle bearing failure in bolted connection – Specimen GP-04

The angle was assumed to deform elastically. A compatibility of specimen deformation was preserved at the top of the gusset plate. The displacement of the top

of the angle was assumed to be approximately equal to the in-plane displacement at the top of the gusset plate free edges. Since the angle is relatively rigid compared to the gusset plate, this assumption appears to be valid.

During the loading of specimen, strain gauges reading were recorded through data acquisition system. As soon as strain localizations occurred in the plate and the stresses begin to redistribute. Figure 4.34 to Figure 4.36 show the strain distributions from 50 kN to 325 kN. The strain gauges values are in micro strain.

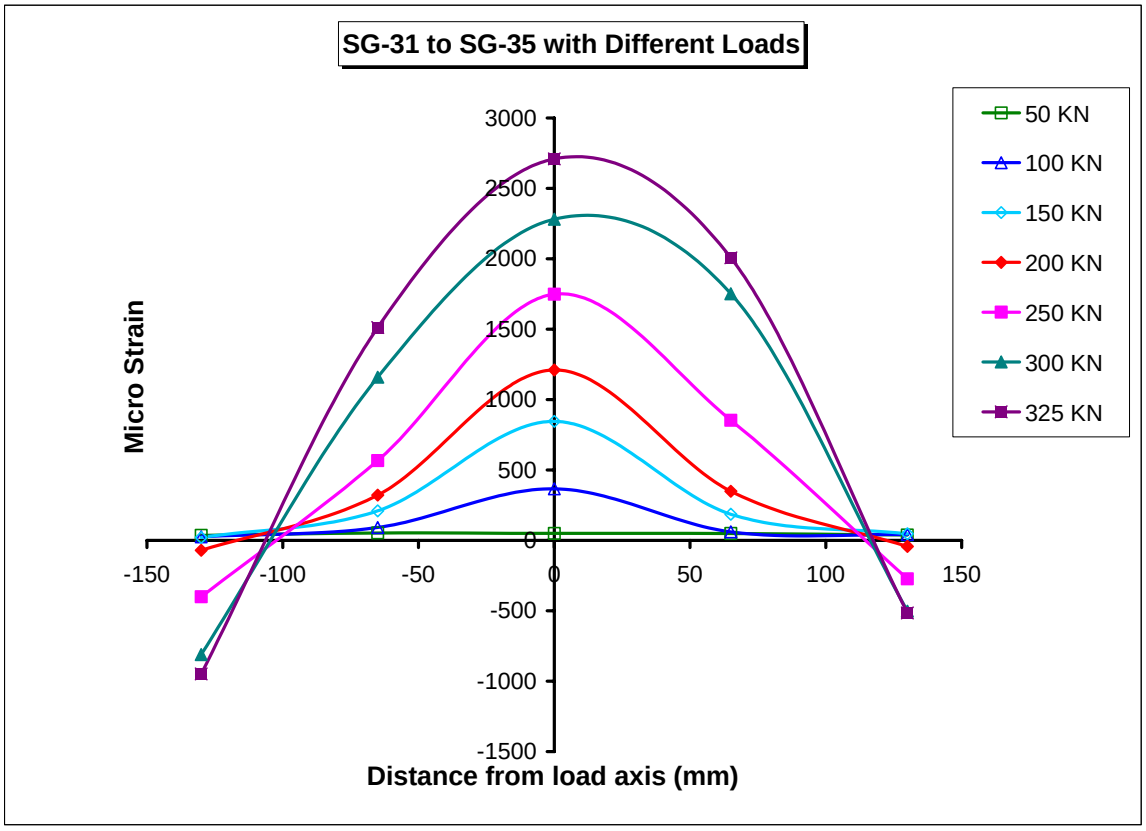


Figure 4. 34 – Strain values for (top) row 3 of specimen GP-04 at different loads

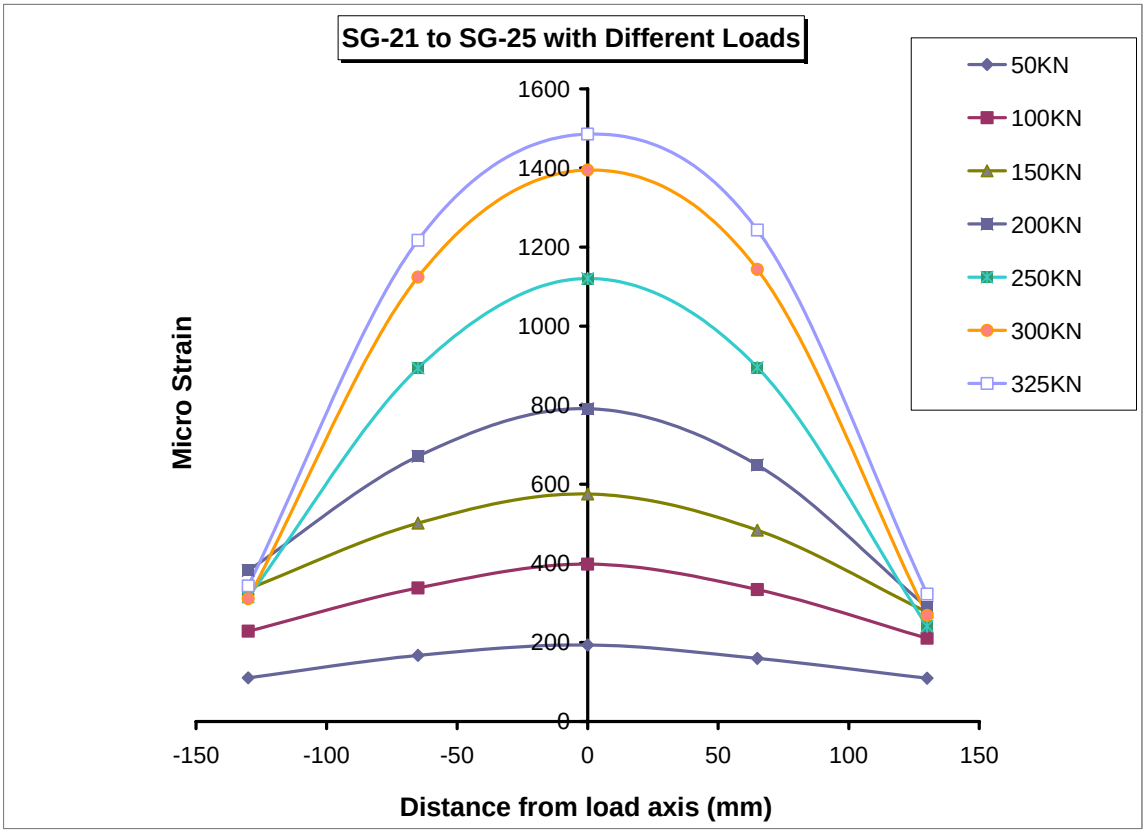


Figure 4. 35 – Strain values for (middle) row 2 of specimen GP-04 at different loads

Since SG-33 was very close (5 mm) to the edge of the hole. As a result, the strain history for this gauge was not good. It was decided to correct the strain data for this gauge and Figure 4.34 shows the corrected values. Because of this problem, the first row of strain gauges was applied at 50 mm away from the edge of hole for all the future tests.

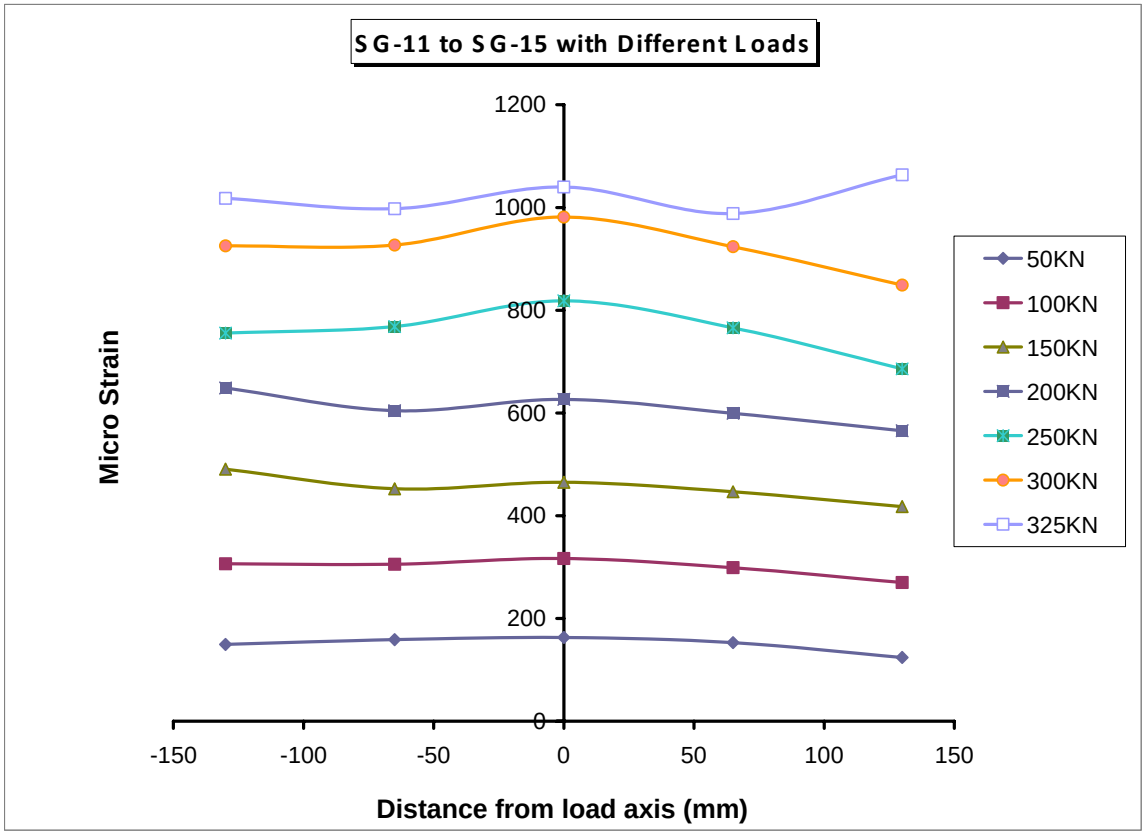


Figure 4. 36 – Strain values for (bottom) row 1 of specimen GP-04 at different loads

When the specimen load is increased beyond 150 kN level, strain level become non-uniform. When the strain reading at the 325 kN load are analyzed, the strain level are generally slightly more than one and half times those recorded at the load of 150 kN level. Figure 4.37 to Figure 4.39 show the strain distribution at different levels on plate surface. The strain gauges values are in micro strain.

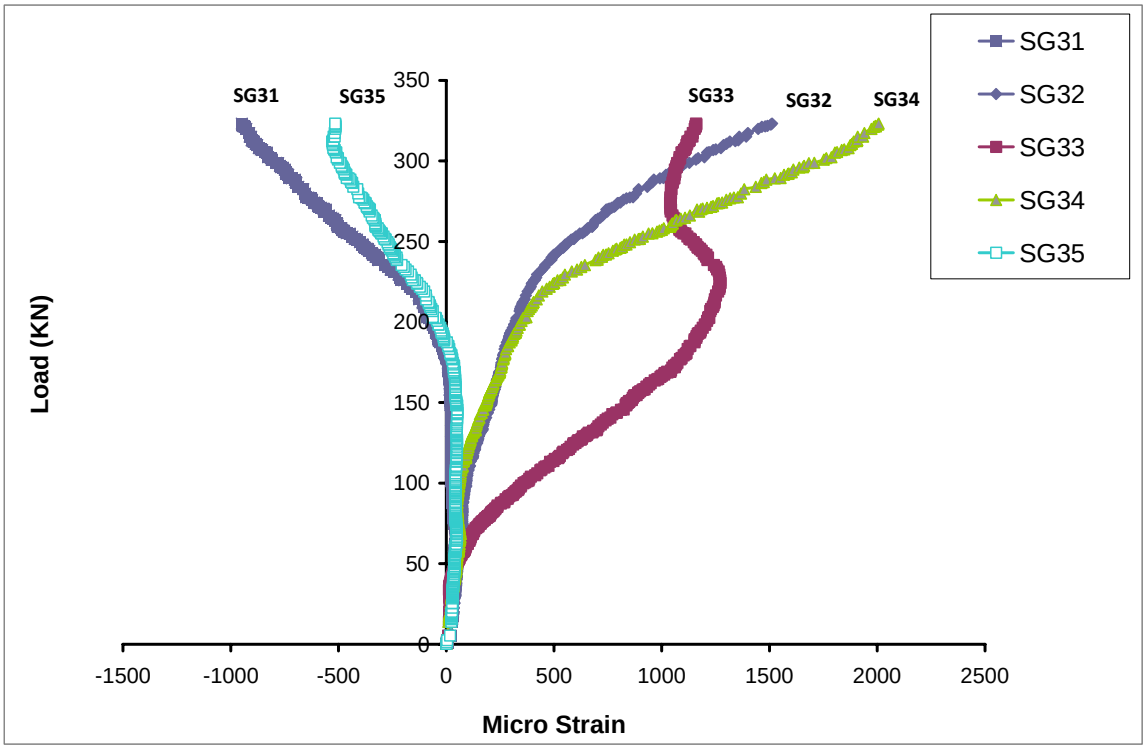


Figure 4. 37 – Strain vs. load for (top) row 3 of specimen GP-04

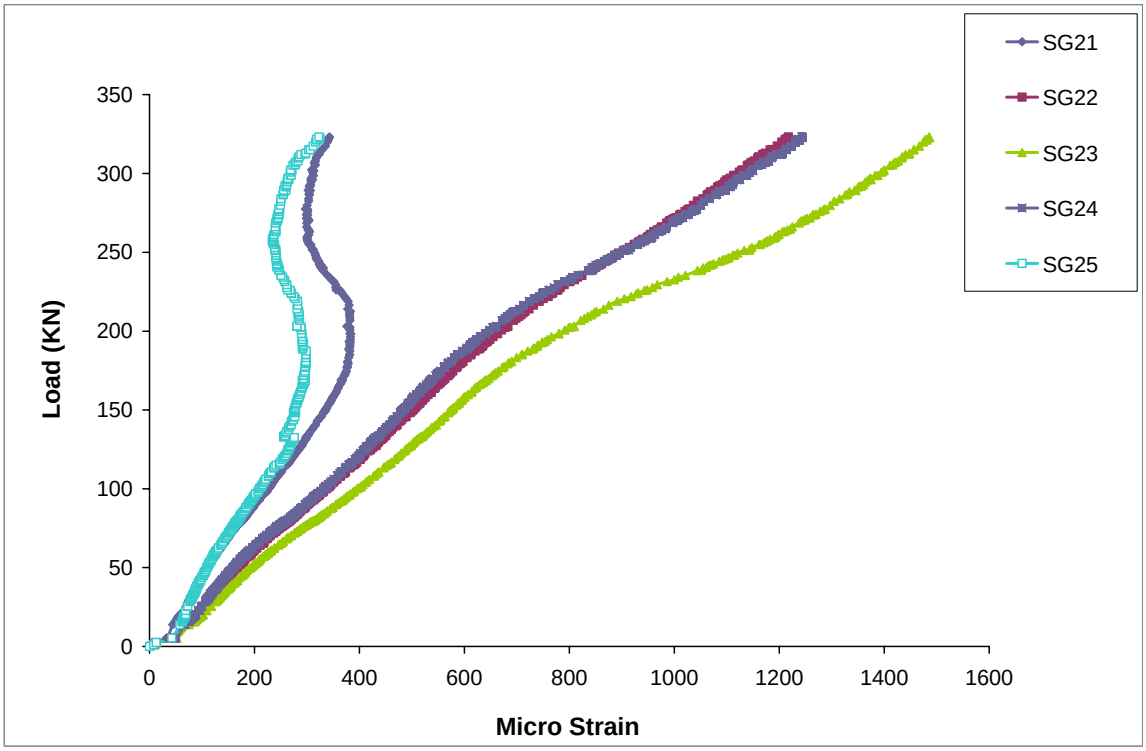


Figure 4. 38 – Strain vs. load for (middle) row 2 of specimen GP-04

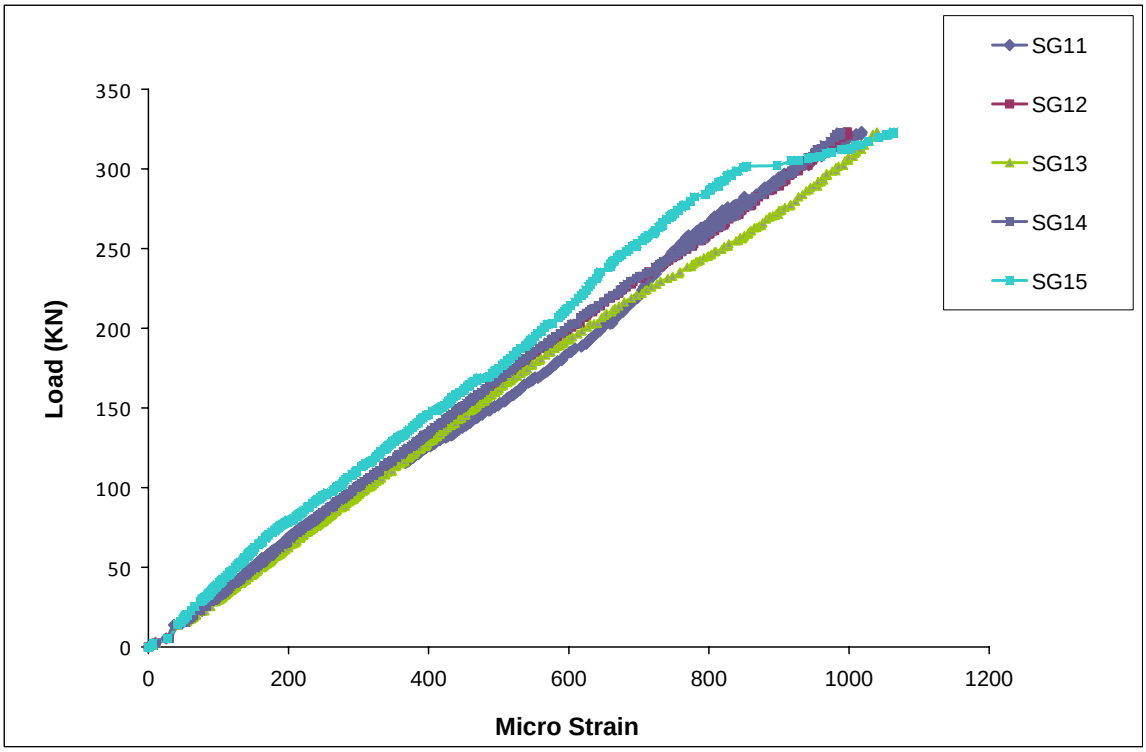


Figure 4. 39 – Strain vs. load for (bottom) row 1 of specimen GP-04

## 4.9 Specimen GP-05

Specimen GP-05 is a gusset plate of 7.0 mm thickness with 850 mm length and 500 mm width. One 38.1 mm (1.5 in) diameter SAE-Grade 8 (ASTM-A354) high strength bolt was used to connect the angle to the gusset plate. The diameter of hole was 40 mm. A 150 x 150 x 10.2 mm angle section was used in this test. The locations of first row of strain gauges were 50 mm below the edge of the hole. The other two rows were installed at 100 mm each apart. There was also one row of strain gauge near the support in order to observe the effect of strain distribution on plate surface. Figure 4.40 shows the location of strain gauge and LVDTs which were used for this specimen. There were three LVDTs (LVDT-1, LVDT-2, LVDT-3) located on the left, middle and right side of the front plate surface. There was also one more 100 mm (4 in) spring loaded LVDT (LVDT-4) between the loading jack and load cell plate.

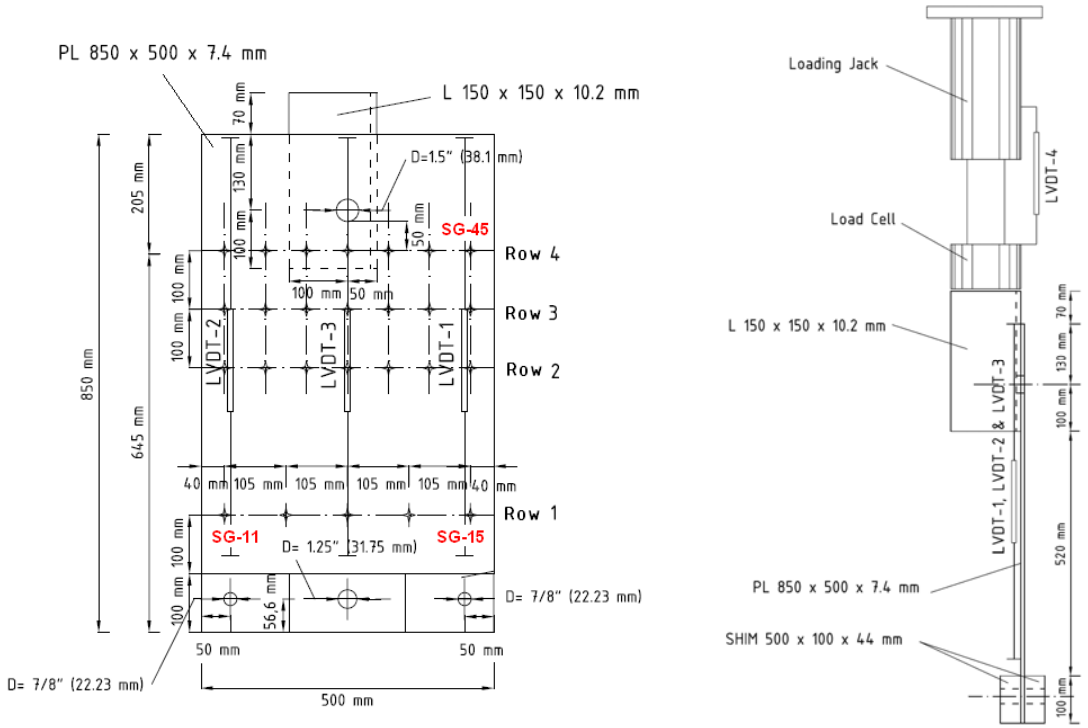


(a) Strain gauge location (b) LVDT(s) location

Figure 4. 40 – Locations of strain gauges and LVDTs in specimen GP-05

The displacement was recorded by the LVDTs attached to the plate surface and jack. The load deformation plot is not shown for this specimen because the output of LVDT which was mounted between jack and load cell was unacceptable. Also, due to the local buckling of plate during the test, the outputs of LVDTs which connected to plate surface were unacceptable (Figure 4.41(b)). Hence, no load-deformation plot is available for this specimen and the next test (GP-06) was conducted as a repeat test for GP-05 such that load-deformation plot as well as strain plots can be obtained. The test GP-05 was discontinued because of load cell capacity limitation. The maximum load recorded from this specimen was 551.8 kN (Table 4.3).

After the completion of the test, the failed gusset plate specimen was examined. It was observed that the specimen failed in tension due a bearing failure of the plate material between the bolt holes of the connection. The failed plate material is shown in Figure 4.41(d). The bolt hole in the connection had deformed due to the bearing of the bolts under load. The final length of top hole was 40.7 mm.


(a) Test setup

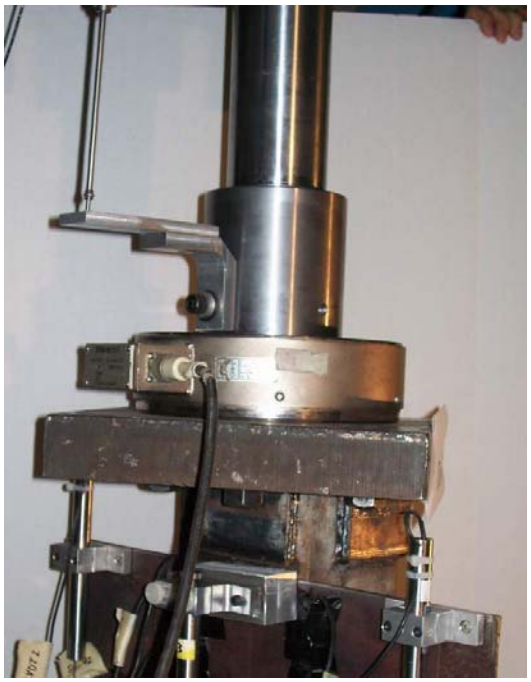

(b) LVDT location on jack

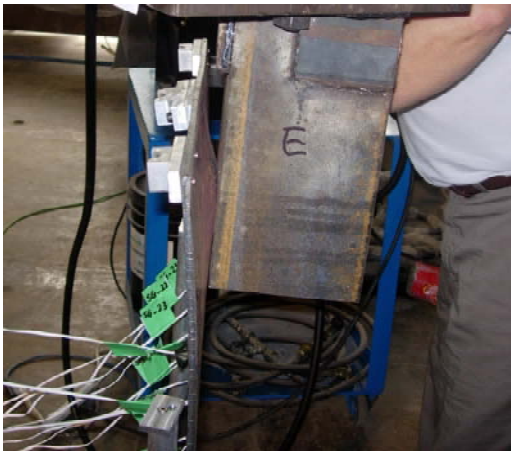

(c) Local plate buckling


(d) Plate hole elongation

Figure 4. 41 – Plate bearing failure in bolted connection – Specimen GP-05

The angle was assumed to deform elastically. A compatibility of specimen deformation was preserved at the top of the gusset plate. The displacement of the top of the angle was assumed to be approximately equal to the in-plane displacement at the top of the gusset plate free edges. Since the angle is relatively rigid compared to the gusset plate, this assumption appears to be valid.

During the loading of specimen, strain gauges reading were recorded through data acquisition system. As soon as local yielding occurred in the plate and the stresses began to redistribute, the strain readings were localized. Figure 4.42 to Figure 4.45 show the strain distributions from 50 kN to 550 kN. The strain gauges values are in micro strain.

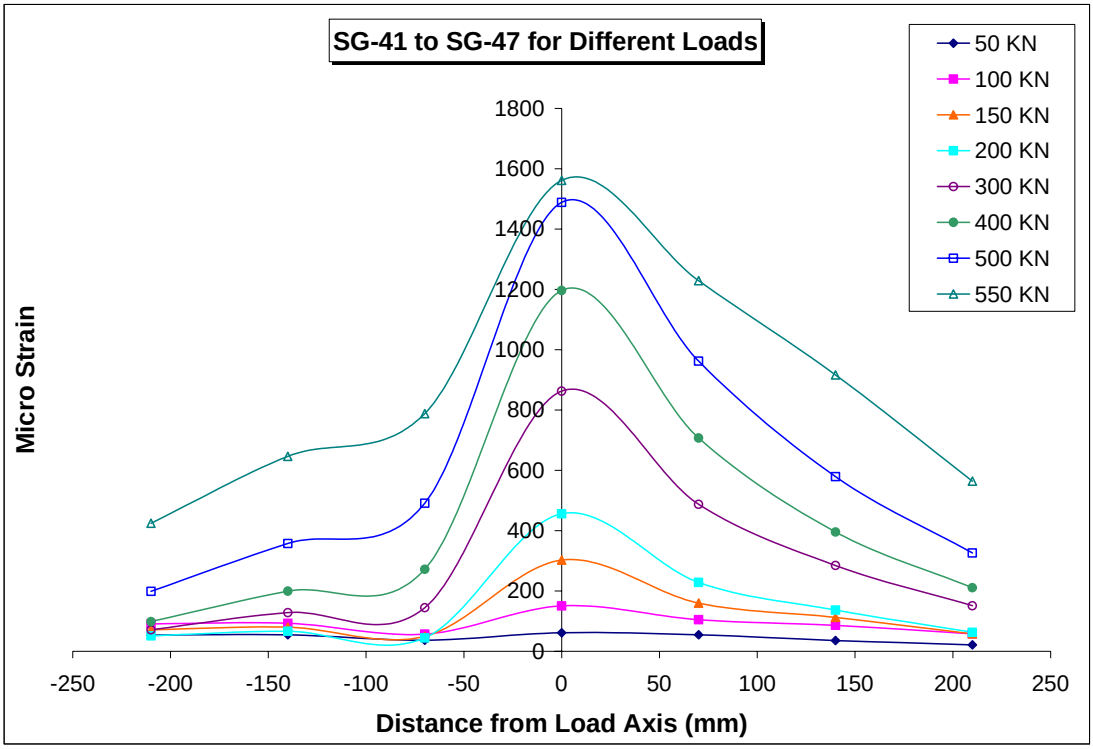


Figure 4. 42 – Strain values for (top) row 4 of specimen GP-05 at different loads

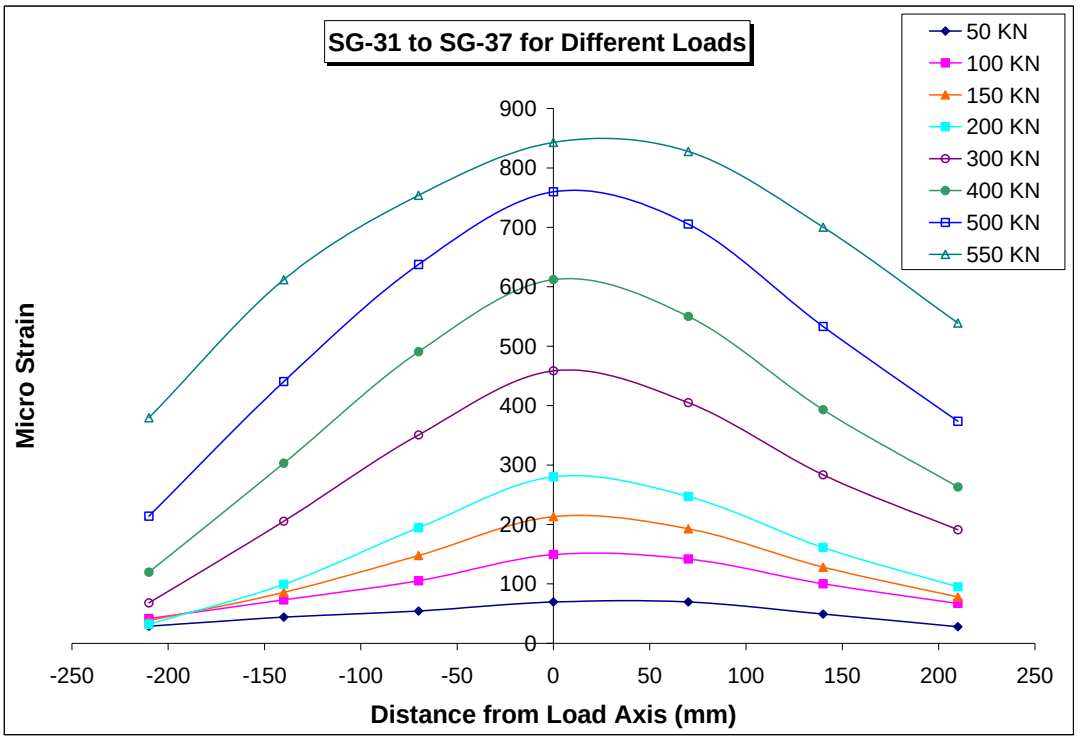


Figure 4. 43 – Strain values for (middle) row 3 of specimen GP-05 at different loads

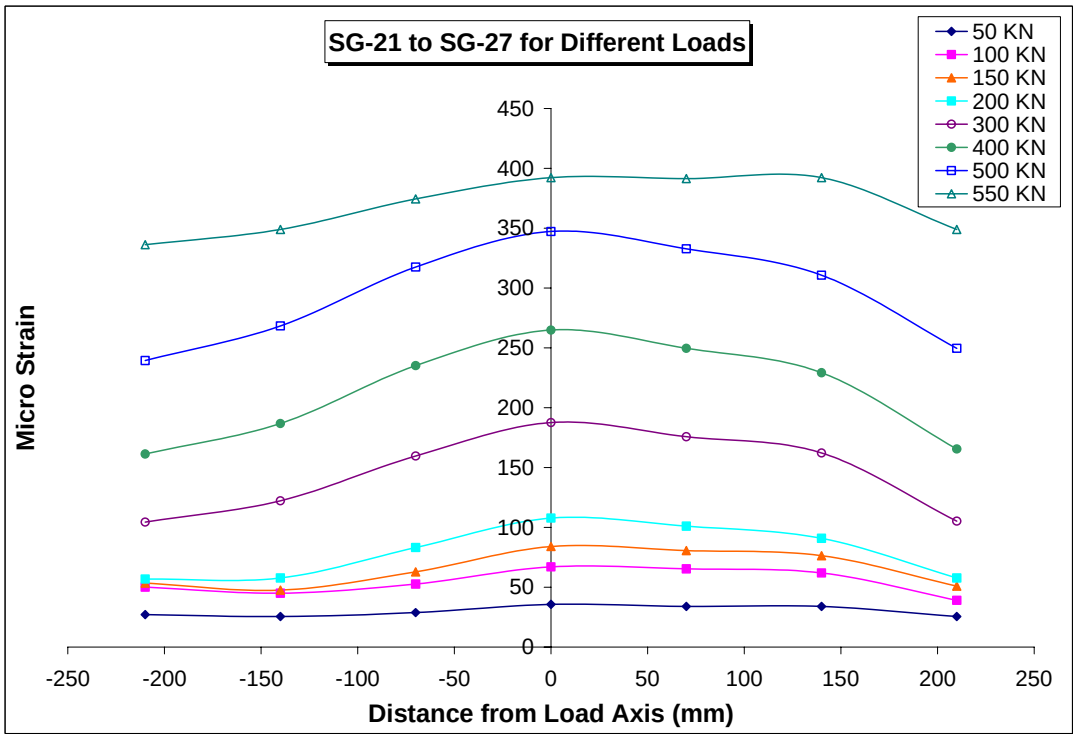


Figure 4. 44 – Strain values for (bottom) row 2 of specimen GP-05 at different loads

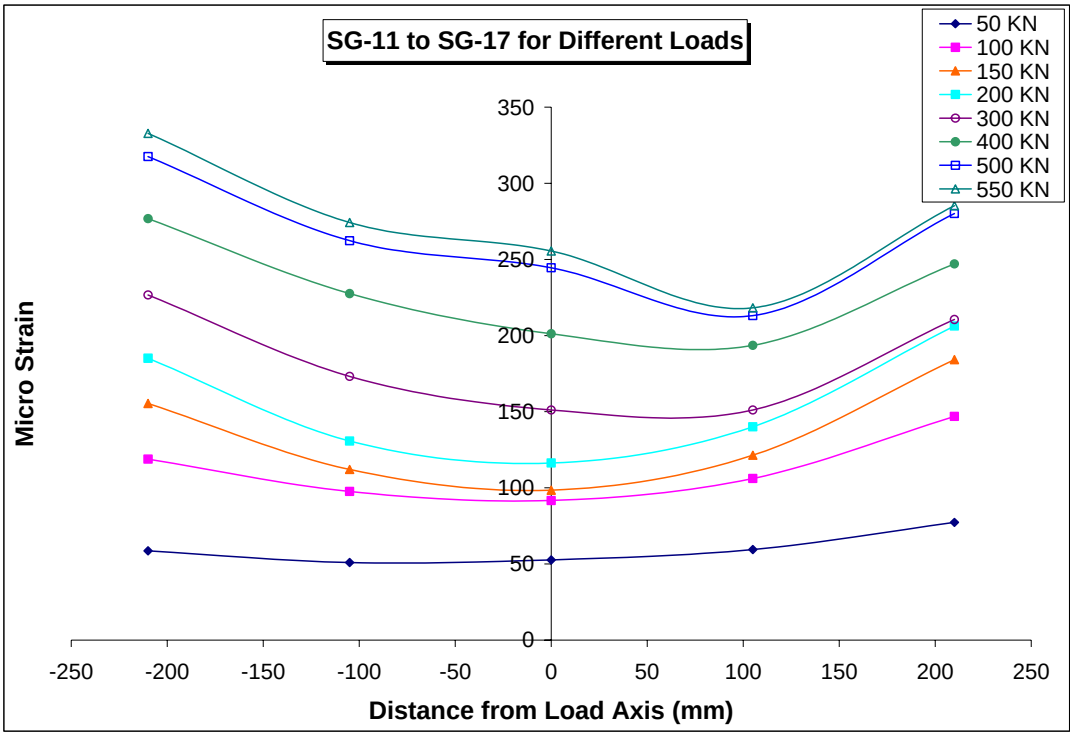


Figure 4. 45 – Strain values for (support) row 1 of specimen GP-05 at different loads

When the specimen load is increased beyond 350 kN level, strain level are changed. When the strain reading at the 550 kN load are analyzed, the strain level are generally slightly more than one and half times those recorded at the 350 kN level. Figure 4.46 to Figure 4.49 show the strain distribution at different levels on plate surface. The strain gauges values are in micro strain.

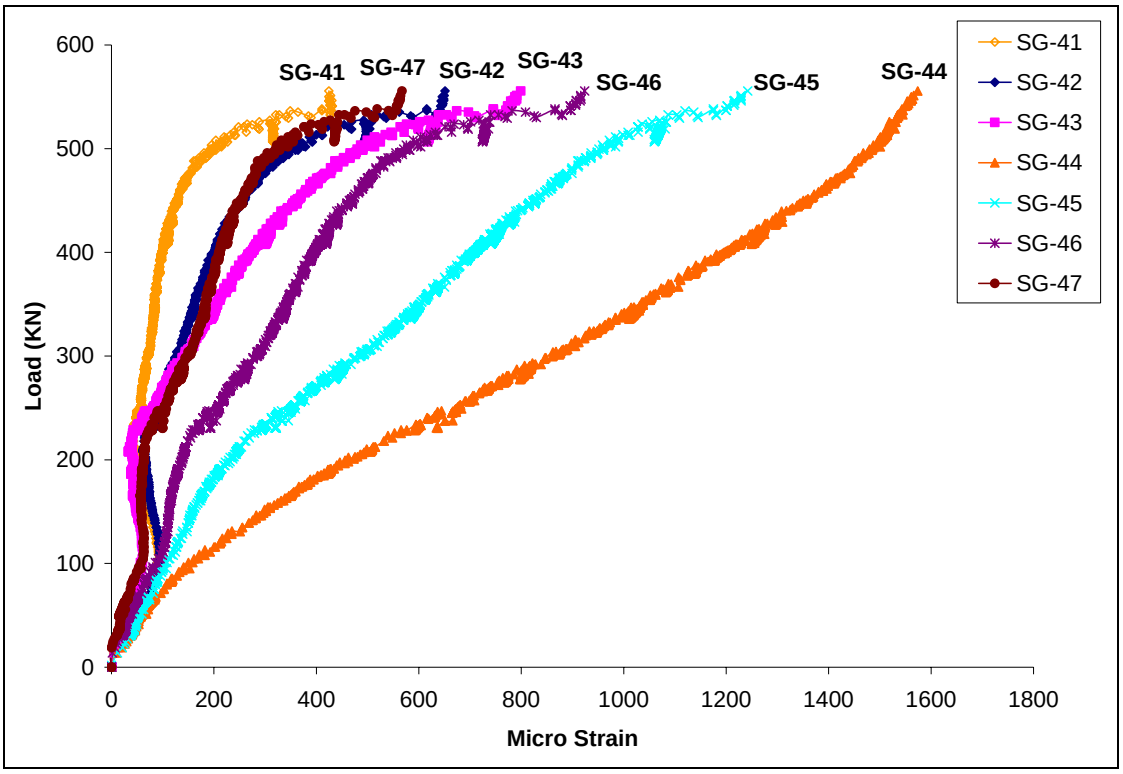


Figure 4. 46 – Strain vs. load for (top) row 4 of specimen GP-05

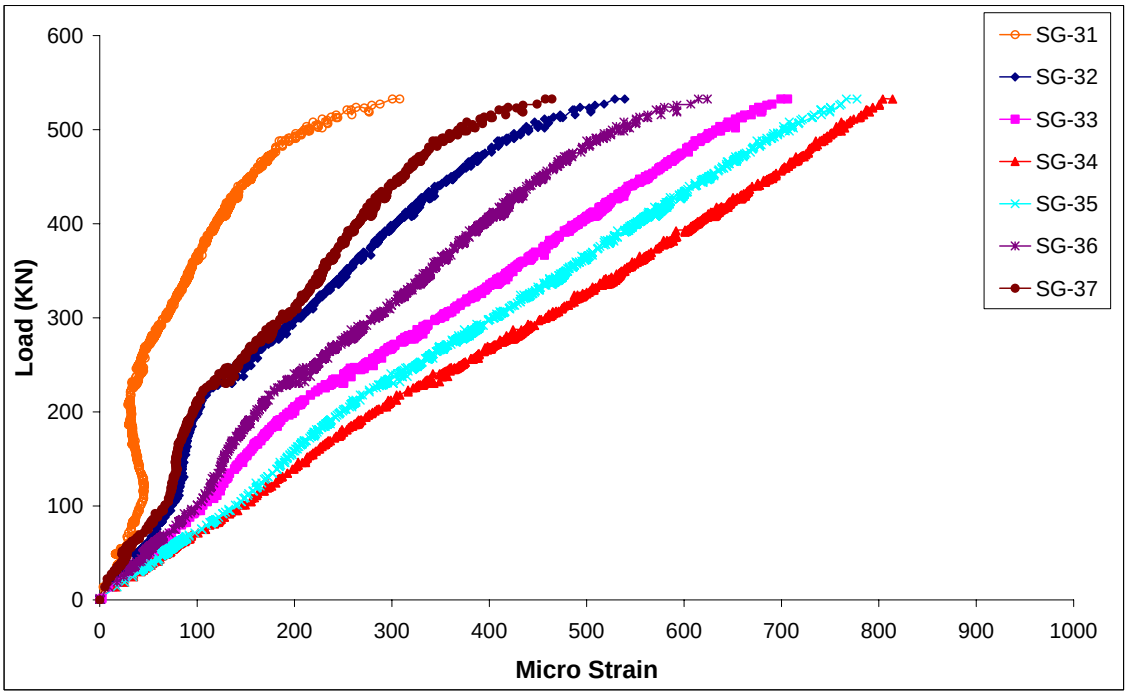


Figure 4. 47 – Strain vs. load for (middle) row 3 of specimen GP-05

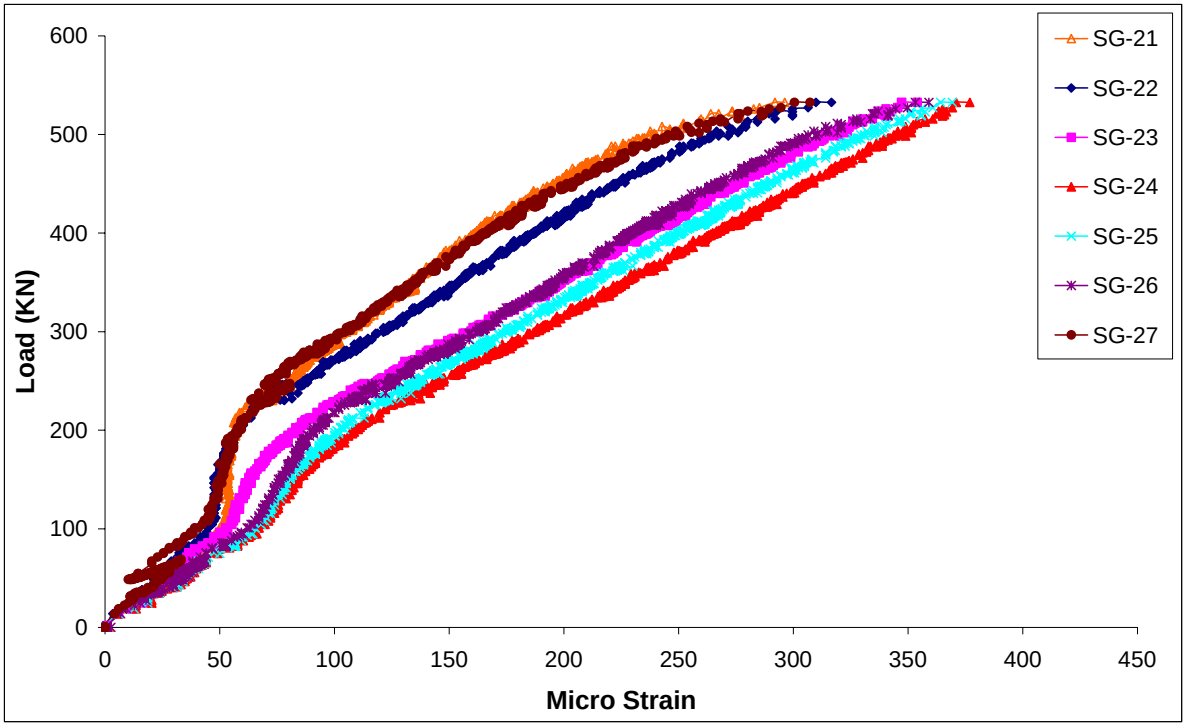


Figure 4. 48 – Strain vs. load for (bottom) row 2 of specimen GP-05

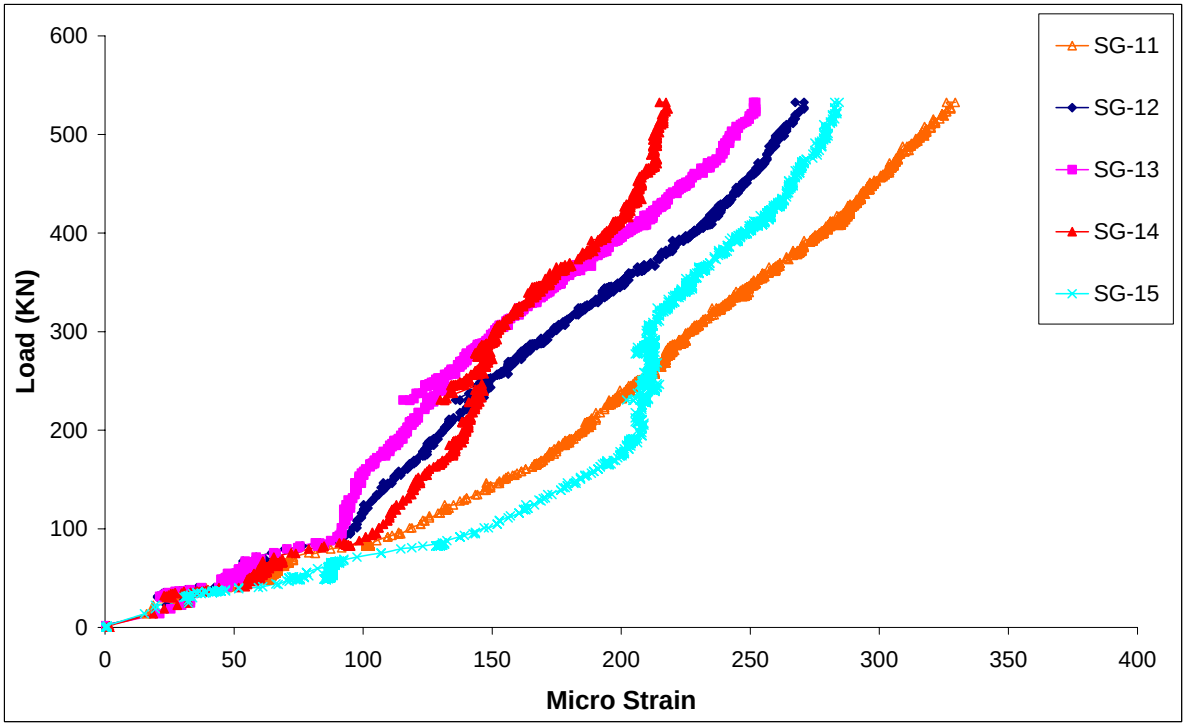


Figure 4. 49 – Strain vs. load for (support) row 1 of specimen GP-05

## 4.10 Specimen GP-06

Specimen GP-06 is a gusset plate of 7.0 mm thickness with 720 mm length and 500 mm width and hence, this specimen is similar to GP-05 and this test was undertaken as a repeat test for GP-05. Since the capacity of load cell for specimen GP-05 was not enough (450 kN), a higher capacity universal load cell (900 kN) was used for GP-06 and subsequent tests. Also, a new and higher capacity universal loading jack (200 ton) was used for all the following specimens including GP-06. One 38.1 mm (1.5 in) diameter SAE-Grade 8 (ASTM-A354) high strength bolt was used to connect the angle to the gusset plate. The diameter of hole was 40 mm. A 150 x 150 x 10.2 mm angle section was used in this test. The locations of first row of strain gauges were 50 mm below the hole. The other three rows were installed at 100 mm each apart. Figure 4.50 shows the location of strain gauge and LVDTs which were used for this specimen. There were two LVDT located on the front and back of the plate surface. There was also two 100 mm (4 in) spring loaded LVDT on the front and back of jack.

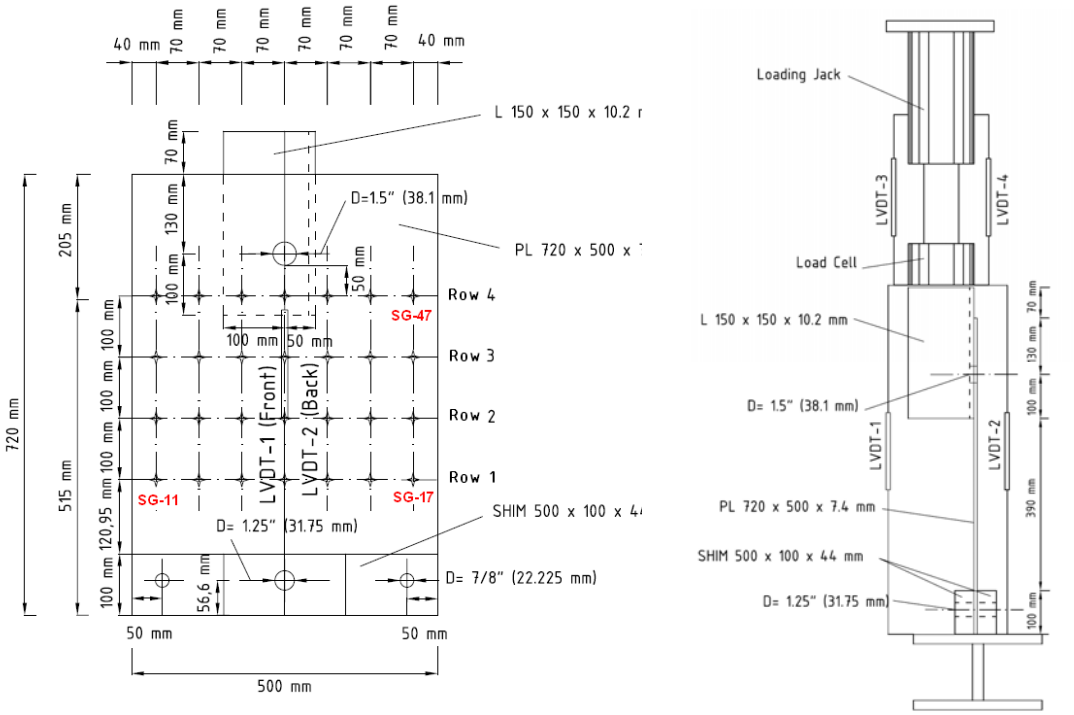


(a) Strain gauge location (b) LVDT(s) location

Figure 4. 50 – Locations of strain gauges and LVDTs in specimen GP-06

The plate remained in elastic range until a load of about 160 kN and after that the plastic deformation started and the elongation of the hole indicate that the plastic deformation continued until the tearing is happened. This test was discontinued when the load capacity started to drop. Figure 4.51 shows the load versus axial displacement response of specimen GP-06 through its loading which obtained from information of LVDT attached on angle and jack. The deformation of the gusset plate, the angle and the slip in the angle to gusset plate connection was recorded as total displacement.

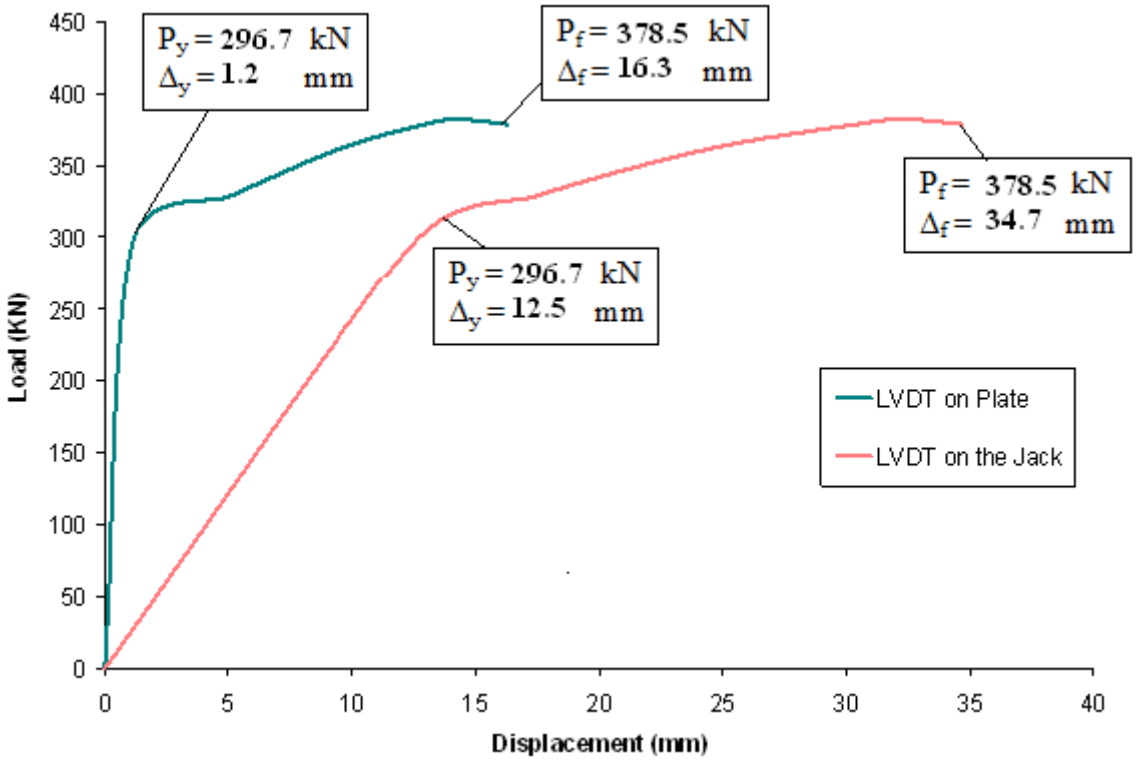


Figure 4. 51 – Load vs. axial displacement response of the gusset plate from LVDT located on plate (LVDT-1) and on the jack (LVDT-4) - Specimen GP-06

As it is shown in Figure 4.51, the specimen response under tension is reasonably stable. The load carrying capacity of the specimen increased as the deformation level increased. The out-of-plane plate bending of specimen was accompanied by the increase in axial deformation and drop in load carrying capacity.

After the completion of the test, the failed gusset plate specimen was examined. It was observed that the specimen failed in tension due a bearing failure of the plate material between the bolt holes of the connection. It was also observed that the top hole elongated and some tearing happens (Figure 4.52(d)). The bolt hole in the connection had elongated by 8.1 mm due to the bearing of the bolts under load. The final length of top hole was 39.8 mm.

(a) Test setup

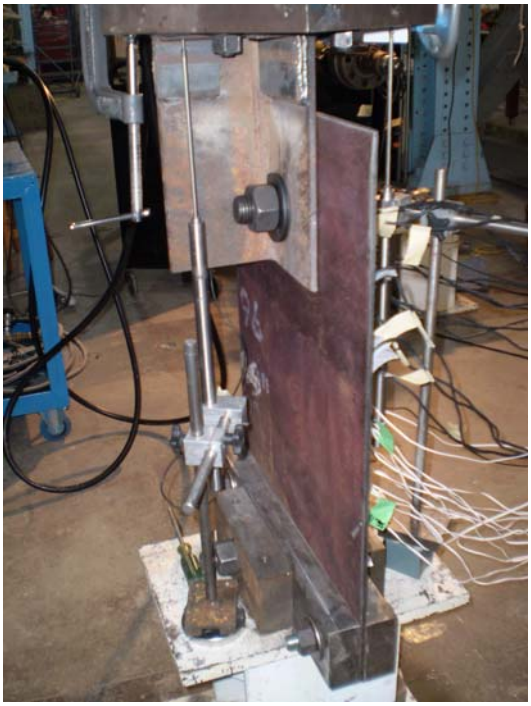

(b) LVDT location on angle

(c) Plate buckling


(d) Plate top hole elongation

Figure 4. 52 – Plate bearing failure in bolted connection – Specimen GP-06

The angle was assumed to deform elastically. A compatibility of specimen deformation was preserved at the top of the gusset plate. The displacement of the top of the angle was assumed to be approximately equal to the in-plane displacement at the top of the gusset plate free edges. Since the angle is relatively rigid compared to the gusset plate, this assumption appears to be valid.

During the loading of specimen, strain gauges reading were recorded through data acquisition system. As soon as local yielding occurred in the plate at load about 295 kN and the strain began to redistribute, the strains localized. Figure 4.53 to Figure 4.56 show the strain distributions from 50 kN to 350 kN. The strain gauges values are in micro strain.

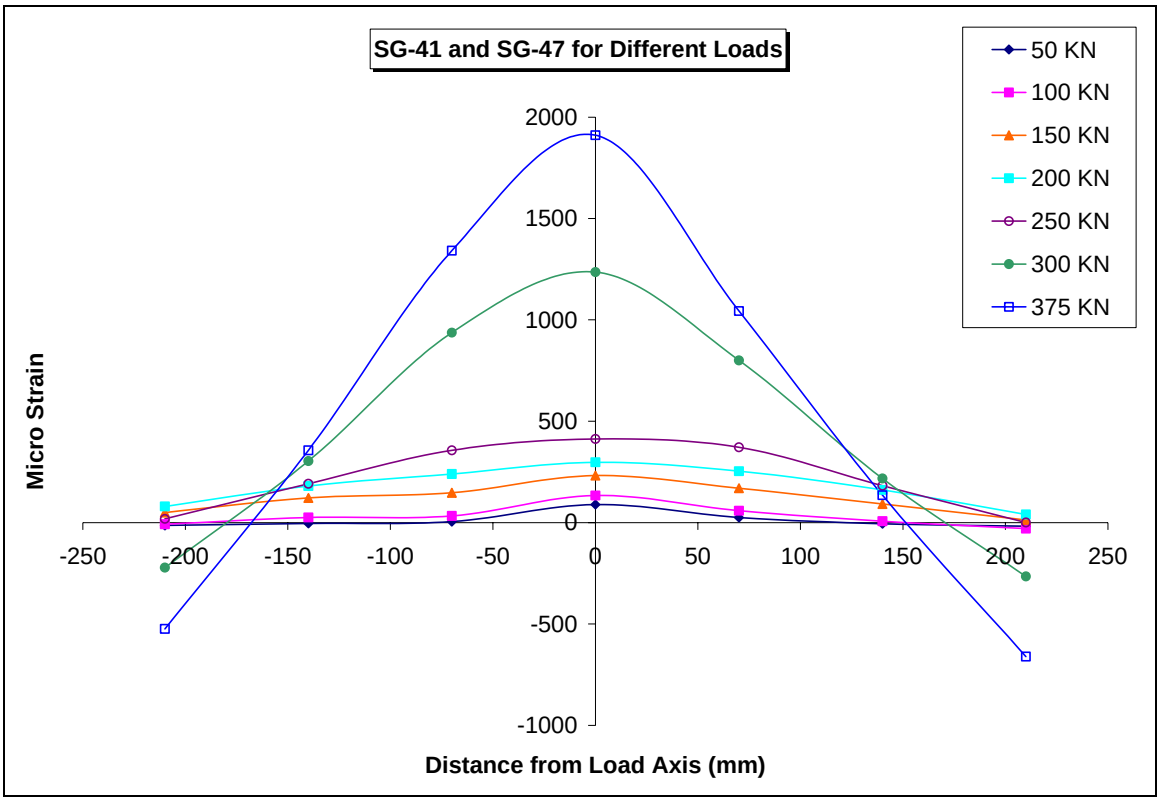


Figure 4. 53 – Strain values for (top) row 4 of specimen GP-06 at different loads

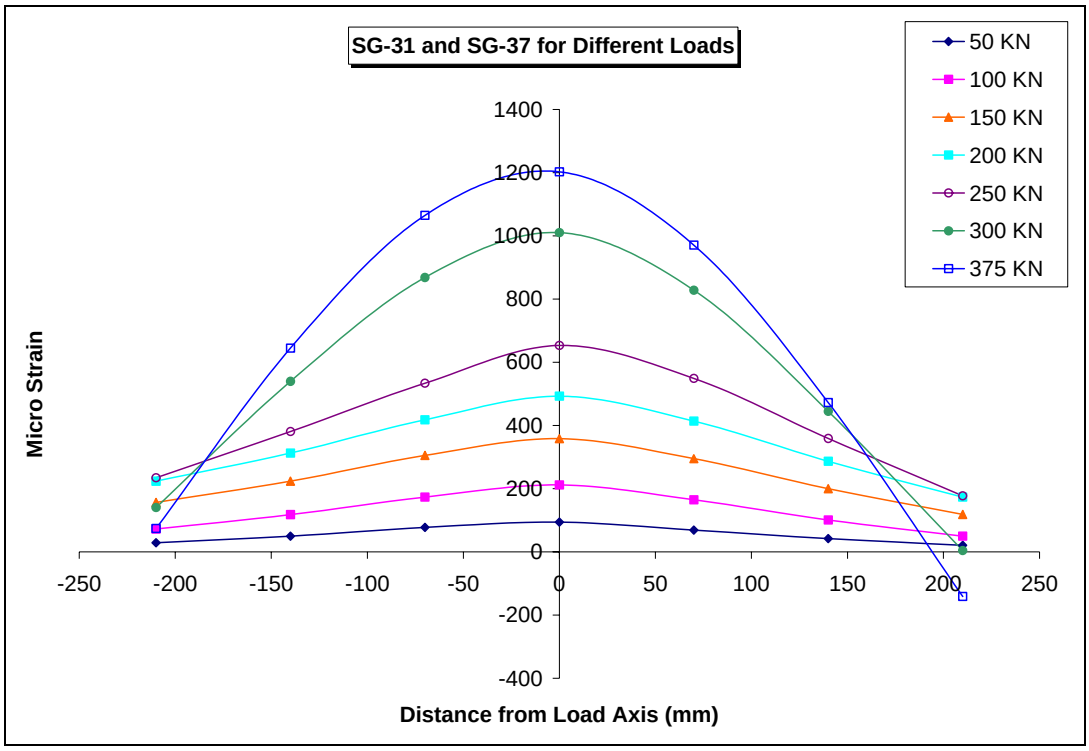


Figure 4. 54 – Strain values for (middle) row 3 of specimen GP-06 at different loads

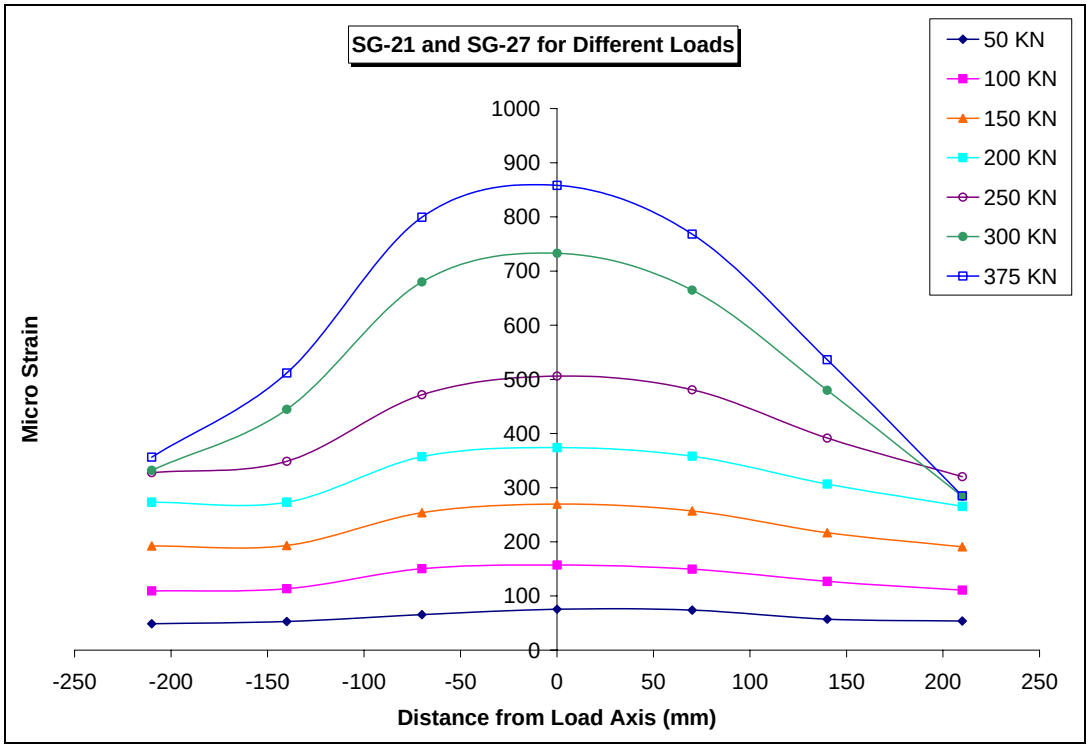


Figure 4. 55 – Strain values for (lower) row 2 of specimen GP-06 at different loads

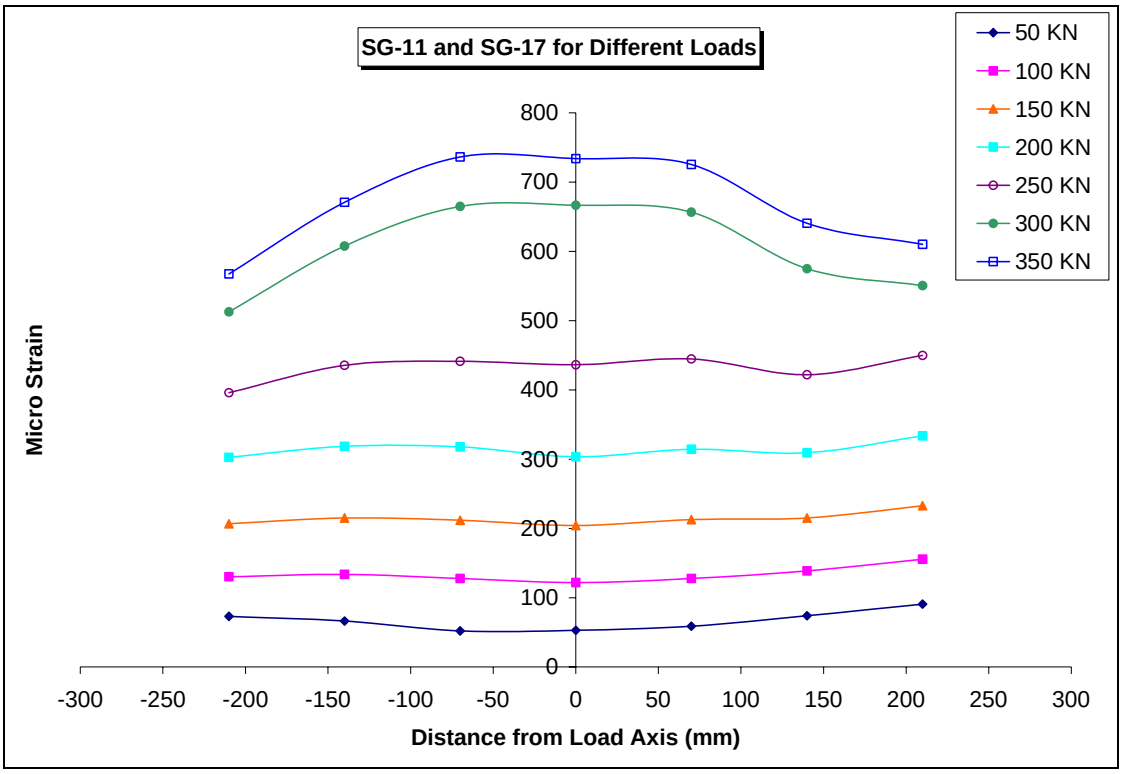


Figure 4. 56 – Strain values for (bottom) row 1 of specimen GP-06 at different loads

When the specimen load is increased beyond the yield load 150 kN, strain levels were changed. When the strain reading at the 350 kN load are analyzed, the strain level are generally slightly more than three times those recorded at the 150 kN level. Figure 4.57 to Figure 4.60 show the strain distribution at different levels on plate surface. The strain gauges values are in micro strain.

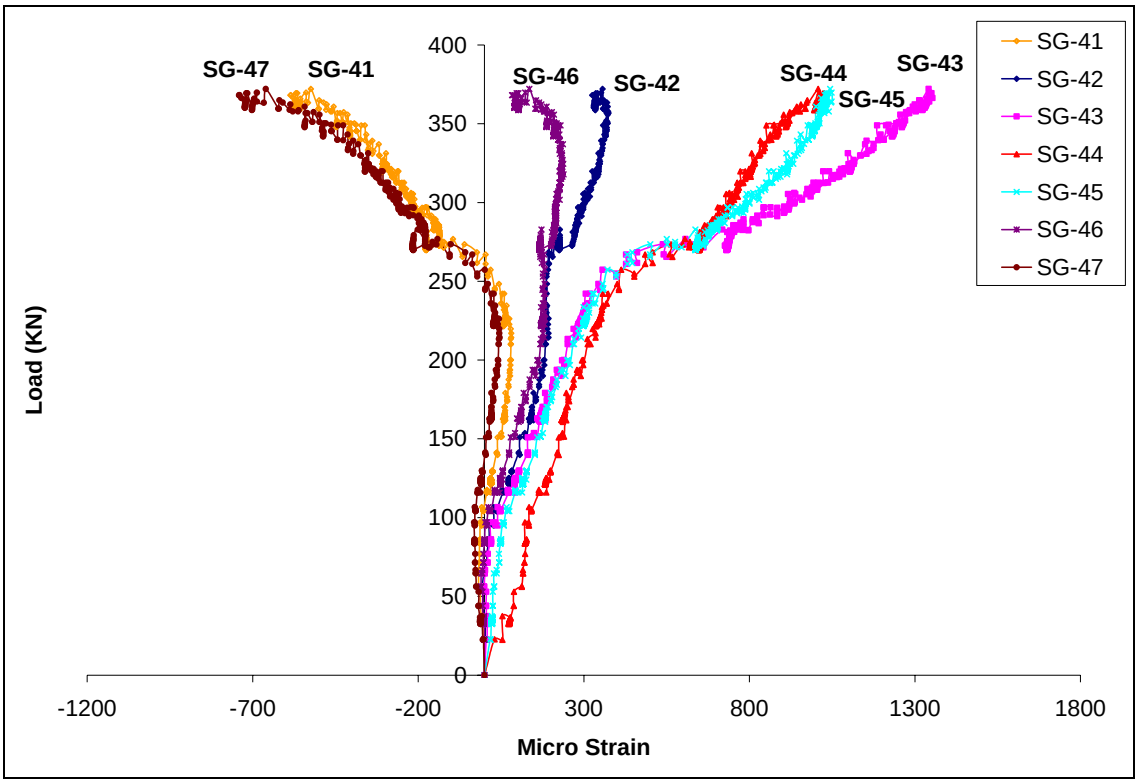


Figure 4. 57 – Strain vs. load for (top) row 4 of specimen GP-06

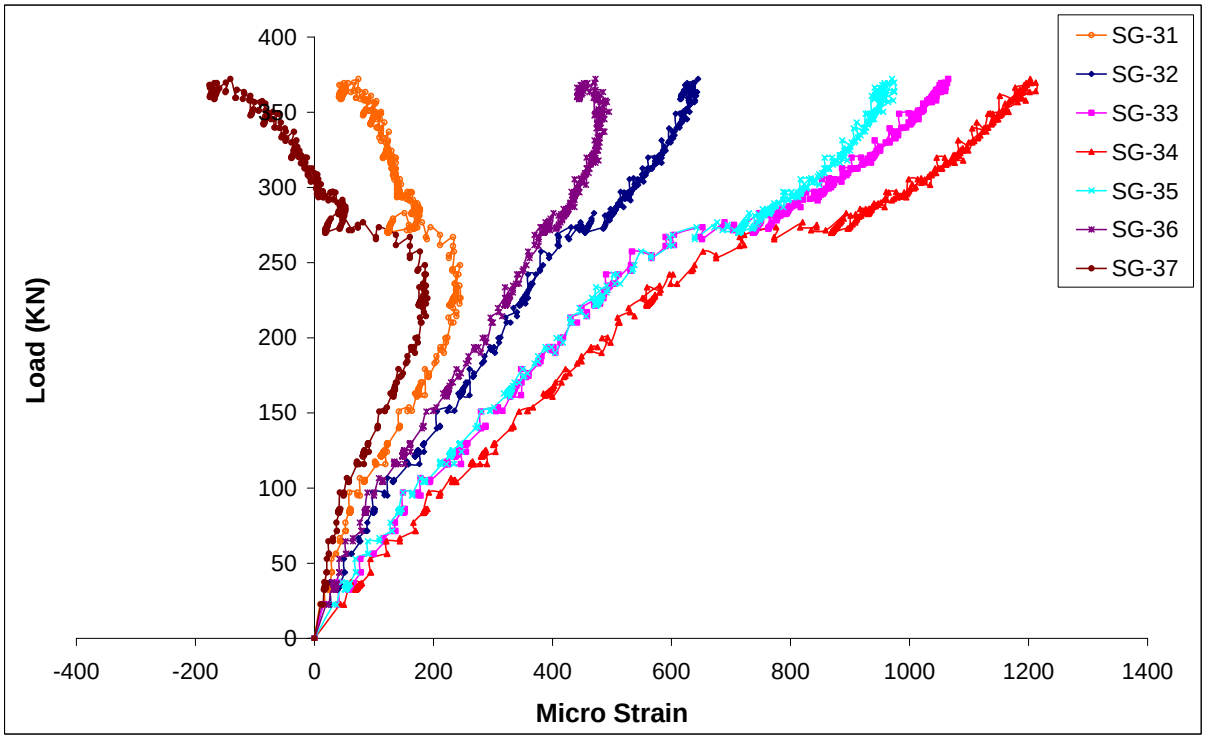


Figure 4. 58 – Strain vs. load for (middle) row 3 of specimen GP-06

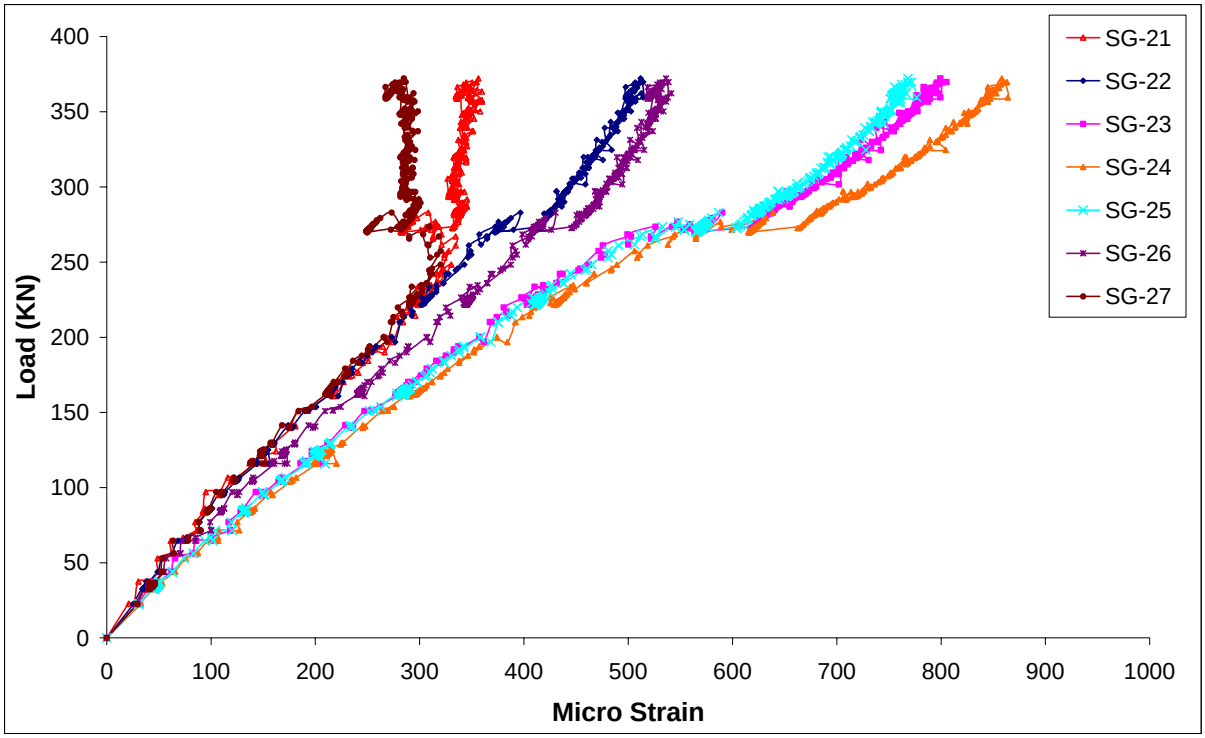


Figure 4. 59 – Strain vs. load for (lower) row 2 of specimen GP-06

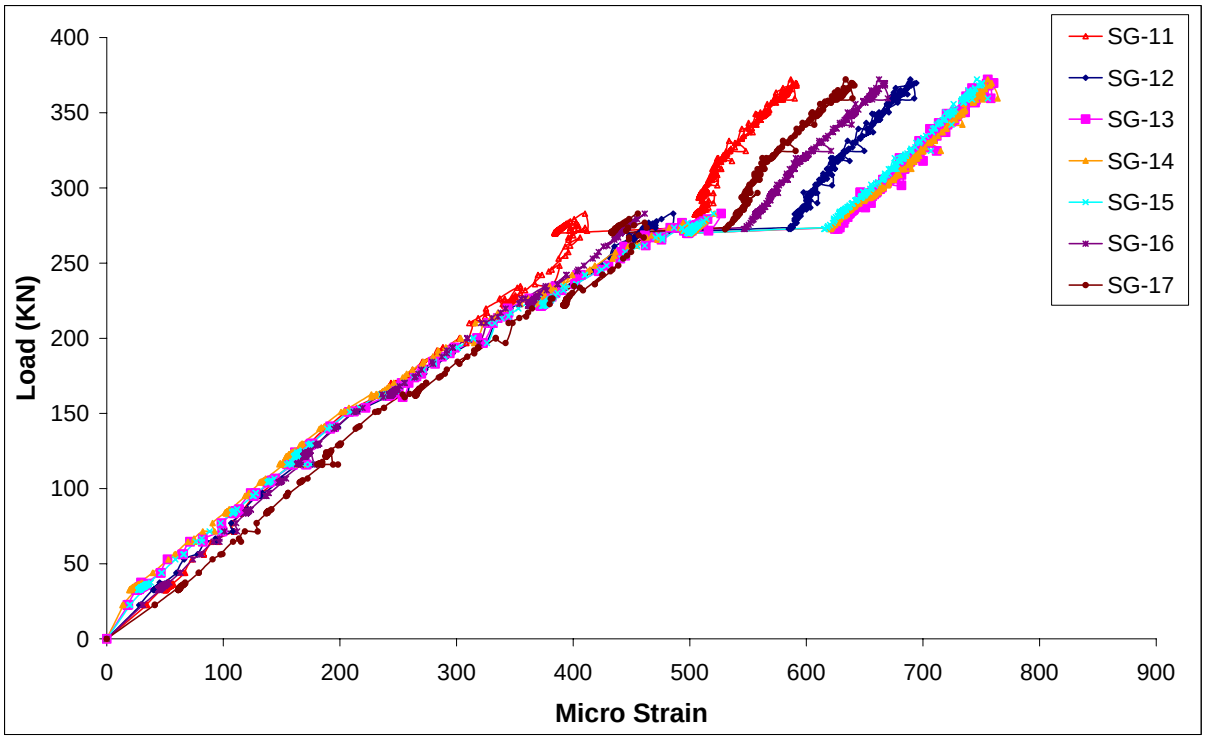


Figure 4. 60 – Strain vs. load for (bottom) row 1 of specimen GP-06

### 4.11 Specimen GP-07

Specimen GP-07 is a gusset plate of 7.0 mm thickness with 720 mm length and 500 mm width. One 38.1 mm (1.5 in) diameter SAE-Grade 8 (ASTM-A354) high strength bolt was used to connect the angle to the gusset plate. The diameter of hole was 40 mm. A 150 x 150 x 10.2 mm angle section was used in this test. This specimen is similar to GP-06 except the far end boundary condition was changed to fix by welding the bottom end of the plate to the thick shim plates which were bolted to the steel pedestal. Similar to GP-06, the locations of first row of strain gauges were 50 mm below the hole. The other three rows were installed with 100 mm offset between two rows. Figure 4.61 shows the location of strain gauge and LVDTs which were used for desired plate. There were two LVDT (LVDT-1 and LVDT-2) located on front and back of the plate surface. There was also one 100 mm (4 in) spring loaded LVDT (LVDT-3) in the front of jack.

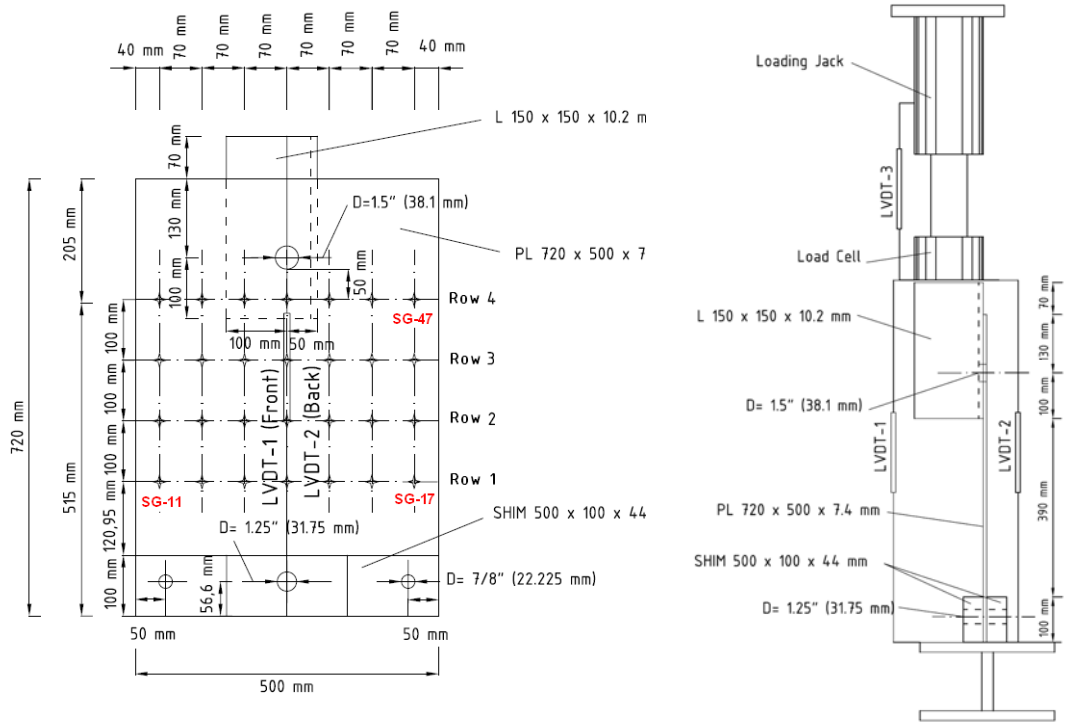


(a) Strain gauge location

(b) LVDT(s) location

Figure 4. 61 – Locations of strain gauges and LVDTs in specimen GP-07

The global behaviour of plate remains in elastic range until a load of about 250 kN and after that the plastic deformation started as the elongation of the hole increased and continued until the tearing is happened. Because of the failure at the bottom of the plate and rupturing of the welds at the bottom support, the test was discontinued and the tearing was not occurred in the plate. Figure 4.62 shows the load versus axial displacement response of specimen GP-07 through its loading which obtained from information of LVDT attached on angle and on the jack. The deformation of the gusset plate, the angle and the slip in the angle to gusset plate connection was recorded as total displacement. The maximum load obtained from this specimen is about 349.5 kN.

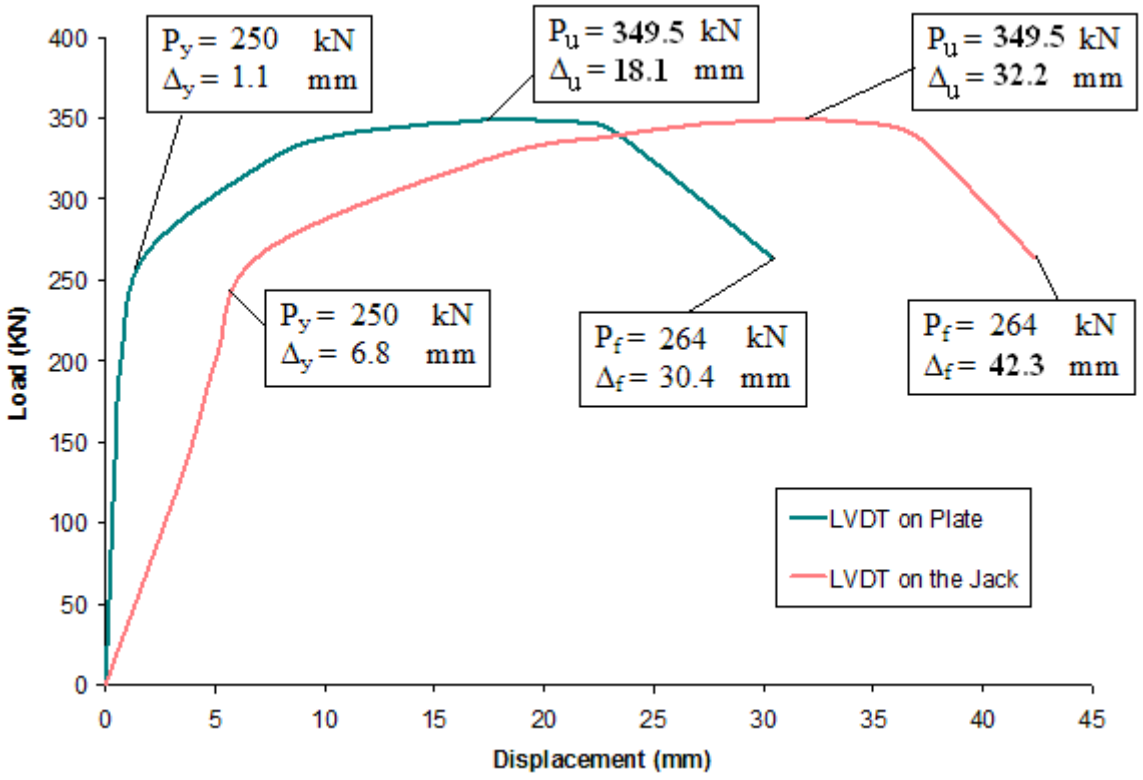


Figure 4. 62 – Load vs. axial displacement response of the gusset plate from LVDT located on plate and on the jack- Specimen GP-07

As it is shown in Figure 4.62, the specimen response under tension is reasonably stable. The load carrying capacity of the specimen increased as the deformation level

increased. The out-of-plane plate bending of specimen was accompanied by the increase in axial deformation and drop in load carrying capacity. The test was discontinued because the weld at the bottom support ruptured and plate specimen became rotated in its plane (Figure 4.63(c)).

After the completion of the test, the failed gusset plate specimen was examined. It was observed that the specimen failed in tension due a bearing failure of the plate material between the top bolt holes of the connection. The failed plate material is shown in Figure 4.63(d). The bolt hole in the connection had deformed by 10.8 mm due to the bearing of the bolts under load. The final length of hole was 48.85 mm.

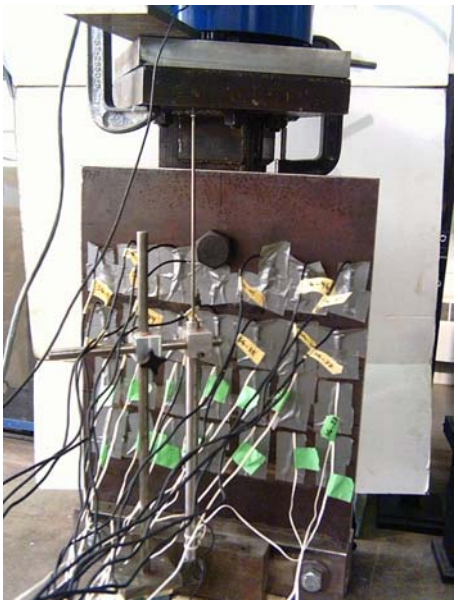

(a) Test setup


(b) LVDT location on angle

(c) Weld rupture at the bottom end

(d) Failed plate material in bolt connection

Figure 4. 63 – Plate bearing failure in bolted connection – Specimen GP-07

The angle was assumed to deform elastically. A compatibility of specimen deformation was preserved at the top of the gusset plate. The displacement of the top of the angle was assumed to be approximately equal to the in-plane displacement at the top of the gusset plate free edges. Since the angle is relatively rigid compared to the gusset plate, this assumption appears to be valid.

During the loading of specimen, strain gauges reading were recorded through data acquisition system. As soon as local yielding occurred at load about 250 kN in the plate and the stresses begin to redistribute, the strain become localized. Figure 4.64 to Figure 4.67 show the strain distributions from 50 kN to 350 kN. The strain gauges values are in micro strain.

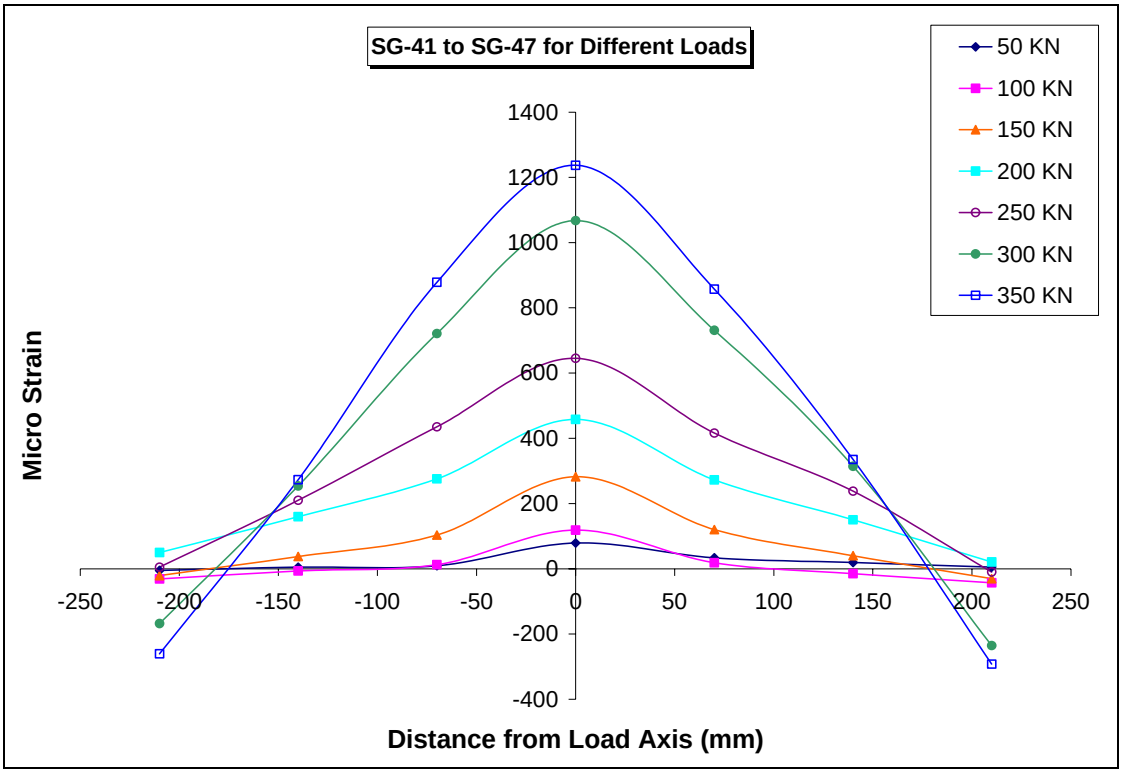


Figure 4. 64 – Strain values for (top) row 4 of specimen GP-07 at different loads

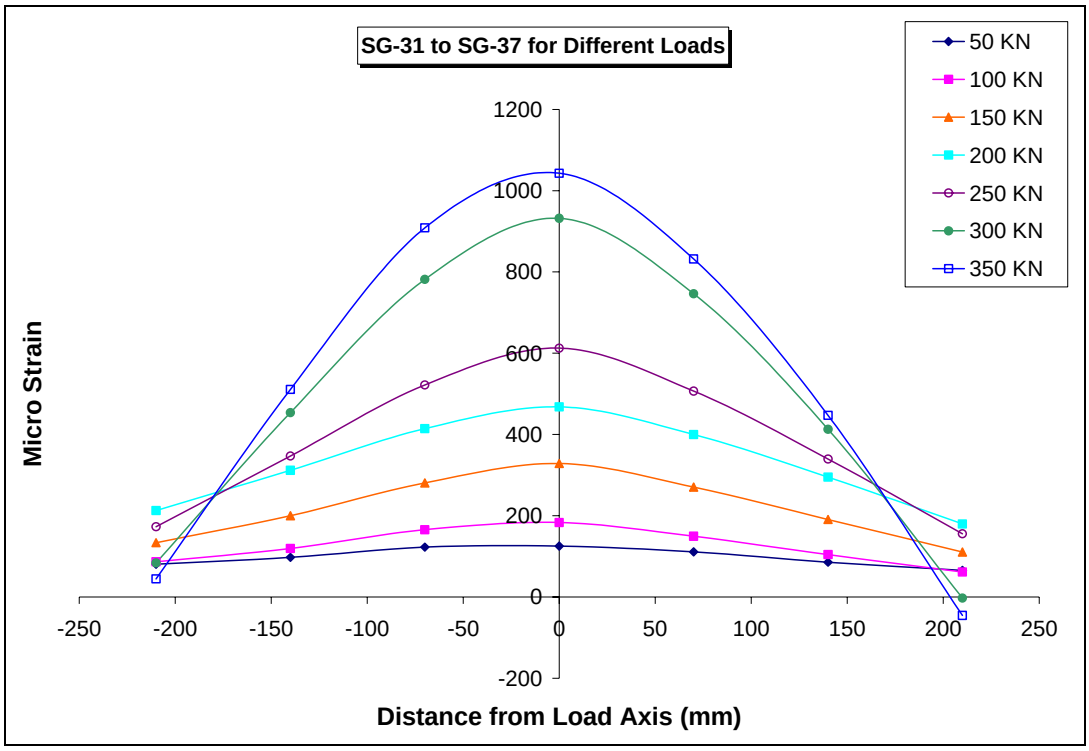


Figure 4. 65 – Strain values for (middle) row 3 of specimen GP-07 at different loads

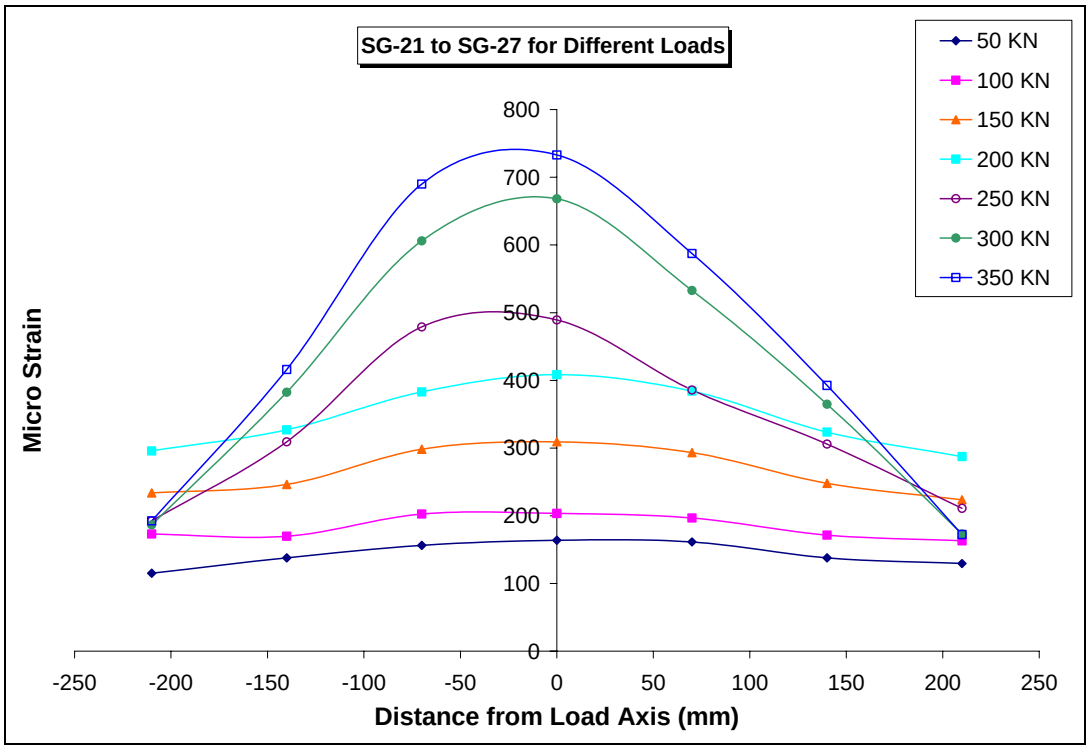


Figure 4. 66 – Strain values for (lower) row 2 of specimen GP-07 at different loads

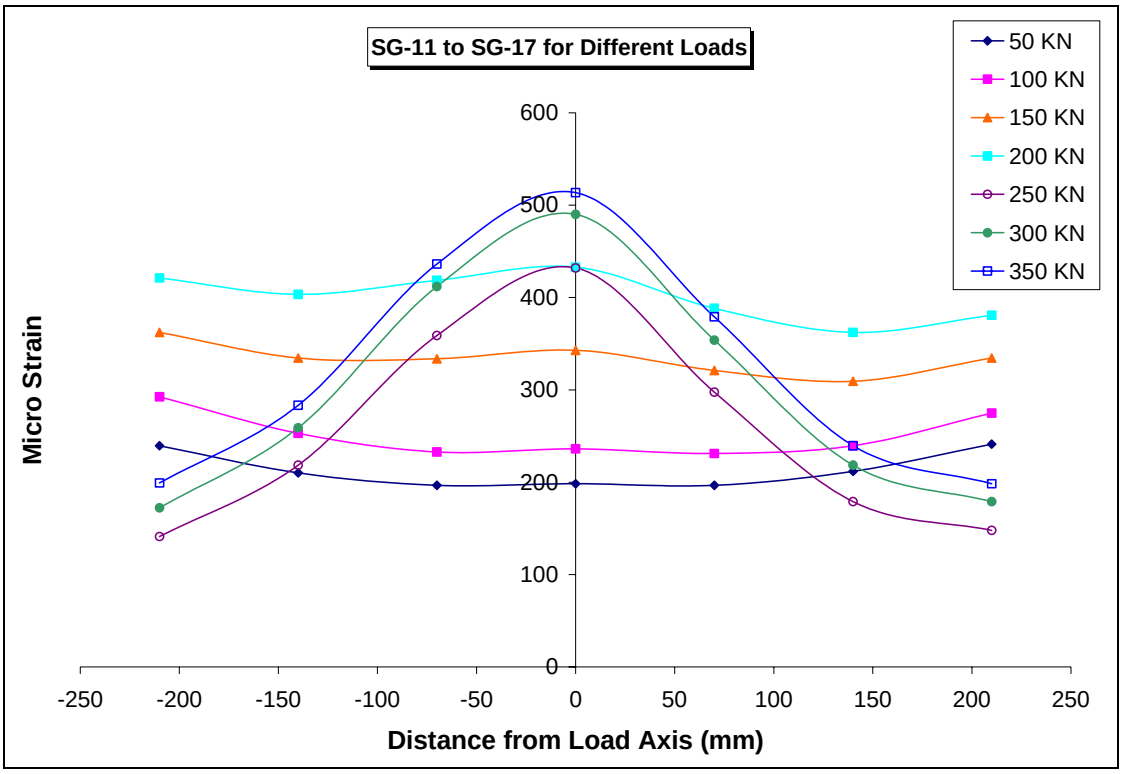


Figure 4. 67 – Strain values for (bottom) row 1 of specimen GP-07 at different loads

When the specimen load is increased beyond 250 kN yield load, strain value become non-uniform due to strain localization. When the strain reading at the 325 kN load are analyzed, the strain level are generally slightly less than two times those recorded at the 250 kN level. Figure 4.68 to Figure 4.71 show the strain distribution at different levels on plate surface. The strain gauges values are in micro strain. It should be noted that the maximum strain value (SG-44) is less than yield strain (0.0021) though it does not mean the yielding did not occur at the hole.

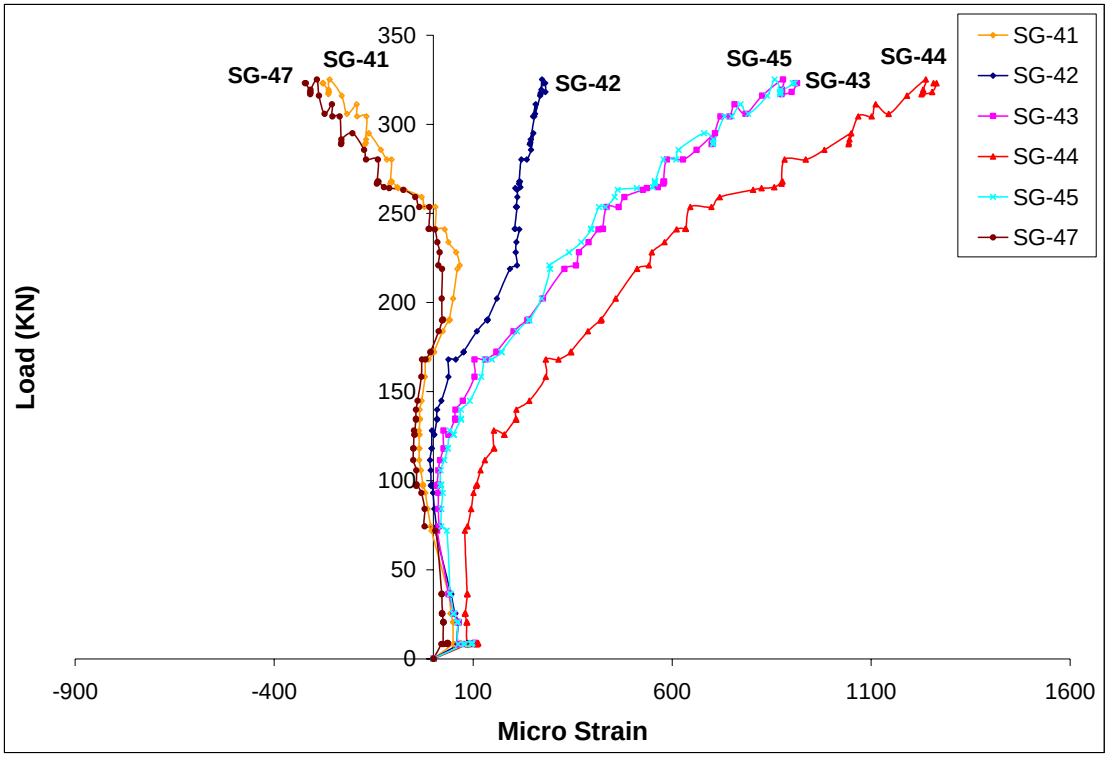


Figure 4. 68 – Strain vs. load for (top) row 4 of specimen GP-07

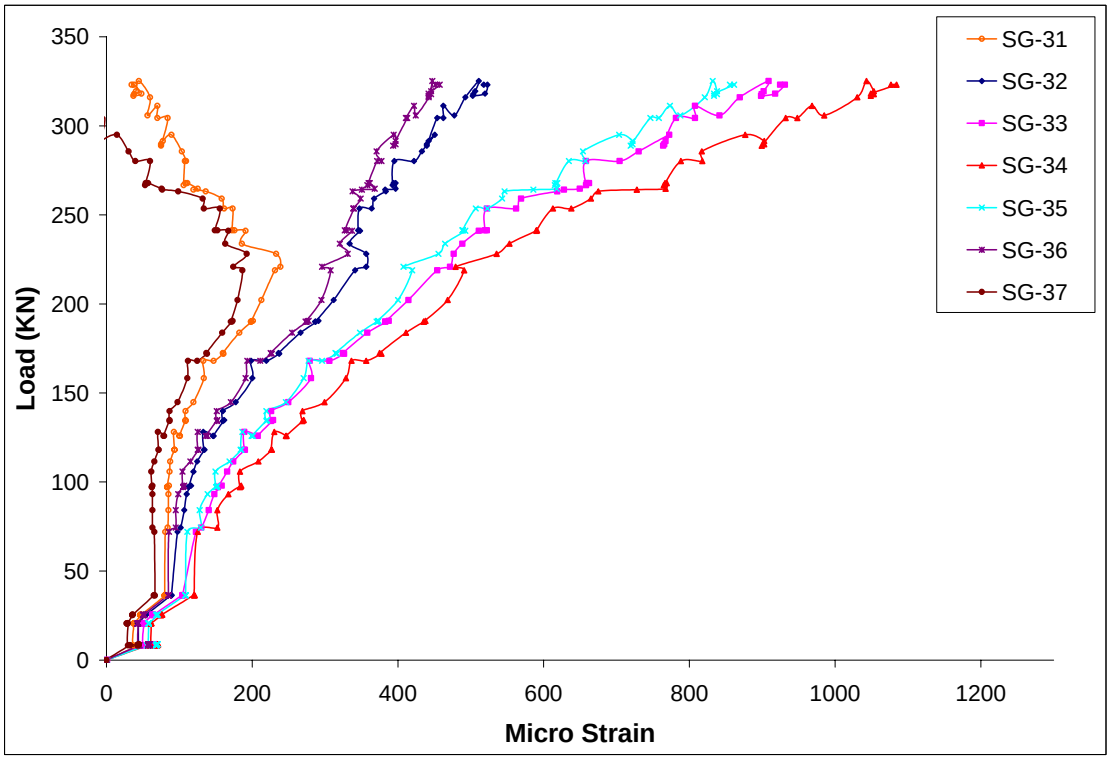


Figure 4. 69 – Strain vs. load for (middle) row 3 of specimen GP-07

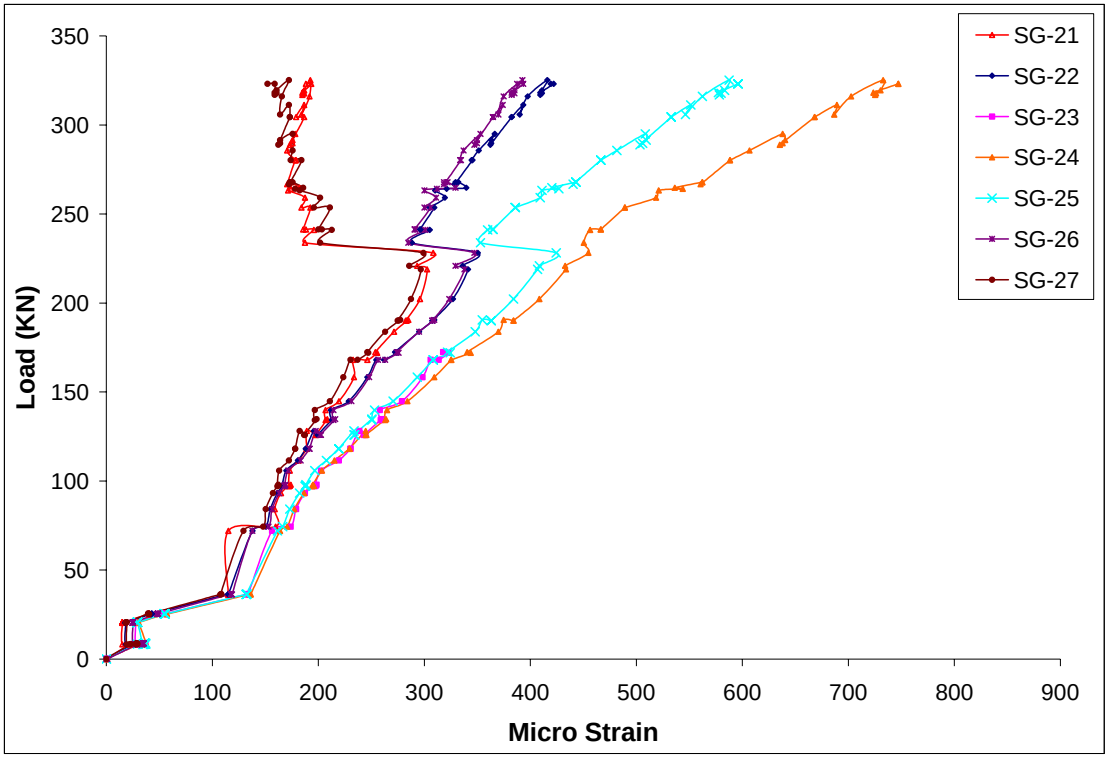


Figure 4. 70 – Strain vs. load for (lower) row 2 of specimen GP-07

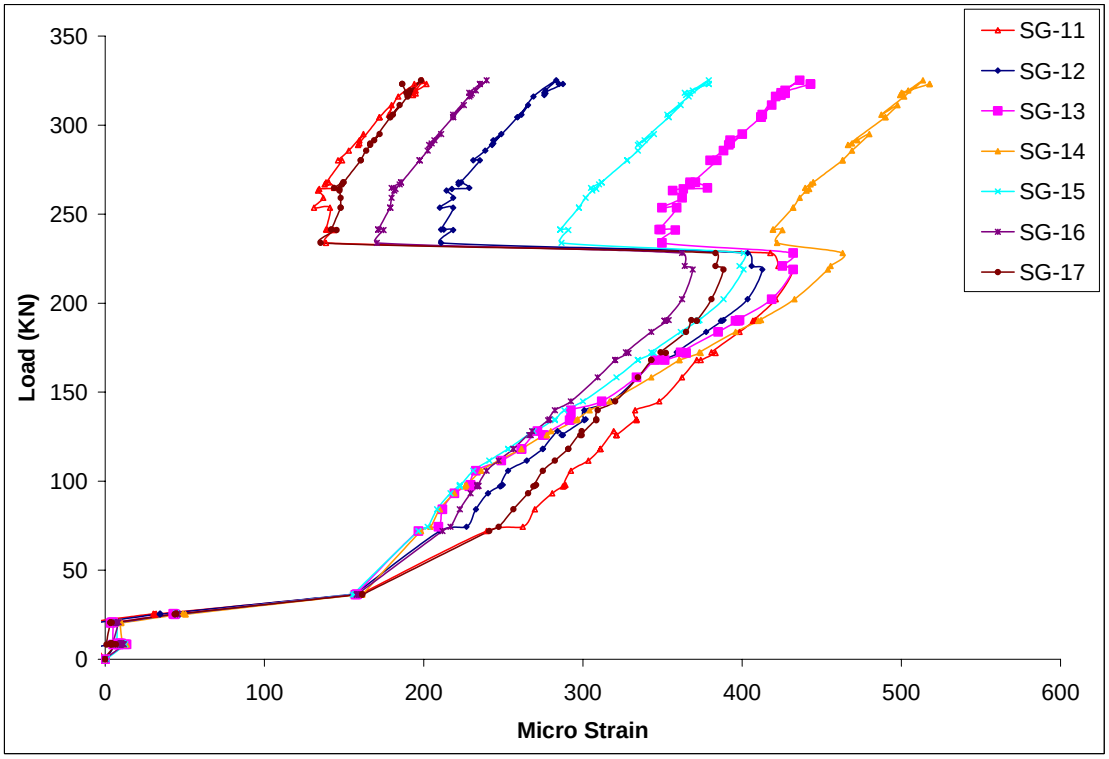


Figure 4. 71 – Strain vs. load for (bottom) row 1 of specimen GP-07

## 4.12 Specimen GP-08

Specimen GP-08 is a gusset plate of 7.0 mm thickness with 590 mm length and 500 mm width. Except the length of plate, this specimen was identical to GP-07. Also, the far-end boundary condition was changed from fixed (welded) to hinge (pinned) because the weld at far-end for GP-07 ruptured. Hence, specimens GP-06 and GP-08 are similar specimen. The objective of testing GP-08 was to capture more plastic deformation (more than what happened in GP-06) in the specimen. One 38.1 mm (1.5 in) diameter SAE-Grade 8 (ASTM-A354) high strength bolt was used to connect the angle to the gusset plate. A 150 x 150 x 10.2 mm angle section was used in this test. The diameter of top hole was 40 mm. The far-end condition for this specimen was changed back to pinned and so no welding was used at far end. The locations of first row of strain gauges were 50 mm below the hole. The other two rows were installed at 100 mm each apart. Figure 4.72 shows the location of strain gauge and LVDTs which were used for this specimen.

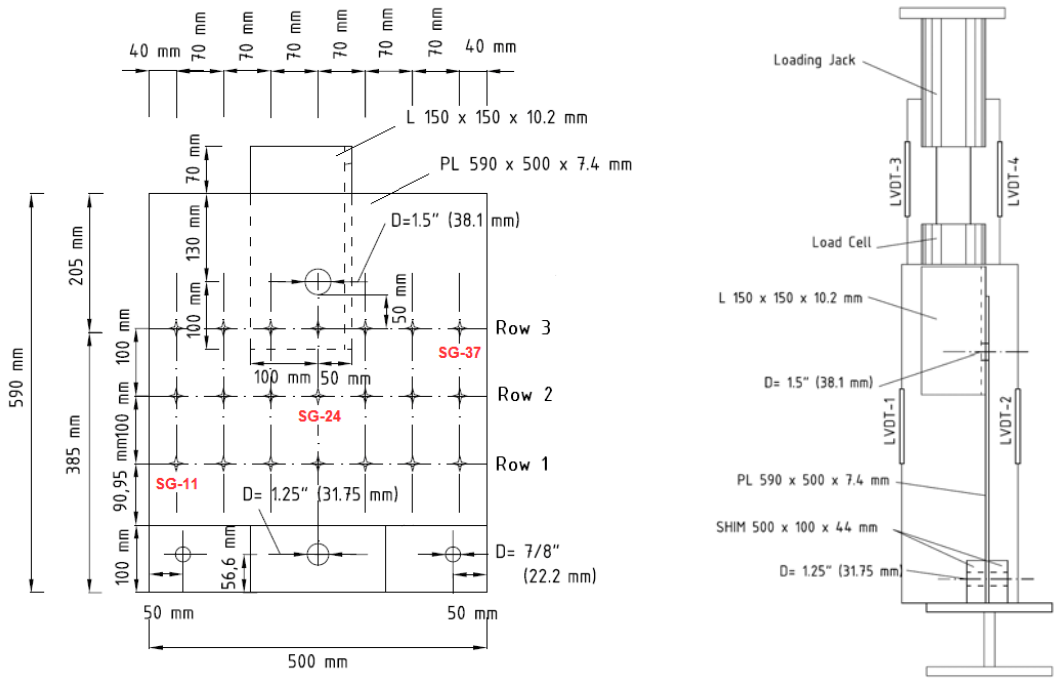


(a) Strain gauge location (b) LVDT(s) location

Figure 4. 72 – Locations of strain gauges in specimen GP-08

There were two LVDT (LVDT-1 and LVDT-2) located on front and back of the plate. There were also two 152.4 mm (6 in) spring and free core loaded LVDT (LVDT-3 and LVDT-4) in the front and back of load cell and jack connection, respectively.

The plate remained in elastic range until a load of about 300 kN (yield load) and after that the plastic deformation started as the elongation of the hole increased and continued until the tearing is happened. The test is continued until reaching the plastic range and the tearing is occurred in the plate. Figure 4.73 shows the load versus axial displacement response of specimen GP-07 through its loading which obtained from information of LVDT attached on angle and on the jack, respectively. The deformation of the gusset plate, the angle and the slip in the angle to gusset plate connection was recorded as total displacement. The maximum load capacity obtained from this specimen was 422.6 kN.

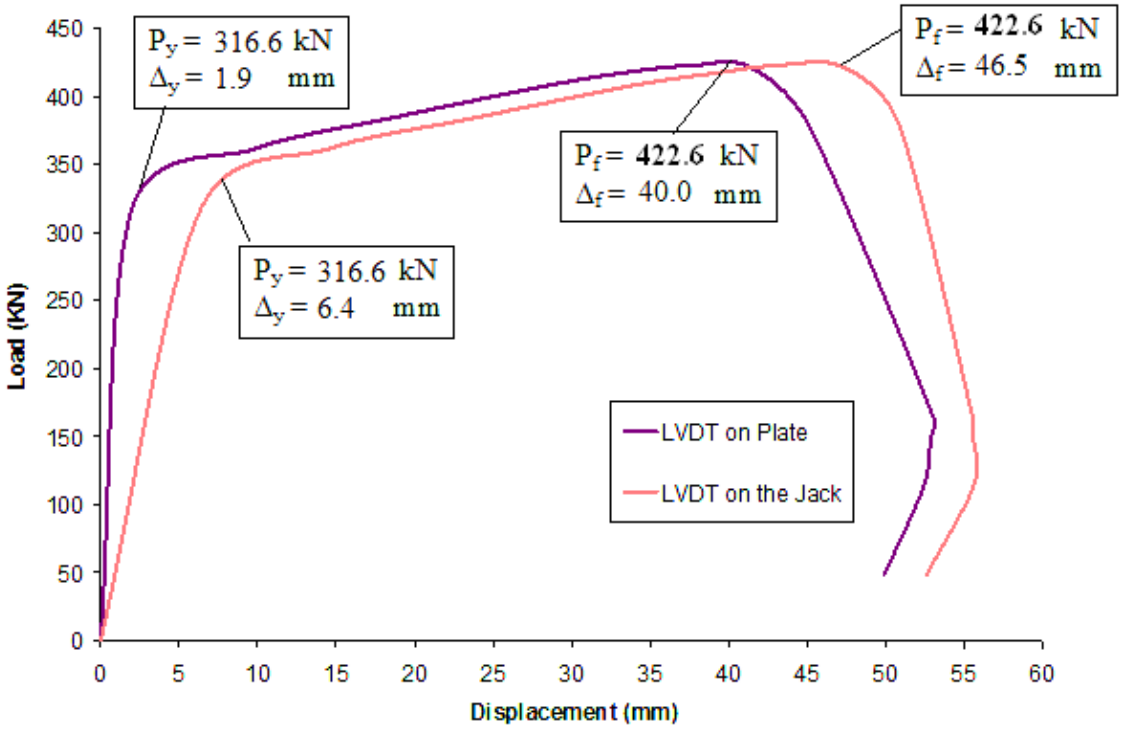


Figure 4. 73 – Load vs. axial displacement response of the gusset plate from LVDT located on plate and on the jack (LVDT-1 and LVDT-3) - Specimen GP-08

As it is shown in Figure 4.73, the specimen response under tension is reasonably stable. The load carrying capacity of the specimen increased as the deformation level increased. The out-of-plane plate bending of specimen was accompanied by the increase in axial deformation and drop in load carrying capacity.

After the completion of the test, the failed gusset plate specimen was examined. It was observed that the specimen failed in tension due a bearing failure of the plate material between the bolt holes of the connection. The failed plate material is shown in Figure 4.74(d). The final elongation of top hole was measured as 94.7 mm. Hence, the bolt hole in the connection had elongated by 56.6 mm due to the bearing of the bolts under load.

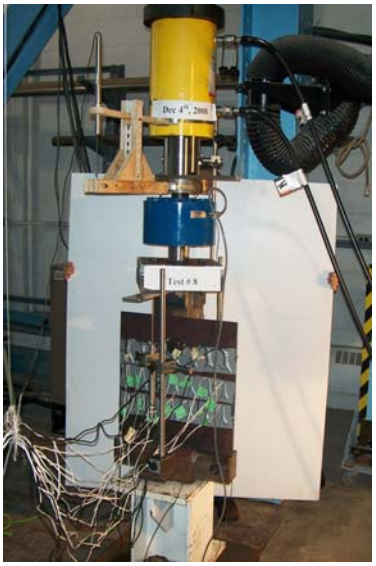

(a) Test setup

(b) LVDT location on angle

(c) Top hole tearing


(d) Top hole elongation

Figure 4. 74 – Plate bearing failure in bolted connection – Specimen GP-08

The angle was assumed to deform elastically. A compatibility of specimen deformation was preserved at the top of the gusset plate. The displacement of the top of the angle was assumed to be approximately equal to the in-plane displacement at the top of the gusset plate free edges. Since the angle is relatively rigid compared to the gusset plate, this assumption appears to be valid.

During the loading of specimen, strain gauges reading were recorded through data acquisition system. As soon as local yielding occurred in the plate at 300 kN and the stresses began to redistribute, the strains localized. Figure 4.75 to Figure 4.77 show the strain distributions from 50 kN to 420 kN. The strain gauges values are in micro strain.

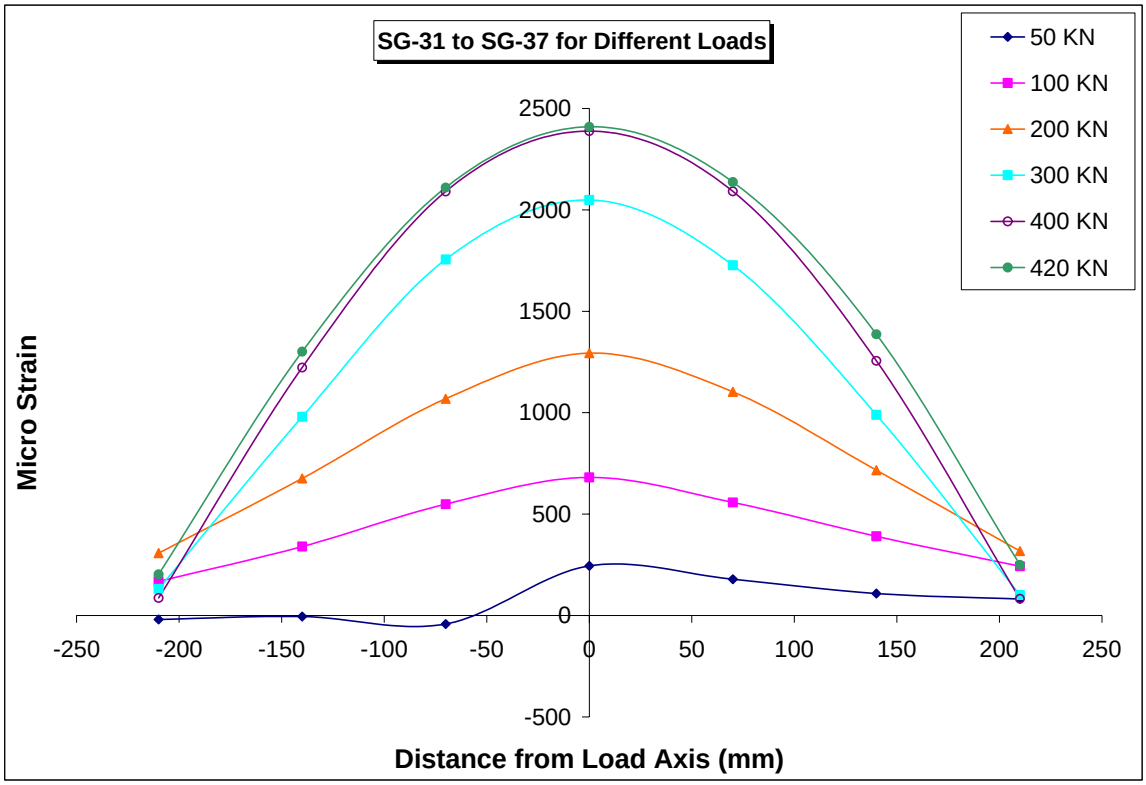


Figure 4. 75 – Strain values for (top) row 3 of specimen GP-08 at different loads

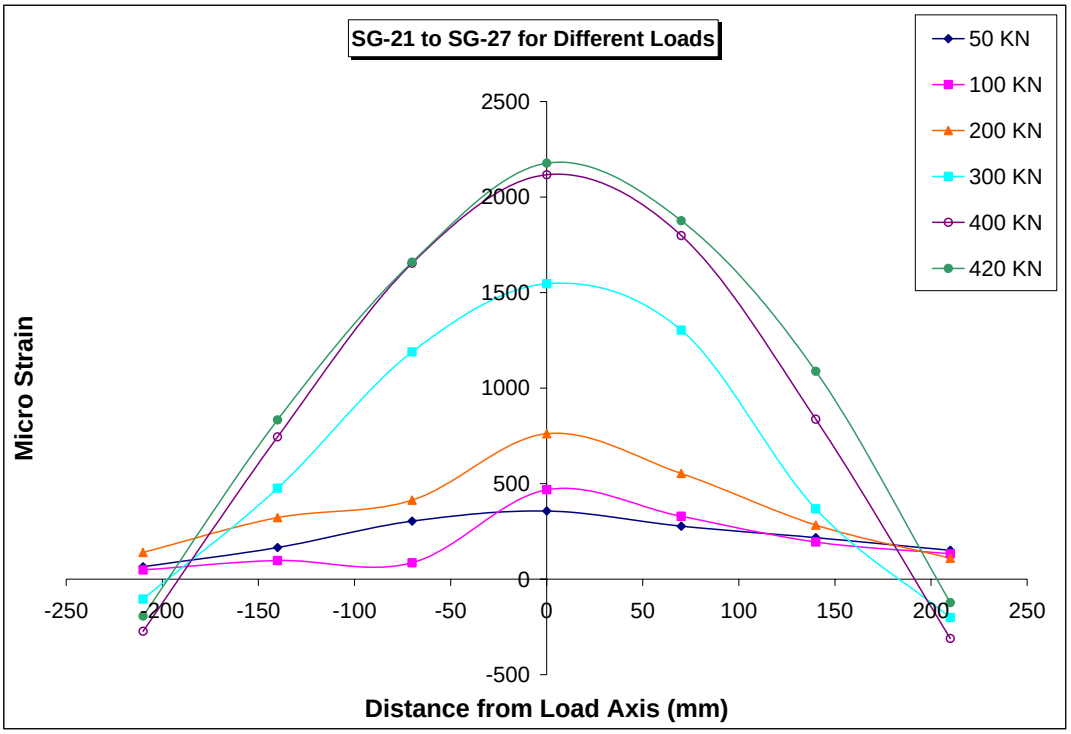


Figure 4. 76 – Strain values for (middle) row 2 of specimen GP-08 at different loads

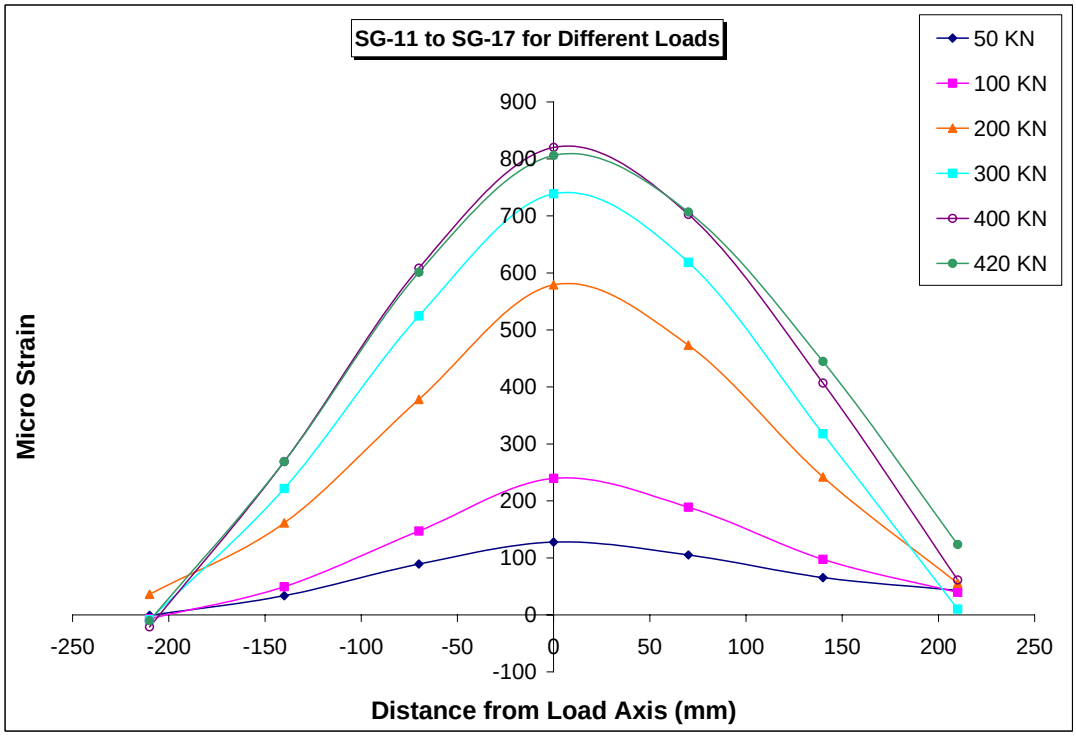


Figure 4. 77 – Strain values for (lower) row 1 of specimen GP-08 at different loads

When the specimen load is increased beyond 250 kN (yield load), strain level are changed. When the strain reading at the 420 kN load are analyzed, the strain level are

generally slightly less than two times those recorded at the 250 kN level. Figure 4.78 to Figure 4.80 show the strain distribution at different levels on plate surface. The strain gauges values are in micro strain.

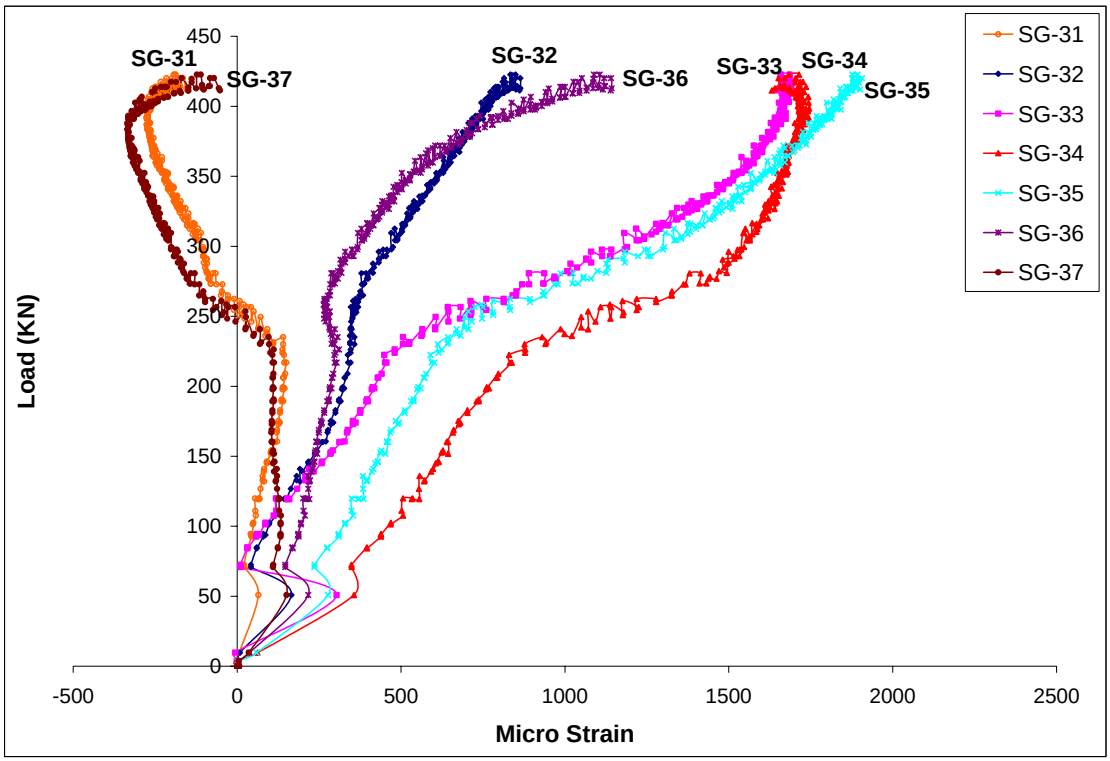


Figure 4. 78 – Strain vs. load for (middle) row 3 of specimen GP-08

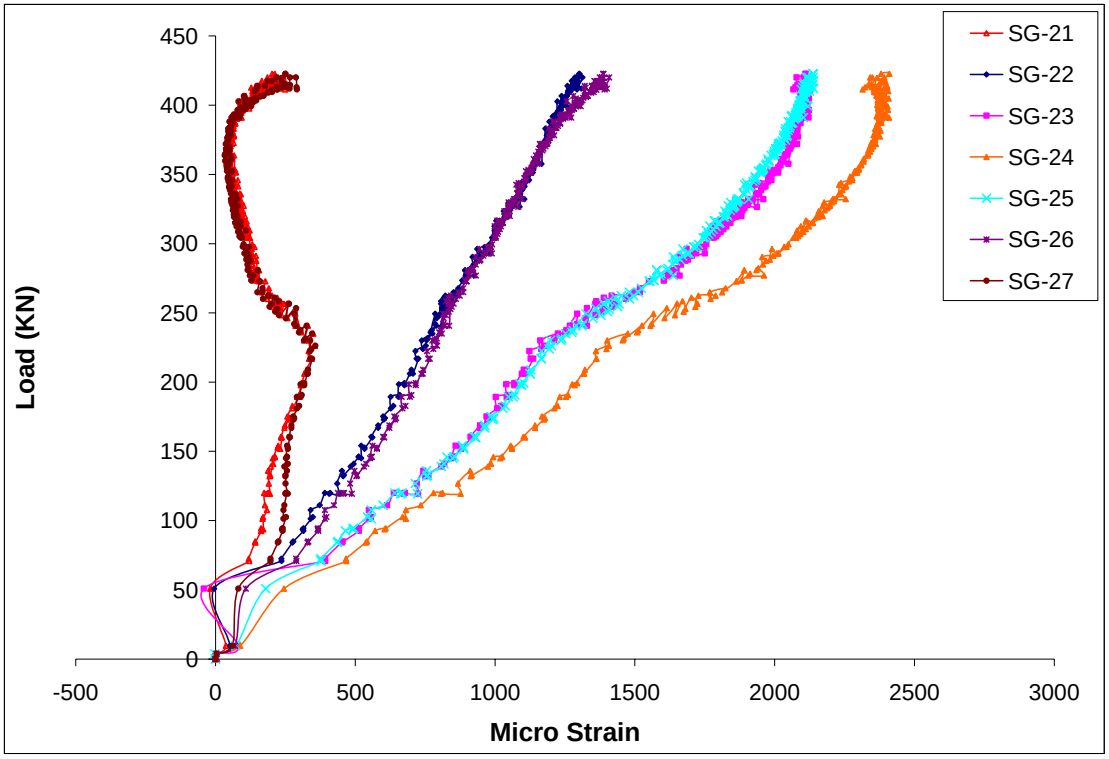


Figure 4. 79 – Strain vs. load for (lower) row 2 of specimen GP-08

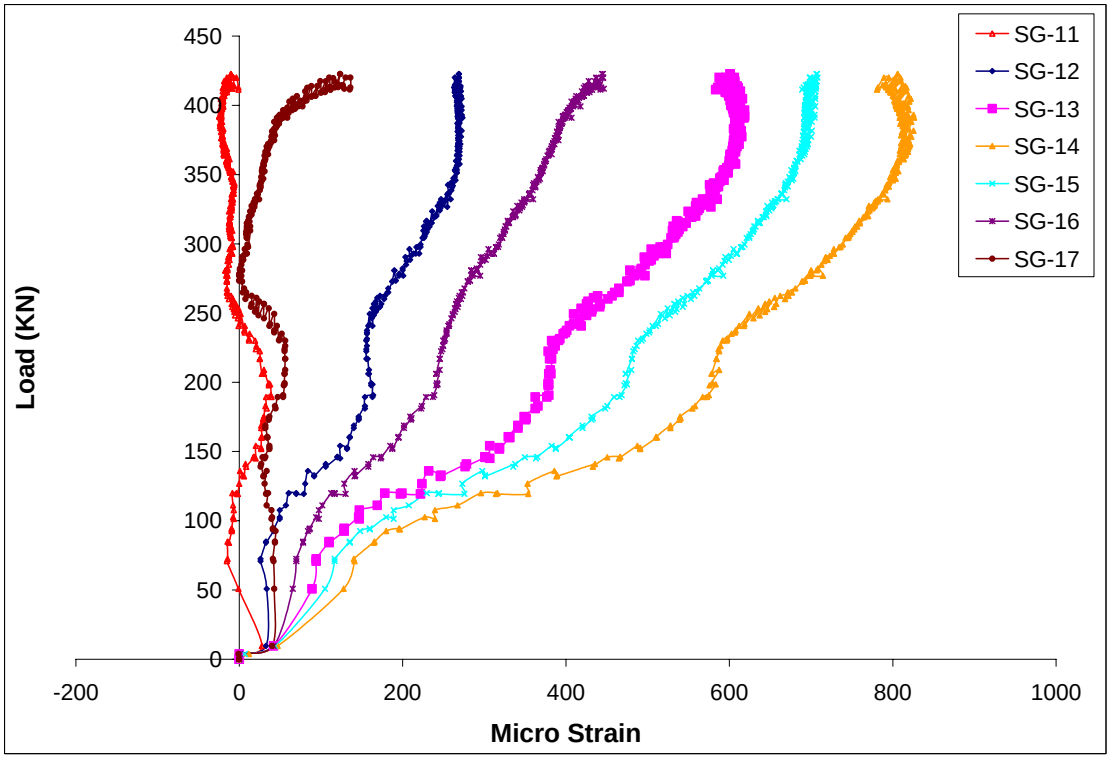


Figure 4. 80 – Strain vs. load for (bottom) row 1 of specimen GP-08

## 4.13 Specimen GP-09

This is the first specimen with two bolts. Specimen GP-09 is a gusset plate of 6.9 mm thickness with 640 mm length and 500 mm width. Two 38.1 mm (1.5 in) diameter SAE-Grade 8 (ASTM-A354) high strength bolt was used to connect the angle to the gusset plate. The specimen was a plate with two bolts. A 150 x 150 x 10.2 mm angle section was used in this test. Diameter of each hole was 40 mm. The far-end condition was pinned. The location of first row (row 4) of strain gauges was between the two holes (65 mm from center of both holes). The center to center distance between two holes was 130 mm.

The first row (row 2) below the bottom hole was at 50 mm away (70 mm away from center of hole). The subsequent rows were at 70 mm and 100 mm centers as shown in Figure 4.89. Figure 4.81 shows the location of strain gauges which were used for this specimen. Two LVDTs (LVDT-1 and LVDT-2) were used one on front face of plate and back of the plate. There were also two 152.4 mm (6 in) spring and free core loaded LVDT (LVDT-3 and LVDT-4) in the front and back of load cell and jack connection, respectively.

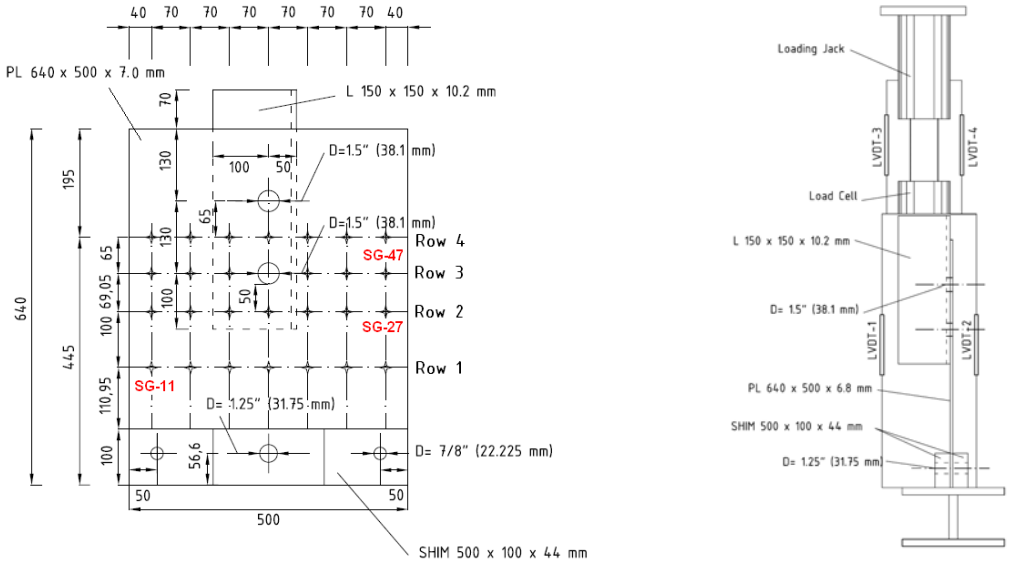


(a) Strain gauge location (b) LVDT(s) location

Figure 4. 81 – Locations of strain gauges in specimen GP-09

The plate remained in elastic range until a load about 280 kN (yield load) and after that the plastic deformation started because of the elongation in holes. This deformation can continue until the tearing occurs above top hole or until the bolt fails in shear. The test was continued until reaching the plastic range but the tearing did not occur in the plate, neither, the bolt failed in shear. Figure 4.82 shows the load versus axial displacement response of specimen GP-09 which obtained using LVDT attached on angle that is at the front and back of the plate and on the jack. The deformation of the gusset plate, the angle and the slip in the angle to gusset plate connection was recorded as total displacement. The maximum load capacity was recorded as 549.3 kN.

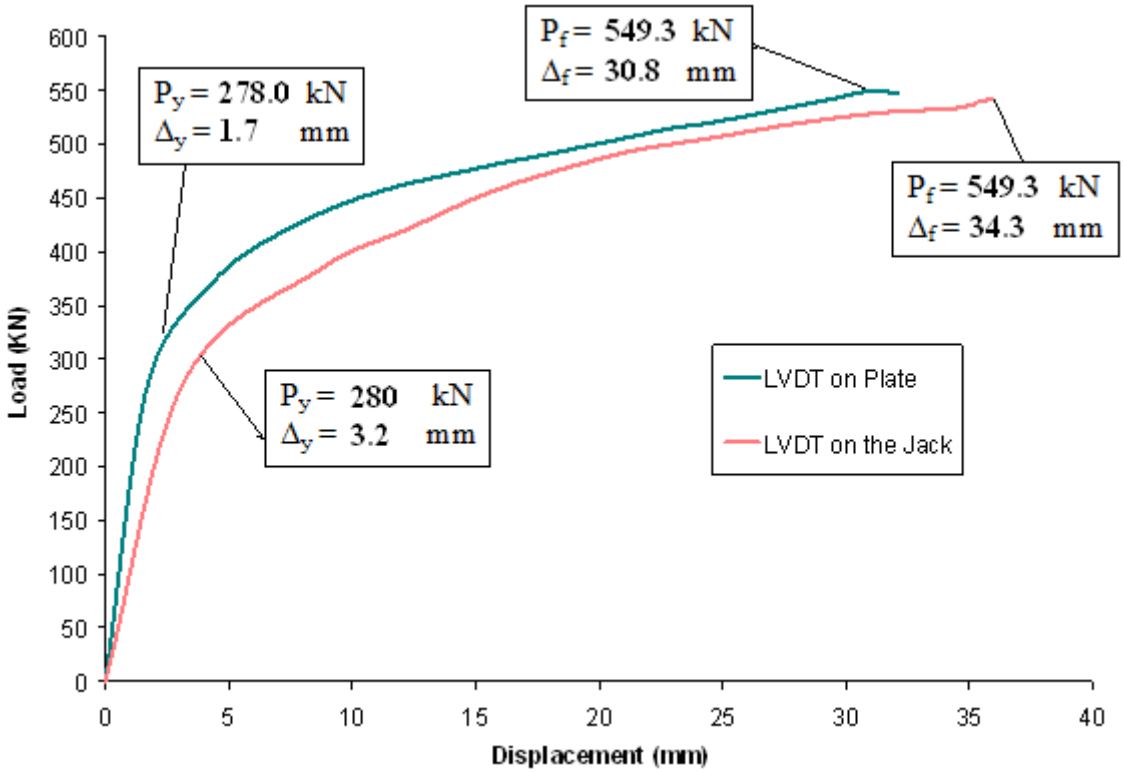


Figure 4. 82 – Load vs. axial displacement response of the gusset plate from LVDT located on plate and on the jack (LVDT-1 and LVDT-4) - Specimen GP-09

As it is shown in Figure 4.82, the specimen response under tension load was increasing reasonably and finally became stable. The load carrying capacity of the

specimen increased as the deformation level increased. The out-of-plane plate bending of specimen was accompanied by the increase in axial deformation and drop in load carrying capacity. The test was discontinued due to serve out-of-plane buckling of plate.

After the completion of the test, the failed gusset plate specimen was examined. It was observed that the specimen failed in tension due a bearing failure of the plate at both bolt holes of the connection. The failed plate material is shown in Figure 4.83. The bolt holes in the connection had elongated by 8.6 mm due to the bearing of the bolt holes under load (Figure 4.83(d)). Hence, the final length of each top hole was 40.4 mm.


(a) Test setup

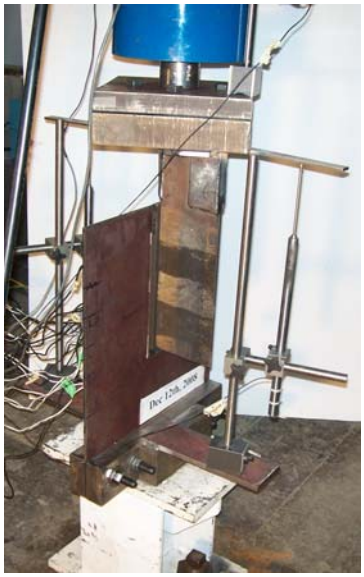

(b) LVDT location on angle


(c) Local out-of-plane buckling of plate top end


(d) Elongation of bolt holes

Figure 4. 83 – Plate bearing failure in bolted connection – Specimen GP-09

The angle was assumed to deform elastically. A compatibility of specimen deformation was preserved at the top of the gusset plate. The displacement of the top of the angle was assumed to be approximately equal to the in-plane displacement at the top of the gusset plate free edges. Since the angle is relatively rigid compared to the gusset plate, this assumption appears to be valid.

During the loading of specimen, strain gauges reading were recorded through data acquisition system. As soon as local yielding occurred in the plate and the strains localized and began to redistribute. Figure 4.84 to Figure 4.87 show the strain distributions from 50 kN to 550 kN. The strain gauges values are in micro strain.

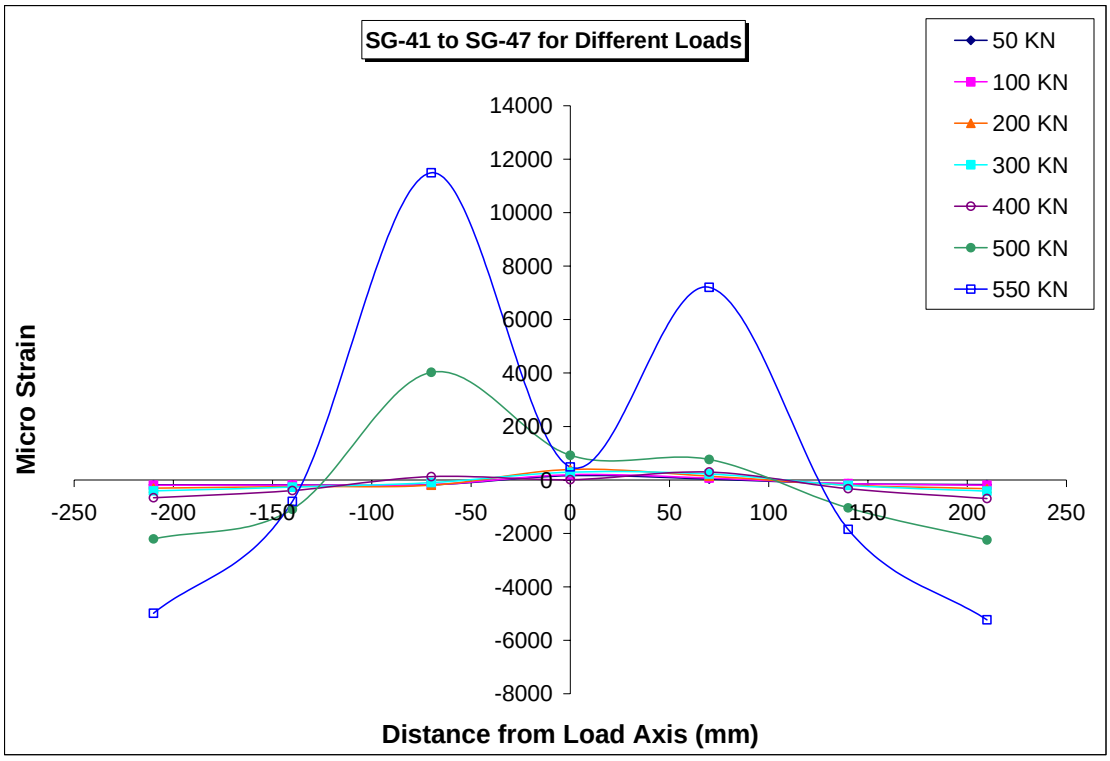


Figure 4. 84 – Strain values for (top) row 4 of specimen GP-09 at different loads

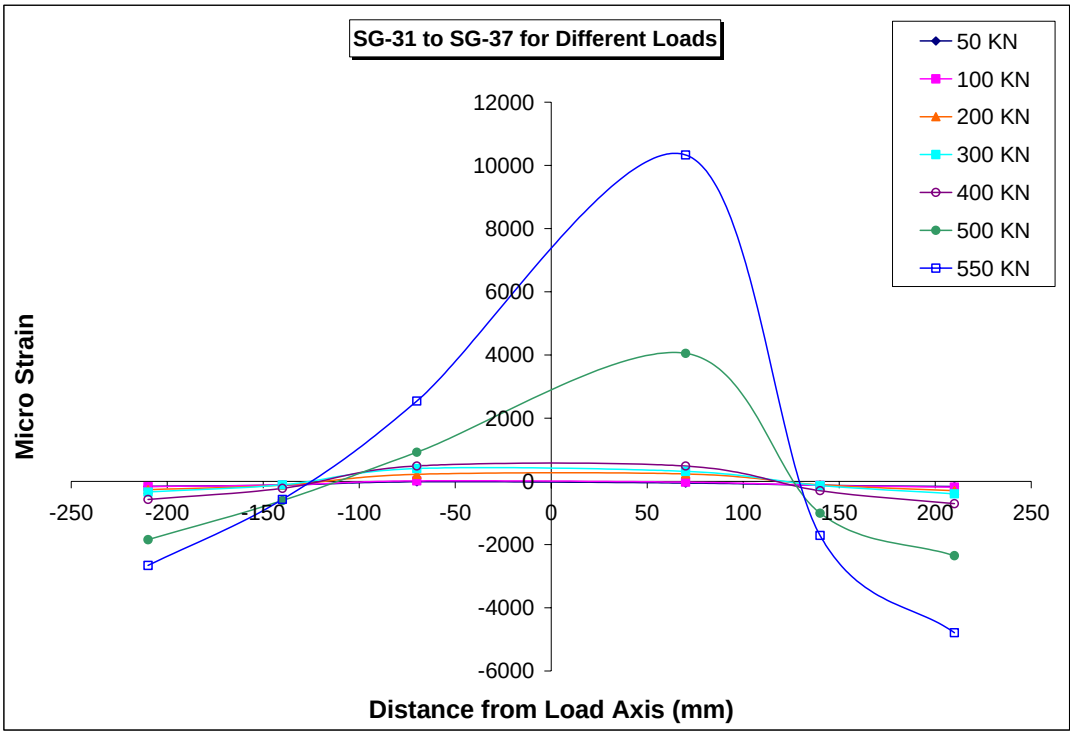


Figure 4. 85 – Strain values for (middle) row 3 of specimen GP-09 at different loads

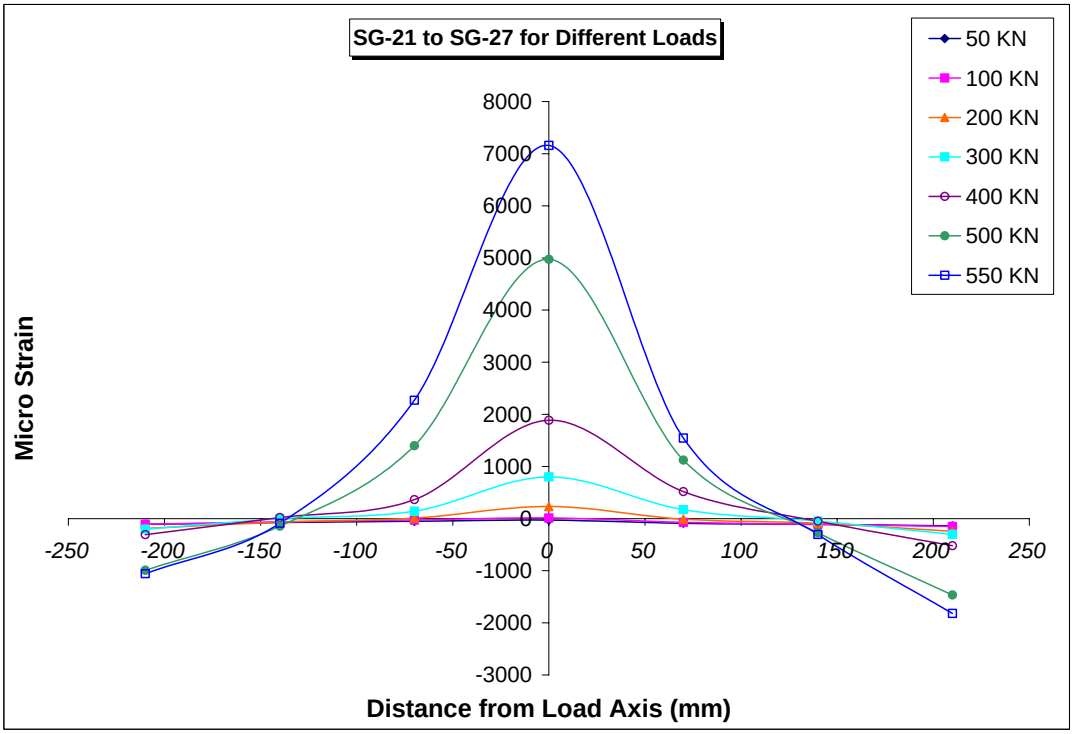


Figure 4. 86 – Strain values for (lower) row 2 of specimen GP-09 at different loads

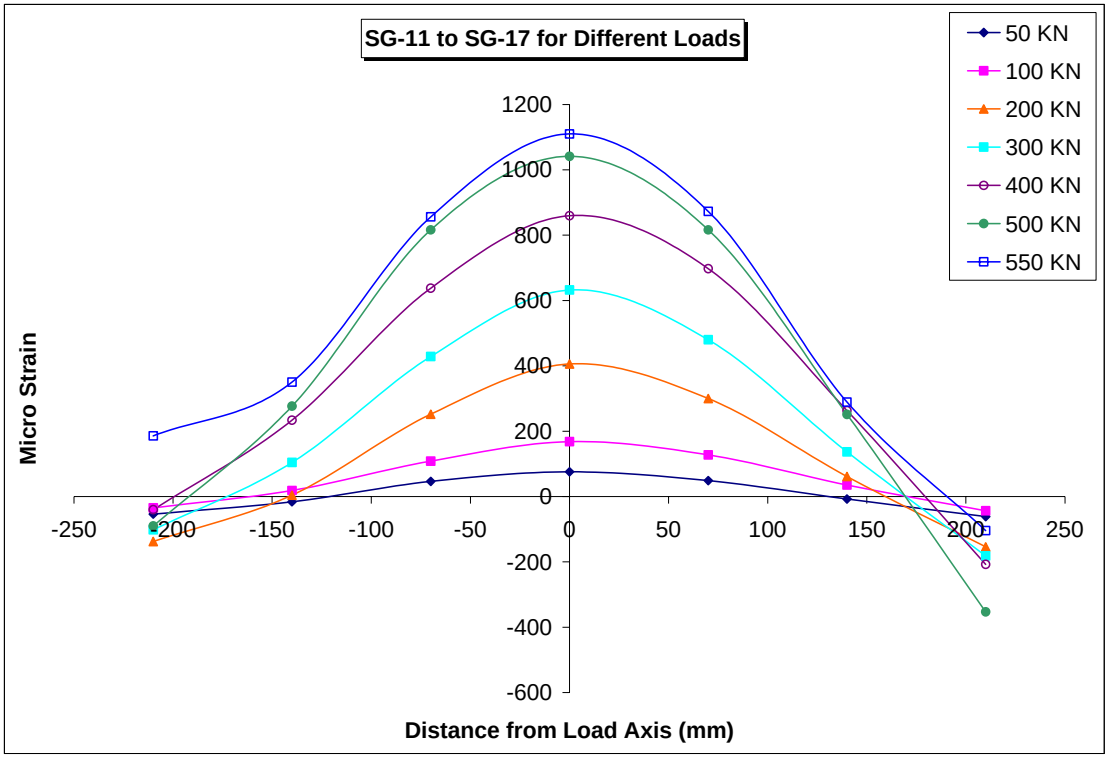


Figure 4. 87 – Strain values for (bottom) row 1 of specimen GP-09 at different loads

When the specimen load is increased beyond 280 KN level (yield load), strain values become non-uniform. When the strain reading at the 550 kN load are analyzed, the strain level are generally slightly more than one and half times those recorded at the 280 KN level. Figure 4.88 to Figure 4.91 show the strain distribution at different levels on plate surface. The strain gauges values are in micro strain.

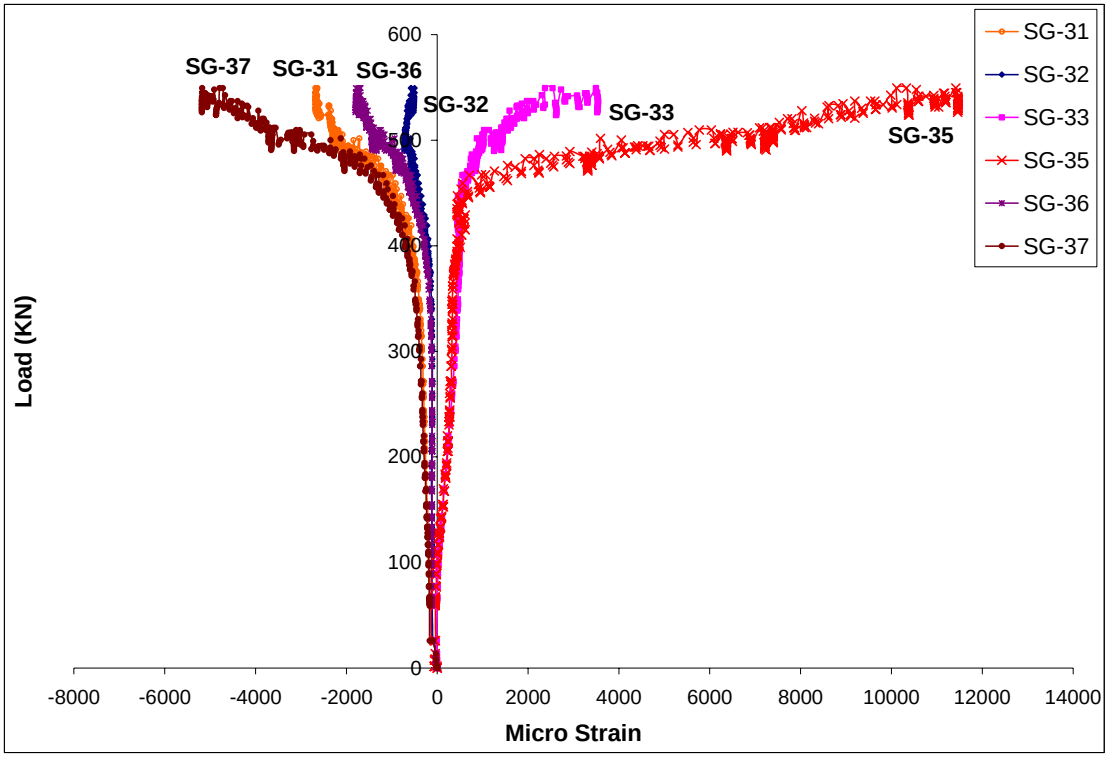


Figure 4. 88 – Strain vs. load for (top) row 4 of specimen GP-09

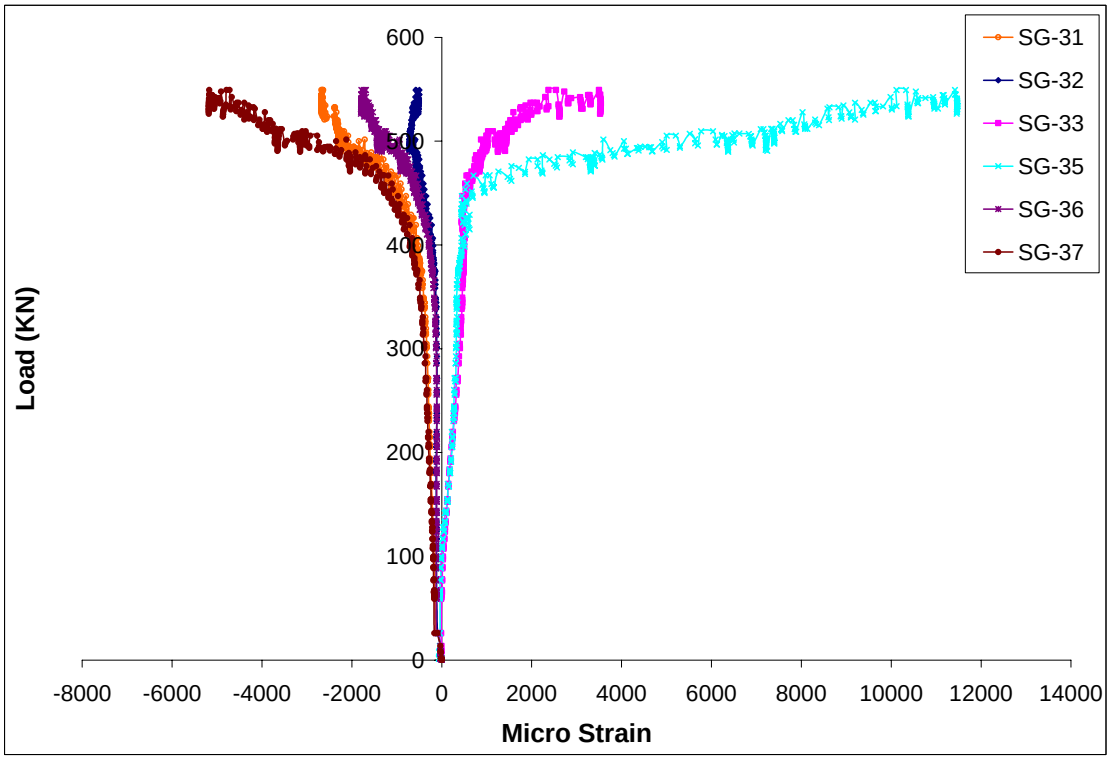


Figure 4. 89 – Strain vs. load for (middle) row 3 of specimen GP-09

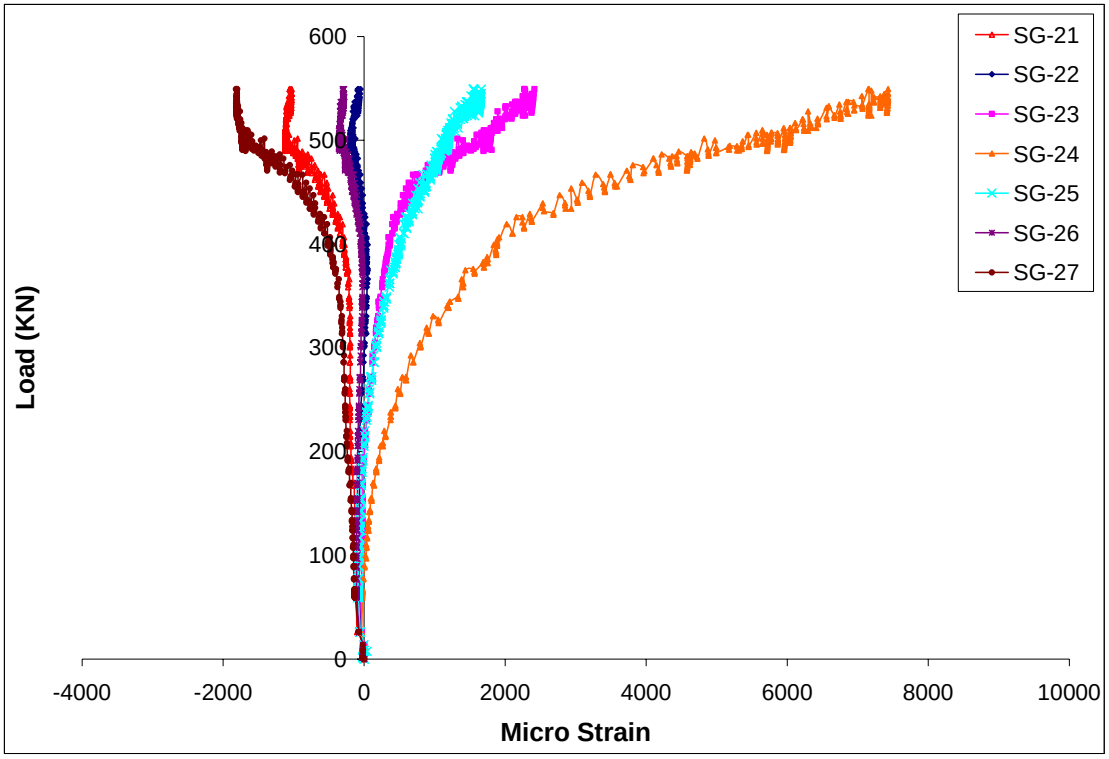


Figure 4. 90 – Strain vs. load for (lower) row 2 of specimen GP-09

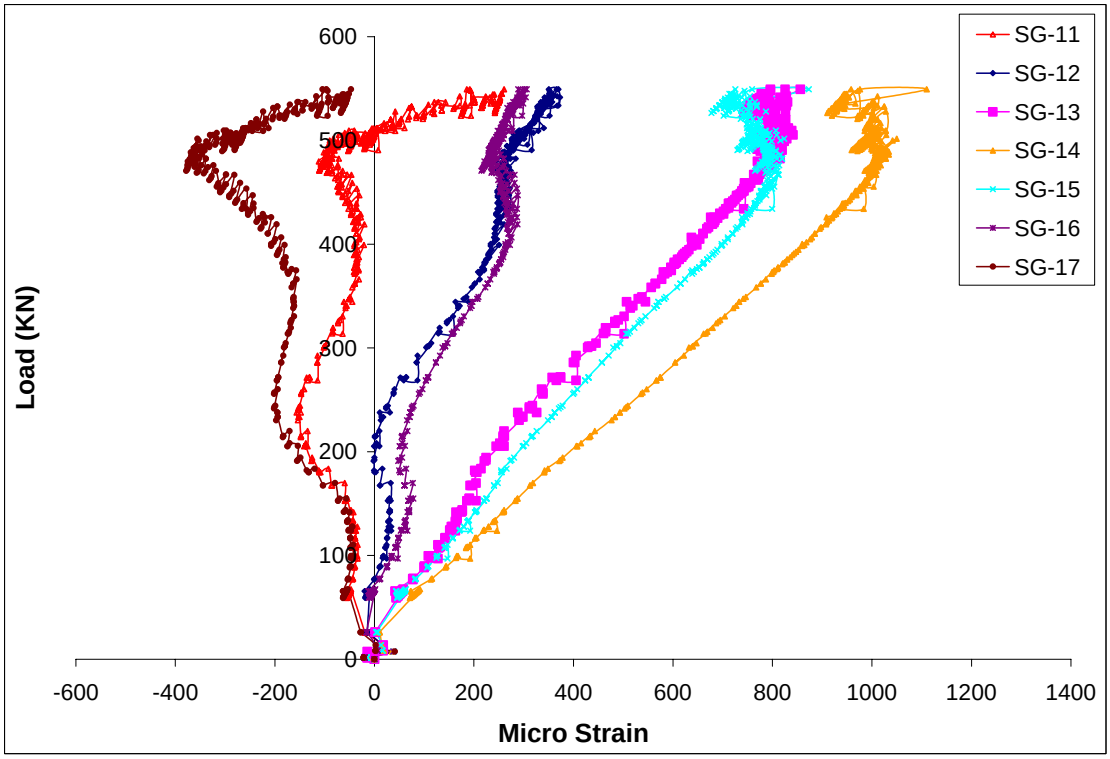


Figure 4. 91 – Strain vs. load for (bottom) row 1 of specimen GP-09

## 4.14 Specimen GP-10

Specimen GP-10 is the second specimen with two bolts and it was a gusset plate of 6.9 mm thickness with 620 mm length and 500 mm width. This specimen was almost identical to GP-09 (except length is 20 mm different). The intention was to repeat test of specimen GP-09. Specimen GP-09 had severe out-of-plane buckling at top end because the bolts were just snug tight using a manual wrench. However, in specimen GP-10, the bolts were tightened using power wrench to minimize the out-of-plane buckling.

Two 38.1 mm (1.5 in) diameter SAE-Grade 8 (ASTM-A354) high strength bolt was used to connect the angle to the gusset plate. The specimen was a plate with two bolts. The diameter of each hole was 40 mm. A 150 x 150 x 10.2 mm angle section was used in this test. Similar to GP-09, the far-end condition was pinned for GP-10.

The location of first row (row 4) of strain gauges was between the two holes (65 mm from centers of both holes). The first row below the bottom hole was at 50 mm away (70 mm away from center of hole). The subsequent rows were at 70 mm and 100 mm centers (Figure 4.92) and therefore, identical to GP-09. Figure 4.92 shows the location of strain gauge and LVDTs which were used for this specimen. There were two LVDT (LVDT-1 and LVDT-2) located on front face of plate and back of the plate. There were also two 152.4 mm (6 in) spring loaded LVDT (LVDT-3 and LVDT-4) in the front and back of load cell and jack connection, respectively. Hence, locations of LVDTs were also identical to GP-09.

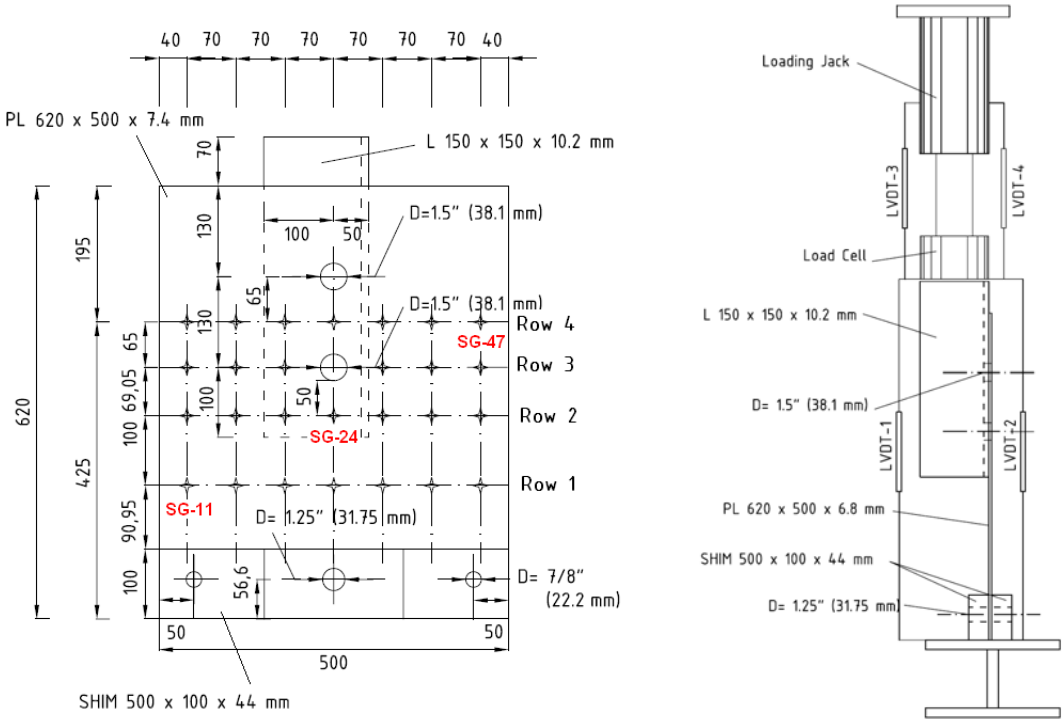


(a) Strain gauge location (b) LVDT(s) location

Figure 4. 92 – Locations of strain gauges and LVDTs in specimen GP-10

The plate remained in elastic range until a load of about 270 kN and after that the plastic deformation started because of the elongation in holes (See Figure 4.94(c)). This deformation continued until the tearing did occurred in top hole. Because of failure in load cell bolts, the test was discontinued and the tearing is not occurred in the plate. It should be noted that 6 bolt of 0.3 mm diameter (5/16 in) Grade 6 were used in between the load cell and top loading plate in this specimen

Figure 4.93 shows the load versus axial displacement response of specimen GP-10 through its loading which obtained from information of LVDT attached on angle and on the jack. The deformation of the gusset plate, the angle and the slip in the angle to gusset plate connection was recorded as total displacement. The maximum load reached was 612.4 kN.

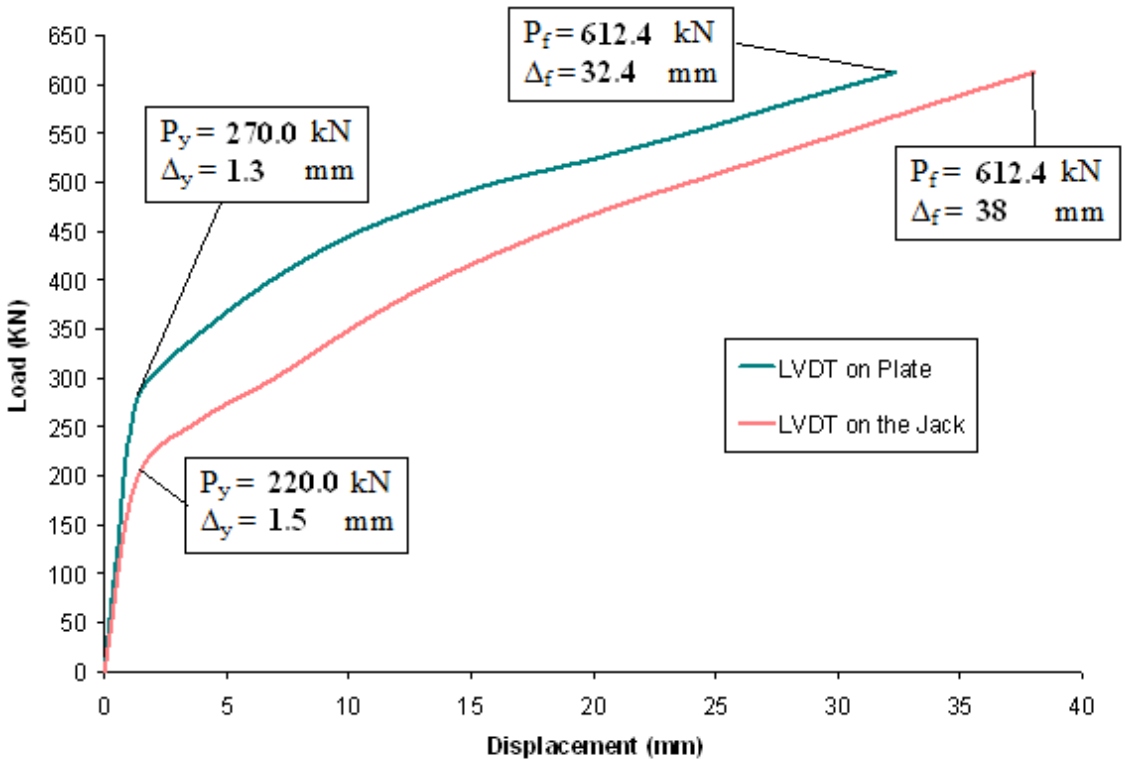


Figure 4. 93 – Load vs. axial displacement response of the gusset plate from LVDT located on plate and on the jack - Specimen GP-10

As it is shown in Figure 4.93, the specimen response under tension load was increasing and finally became stable. The load carrying capacity of the specimen increased as the deformation level increased. The out-of-plane plate bending of specimen was accompanied by the increase in axial deformation and drop in load carrying capacity. The test was discontinued due to failure in load cell bolts. Because of failure in bolts between load cell and top loading plate, 8 bolt of 0.3 mm (5/16 in) of Grade 6 were used in next test.

After the completion of the test, the failed gusset plate specimen was examined. It was observed that the specimen failed in tension due a bearing failure of the plate material between the bolt holes of the connections. The failed plate material is shown in Figure 4.94(d). The bolt hole in the connection had elongated by 9.4 mm due to the

bearing of the bolts under load. Hence, the final deformation at each hole was 41.2 mm.

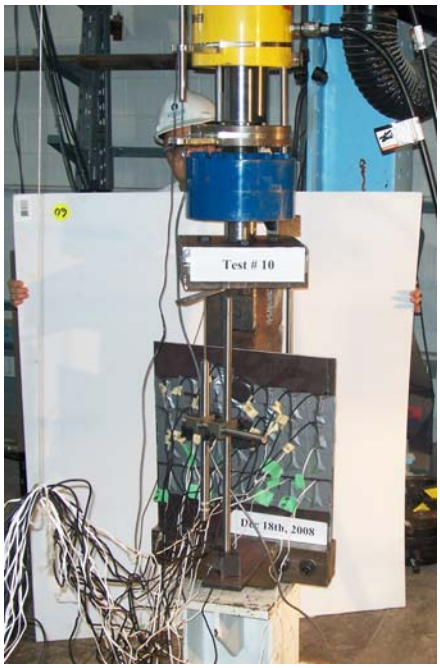


(a) Test setup


(b) LVDT location on angle


(c) Failure in load cell bolts

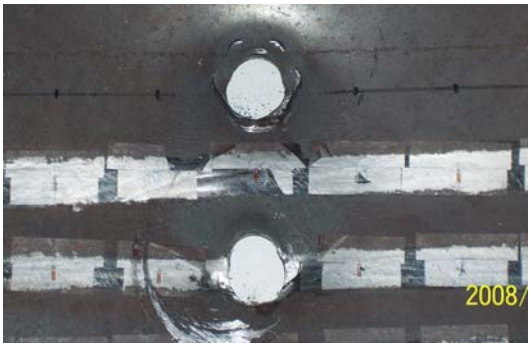


(d) Elongation of the bolt holes

Figure 4. 94 – Plate bearing failure in bolted connection – Specimen GP-10

The angle was assumed to deform elastically. A compatibility of specimen deformation was preserved at the top of the gusset plate. The displacement of the top of the angle was assumed to be approximately equal to the in-plane displacement at the top of the gusset plate free edges. Since the angle is relatively rigid compared to the gusset plate, this assumption appears to be valid.

During the loading of specimen, strain gauges reading were recorded through data acquisition system. As soon as local yielding occurred in the plate and the stresses began to redistribute, the strain readings were localized. Figure 4.95 to Figure 4.98 show the strain distributions from 50 kN to 600 kN. The strain gauges values are in micro strain.

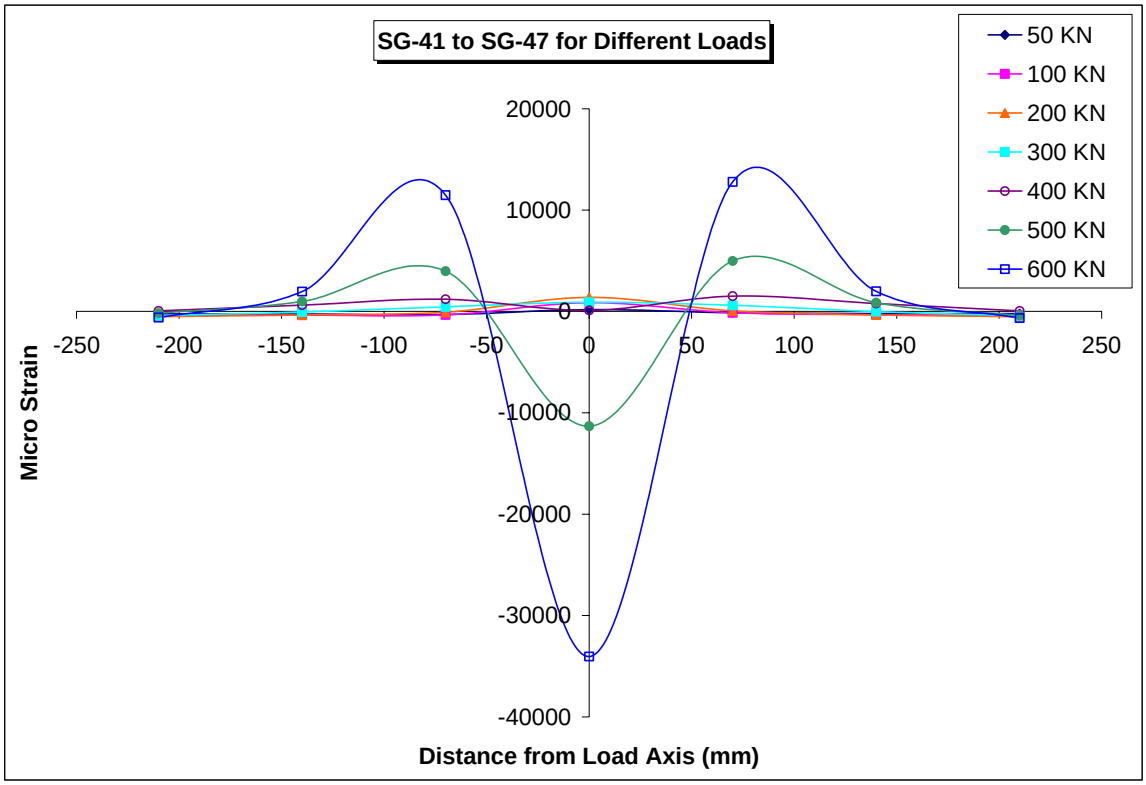


Figure 4. 95 – Strain values for (top) row 4 of specimen GP-10 at different loads

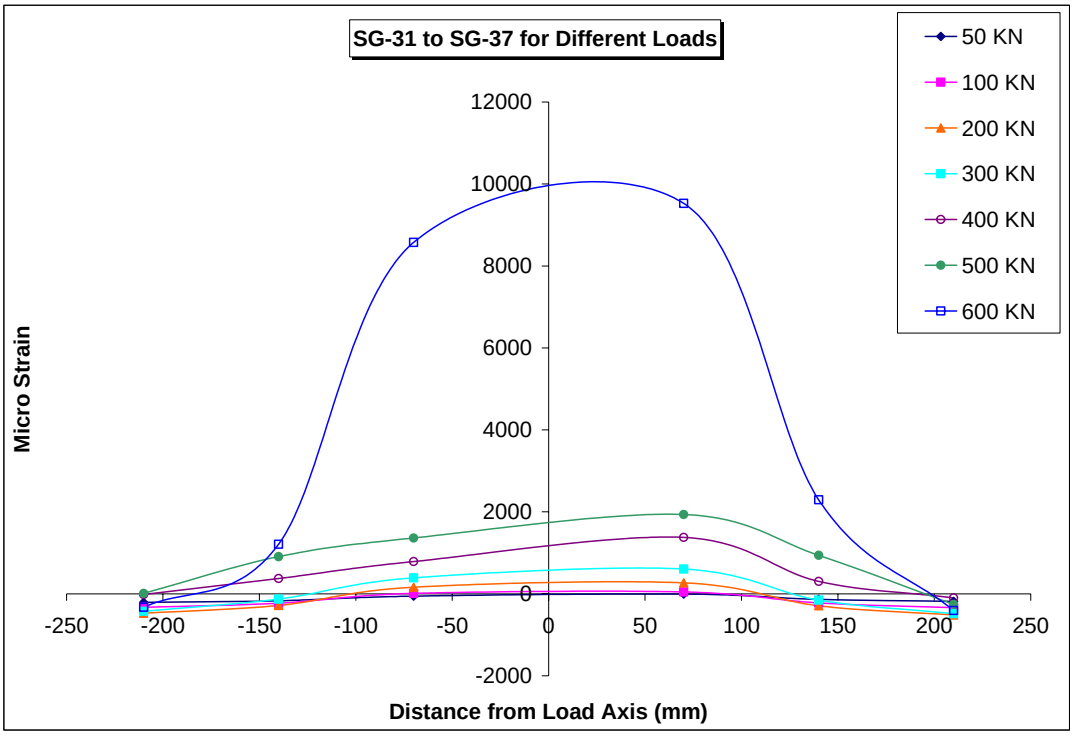


Figure 4. 96 – Strain values for (middle) row 3 of specimen GP-10 at different loads

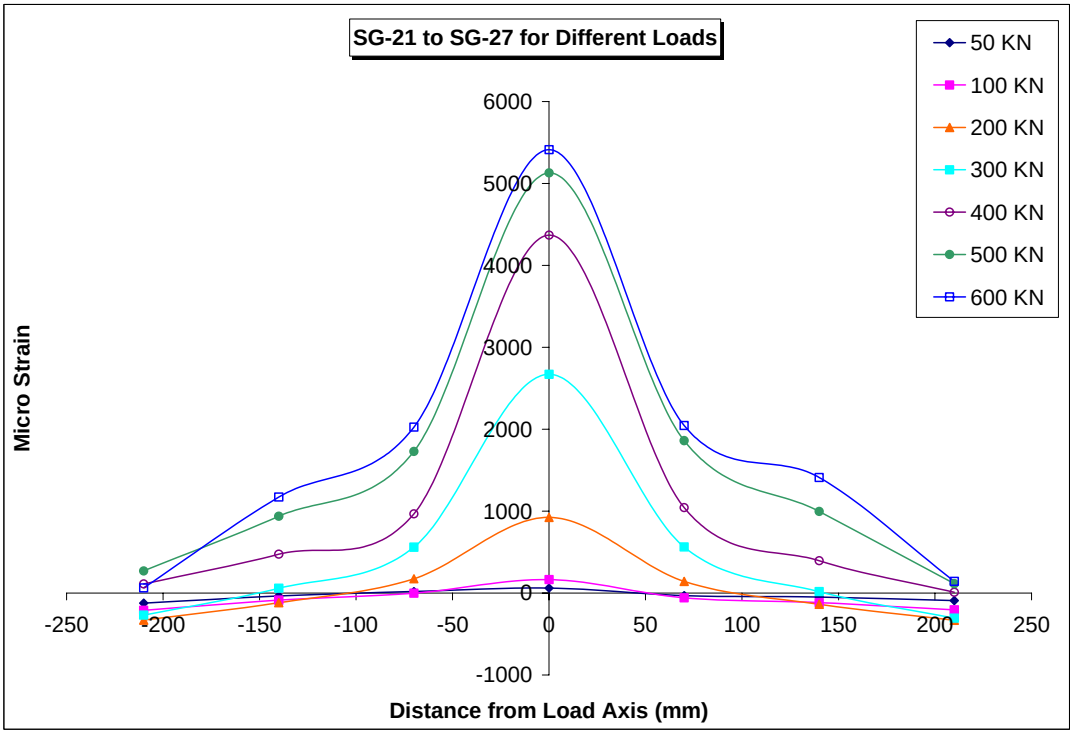


Figure 4. 97 – Strain values for (lower) row 2 of specimen GP-10 at different loads

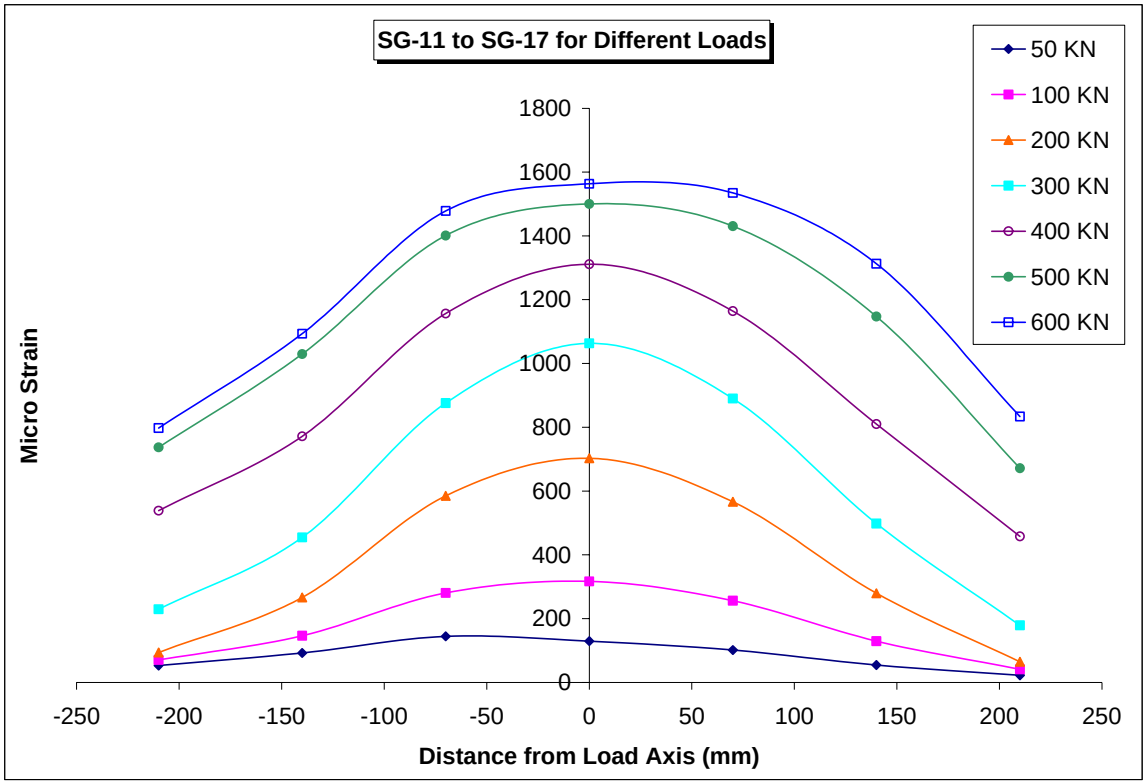


Figure 4. 98 – Strain values for (bottom) row 1 of specimen GP-10 at different loads

When the specimen load is increased beyond 270 kN level (yield load), strain values became non-uniform. When the strain reading at the 600 kN load are analyzed, the strain level are generally slightly less than two times those recorded at the 270 kN level. Figure 4.99 to Figure 4.102 show the strain distribution at different levels on plate surface. The strain gauges values are in micro strain.

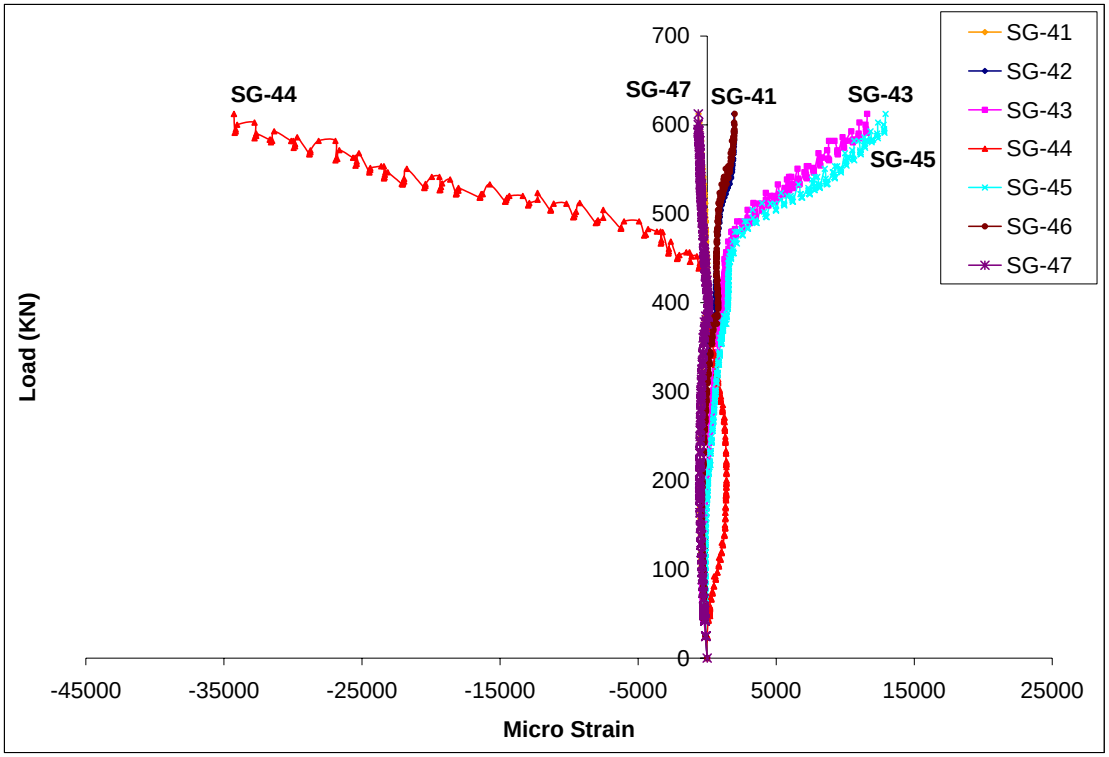


Figure 4. 99 – Strain vs. load for (top) row 4 of specimen GP-10

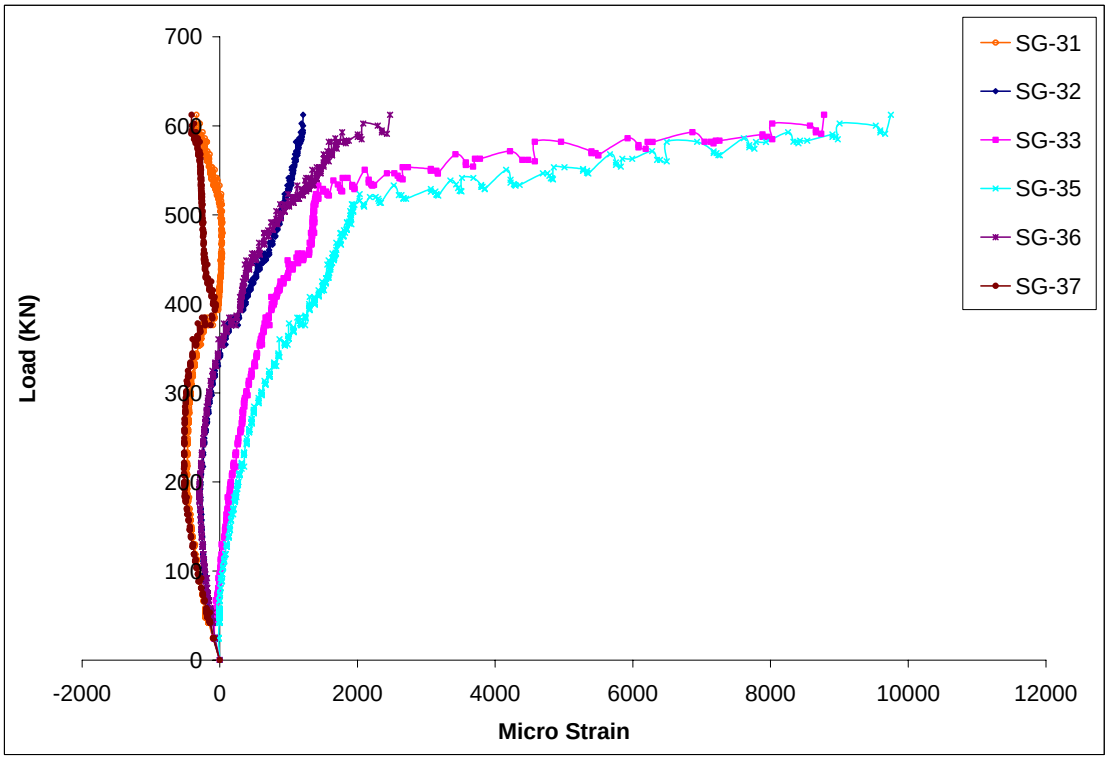


Figure 4. 100 – Strain vs. load for (middle) row 3 of specimen GP-10

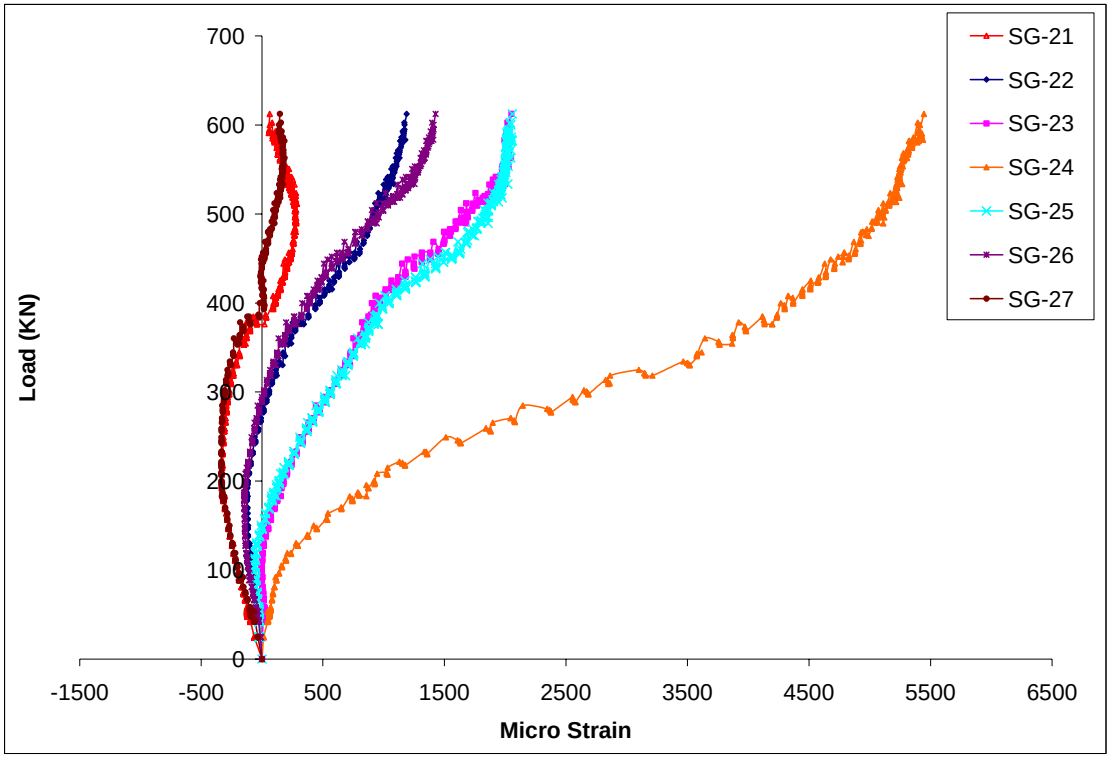


Figure 4. 101 – Strain vs. load for (lower) row 2 of specimen GP-10

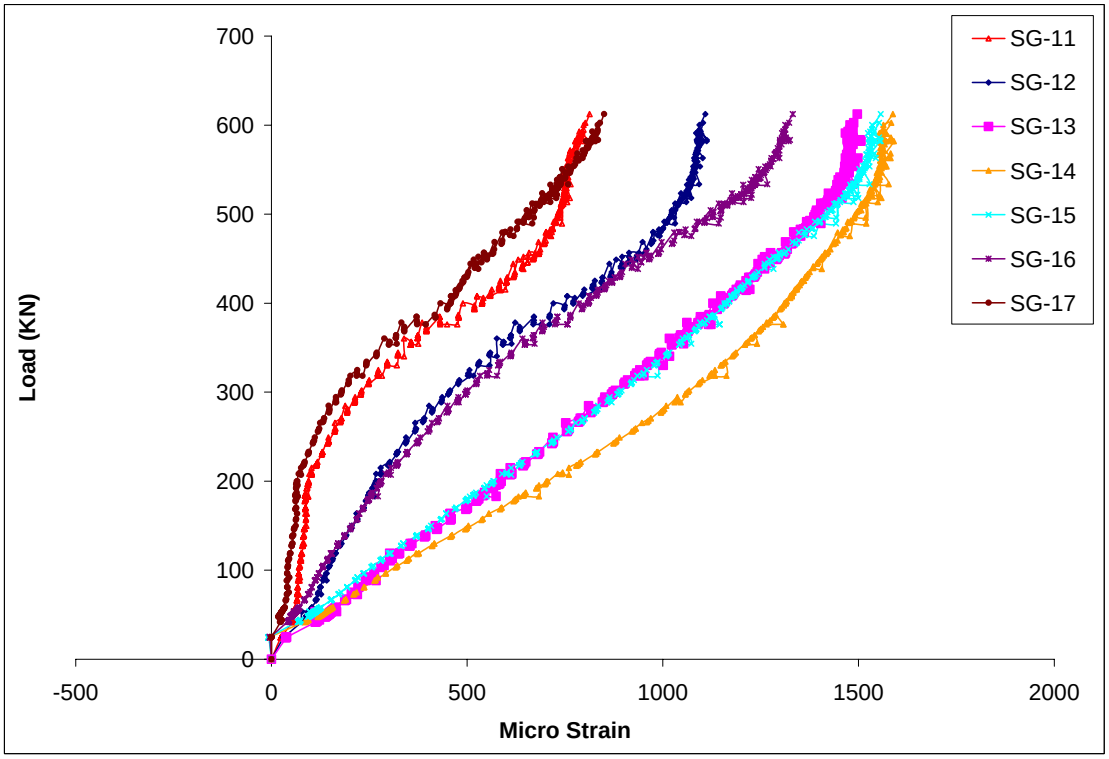


Figure 4. 102 – Strain vs. load for (bottom) row 1 of specimen GP-10

## 4.15 Specimen GP-11

Specimen GP-11 is a gusset plate of 6.9 mm thickness with 635 mm length and 500 mm width. Two 38.1 mm (1.5 in) diameter SAE-Grade 8 (ASTM-A354) high strength bolt was used to connect the angle to the gusset plate. The specimen was a plate with two bolts. A 150 x 150 x 10.2 mm angle section was used in this test. The far-end condition was also pinned. Hence, GP-11 was identical to GP-10 (except length of plate was different by 15 mm). The bearing length of plate above the top-most bolt was reduced from 130 mm to 110 mm in GP-11 to ensure bearing failure occurs in GP-11. The first row of strain gauges below the bottom hole was at 50 mm away (70 mm away from center of hole). The subsequent row was at 100 mm as shown in Figure 4.103.

It should be noted that unlike GP-09 and GP-10, no strain gauges were used in between two holes (Row 4) and also for Row 3 to minimize total number of strain gauges. The intention of the test (GP-11) was to repeat test of specimen GP-10 which was discontinued because of shear failure in bolts in between load cell and top loading plate. The number of bolts was increased to 8 with 0.35 mm (5/16 in) diameter of Grade 6.

Figure 4.103 shows the location of strain gauge and LVDTs which were used for this specimen. There were two LVDT (LVDT-1 and LVDT-2) located on front face of plate and back of the plate. Similar to GP-09 and GP-10, there were also two 152.4 mm (6 in) spring loaded LVDT (LVDT-3 and LVDT-4) in the front and back of load cell and jack connection, respectively.

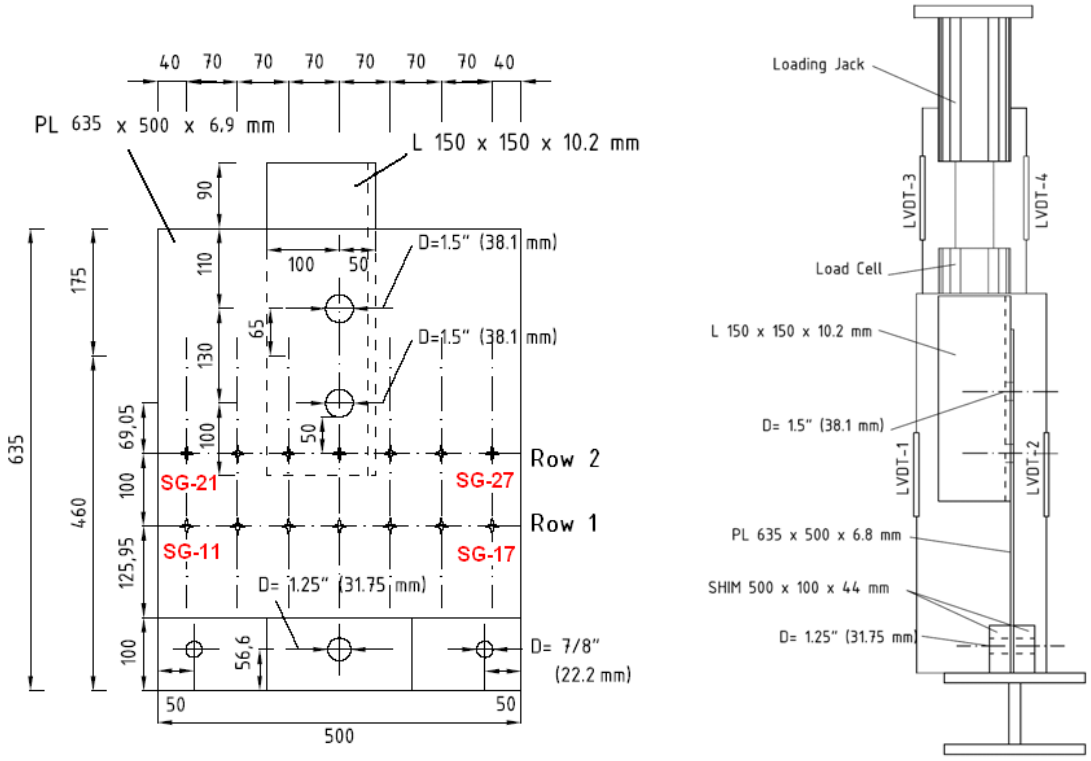


(a) Strain gauge location (b) LVDT(s) location

Figure 4. 103 – Locations of strain gauges and LVDTs in specimen GP-11

The plate remained in elastic range until a load of about 290 kN and after that the plastic deformation started because of the elongation in holes. This deformation continued until the tearing did occurred in top hole. Because sever of out-of-plane buckling at top end of the plate similar to GP-09, the test (GP-11) was discontinued even though no tearing occurred in the plate (Figure 4.105c). Figure 4.104 shows the load versus axial displacement response of specimen GP-11 through its loading which obtained from information of LVDT attached on angle and on the jack. The deformation of the gusset plate, the angle and the slip in the angle to gusset plate connection was recorded as total displacement.

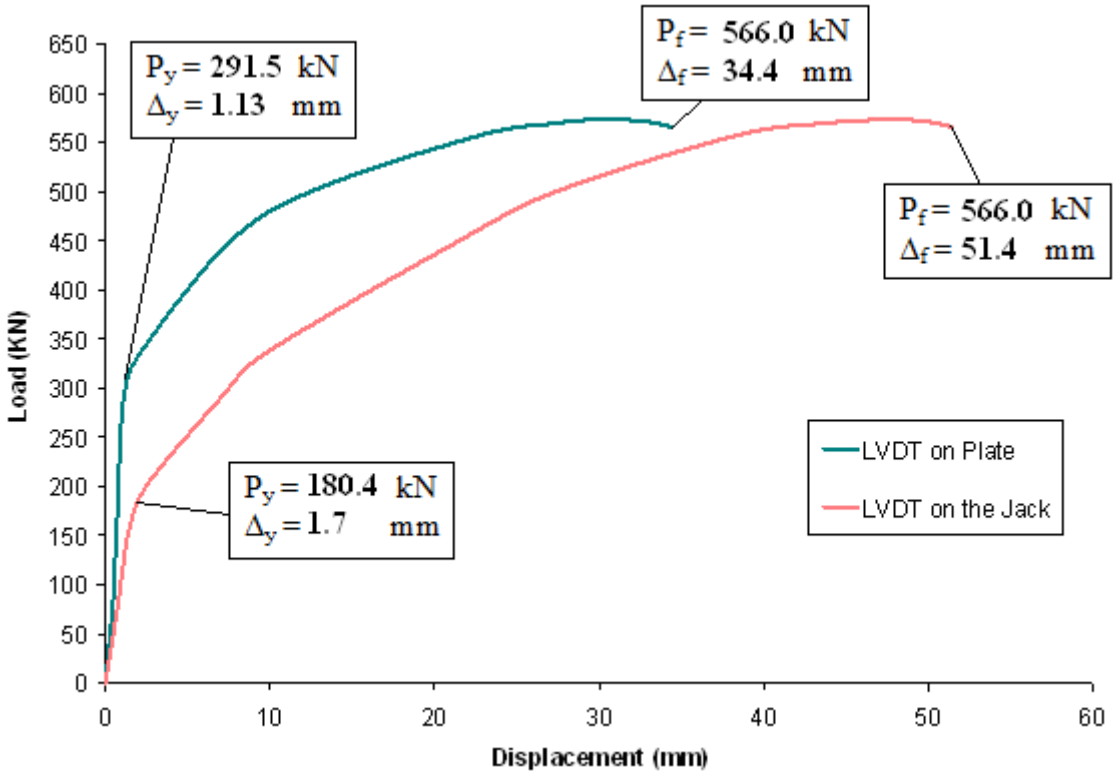


Figure 4. 104 – Load vs. axial displacement response of the gusset plate from LVDT located on plate and on the jack (LVDT-1 and LVDT-4) - Specimen GP-11

As it is shown in Figure 4.104, the specimen response under tension load was increasing and finally became stable. The load carrying capacity of the specimen increased as the deformation level increased. The maximum load reached was 566.0 kN. The out-of-plane plate bending of specimen was accompanied by the increase in axial deformation and drop in load carrying capacity. The test was discontinued due to the limitation of loading jack capacity.

After the completion of the test, the failed gusset plate specimen was examined. It was observed that the specimen failed in tension due a bearing failure of the plate material between the bolt holes of the connections. The failed plate material is shown in Figure 4.105. The bolt hole in the connection had elongated by 9.4 mm due to the bearing of the bolts under load. The final length of each top hole was 41.2 mm.

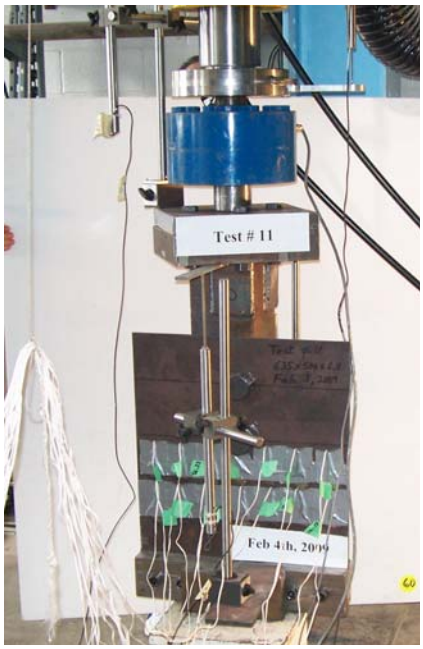


(a) Test setup

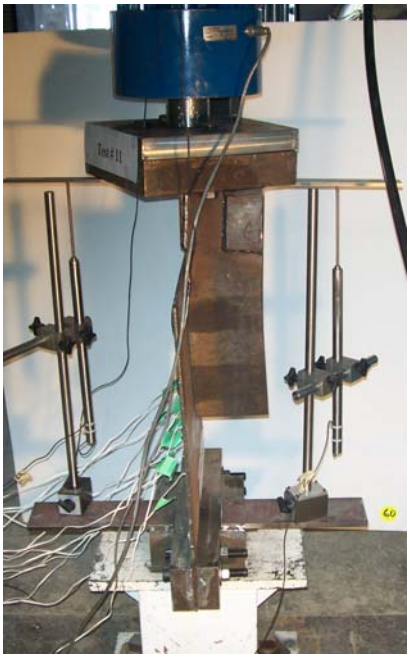

(b) LVDT location on angle

(c) Local out-of-plane buckling of plate top end


(d) Elongation of the bolt holes

Figure 4. 105 – Plate bearing failure in bolted connection – Specimen GP-11

The angle was assumed to deform elastically. A compatibility of specimen deformation was preserved at the top of the gusset plate. The displacement of the top of the angle was assumed to be approximately equal to the in-plane displacement at the top of the gusset plate free edges. Since the angle is relatively rigid compared to the gusset plate, this assumption appears to be valid.

During the loading of specimen, strain gauges reading were recorded through data acquisition system. As soon as local yielding occurred in the plate and the strain localized and began to redistribute. Figure 4.106 to Figure 4.107 show the strain distributions from 50 kN to 550 kN. The strain gauges values are in micro strain.

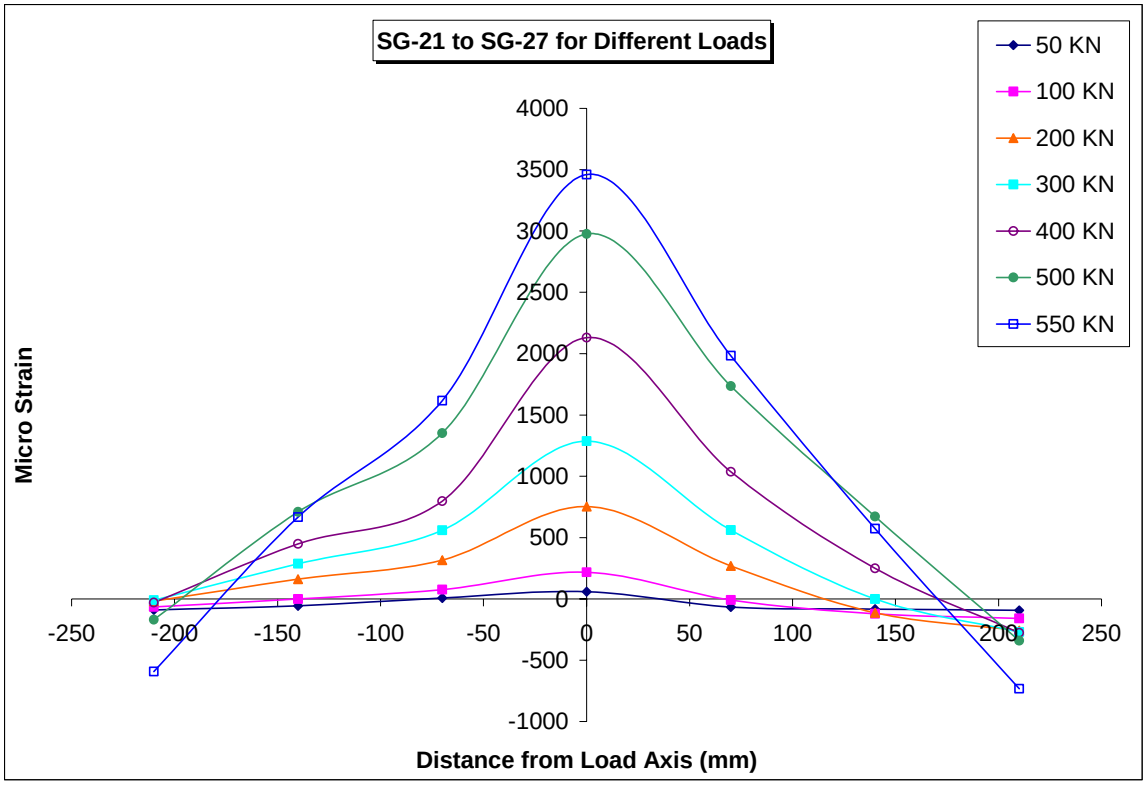


Figure 4. 106 – Strain values for (top) row 2 of specimen GP-11 at different loads

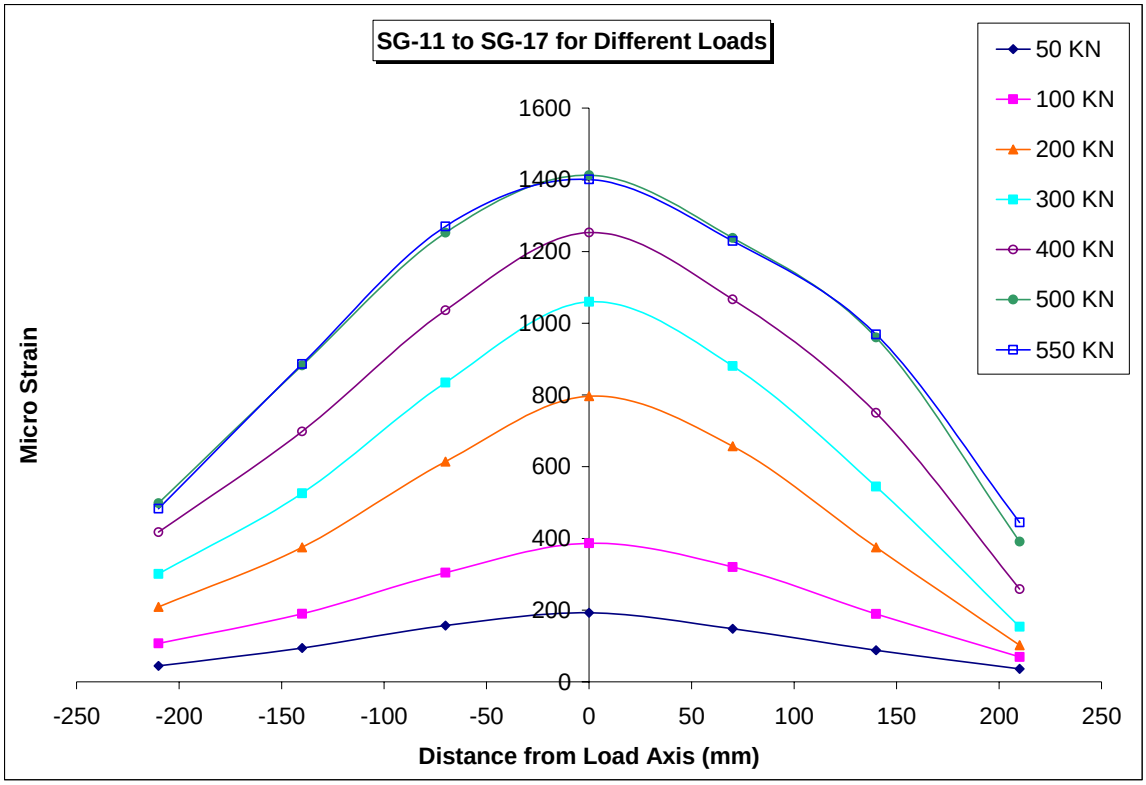


Figure 4. 107 – Strain values for (bottom) row 1 of specimen GP-11 at different loads

When the specimen load is increased beyond 290 kN level (yield load), strain values became non-uniform. When the strain reading at the 550 kN load are analyzed, the strain level are generally slightly less than three times those recorded at the 290 kN level. Figure 4.108 and Figure 4.109 show the strain distribution at different levels on plate surface. The strain gauges values are in micro strain.

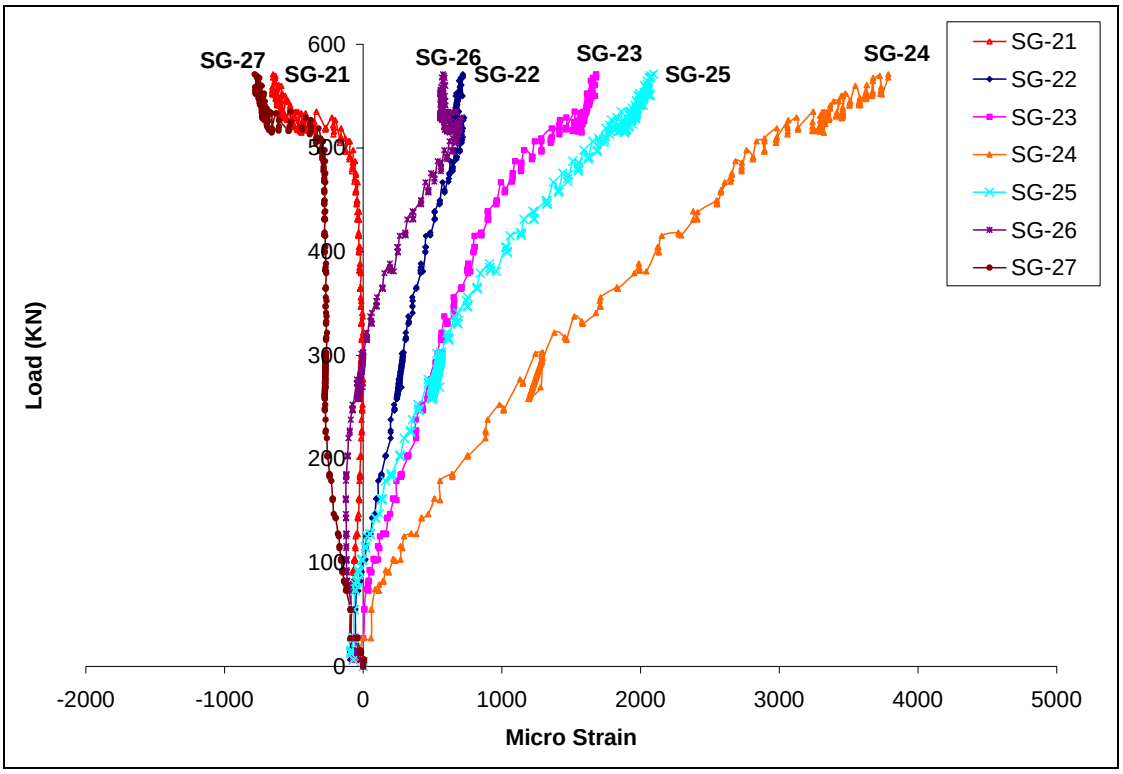


Figure 4. 108 – Strain vs. load for (top) row 2 of specimen GP-11

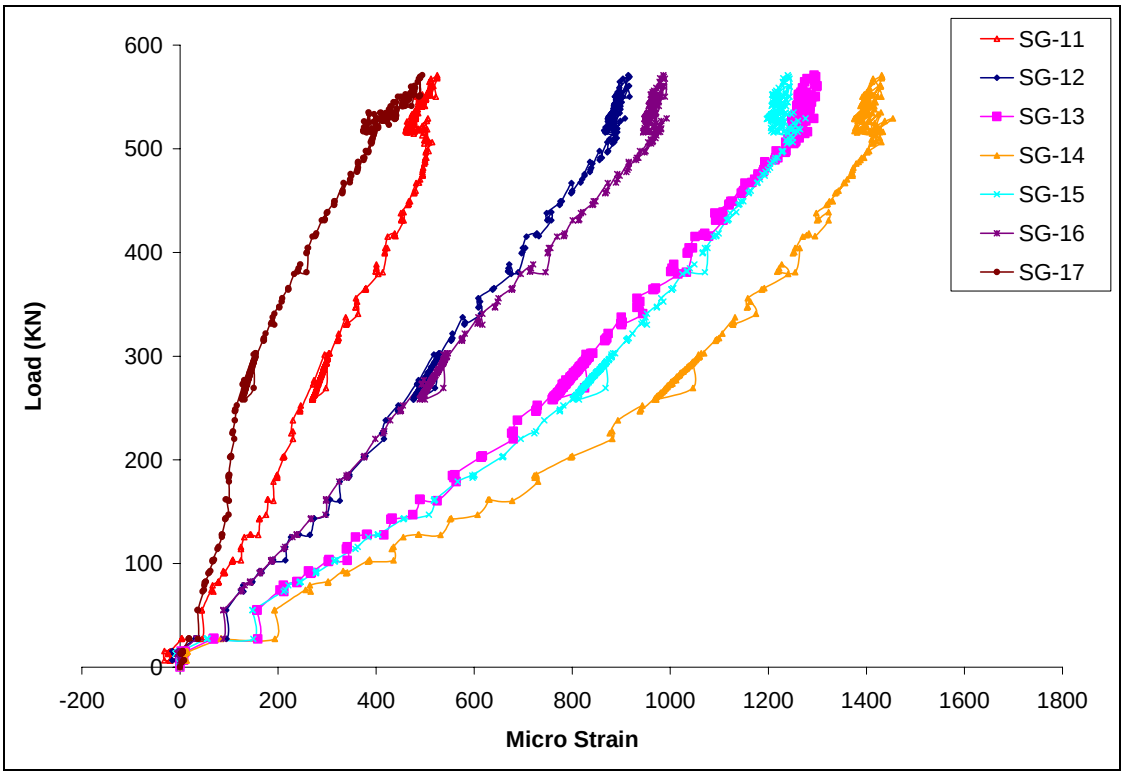


Figure 4. 109 – Strain vs. load for (bottom) row 1 of specimen GP-11

## 4.16 Specimen GP-12

Specimen GP-12 is a gusset plate of 6.5 mm thickness with 490 mm length and 200 mm width. One 38.1 mm (1.5 in) diameter SAE-Grade 8 (ASTM-A354) high strength bolt was used to connect the angle to the gusset plate. The diameter of hole was 40 mm. The specimen was a plate with one bolt. A 150 x 150 x 10.2 mm angle section was used in this test. The far-end condition was pinned. This specimen was used to study the effect of plate width for connections with one bolt. The first row of strain gauges below the bottom hole was at 50 mm away (70 mm away from center of hole). The subsequent row was at 100 mm each apart as shown in Figure 4.110. Figure 4.110 shows the location of strain gauge and LVDTs which were used for this specimen. Only two rows of strain gauges below the top hole were installed. Two LVDTs (LVDT-1 and LVDT-2) were used one on front and back of the plate. There were also two 152.4 mm (6 in) spring loaded LVDTs (LVDT-3 and LVDT-4) in the front and back of load cell and jack connection, respectively.

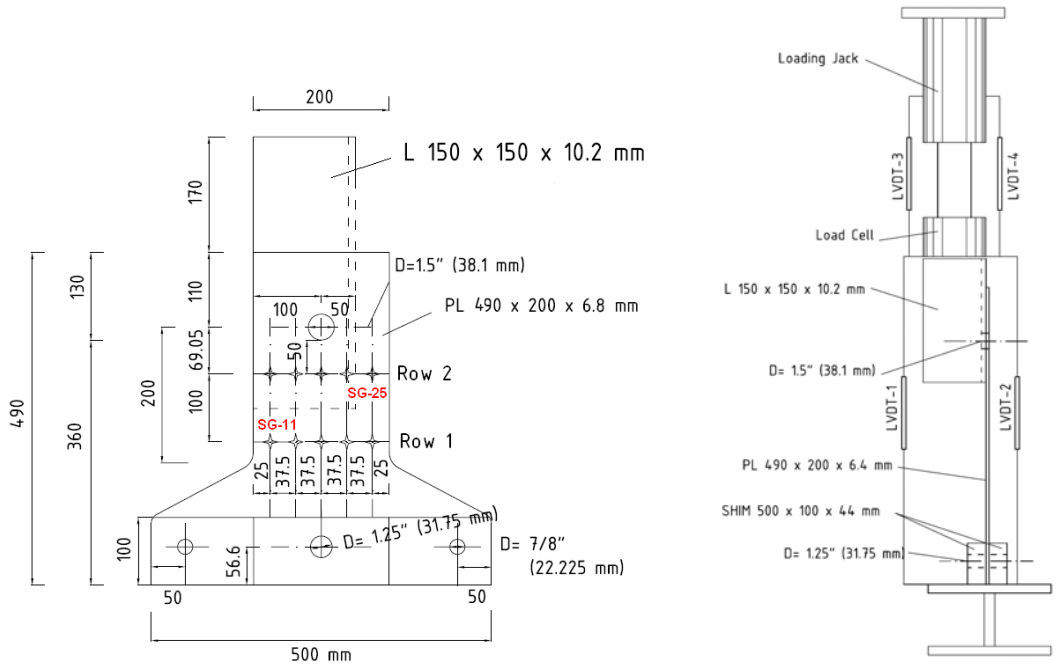


(a) Strain gauge location (b) LVDT(s) location

Figure 4. 110 – Locations of strain gauges and LVDTs in specimen GP-12

The plate remained in elastic range until a load of about 230 kN and after that the plastic deformation started because of the elongation in holes. The test was continued until a severe (about 50 mm) out-of-plane buckling occurred at the top end of the plate and a long crack above the top hole appeared. Figure 4.111 shows the load versus axial displacement response of specimen GP-12 which obtained from information of LVDT attached on angle and on the jack. The deformation of the gusset plate, the angle and the slip in the angle to gusset plate connection was recorded as total displacement.

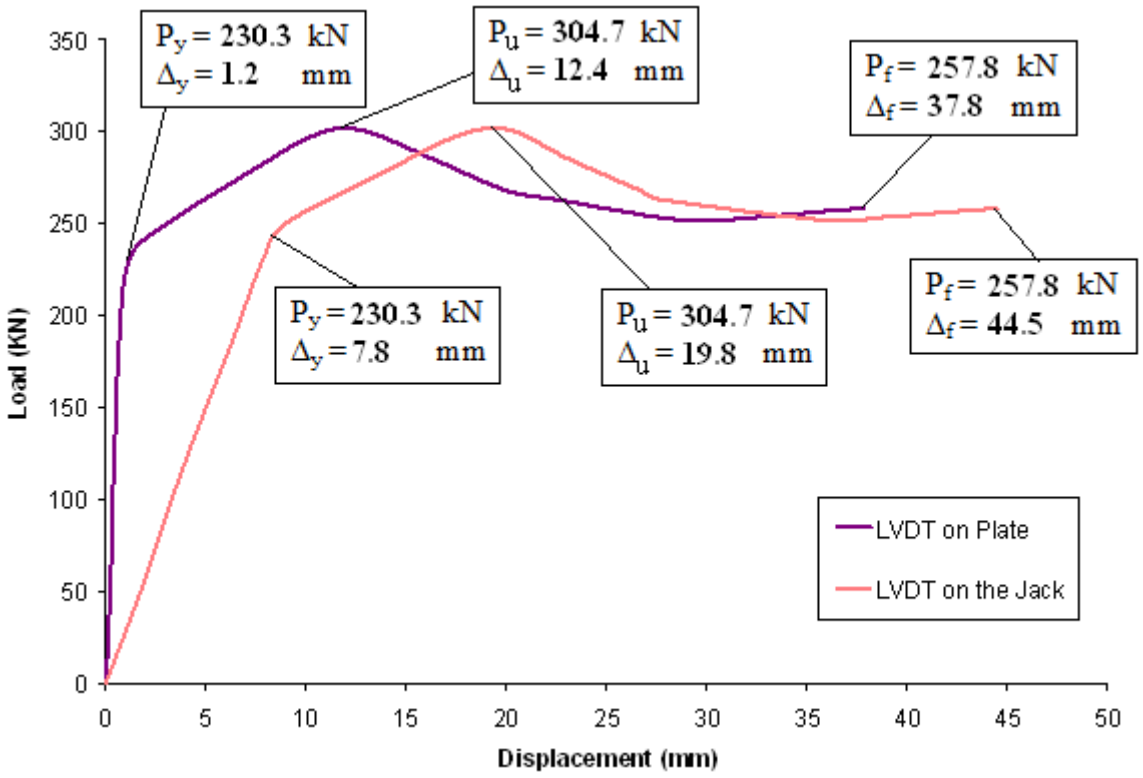


Figure 4. 111 – Load vs. axial displacement response of the gusset plate from LVDT located on plate and on the jack - Specimen GP-12

As it is shown in Figure 4.111, the specimen response under tension load was increasing and finally became stable. The load carrying capacity of the specimen increased as the deformation level increased. The maximum load reached was 304.7 kN. The out-of-plane plate bending of specimen was accompanied by the increase in

axial deformation and drop in load carrying capacity. The test was discontinued due to serve out-of-plane buckling in the plate above the bolt and hole.

After the completion of the test, the failed gusset plate specimen was examined. It was observed that the specimen failed in tension due a bearing failure of the plate material between the bolt hole in the connection. The failed plate material is shown in Figure 4.112(c). The bolt hole in the connection had elongated by 39.2 mm due to the bearing of the bolts under load. The final length of hole was 77.3 mm.

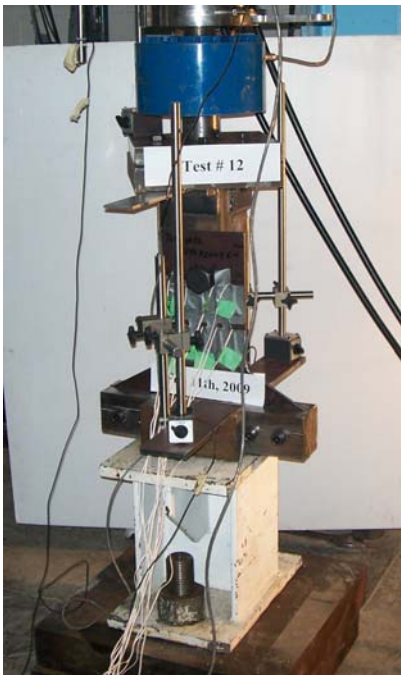


(a) Test setup

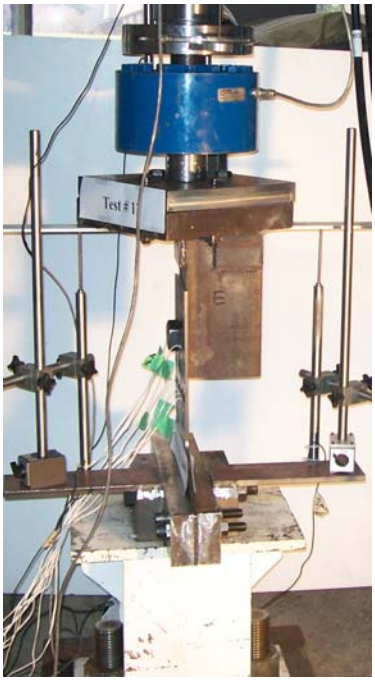

(b) LVDT location on angle


(c) Local buckling of plate


(d) Elongation of the bolt hole

Figure 4. 112 – Plate bearing failure in bolted connection – Specimen GP-12

The angle was assumed to deform elastically. A compatibility of specimen deformation was preserved at the top of the gusset plate. The displacement of the top of the angle was assumed to be approximately equal to the in-plane displacement at the top of the gusset plate free edges. Since the angle is relatively rigid compared to the gusset plate, this assumption appears to be valid.

During the loading of specimen, strain gauges reading were recorded through data acquisition system. As soon as local yielding occurred in the plate and the strains localized and began to redistribute. Figure 4.113 and Figure 4.114 show the strain distributions from 50 kN to 300 kN. The strain gauges values are in micro strain.

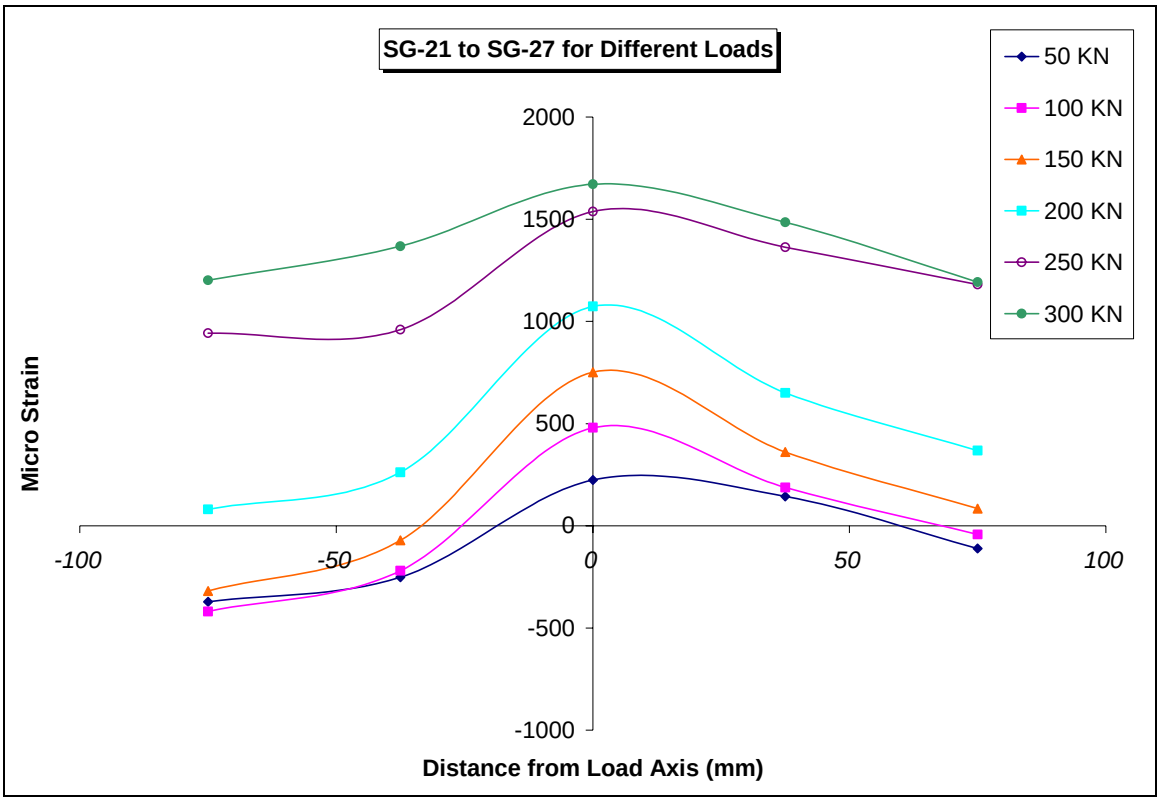


Figure 4. 113 – Strain values for (top) row 2 of specimen GP-12 at different loads

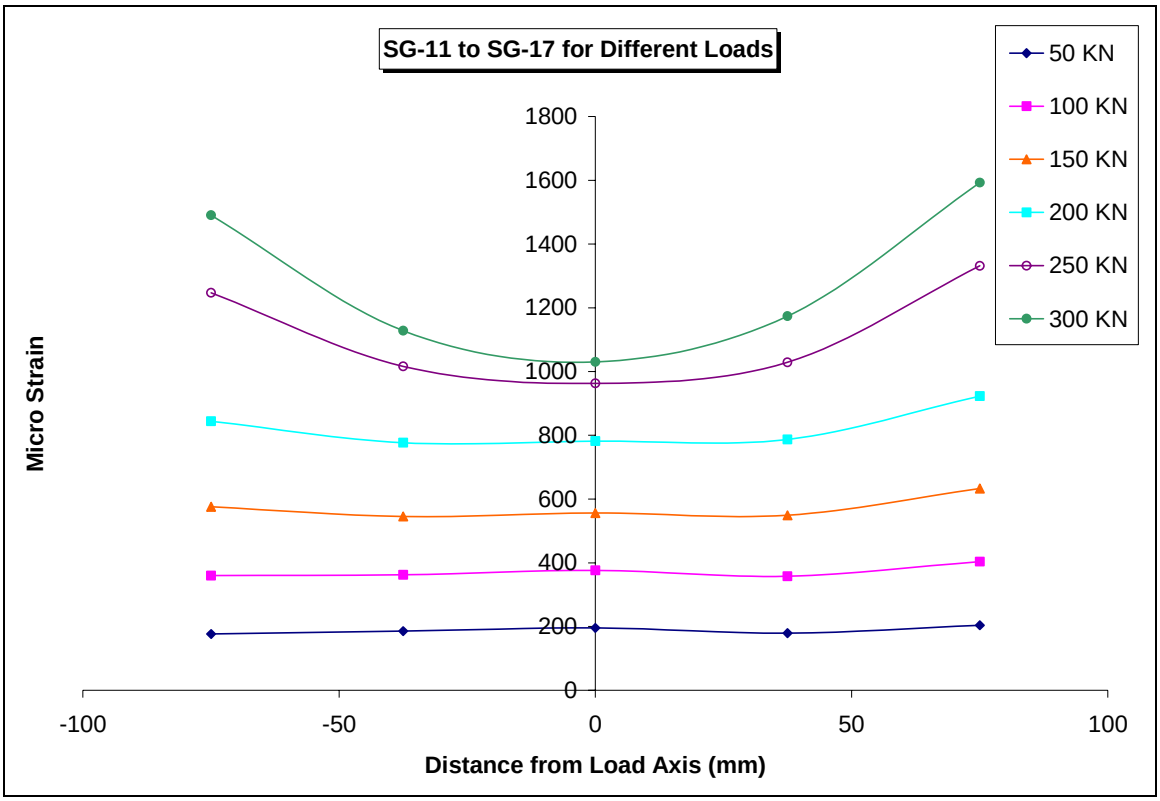


Figure 4. 114 – Strain values for (bottom) row 1 of specimen GP-12 at different loads

When the specimen load is increased beyond 230 kN level, strain values became non-uniform. When the strain reading at the 300 kN load are analyzed, the strain level are generally slightly more than one and half times those recorded at the 230 kN level. Figure 4.115 and Figure 4.116 show the strain distribution at different levels on plate surface. The strain gauges values are in micro strain. Due to the large out-of-plane buckling of plate, the strain value of different row did not change and reached to a constant limit about 1600 micro strain.

It is also observed that strain value never reached yield level (1900 micro strain) though this doesn't mean that plate did not yield elsewhere. In fact, the plate yielded and experienced severs plastic deformation at and near the hole. Since no strain gauges could be installed at those locations, strain values at those locations could not be captured.

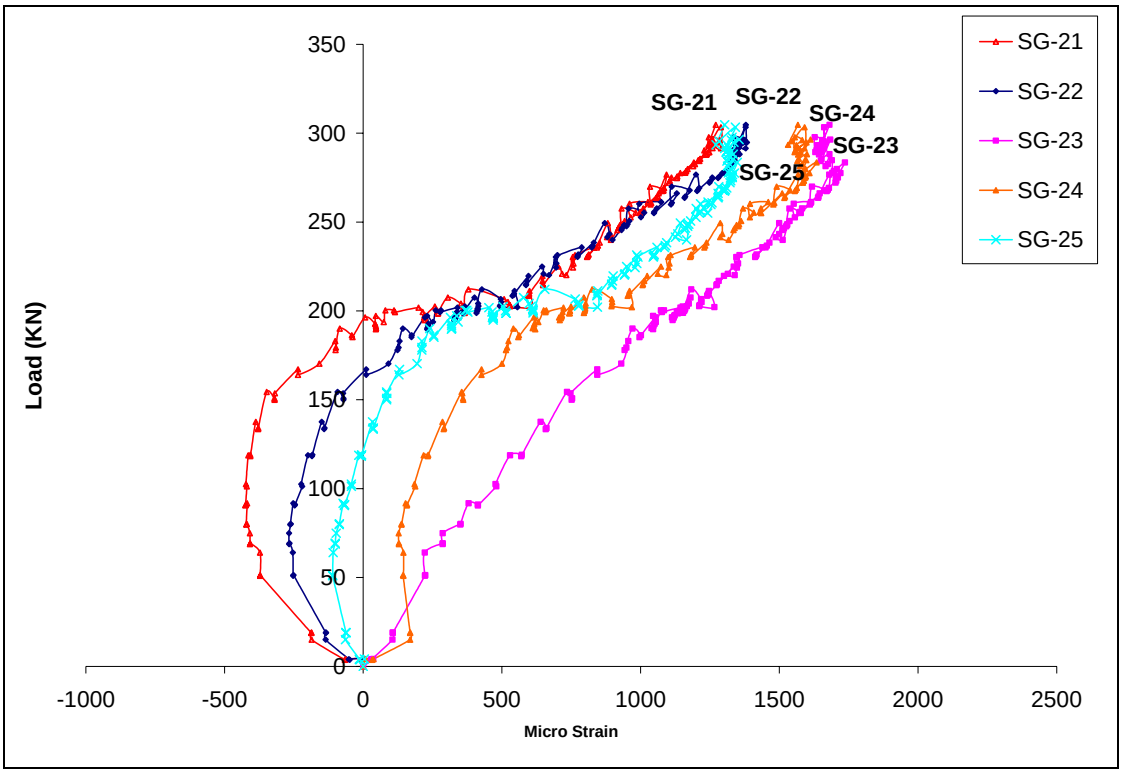


Figure 4. 115 – Strain vs. load for (top) row 2 of specimen GP-12

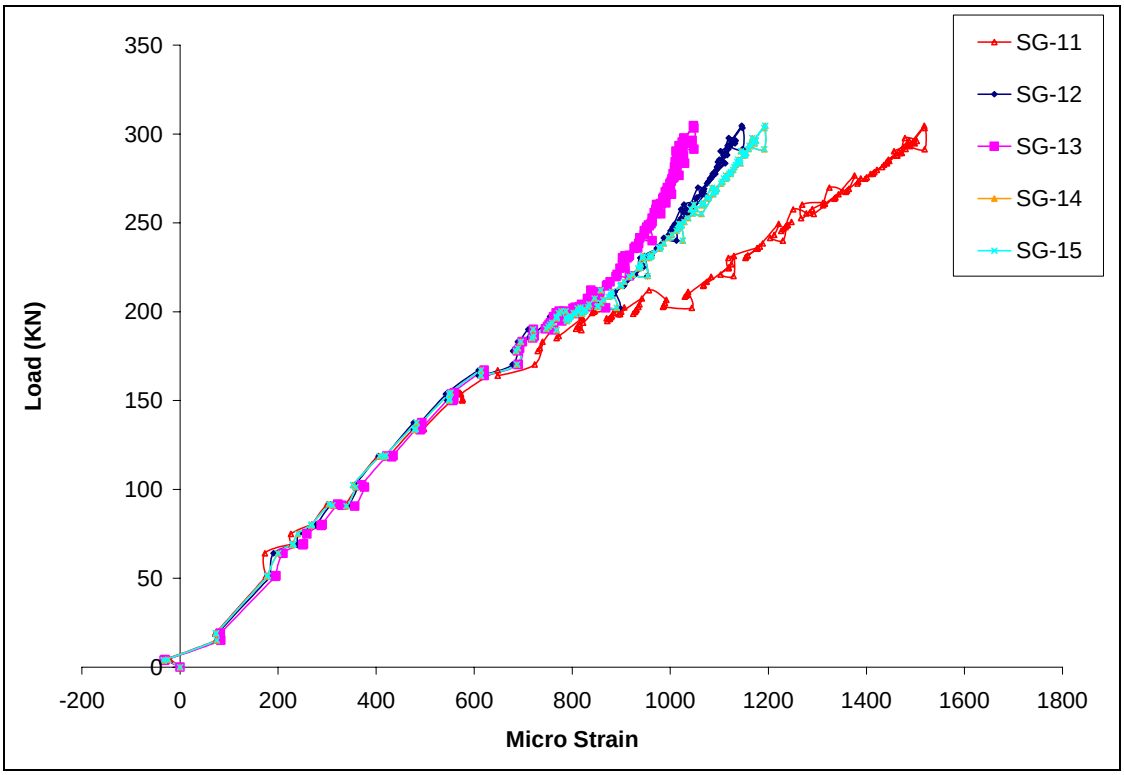


Figure 4. 116 – Strain vs. load for (bottom) row 1 of specimen GP-12

## 4.17 Failure Mode

It has been found that the failure occurs either in the bolt by shear or due to tearing in the angle if the sizes of the bolt (22 mm) and angle (75 x 75 x8.3 mm) are smaller and very similar to what is used in real construction for communication tower (See specimen GP-01 and its repeat test). However, the failure mode changes to bearing failure of the plate if the bolt and angle sizes are made larger (150 x 150 x 10.2 mm for angle and 38.1 mm for bolt) irrespective of one or two bolt connections (See specimen GP-02 to GP-12). It has also been found that the clear distance between the top hole and top edge of the plate does not change the failure mode. However, the gusset plate softens earlier if this distance is reduced (See specimen GP-02, GP-03, GP-11 and GP-12).

## 4.18 Load Balance

The strain-load curve for each test was used for load balance. The strain values in elastic range almost change linearly and have relationship with applied load to specimen. So, in order to check the strain value and validity of test, an applied load in the elastic range of each specimen was selected and compared with calculated load. Table 4.4 shows the load balance for each specimen in elastic range. It is worth mentioning that load balance was checked at the top row of strain gauges (first row below the hole for one-bolt connection and first row below the bottom hole for two-bolt connections). The estimated load (column 6 of Table 4.4) was calculated using the following formula.

$$P = A \cdot E \cdot t \qquad (4.1)$$

Where;

$P$ = Estimated load on specimen
$A$ = Area under the strain-plate width curve for top row of strain gauge
$E$ = Modulus of elasticity of plate material

$t$ = Thickness of plate

The area under the curve was determined using Simpson's method and a typical calculation for specimen GP-08 is shown in Figure 4.117. It should be noted that the total width of this plate specimen is 500 mm. The detailed calculations for estimated loads for specimens GP-04, GP-08, GP-09, GP-10, GP-11, and GP-12 are shown in Appendix.

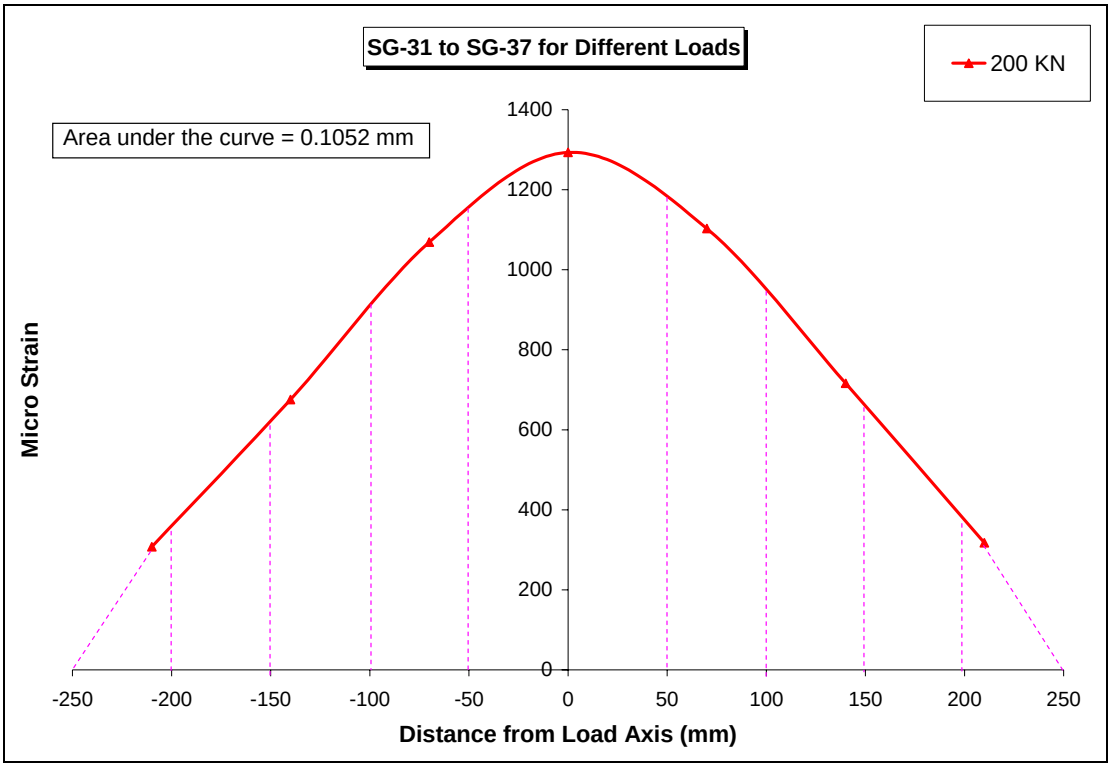


Figure 4. 117 - Calculation of area under the strain distribution curve based on Simpson's method for Specimen GP-08

It should be noted that the load balance was calculated when the specimen is in elastic range (global behaviour is still elastic). No attempt was made to check the load balance in the elastic-plastic (once the specimen global behaviour became non-linear) range because the strains localizes and thus, the load balance at a particular section of the plate does not work. For example, for specimen GP-04, at load 170 kN, the estimated load is 135 kN.

Table 4. 4 – Load balance calculation for Specimen GP-01 to GP-12

| Specimen | Yield Load (kN) | Area under strain-distance curve (mm) | Thickness of plate (mm) | Selected Load (kN) | Estimated Load (kN) |
|---|---|---|---|---|---|
| GP-01 | 135.0 | 0.0357 | 12.8 | 100 | 91.8 |
| GP-02 | 95.0 | 0.0369 | 6.4 | 50 | 47.5 |
| GP-03 | 110.0 | --- | 6.4 | --- | --- |
| **GP-04** | **152.9** | **0.0736** | **6.4** | **100** | **94.7** |
| GP-05 | --- | 0.0608 | 7.0 | 100 | 85.5 |
| GP-06 | 296.7 | 0.1010 | 7.0 | 150 | 142.1 |
| GP-07 | 250.0 | 0.0916 | 7.0 | 150 | 128.9 |
| **GP-08** | **316.6** | **0.1052** | **7.0** | **150** | **148.0** |
| **GP-09** | **278.0** | **0.1268** | **6.9** | **200** | **175.9** |
| **GP-10** | **270.0** | **0.1350** | **6.9** | **200** | **187.2** |
| **GP-11** | **291.5** | **0.1319** | **6.9** | **200** | **182.9** |
| **GP-12** | **230.3** | **0.0726** | **6.5** | **100** | **94.9** |

## 4.19 Effective Width Calculation

Failure in the gusset plate occurred either due to bolt shear or due to bearing of plate above the top bolt and/or out-of-plane bending of the plate portions above the top bolt. It is expected the shear failure in the bolt will govern for usual size bolts of this type of gusset plate connections. However, to preclude shear failure of bolts, much larger diameter bolts were used in this investigation. None of the specimens experienced gross section yielding or nor net section failure.

However, for convenience in design, if the concept of effective width is used, the following procedure can be adopted. For gusset plate with one bolt, the angle of load dispersion and effective plate width has no physical meaning because Whitmore's model can not be applied. This is because many lines can be drawn through one bolt hole. For gusset plate connection with two bolts, the angle of load dispersion and effective plate widths were calculated as shown by the following equation.

$$P_y = w \cdot t \cdot f_y \tag{4.1}$$

Therefore,

$$w = \frac{P_y}{t \cdot f_y} \tag{4.2}$$

Where;

$P_y$ = Yield load of gusset plate connection

$t$ = Thickness of the gusset plate

$w$ = Effective gusset plate width

$f_y$ = Yield stress obtained from coupon test of gusset plate

The values of $P_y$ (yield load) were found from the global load-deformation plots. The thickness of steel plate, $t$, was measured. Therefore, the effective gusset plate width,

*w*, was calculated from above equation and also the angle of load dispersion was determined. Table 4.5 compares the *w* values obtained from this study using above equation and based on Whitmore's model. It can be noticed that for gusset plate connection with two bolts, the angle of dispersion is approximately one half of angle (60 degree) as suggested by Whitmore. This is because the failure mode is not due to yielding of plate, rather due to bearing failure of the plate.

Table 4. 5 - Calculation of effective width for one and two bolt connection with ultimate load method - Specimen GP-01 to GP-12

| Specimen | Yield Load ($P_y$) (kN) | Yield Stress ($f_y$) (MPa) | Plate Thick. (mm) | No. of Bolts | Effective plate width ($w$) (mm) | Distance from bolt center (mm) | Angle with bolt axis (Deg.) | Total angle (Deg.) | w/t ratio | Whitmore's effective width (Deg.) | Whitmore's dispersion angle (Deg.) |
|---|---|---|---|---|---|---|---|---|---|---|---|
| GP-01 | 135.0 | --- | 12.8 | 1 | --- | 60.0 | --- | --- | --- | --- | --- |
| GP-02 | 95.0 | 358.9 | 6.4 | 1 | 41.4 | 75.0 | --- | --- | 6.5 | --- | --- |
| GP-03 | 110.0 | 358.9 | 6.4 | 1 | 47.9 | 20.0 | --- | --- | 7.5 | --- | --- |
| **GP-04** | **224.4** | **358.9** | **6.4** | **1** | **98.0** | **19.3** | --- | --- | **15.3** | --- | --- |
| GP-05 | --- | 364.4 | 7.0 | 1 | --- | 70.0 | --- | --- | --- | --- | --- |
| GP-06 | 296.7 | 364.4 | 7.0 | 1 | 116.3 | 70.0 | --- | --- | 16.6 | --- | --- |
| GP-07 | 250.0 | 364.4 | 7.0 | 1 | 98.0 | 70.0 | --- | --- | 14.0 | --- | --- |
| **GP-08** | **316.6** | **364.4** | **7.0** | 1 | **124.1** | **70.0** | --- | --- | **17.7** | --- | --- |
| **GP-12** | **278.0** | **362.0** | **6.5** | 1 | **118.1** | **70.0** | --- | --- | **18.2** | --- | --- |
| **GP-09** | **270.0** | **378.1** | **6.9** | **2** | **103.5** | **200.0** | **14.5** | **29.0** | **15.0** | **230.9** | **60.0** |
| **GP-10** | **291.5** | **378.1** | **6.9** | **2** | **111.7** | **200.0** | **15.6** | **31.2** | **16.2** | **230.9** | **60.0** |
| **GP-11** | **230.3** | **378.1** | **6.9** | **2** | **88.3** | **200.0** | **12.4** | **24.9** | **12.8** | **230.9** | **60.0** |

## 4.20 Summary

The following items are presented as a summary of this chapter:

1. The test matrix shows details of the changes in experimental factor such as: plate size, plate thickness, far-end boundary condition, number of bolts and number of LVDTs. The information about bolt size and bolt grade was also presented in this table. The plate size was varied from 350 x 300 to 850 x 500 and the thickness was also varied from 6.4 to 7.0 mm.

2. The modules of elasticity for plate with 6.4, 6.5, 6.9 and 7.0 mm thickness was about 210, 212 and 200 GPa, respectively. The tensile strength for these plates was 515, 500 and 520 MPa.

3. The ultimate tensile load was related to the size of the plate, bolt hole position and plate thickness which was varied between 143.0 to 621.0 kN.

4. Specimens GP-01 to GP-08 and GP-12 were used for one bolt connection and specimens GP-09 to GP-11 were used for two bolt connections. The far-end boundary condition for different test were either fixed or hinged.

5. The amount of strain during the test was determined by installing strain gauges on plate surface in different rows. One of the rows was near the bolt hole and the others indicated the strain variation on plate surface.

6. In all the specimens, the plate remained in the elastic range until the yield load and after which plastic deformation began to occur. The elongation of the hole indicated that the plastic deformation continued until ultimate rupture and tearing occurred.

7. The displacements were recorded by the LVDTs attached to the plate surface or angle. The deformation of the gusset plate, the angle and the slip in the angle to gusset plate connection were recorded as total displacement.

8. During the loading of the specimen, strain gauges reading were recorded through data acquisition system. As soon as local yielding occurred in the plate and the stresses began to redistribute and the strains were localized.

9. For gusset plate with one bolt, the angle of load dispersion and effective plate width has no physical meaning because Whitmore's model can not be applied. This is because many lines can be drawn through one bolt hole. For gusset plate connection with two bolts, the angle of load dispersion and effective plate widths were calculated as shown by the equation.

# 5. FINITE ELEMENT ANALYSIS AND VALIDATION

## 5.1 Introduction

In this chapter, a numerical investigation of the behaviour of gusset plate connected to a splice member with one or two bolt performed using the finite element program ABAQUS (2004), version 6.6 is described and the results of the investigation is presented. The investigation comprised of two phases. In the first phase, finite element models were developed predict the behaviour of gusset plate connection under monotonic tension loading with one bolt. In this phase, the models were validated with data from experimental investigations which performed for gusset plate under monotonic tension loading. In second phase of the investigation, the finite element models expanded to include the two bolt connection and the validation of finite element model was conducted.

This chapter focuses on the development of the finite element models used in the first phase of the investigation. The validation of these models will be presented and discussed in the second phase. The basic steps involved in the first phase of the investigation were as follows:

(1) A linear elastic mesh study of a gusset plate connection was preformed to determine the level of mesh refinement required to ensure convergence.
(2) Inelastic behaviour was incorporated in the gusset plate connection model from step (1) and the models were loaded monotonically in tension well beyond first yield. In this step, the effects of mesh refinement, material strain hardening, contact and bolt model were studied.

The results of finite element analysis were validated by comparing to the test result from monotonic tension loading for one and two bolt connection. The amounts of

displacement were measured in the tests and the variation of axial load vs. displacement behaviour is used as a basis for comparison. The numerical models are validated by comparison with the experimental results.

## 5.2 Linear Elastic Mesh Study

The main purpose of the linear elastic mesh study was to determine the level of mesh refinement required to ensure convergence. In this step, four different finite element meshes were used to model the experimental specimen result (see Figure 5.1). For each mesh, the ABAQUS solid element with 8-node and incompatible mode (C3D8I) was used to model the gusset plate and angle which is splice to gusset plate with bolts. Since the bolt did not deform or shear, it was modeled as analytical rigid, connecting the holes in gusset plate and angle that corresponded with the bolt locations. Linear elastic material properties were assigned to all gusset plate and angle elements. The modulus of elasticity used in the linear elastic material was 201,000 MPa, based on results obtained from the coupon test. The rotational and translational degrees of freedom at the nodes along the connected edge of gusset plate and angle were applied based on the different condition of experiment. The load was applied through the reference node 115 mm away from angle surface and is retrained with the surface of angle. This reference node is also used for applying the desired displacement to model. Figure 5.2 shows a typical gusset plate model used for the linear elastic mesh study. The finite element model of angle member is also shown in Figure 5.3. Figure 5.4 and 6.5 shows the complete model of angle and gusset plate connection with one bolt and two bolts, respectively.

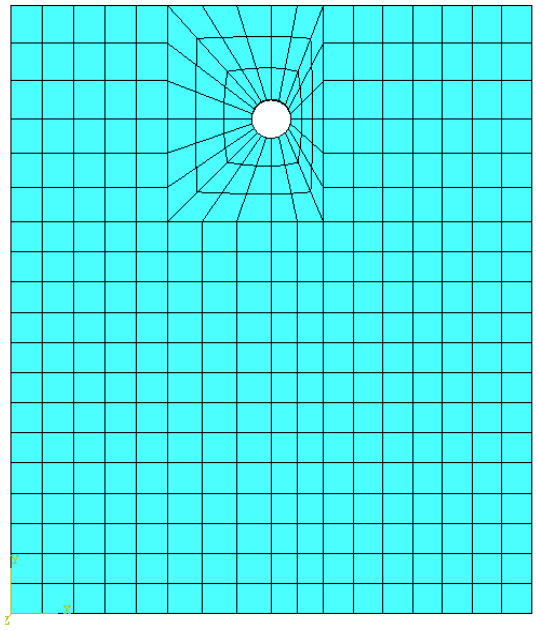

(a) Mesh 1

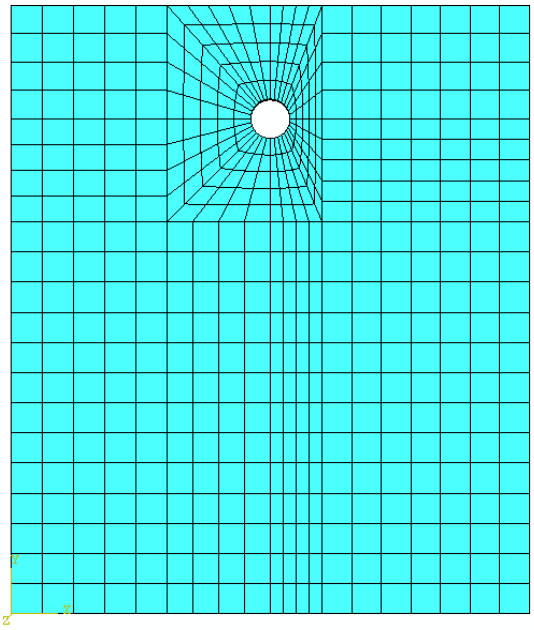

(b) Mesh 2

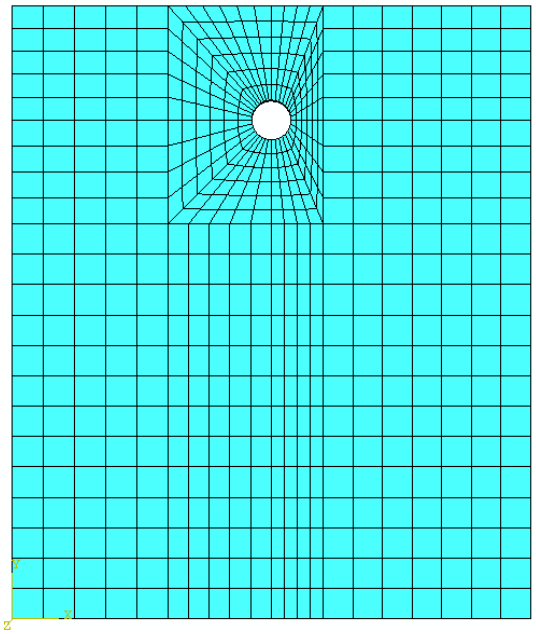

(c) Mesh 3

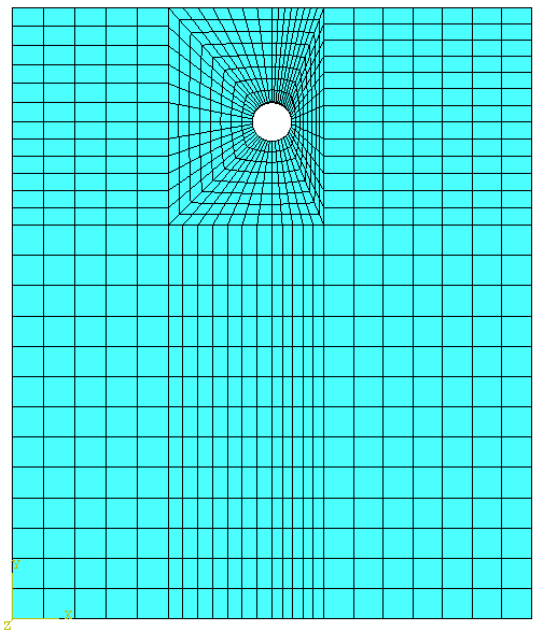

(d) Mesh 4

Figure 5. 1 - Gusset plate meshes used for linear elastic mesh study

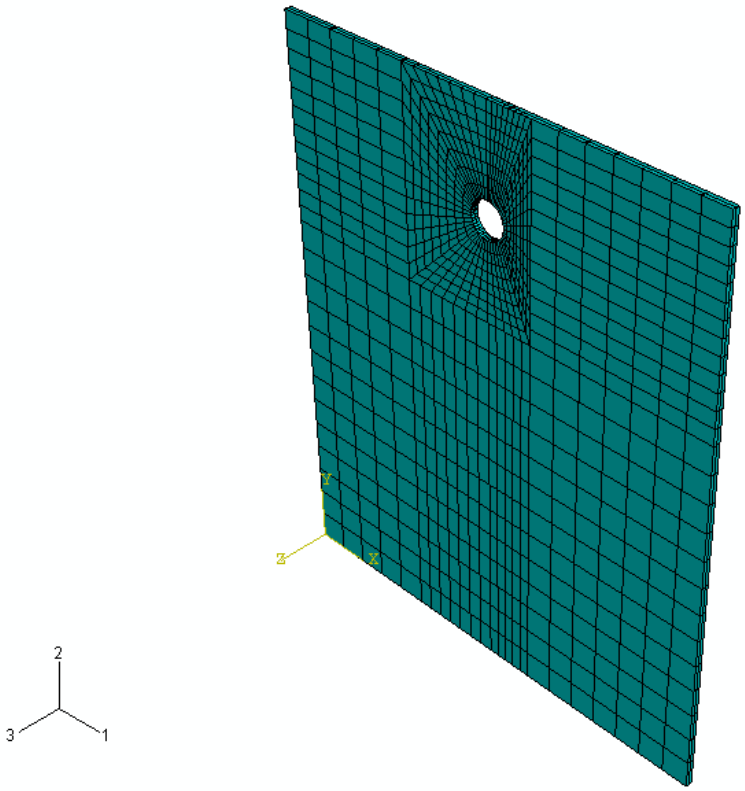


Figure 5. 2 - ABAQUS gusset plate connection model with one bolt connection

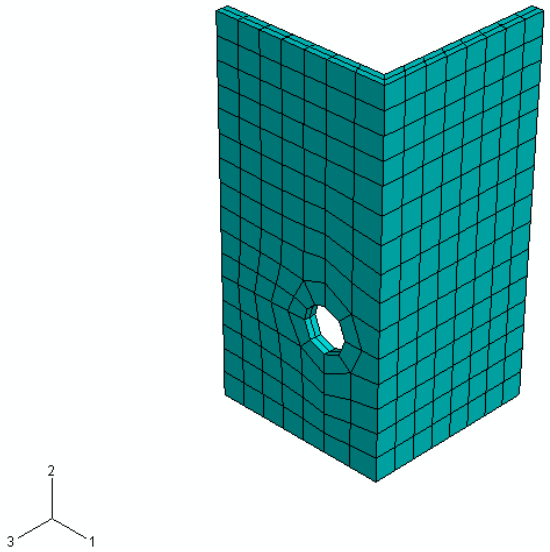


Figure 5. 3 – ABAQUS splice member (angle) model with one bolt connection

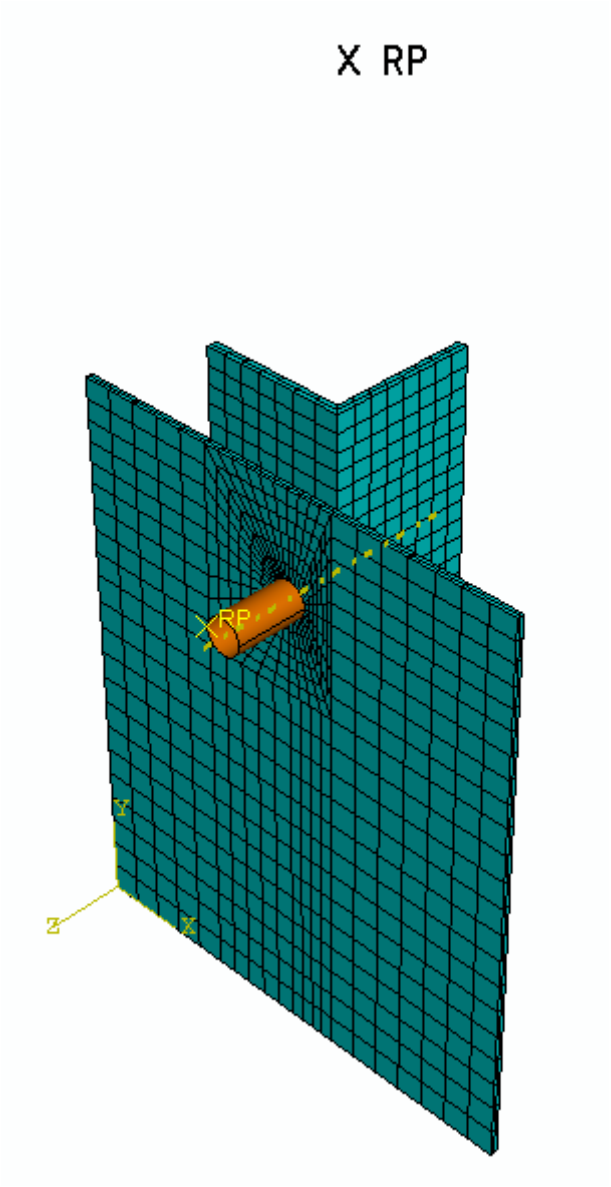


Figure 5. 4 – ABAQUS complete model of gusset plate and angle connection with one bolt connection

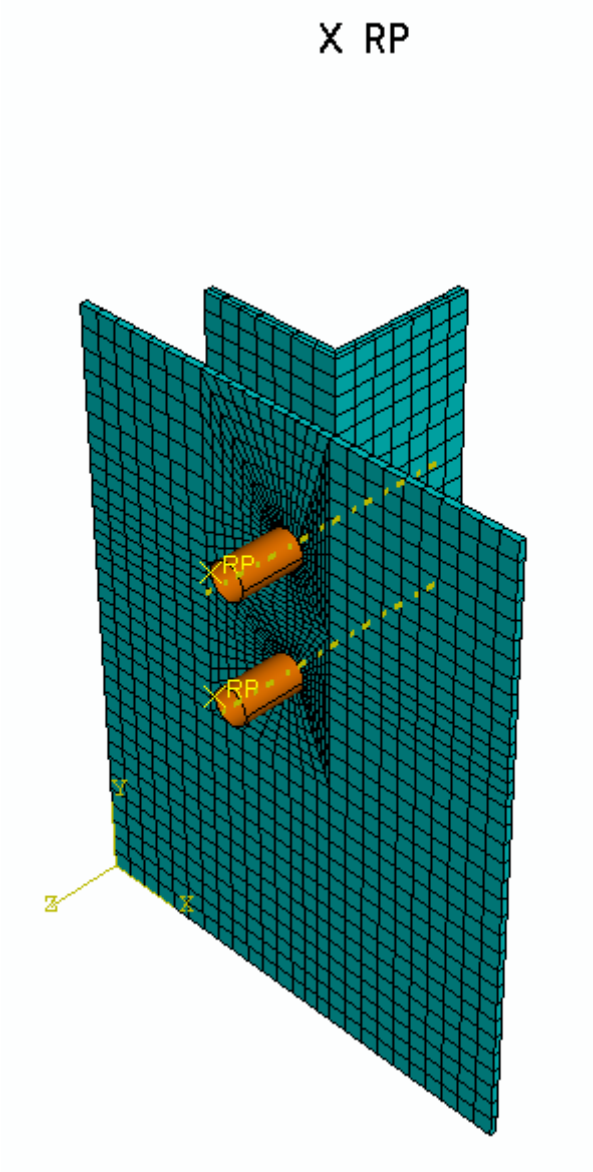


Figure 5. 5 – ABAQUS complete model of gusset plate and angle connection with two bolt connection

A mesh study was conducted using linear elastic model to investigate the stress distribution in a gusset plate and to determine the level of mesh refinement that would be required for modeling the gusset plate connection under monotonic loading. For the linear elastic mesh study, a predetermined load in elastic range was applied to each model. Axial displacement and Von Mises stress output at the element below the hole was compared for the various meshes. Axial displacement output was used primarily, however, in selecting the sufficient level of mesh refinement.

Four different meshes with the number of solid elements ranging from 394 to 1071 were investigated. Table 5.1 and Figure 5.6 compare axial displacement, U (in-plane), and Von Mises stress, VM (max), for four levels of mesh refinement. The axial displacement was illustrated to converge to a constant value as the level of mesh refinement is increased. The third finest mesh (Mesh 3 in Figure 5.1(c)) appears to be adequate for predicting displacements in the elastic range. Refinement beyond this point appears to have little effect on axial displacement.

Table 5. 1– Linear elastic mesh study – summary of results

| Finite Element Model | Mesh Number | Number of Elements | Von Mises Stress (MPa) | In-Plane Displacement (mm) |
|---|---|---|---|---|
| MS1 | Mesh 1 | 394 | 4963.12 | 51.29 |
| MS2 | Mesh 2 | 598 | 5463.00 | 51.92 |
| MS3 | Mesh 3 | 916 | 5735.84 | 53.28 |
| MS4 | Mesh 4 | 1071 | 5758.52 | 53.39 |

Note: VM = Von Mises stress value
U (in-plane) = in-plane displacement
Mesh numbers correspond to gusset plate meshes shown in Figure 5.1

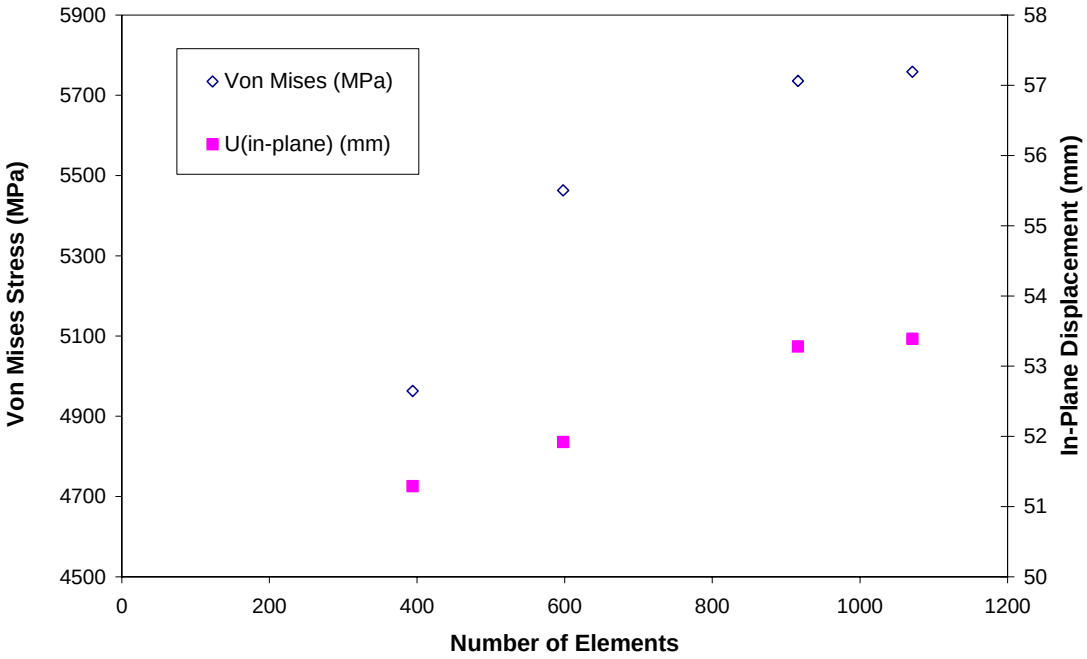


Figure 5. 6 – Linear elastic mesh study – Summary of results.

The Von Mises stress contour plots for each level of mesh refinement, shown in Figure 5.7 and 5.8, indicate that the highest stresses and maximum stress gradients occurs near the last rows of bolt in case of two bolt and near the bolt hole in case of one bolt, respectively.

In Table 5.1 (or Figure 5.6), Von Mises stress can be seen to be increasing as the mesh is refined. In Figure 5.7 and 5.8, it is apparent that the Von Mises stresses away from the bolts are converging. Since analytical rigid were used to model the bolt(s), it was felt that a precise value of Von Mises stress (determined using this bolt model) would not be a value that could be related directly to the stress in actual connection. Since it was the general load versus displacement behaviour of the gusset plate that was of most interest in this study, several attempts was made to refine the mesh to achieve convergence of Von Mises stress.

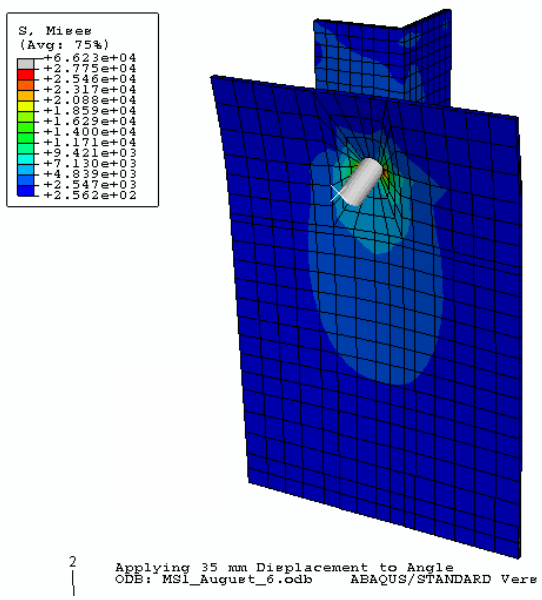


(a) – Mesh 1

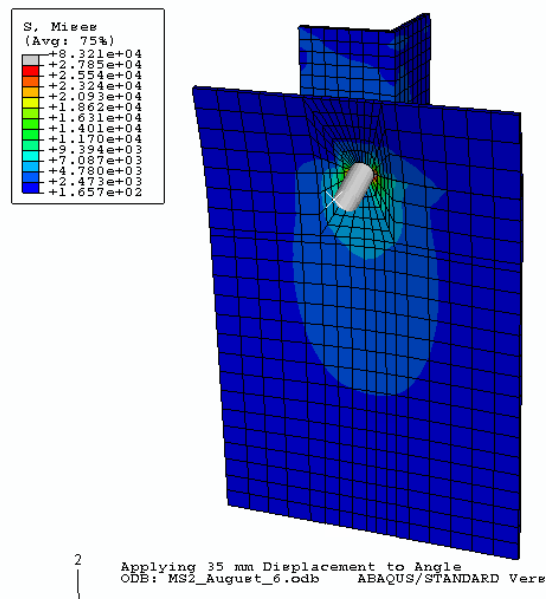


(b) – Mesh 2

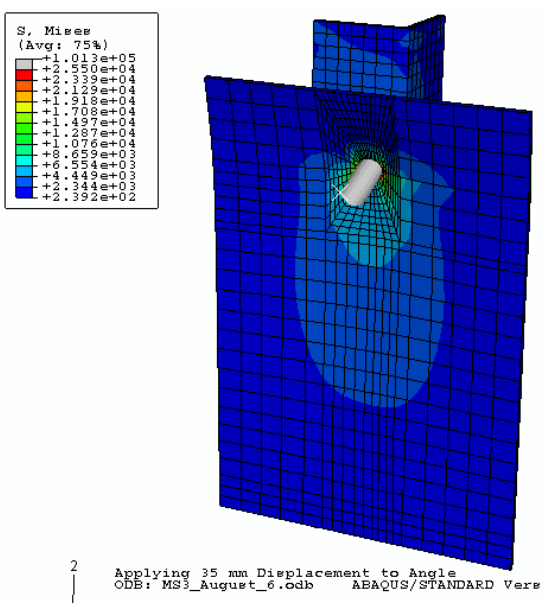


(c) – Mesh 3

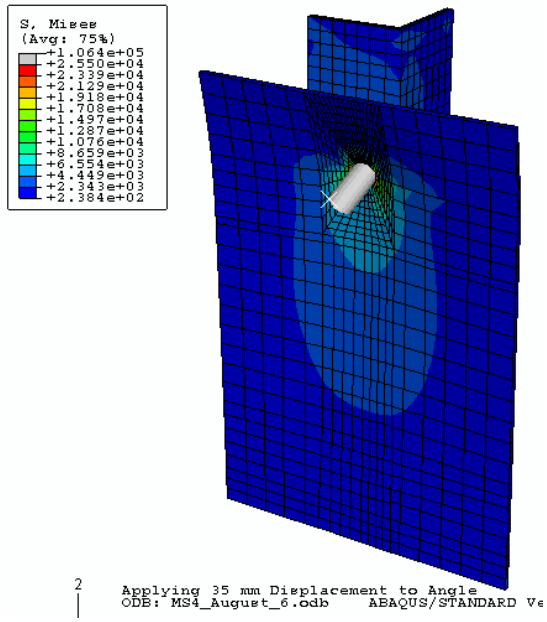


(d) – Mesh 4

Figure 5. 7 – Von Mises stress contour plots from linear elastic mesh study for one bolt connection.

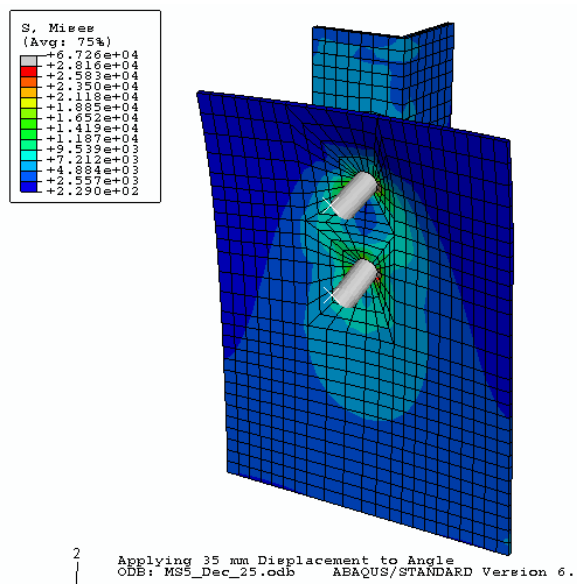


(a) – Mesh 1

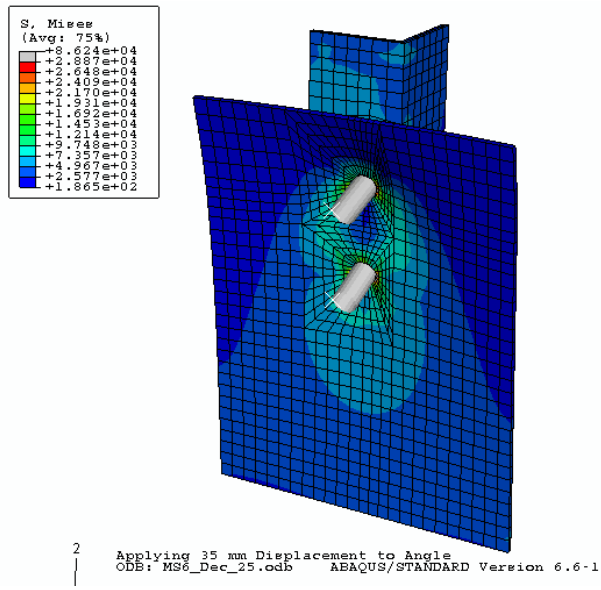


(b) – Mesh 2

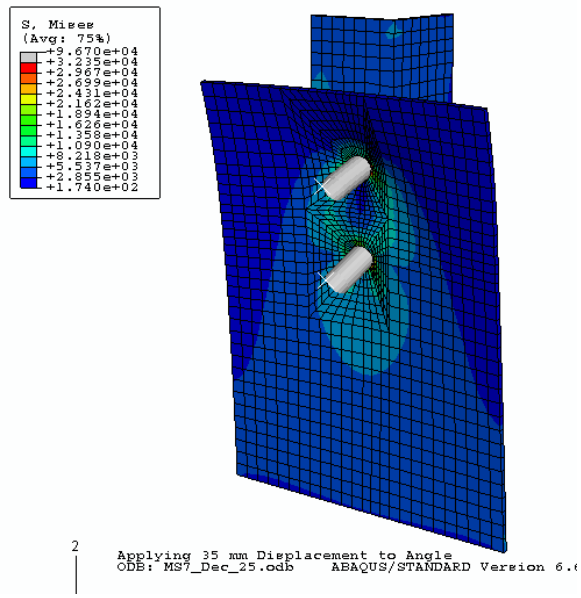


(c) – Mesh 3

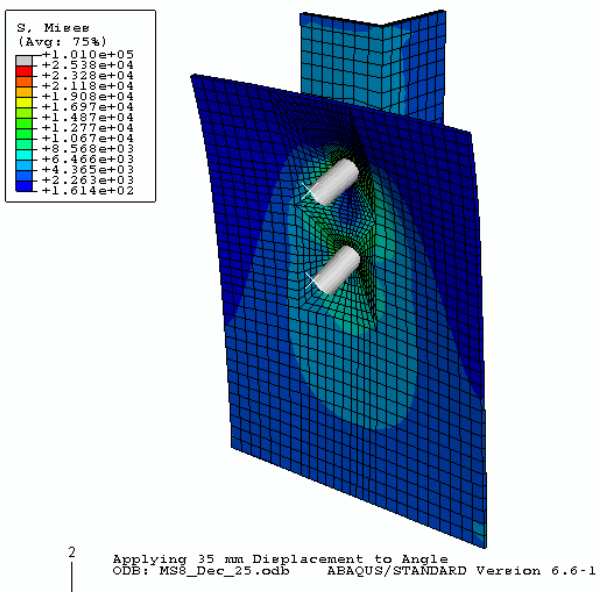


(d) – Mesh 4

Figure 5. 8 – Von Mises stress contour plots from linear elastic mesh study for two bolt connection.

## 5.3 Inelastic Analysis

For this portion of the analysis, nonlinear material behaviour was considered so that the behaviour of the gusset plate was investigated beyond the elastic range. Isotropic strain hardening materials model was developed based on the results from tension coupon tests. True stress versus plastic strain material properties used in ABAQUS (See Figure 5.9(a) and 5.9(b)).

In order to investigate the behaviour of the gusset plate connection loaded monotonically in tension up to and beyond yield, the models developed for the linear elastic mesh study were modified to incorporate nonlinear material behaviour. At this level, the effects of mesh refinement, material strain hardening, analytical rigid (bolt) and contact surface on model were studied.

ABAQUS models that were constructed to study the behaviour of gusset plate connections loaded monotonically in tension were designated MT1 to MT28. Descriptions of these models can be found in Table 5.2. This resulted in four levels of mesh refinement and different size of plate. The strain hardening model was performed for plastic behaviour of material property. The boundary and loading conditions were the same as those described in the test matrix section.

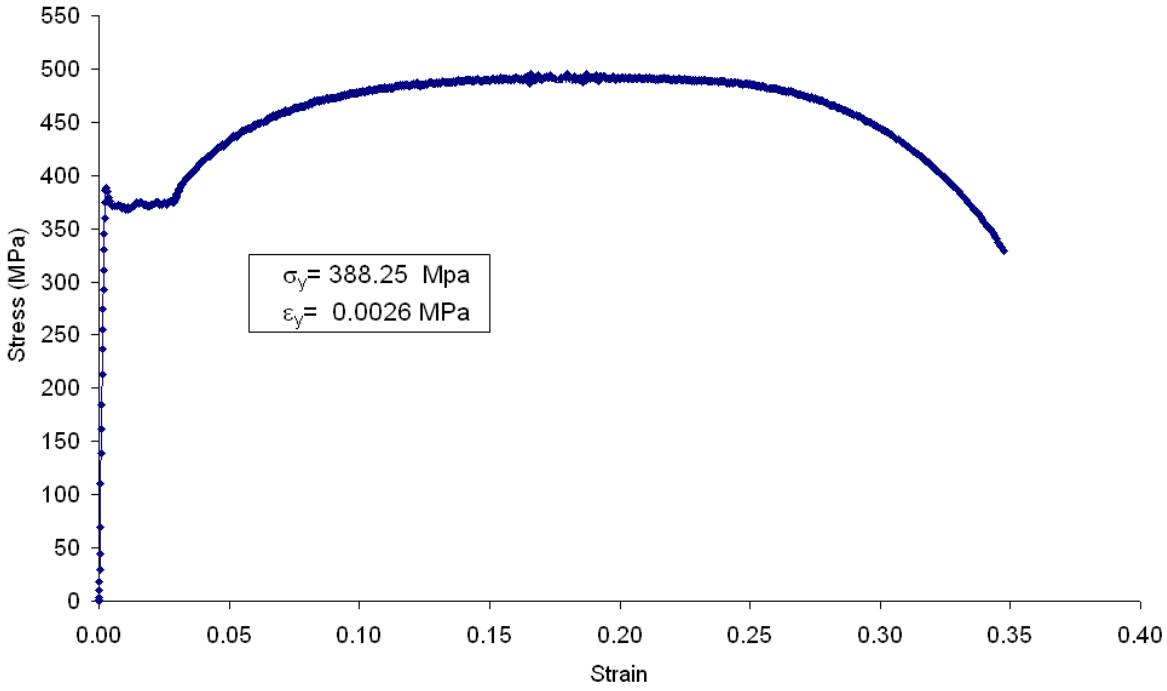


(a) – Typical engineering stress versus strain behaviour for plate obtained from tension coupon test

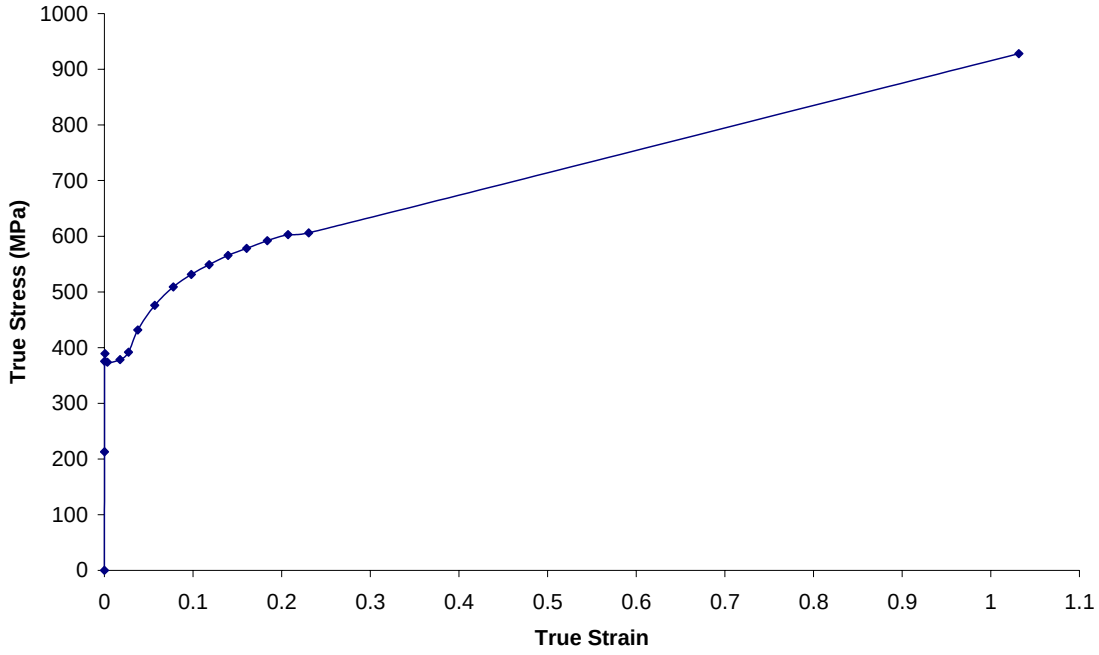


(b) – Typical true stress versus true strain for plate used in ABAQUS

Figure 5. 9 – Material properties for finite element models

Table 5. 2 – Summary of finite element models for different size of plate with one and two bolt connection

| Test No. | Model | Specimen | Mesh | Material Model | Shape | Note |
|---|---|---|---|---|---|---|
| (a) Linear Elastic Mesh Study Models | | | | | | |
| One Bolt Connection | MS1 | PL_720_500_1 | 1 | elastic | Rectangular | |
| | MS2 | PL_720_500_2 | 2 | elastic | Rectangular | |
| | MS3 | PL_720_500_3 | 3 | elastic | Rectangular | |
| | MS4 | PL_720_500_4 | 4 | elastic | Rectangular | |
| Two Bolt Connection | MS5 | PL_640_500_1 | 1 | elastic | Rectangular | |
| | MS6 | PL_640_500_2 | 2 | elastic | Rectangular | |
| | MS7 | PL_640_500_3 | 3 | elastic | Rectangular | |
| | MS8 | PL_640_500_4 | 4 | elastic | Rectangular | |
| (b) Monotonic Tension Loading Models | | | | | | |
| Test #4 (One Bolt) | MT1 | PL_710_305_1 | 1 | strain hardening | Rectangular | |
| | MT2 | PL_710_305_2 | 2 | strain hardening | Rectangular | |
| | MT3 | PL_710_305_3 | 3 | strain hardening | Rectangular | |
| | MT4 | PL_710_305_4 | 4 | strain hardening | Rectangular | |
| Test #7 (One Bolt) | MT5 | PL_720_500_1 | 1 | strain hardening | Rectangular | |
| | MT6 | PL_720_500_2 | 2 | strain hardening | Rectangular | |
| | MT7 | PL_720_500_3 | 3 | strain hardening | Rectangular | |
| | MT8 | PL_720_500_4 | 4 | strain hardening | Rectangular | |
| Test #8 (One bolt) | MT9 | PL_585_500_1 | 1 | strain hardening | Rectangular | |
| | MT10 | PL_585_500_2 | 2 | strain hardening | Rectangular | |
| | MT11 | PL_585_500_3 | 3 | strain hardening | Rectangular | |
| | MT12 | PL_585_500_4 | 4 | strain hardening | Rectangular | |
| Test #9 (Two bolt) | MT13 | PL_640_500_1 | 1 | strain hardening | Rectangular | |
| | MT14 | PL_640_500_2 | 2 | strain hardening | Rectangular | |
| | MT15 | PL_640_500_3 | 3 | strain hardening | Rectangular | |
| | MT16 | PL_640_500_4 | 4 | strain hardening | Rectangular | |

Table 5.2 – Summary of finite element models for different size of plate with one and two bolt connection (continued)

| Test No. | Model | Specimen | Mesh | Material Model | Shape | Note |
|---|---|---|---|---|---|---|
| (b) Monotonic Tension Loading Models | | | | | | |
| Test #10 (Two bolt) | MT17 | PL_620_500_1 | 1 | strain hardening | Rectangular | |
| | MT18 | PL_620_500_2 | 2 | strain hardening | Rectangular | |
| | MT19 | PL_620_500_3 | 3 | strain hardening | Rectangular | |
| | MT20 | PL_620_500_4 | 4 | strain hardening | Rectangular | |
| Test #11 (Two Bolt) | MT21 | PL_635_500_1 | 1 | strain hardening | Rectangular | |
| | MT22 | PL_635_500_2 | 2 | strain hardening | Rectangular | |
| | MT23 | PL_635_500_3 | 3 | strain hardening | Rectangular | |
| | MT24 | PL_635_500_4 | 4 | strain hardening | Rectangular | |
| Test #12 (One Bolt) | MT25 | PL_490_200_1 | 1 | strain hardening | Rectangular | |
| | MT26 | PL_490_200_2 | 2 | strain hardening | Rectangular | |
| | MT27 | PL_490_200_3 | 3 | strain hardening | Rectangular | |
| | MT28 | PL_490_200_4 | 4 | strain hardening | Rectangular | |

Subsequent to the investigation of mesh refinement, the third finest mesh (Mesh 3 in Figure 5.1) was adopted and modified to evaluate the effects of fixed or pinned far end and bolt model.

The effect of friction between angle and plate surface was simulated by surface-to-surface contact. This surface-to-surface contact could carry out the load through angle to plate and is affected on the area below and top of the hole in plate. To study the effect of the bolt on plate and angle the tie contact was developed between the outer peripheral surface of bolt and inner peripheral surface of holes in plate and angle, respectively. Figure 5.10 and 5.11 shows the different contact and far-end boundary condition for one and two bolt connection, respectively.

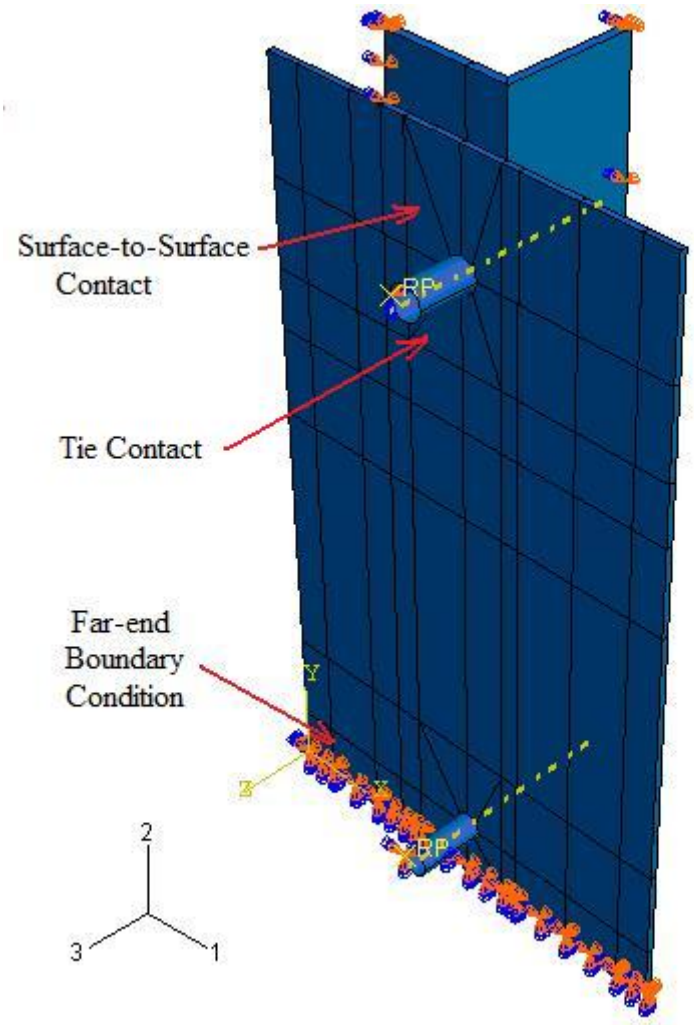


Figure 5. 10 - ABAQUS gusset plate with one bolt connection model including contact and far-end boundary condition

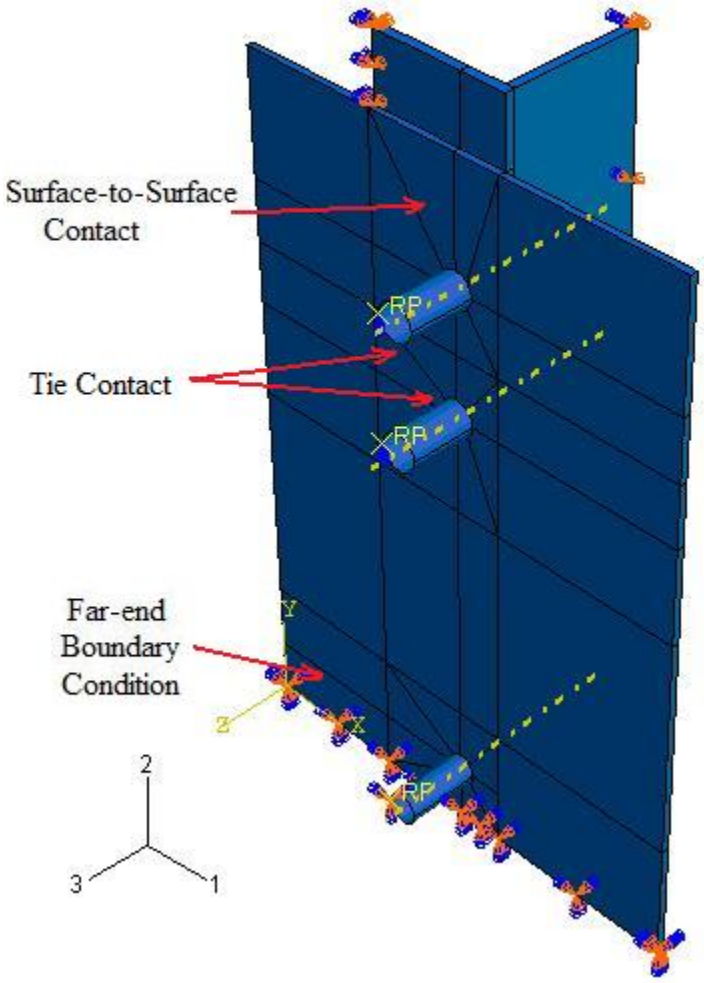


Figure 5. 11 - ABAQUS gusset plate with two bolt connection model including contact and far-end boundary condition.

Figure 5.12 to 5.18 shows the deformed configuration of seven gusset plate models loaded monotonically in tension. As can be seen in these figures, most of the element distortion is occurring in the elements just beyond the bolt in one bolt connection and it was occurred in last row of bolts in two bolt connection of gusset plate. The upper surface of the plate has out-of-plane buckling during the loading. This was also indicated in finite element model and has a good agreement with test condition.

The tearing of the plate occurred in several test and it was determined that the location of the bolt from plate edge affected the tearing but the bearing of the plate near the bolt hole was observed in all tests.

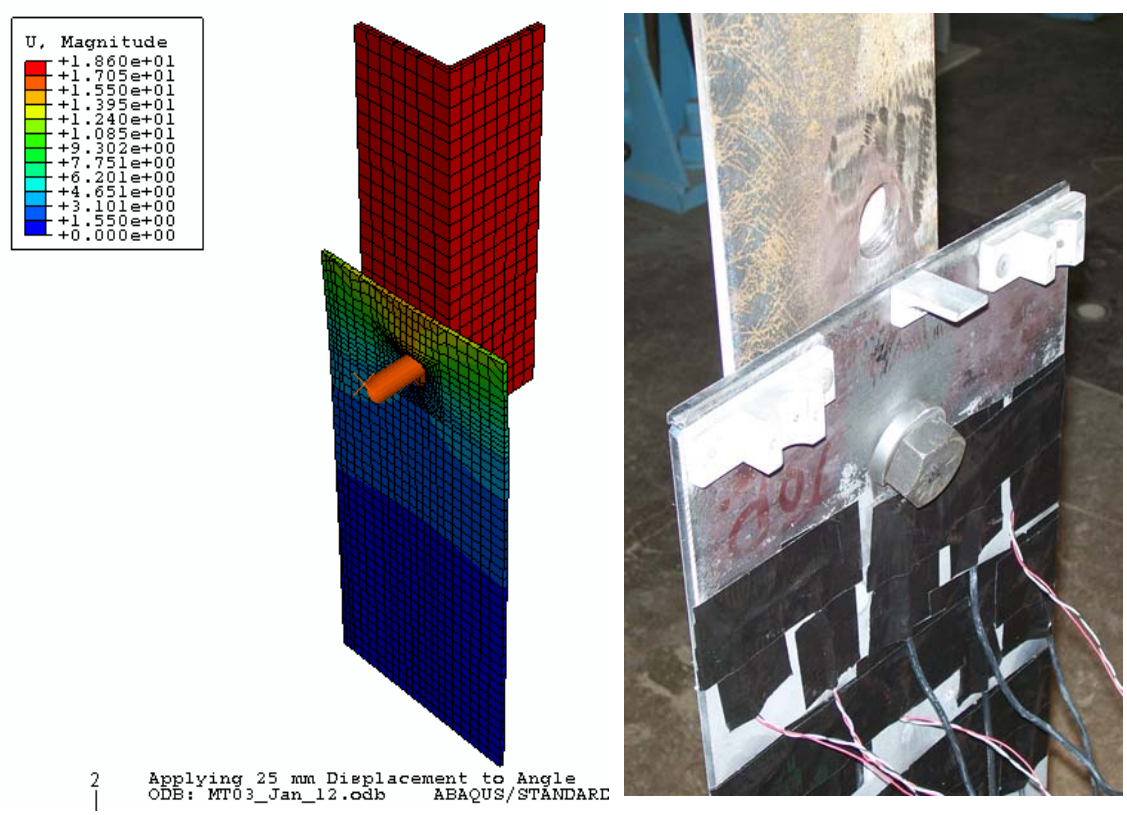


(a) Finite element model of Test #4 (b) Deformed specimen Test #4

Figure 5. 12 – Deformed configuration of gusset plate model with one bolt connection (MT-3) loaded monotonically in tension (Model of Test #4)

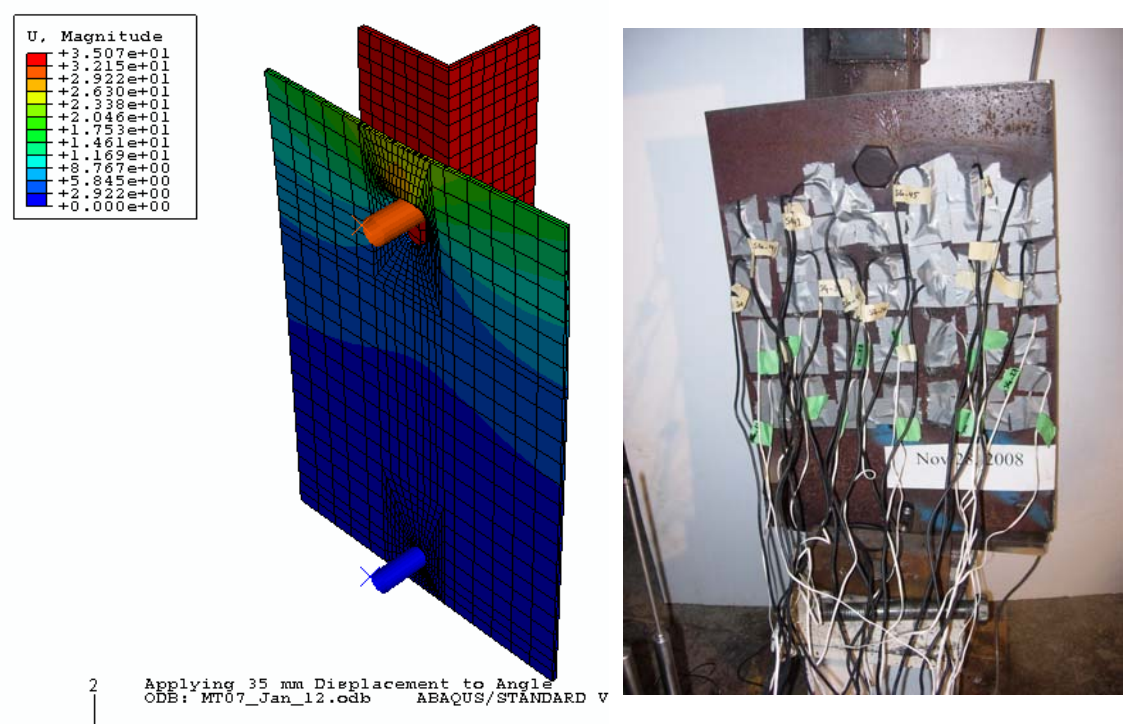


(a) Finite element model of Test #7 (b) Deformed specimen Test #7

Figure 5. 13 – Deformed configuration of gusset plate model with one bolt connection (MT-7) loaded monotonically in tension (Model of Test #7)

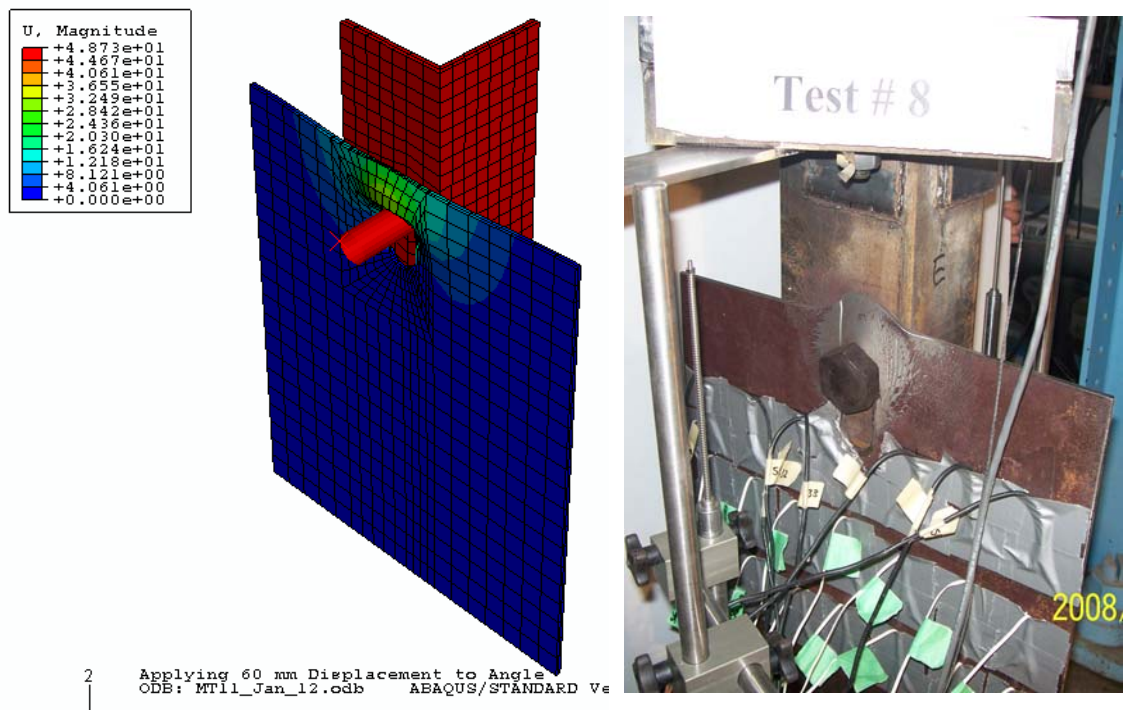


(a) Finite element model of Test #8 (b) Deformed specimen Test #8

Figure 5. 14 – Deformed configuration of gusset plate model with one bolt connection (MT-11) loaded monotonically in tension (Model of Test #8)

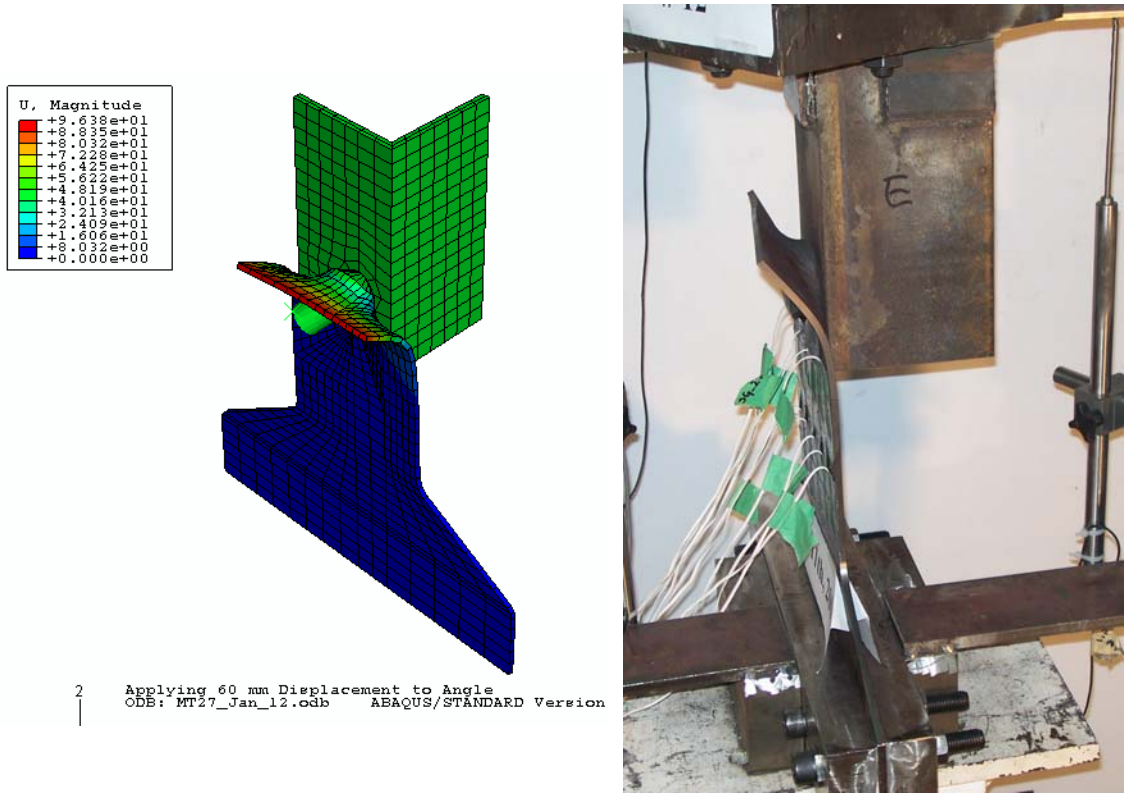


(a) Finite element model of Test #12 (b) Deformed specimen Test #12

Figure 5. 15 – Deformed configuration of gusset plate model with one bolt connection (MT-27) loaded monotonically in tension (Model of Test #12)

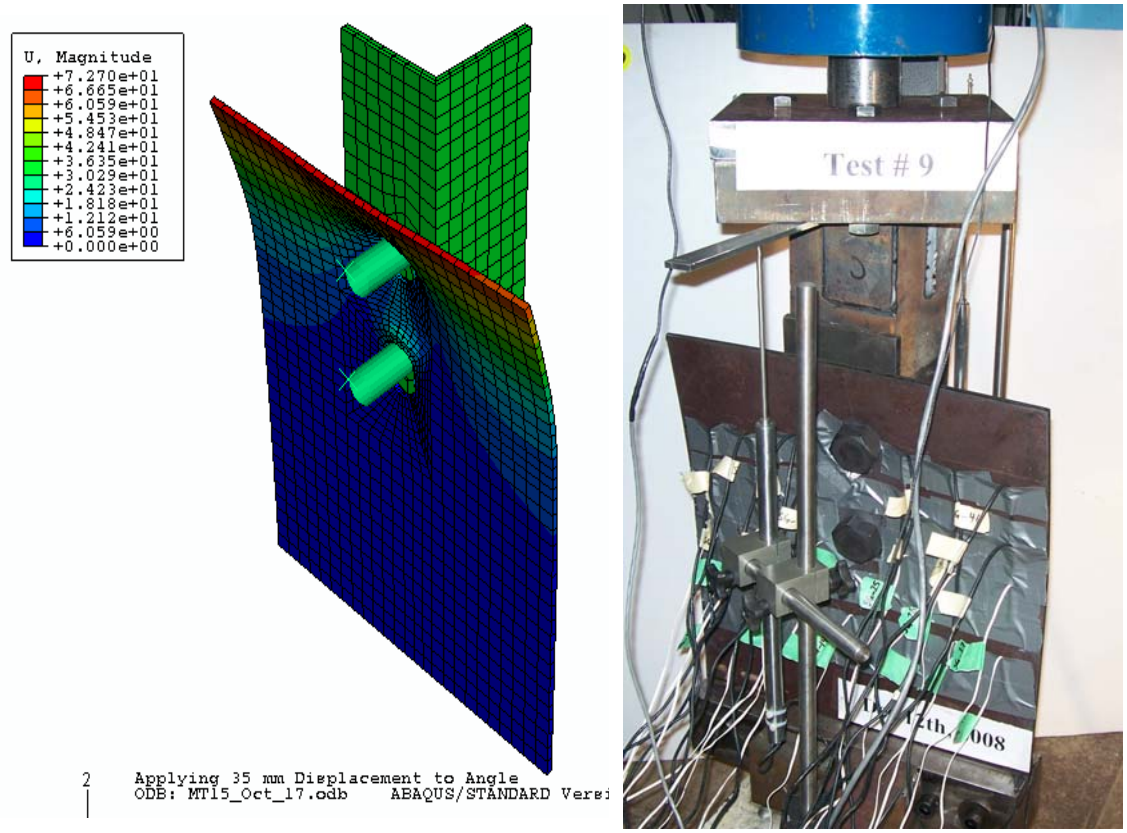


(a) Finite element model of Test #9 (b) Deformed specimen Test #9

Figure 5. 16 – Deformed configuration of gusset plate model with two bolt connection (MT-15) loaded monotonically in tension (Model of Test #9)

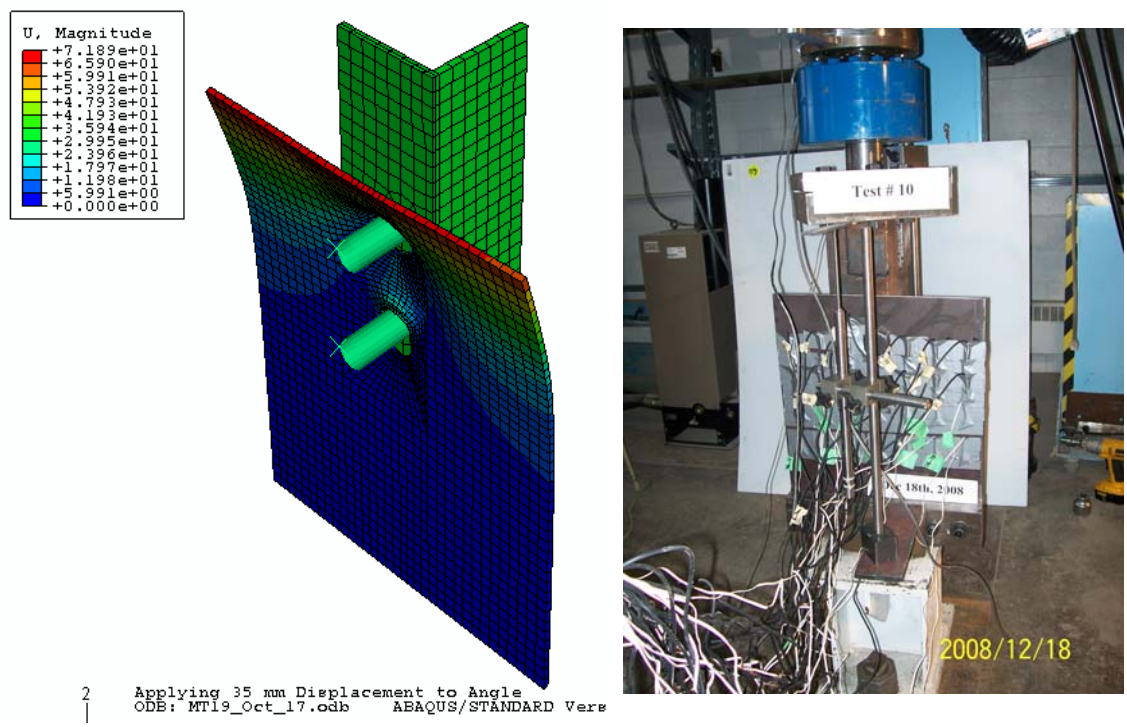


(a) Finite element model of Test #10 (b) Deformed specimen Test #10

Figure 5. 17 – Deformed configuration of gusset plate model with two bolt connection (MT-19) loaded monotonically in tension (Model of Test #10)

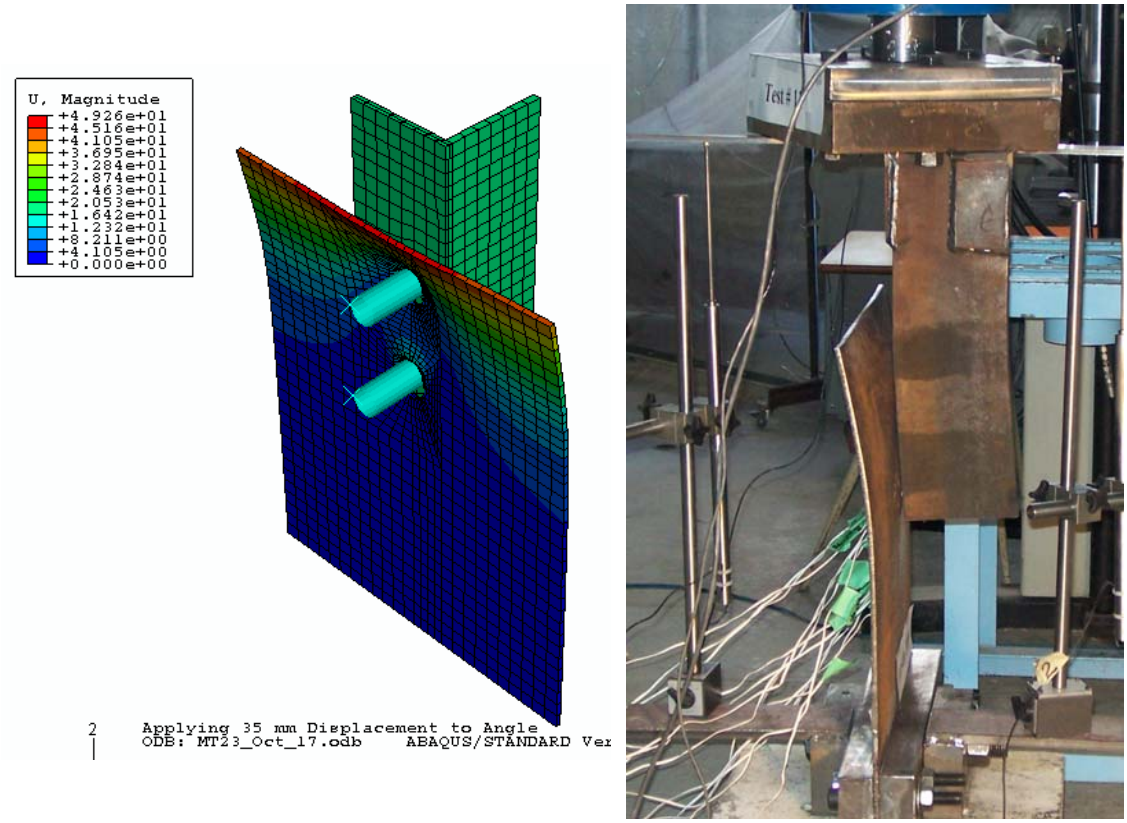


(a) Finite element model of Test #11 (b) Deformed specimen Test #11

Figure 5. 18 – Deformed configuration of gusset plate model with two bolt connection (MT-23) loaded monotonically in tension (Model of Test #11)

For the levels of mesh refinement investigated, the effect of mesh refinement on monotonic tension load-displacement behaviour appears to have some difference and then begin to converge. Figure 5.19 shows that as the mesh are refined, the ultimate tensile capacity of the model decrease slightly. The difference between subsequent refinements appears to diminish as the mesh is refined. The third finest mesh (Mesh 3 in Figure 5.2(c)) was selected for the remaining monotonic tension analysis.

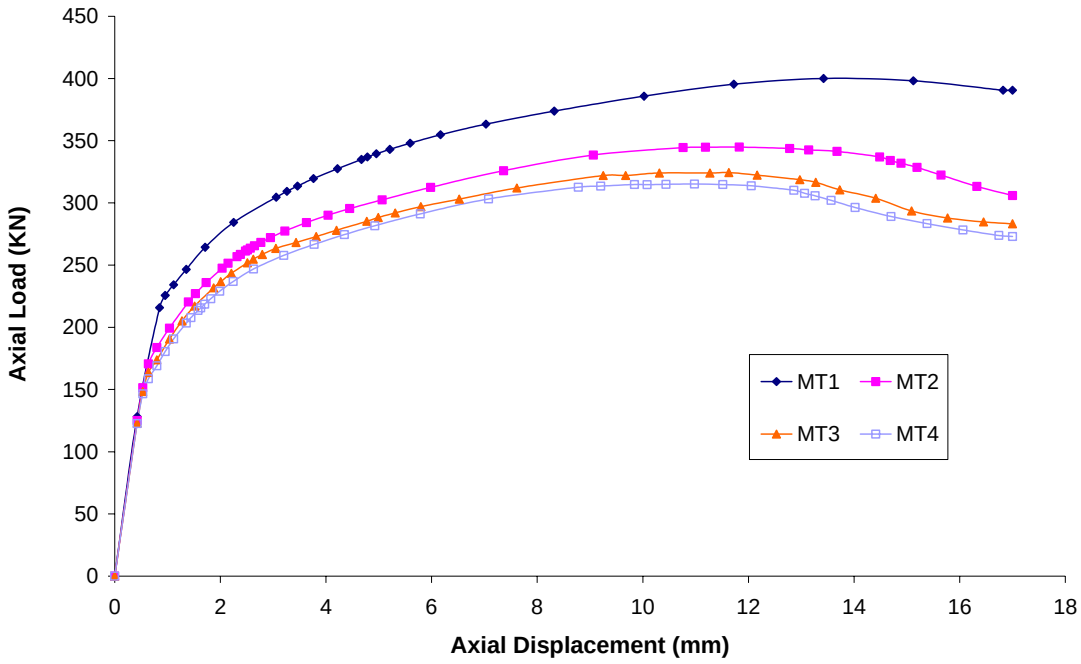


Model Description:

MT1 - Mesh 1, isotropic strain hardening material model

MT2 - Mesh 2, isotropic strain hardening material model

MT3 - Mesh 3, isotropic strain hardening material model

MT4 - Mesh 4, isotropic strain hardening material model

Figure 5. 19 – Effect of mesh refinement for plate 710 × 305 × 6.4 mm with one bolt connection (GP-04)

In studying the effects of mesh refinement along with detailed, surface-to-surface contact, tie contact and analytical rigid (bolt) with inelastic material properties were constructed. In Figures 5.20 to 5.25, the models that used the isotropic strain hardening material for different size of plate are shown. There is a good convergence in mesh refinement in all finite element models.

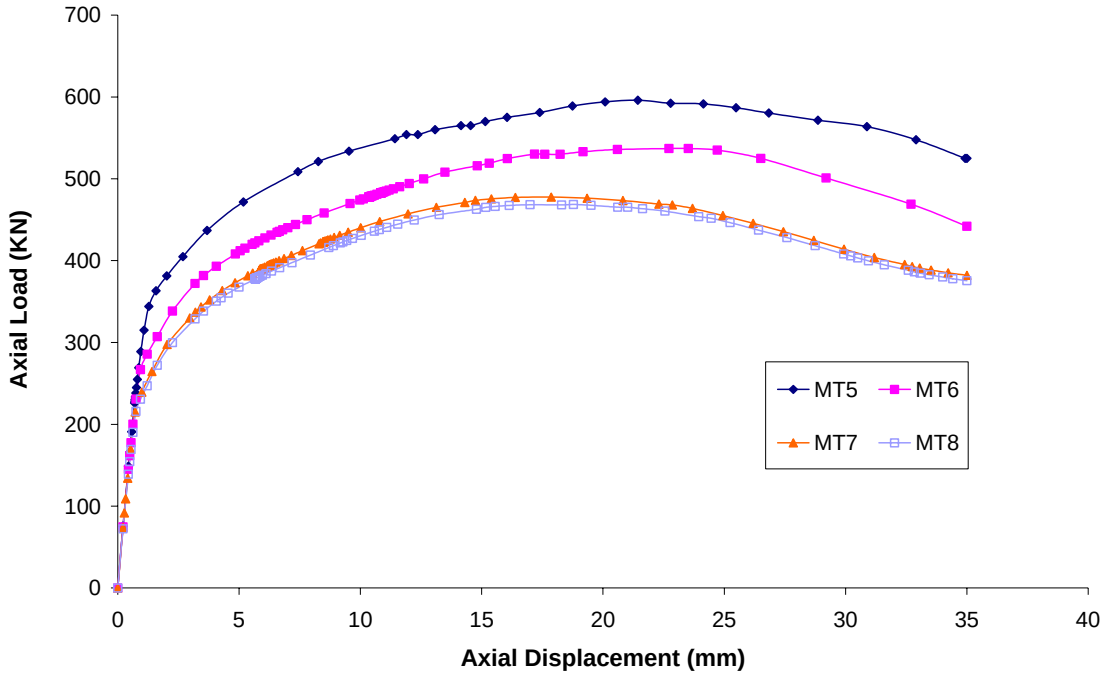


Model Description:

MT5 - Mesh 1, isotropic strain hardening material model

MT6 - Mesh 2, isotropic strain hardening material model

MT7 - Mesh 3, isotropic strain hardening material model

MT8 - Mesh 4, isotropic strain hardening material model

Figure 5. 20 – Effect of mesh refinement for plate 720 × 500 × 7.0 mm with one bolt connection (GP-07)

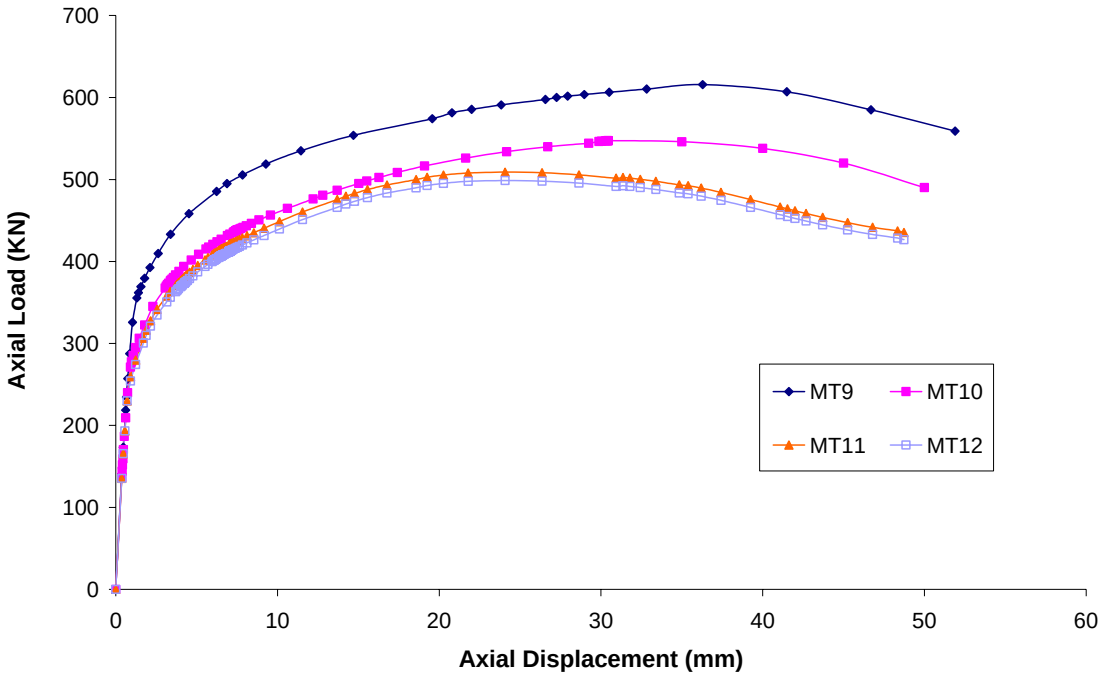


Model Description:

MT9 - Mesh 1, isotropic strain hardening material model

MT10 - Mesh 2, isotropic strain hardening material model

MT11 - Mesh 3, isotropic strain hardening material model

MT12 - Mesh 4, isotropic strain hardening material model

Figure 5. 21 – Effect of mesh refinement for plate 590 × 500 × 7.0 mm with one bolt connection (GP-08)

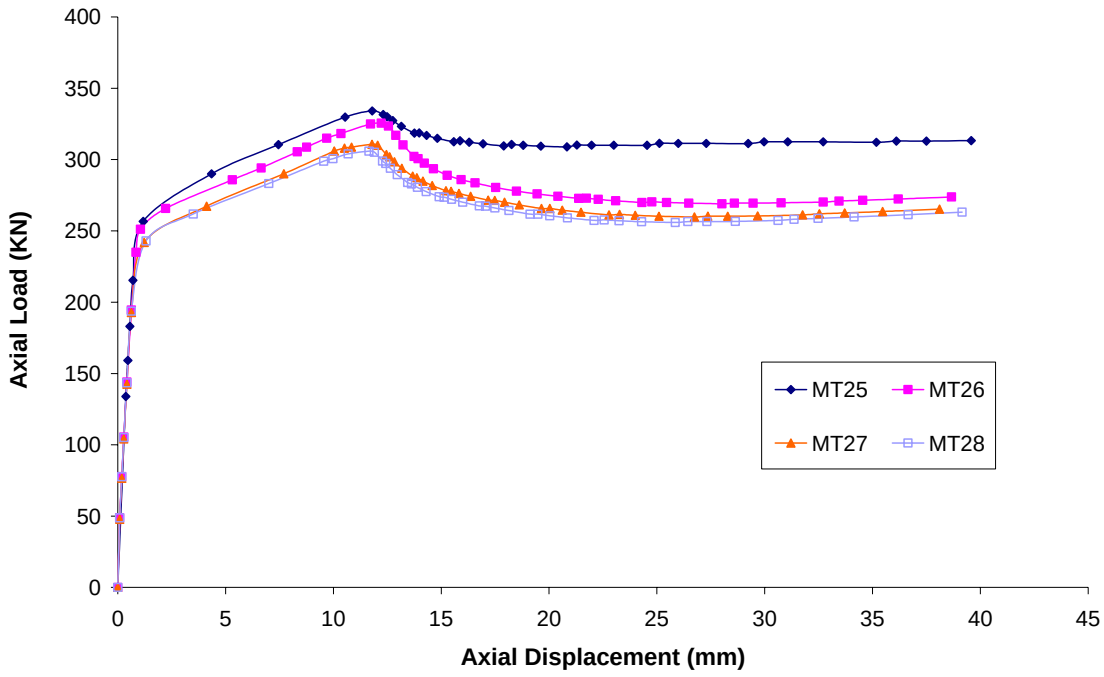


Model Description:

MT25 - Mesh 1, isotropic strain hardening material model

MT26 - Mesh 2, isotropic strain hardening material model

MT27 - Mesh 3, isotropic strain hardening material model

MT28 - Mesh 4, isotropic strain hardening material model

Figure 5. 22 – Effect of mesh refinement for plate 490 × 200 × 6.5 mm with one bolt connection (GP-12)

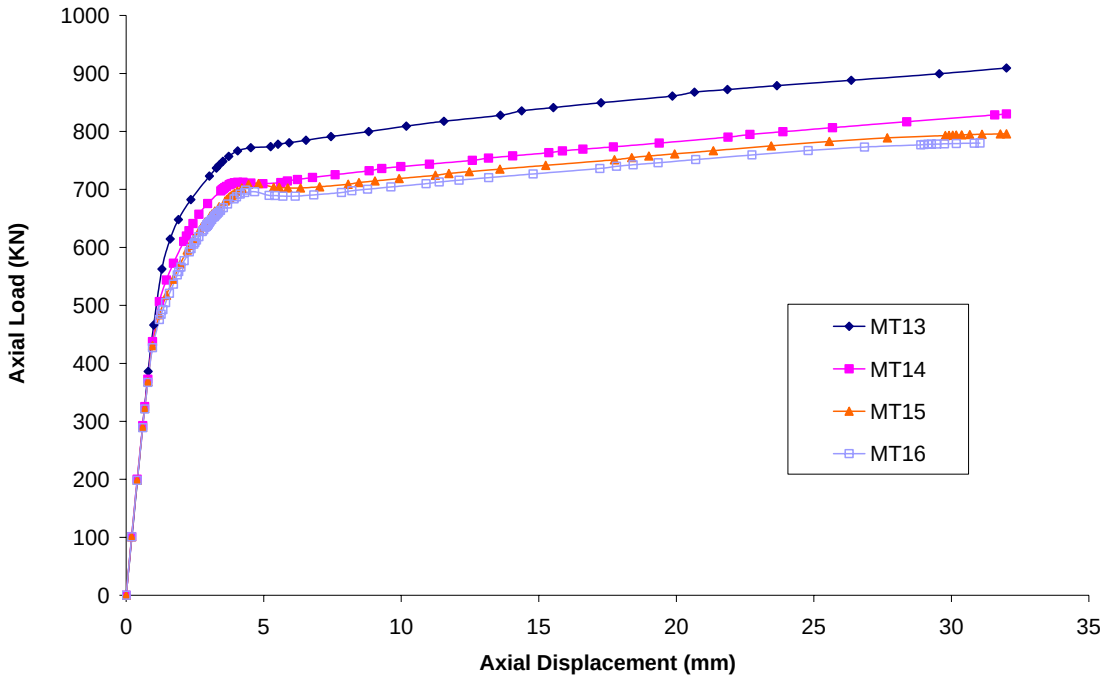


Model Description:

MT13 - Mesh 1, isotropic strain hardening material model

MT14 - Mesh 2, isotropic strain hardening material model

MT15 - Mesh 3, isotropic strain hardening material model

MT16 - Mesh 4, isotropic strain hardening material model

Figure 5. 23 – Effect of mesh refinement for plate 640 × 500 × 6.9 mm with two bolt connections (GP-09)

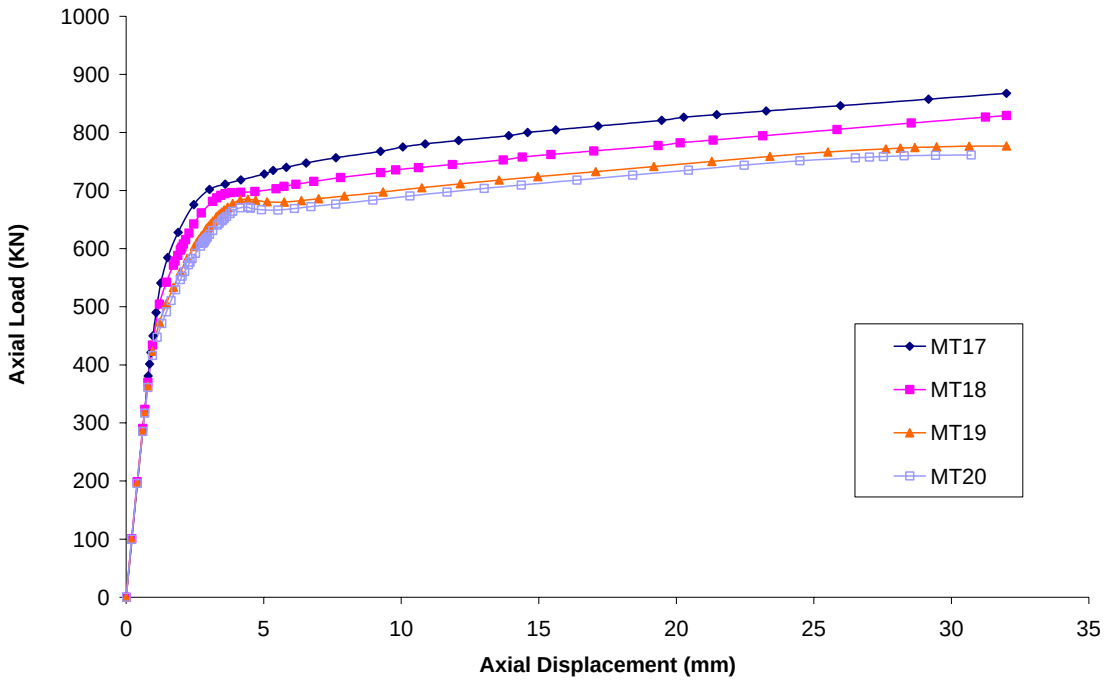


Model Description:

MT17 - Mesh 1, isotropic strain hardening material model

MT18 - Mesh 2, isotropic strain hardening material model

MT19 - Mesh 3, isotropic strain hardening material model

MT20 - Mesh 4, isotropic strain hardening material model

Figure 5. 24 – Effect of mesh refinement for plate 620 × 500 × 6.9 mm with two bolt connections (GP-10)

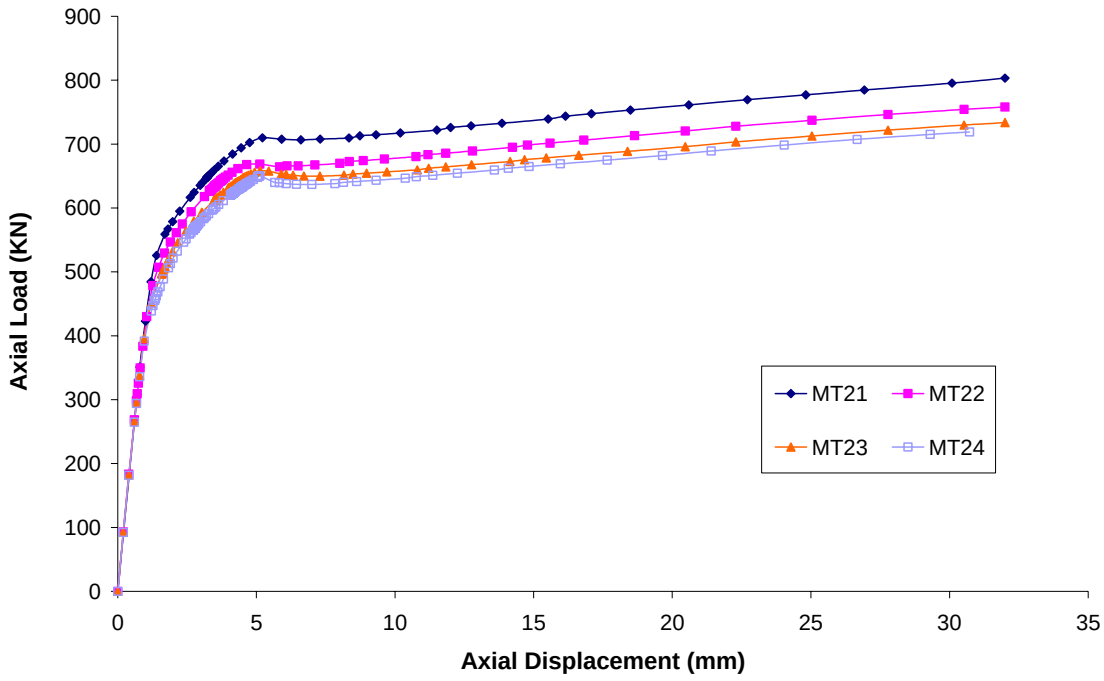


Model Description:

MT21 - Mesh 1, isotropic strain hardening material model

MT22 - Mesh 2, isotropic strain hardening material model

MT23 - Mesh 3, isotropic strain hardening material model

MT24 - Mesh 4, isotropic strain hardening material model

Figure 5. 25 – Effect of mesh refinement for plate 635 × 500 × 6.9 mm with two bolt connections (GP-11)

Table 5.3 compares ultimate loads obtained from the monotonic tension loading analysis using finite element analysis with ultimate tensile loads obtained from the tests. The ratio of finite element analysis to test load value is varied from 1.02 to 1.37.

This ratio has some discrepancy in specimens GP-07 and GP-08 due to the imperfection of simulation. The specimen GP-07 had a failure at the bottom of the plate since the weld ruptured at the far-end and made some rotation in specimen during the test which did not simulate in finite element model. The specimen GP-08 had also a tearing in the left side of the bolt hole during the test condition which did

not simulate in finite element model. However, it seems that there is a good agreement between the result of finite element model and test results for other specimens.

Table 5. 3 – Comparisons of finite element analysis with test results

| Test Specimen | Plate Size (mm) (No of bolts) | Test Measured Capacity (kN) | FE Model | Mesh No. | Material Model | FEA Ultimate Capacity (kN) | FEA/ Test Load Ratio |
|---|---|---|---|---|---|---|---|
| GP-04 | 710 x 305 x 6.4 (1) | 323.2 | MT3 | 3 | isotropic strain hardening | 344.4 | 1.06 |
| GP-07 | 720 x 500 x 7.0 (1) | 349.5 | MT7 | 3 | isotropic strain hardening | 477.3 | 1.37 |
| GP-08 | 590 x 500 x 7.0 (1) | 422.6 | MT11 | 3 | isotropic strain hardening | 507.9 | 1.20 |
| GP-12 | 490 x 200 x 6.5 (1) | 304.7 | MT27 | 3 | isotropic strain hardening | 310.7 | 1.02 |
| GP-09 | 640 x 500 x 6.9 (2) | 549.3 | MT15 | 3 | isotropic strain hardening | 545.9 | 0.99 |
| GP-10 | 620 x 500 x 6.9 (2) | 612.4 | MT19 | 3 | isotropic strain hardening | 623.0 | 1.02 |
| GP-11 | 635 x 500 x 6.9 (2) | 566.0 | MT23 | 3 | isotropic strain hardening | 611.4 | 1.08 |

Note: Mesh numbers correspond to gusset plate meshes shown in Figure 5.1.

In this investigation, no attempt was made to model the tearing of the gusset plate observed in the specimens tested. Again, although this may account for some of the difference, it is believed tearing only occurred in the later stages of the tests, after the ultimate capacity of the gusset plate was reached.

Figures 5.26 to 5.32 show the comparison of axial load versus displacement plots for finite element models with strain hardening model and load versus deformation plot which is obtained from different test. In these figures, it has seen that the curves have a good agreement in elastic range. Due to the local buckling, bolt slip and contact between the surfaces, there is some discrepancy between the graphs in plastic area.

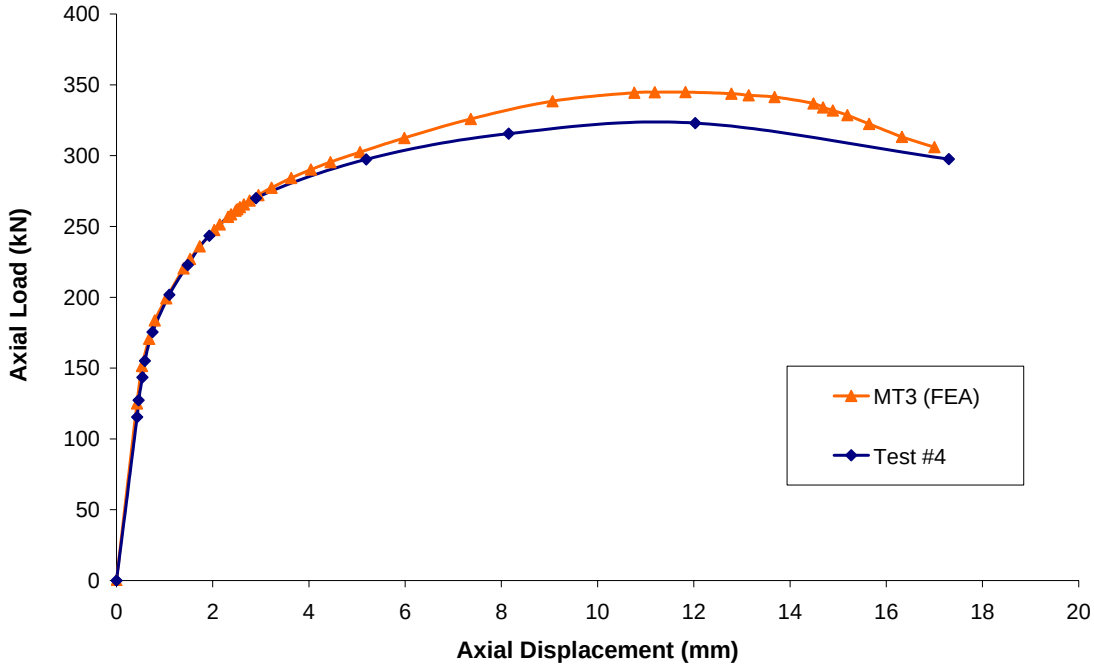


Figure 5. 26 - Comparison with test results of specimen GP-04 (plate 710 x 305 x 6.4 mm) and finite element model with one bolt connection

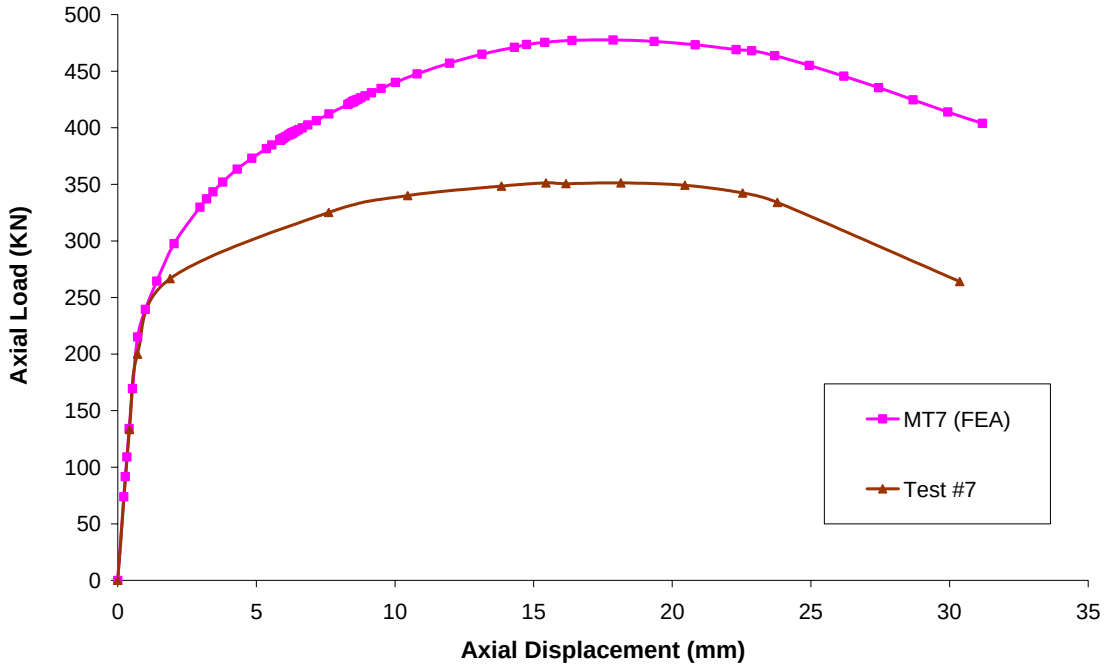


Figure 5. 27 - Comparison with test results of specimen GP-07 (plate 720 x 500 x 7.0 mm) and finite element model with one bolt connection

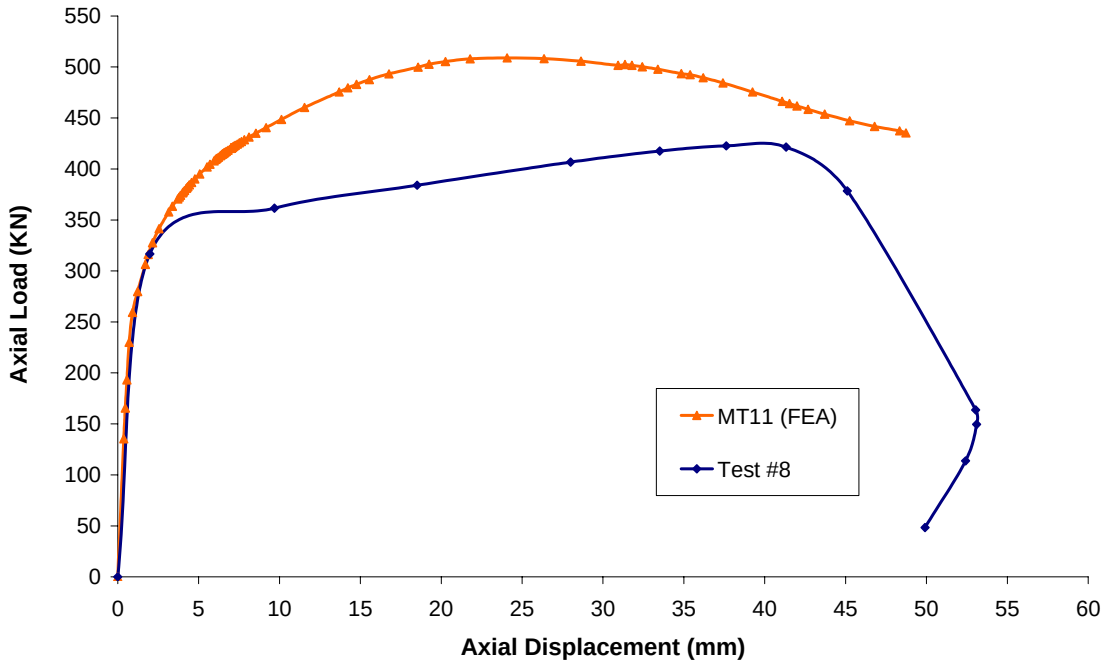


Figure 5. 28 - Comparison with test results of specimen GP-08 (plate 590 x 500 x 7.0 mm) and finite element model with one bolt connection

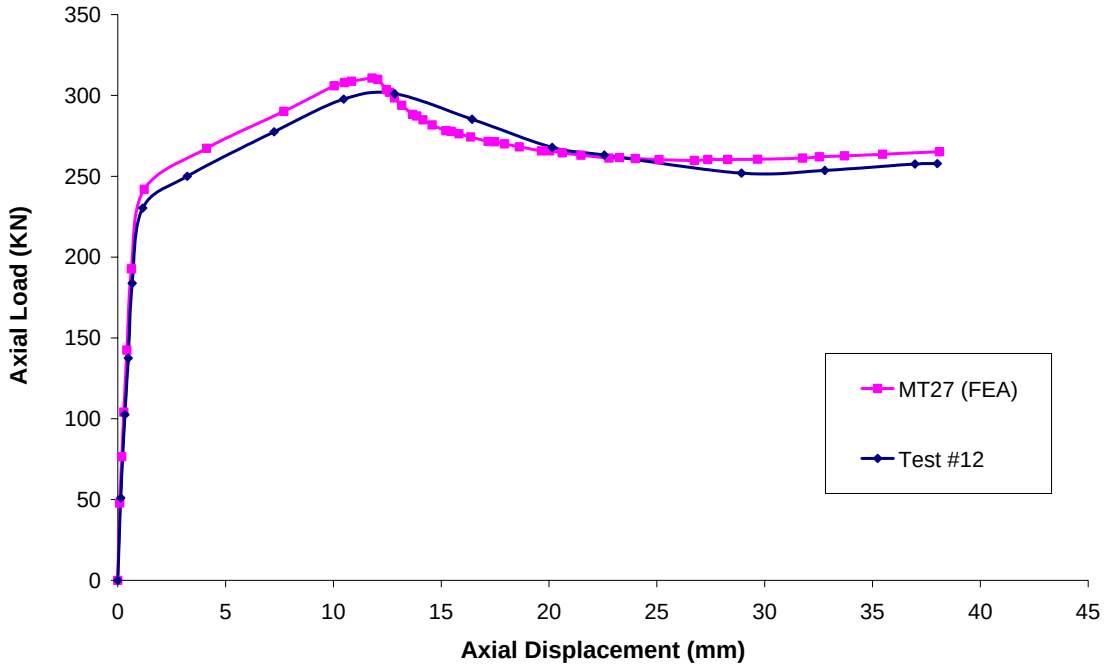


Figure 5. 29 - Comparison with test results of specimen GP-12 (plate 490 x 200 x 6.5 mm) and finite element model with one bolt connection

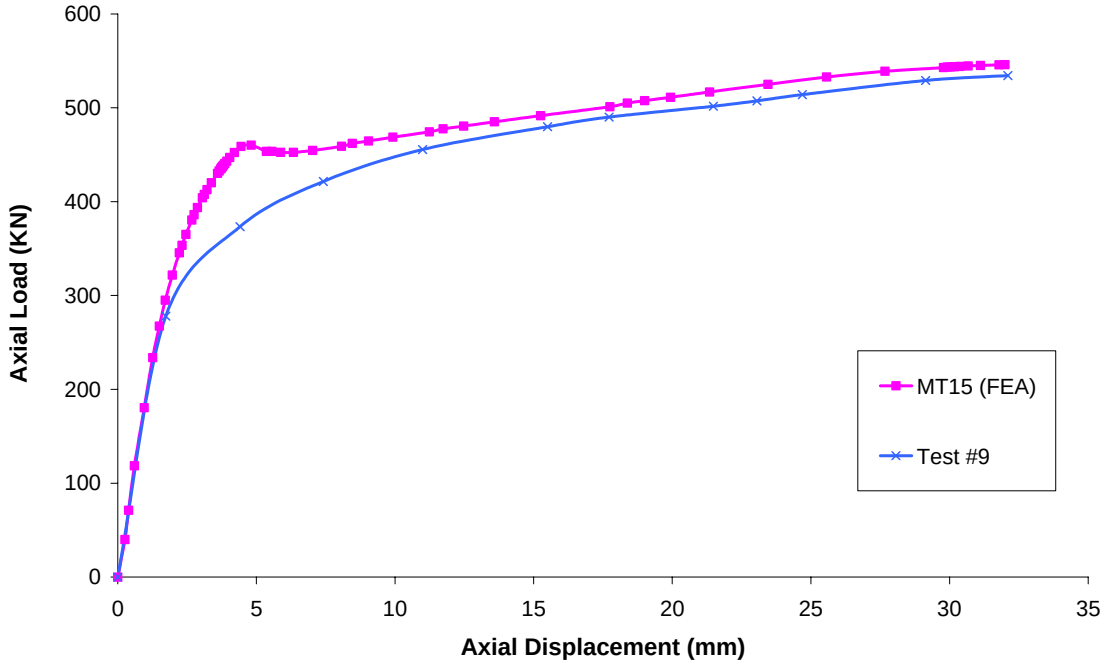


Figure 5. 30 - Comparison with test results of specimen GP-09 (plate 640 x 500 x 6.9 mm) and finite element model with two bolt connections

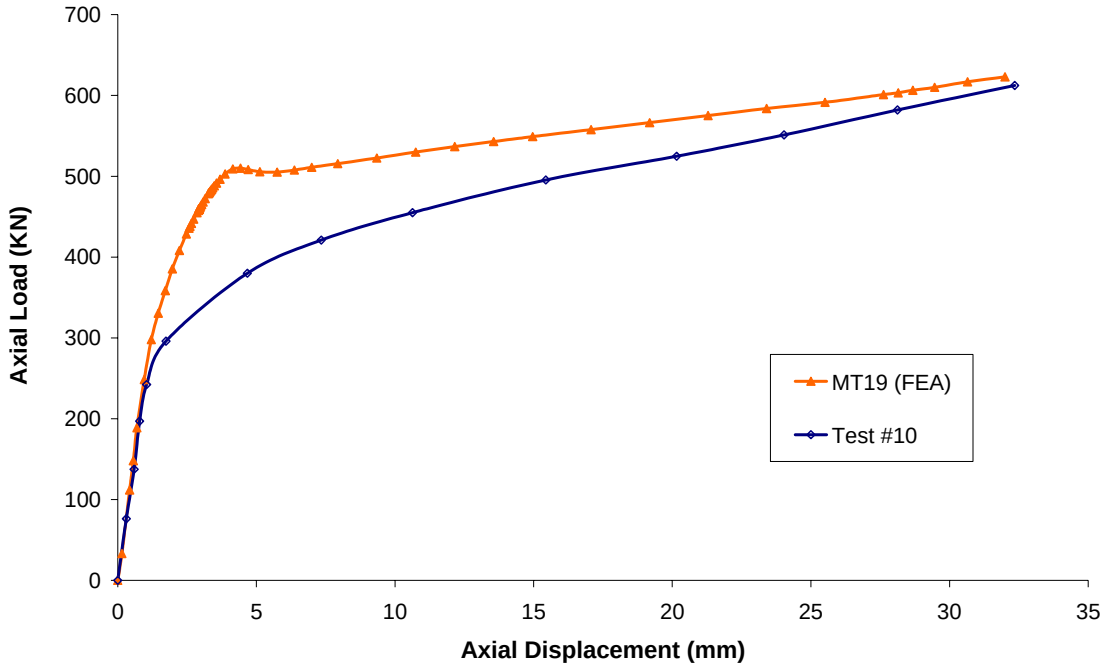


Figure 5. 31 - Comparison with test results of specimen GP-10 (plate 620 x 500 x 6.9 mm) and finite element model with two bolt connections

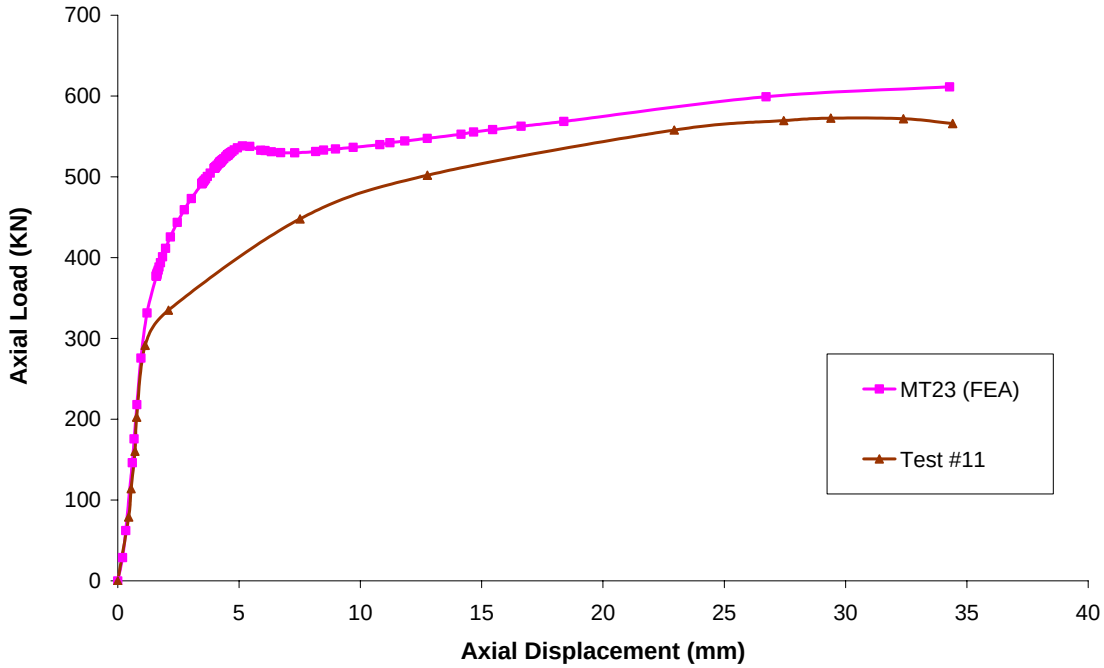


Figure 5. 32 - Comparison with test results of specimen GP-11 (plate 635 x 500 x 6.9 mm) and finite element model with two bolt connections

## 5.4 Summary

The following items are presented as a summary of this chapter:

1. A linear elastic mesh study of a gusset plate connection was preformed to determine the level of mesh refinement required to ensure convergence. The main purpose of the linear elastic mesh study was to determine the level of mesh refinement required to ensure convergence.

2. The ABAQUS solid element with 8-node and incompatible mode (C3D8I) was used to model the gusset plate and angle which is splice to gusset plate with bolts. The bolts were modeled as analytical rigid, connecting the holes in gusset plate and angle that corresponded with the bolt locations. Linear elastic material properties were assigned to all gusset plate and angle elements.

3. Inelastic behaviour was incorporated in the gusset plate connection model from linear elastic mesh study and the models were loaded monotonically in tension well beyond first yield. Isotropic strain hardening materials model was developed based on the results from tension coupon tests

4. The results of finite element analysis were validated by comparing to the test result from monotonic tension loading for one and two bolt connection. The amounts of displacement were measured in the tests and the variation of axial load vs. displacement behaviour is used as a basis for comparison.

5. The effect of friction between angle and plate surface was simulated by surface-to-surface contact. This surface-to-surface contact could carry out the load through angle to plate and is affected on the area below and top of the hole in plate. To study the effect of the bolt on plate and angle the tie

contact was developed between the outer area of bolt and inner area of holes in plate and angle, respectively.

6. A mesh study was conducted using linear elastic model to investigate the stress distribution in a gusset plate and to determine the level of mesh refinement that would be required for modeling the gusset plate connection under monotonic loading.

7. For the linear elastic mesh study, a predetermined load was applied to each model. Axial displacement and Von Mises stress output was compared for the various meshes. Axial displacement output was used primarily, however, in selecting the sufficient level of mesh refinement.

8. From the finite element analysis, it was found that most of the element distortion is occurring in the elements just around the bolt in one bolt connection and it was occurred in last row of bolts in two bolt connection of gusset plate. The upper surface of the plate has out-of-plane buckling during the loading.

9. In studying the effects of mesh refinement, surface-to-surface contact, tie contact and analytical rigid (bolt) with inelastic material properties were constructed. There is good convergence in mesh refinement in all finite element models.

10. Comparison of ultimate loads from the monotonic tension loading analysis with ultimate tensile loads from the test which was done. The ratio of finite element analysis to test load value is varied from 1.02 to 1.3.

11. Axial load versus displacement plots for finite element models with strain hardening model and load versus displacement of test are compared. It

seems that there is a good agreement between the result of finite element model and test results.

# 6. CONCLUSIONS AND RECOMMENDATIONS

## 6.1 Introduction

In this chapter, conclusions and recommendations are presented, based on the results of the experimental and numerical investigation in Chapter 4 and 5.

## 6.2 Conclusions

In the first phase of this investigation, test specimens of gusset plate connections with one bolt and two bolts were made and tested.

- Eight specimens were built with one bolt and three specimens were built with two bolts. The results of these tests provided strain distributions and global load-deformation behaviours. The load-deformation curves were also used to determine the ultimate capacity of the gusset plate connections and to validate finite element models.

- The effective width for two bolts connections were calculated based on yield load of the gusset plate. The comparison of this method shows that the effective width varies from 88.3 mm to 111.7 mm for two-bolt connections.

- The angle of load dispersion and effective width have no significance for one-bolt connection because a large number of references line for measuring the load dispersion angle, can be drown through one bolt hole. The total angle of load dispersion for two-bolt connections varies from 25 degree to 31 degree. This angle is approximately one half of angle (60 degree) as suggested by Whitmore.

In the second phase of this investigation, finite element models were developed and validated using test results of one bolt and two bolts specimens. The finite element models can be used for further study and detailed parametric study.

## 6.3 Recommendations

The following recommendations can be made based on the results of this investigation:

- More tests need to be undertaken for various thicknesses of plate, bolt diameters, and angle dimensions. For gusset plate connection with two bolts, the plate width needs to be varied as well.

- A detailed parametric study needs to be undertaken to investigate the effect of various parameters such as (i) number of bolts: one and two, (ii) bolt diameter, (iii) angle dimensions, (iv) far-end boundary condition: pinned and fixed, (v) material strength, (vi) plate width, and (vii) plate thickness on the effective width.

## REFERENCES

American Institute of Steel Construction, 1989, "Allowable Stress Design and Plastic Design Specifications for Structural Steel Building", 9th Edition, Chicago, IL, USA.

American Institute of Steel Construction, 2005, "Load and Resistance Factor Design Specification for Structural Steel Building", Chicago, IL, USA.

ANSI/TIA 222-G, 2006, "Structural Standards for Steel Antenna Towers and Antenna Supporting Structures", Canadian Standards Association, Rexdale, Ontario.

Architectural Institute of Japan, 1990, "Standard for Limit State Design of Steel Structures", Tokyo, Japan.

Astaneh-Asl, A., Goel, S.C., and Hanson, R.D., 1981, "Behaviour of Steel Diagonal Bracing", ASCE Conference, October 26-31, St. Louis, Missouri.

Barth, K.E., Orbison. J.G. and Nakala, R., 2001, "Behaviour of Steel Tension Members Subjected to Uniaxial Loading", Journal of Constructional Steel Research, Vol. 58, 2002, pp. 1103-1120.

Bjorhovde, R. and Chakrabarti, S.K., 1983, "Test of Full-Size Gusset Plate Connections", Journal of Structural Engineering, Vol. 111, No. 3, pp. 667-684.

CAN/CSA-S16.1, 2006, "Limit States Design of Steel Structures", Canadian Standards Association, Rexdale, Ontario.

CAN/CSA-S37.01, 2001, "Antenna, Towers, and Antenna-Supporting Structures", Canadian Standards Association, Rexdale, Ontario.

Chakrabarti, S.K. and Bjorhovde, R., 1983, “Tests of Full Size Gusset Plate Connections”, Research Report, Department of Civil Engineering, University of Arizona-Tuscan, Arizona.

Cheng J.J.R., Grondin G.Y. and Yam M.C.H., 2000, “Design and Behaviour of Gusset Plate Connections”, Proceeding of the Forth International Workshop on Connections in Steel Structures, Roanoke, VA, USA.

Davis, C.S., 1967, “Computer Analysis of the Stresses in a Gusset Plate”, Thesis presented to the University of Washington in Seattle, in partial fulfillment of the requirements for the degree of Masters of Science.

European Committee for Standardisation, 1992, Eurocode 3: Design of Steel Structures, ENV 1993-1-1, Brussels, Belgium.

Gross, J.L., 1990, “Experimental Study of Gusseted Connections”, Engineering Journal, AISC, Vol. 27, No. 3, Third Quarter, pp. 89-97.

Habbitt, Karlsson and Sorenson Inc., 1995, “ABAQUS/Standard”, User’s Manual Volume I and II, Version 6.6, Oatucket, R.E.

Hardash, S.G. and Bjorhovde, R., 1984, “Gusset Plate Design Utilizing Block-Shear Concepts”, Research Report, Department of Civil Engineering, University of Arizona-Tuscan, Arizona.

Hardin, B.O., 1958, “Experimental Investigation of the Primary Stress Distribution in the Gusset Plates of a Double Plane Pratt Truss Joint with Chord Splice at the Joint”, University of Kentucky Engineering Experiment Station, Bulletin No. 49.

Hu, S. Z., and Cheng, J.J.R, 1987, “Compressive Behaviour of Gusset Plate Connections”, Structural Engineering Report No. 153, Department of Civil Engineering, University of Alberta, Edmonton, Alberta.

Huns B.B.S., Grondin G. Y. and Driver R.G., 2004, “Tension and Shear Block Failure of Bolted Gusset Plates”, Canadian Journal of Civil Engineering, Vol. 33, pp. 395-408.

Irvan, W.G., 1957, “Experimental Study of Primary Stresses in Gusset Plate of a Double Plane Pratt Truss”, Bulletin No. 49, University of Kentucky Engineering Experiment Station.

Jain, A.K., Goel. S.C., and Hanson, R.D., 1978, “Inelastic Response of Restrained Steel Tubes”, Journal of the Structural Division, Proceeding of the American Society of Civil Engineers, Vol. 104, St6, pp. 897-910.

Kulak, G.L., Fisher, J.W. and Struik, J.H.A., 1987, Guide to Design Criteria for Bolted and Riveted Joints, John Willey and Sons, Second Edition, New York.

NBCC, 2005, National Building Code of Canada 2005, Associate Committee on the National Building Code, National Research Council of Canada, Ottawa, Ontario.

Rabinovitch, J.S. and Cheng, J.J.R., 1993, “Cyclic Behaviour of Steel Gusset Plate Connections”, Structural Engineering Report No. 191, Department of Civil Engineering, University of Alberta, Edmonton, Alberta.

Redwood, R.G. and Jain, A.K., 1992, “Code Provisions for Seismic Design for Concentrically Braced Steel Frames”, Canadian Journal of Civil Engineering, April, pp. 1025-1031.

Sheng, N., Yam, C.H. and Iu, V.P., 2001, “Analytical Investigation and Design of the Compressive Strength of Gusset Plate Connections”, Journal of Constructional Steel Research, Vol. 58, pp. 1473-1493.

Thornton, W.A., 1984, “Bracing Connections for Heavy Construction”, Engineering Journal, AISC, Vol. 21, No. 3, pp. 139-148.

Topkaya C., 2003, “A Finite Element Parametric Study on Block Shear Failure of Steel Tension Members”, Journal of Constructional Steel Research, Vol. 60, pp. 1615-1635.

Varsarelyi, D.D., 1971, “Tests of Gusset Plate Models”, Journal of the Structural Division, Proceedings of the American Society of Civil Engineers, February, pp. 665-678.

Walbridge S.S., Grondin G.Y. and Cheng J.J.R., 2004, “Gusset Plate Connections under Monotonic and Cyclic Loading”, Canadian Journal of Civil Engineering, Vol. 32, pp. 981-995.

Whitmore, R.E., 1952, “Experimental Investigation of Stresses in Gusset Plates”, Bulletin No. 16, Engineering Experiment Station, University o Tennessee.

Williams, G.C. and Richard, R.M., 1986, “Steel Connection Design Based on Inelastic Finite Element Analysis”, Report of the Department of Civil Engineering and Engineering Mechanics, The University of Arizona.

Yam, C.H.M. and Cheng, J.J.R., 1993, “Experimental Investigation of the Compressive Behaviour of Gusset Plate Connections.”, Structural Engineering Report No. 194, Department of Civil Engineering, University of Alberta, Edmonton, Alberta.

## APPENDIX - DETAILS OF LOAD BALANCE CALCULATIONS

The area under the strain distribution curve was found out using Simpson's method. The calculation was performed in elastic range. The detailed calculations for estimated loads for specimens GP-04, GP-08, GP-12 with one bolt connection are shown in Figure A.1 to A.3. Figure A.4 to A.6 shows the detailed calculation of specimen GP-09, GP-10 and GP-11 with two bolt connection.

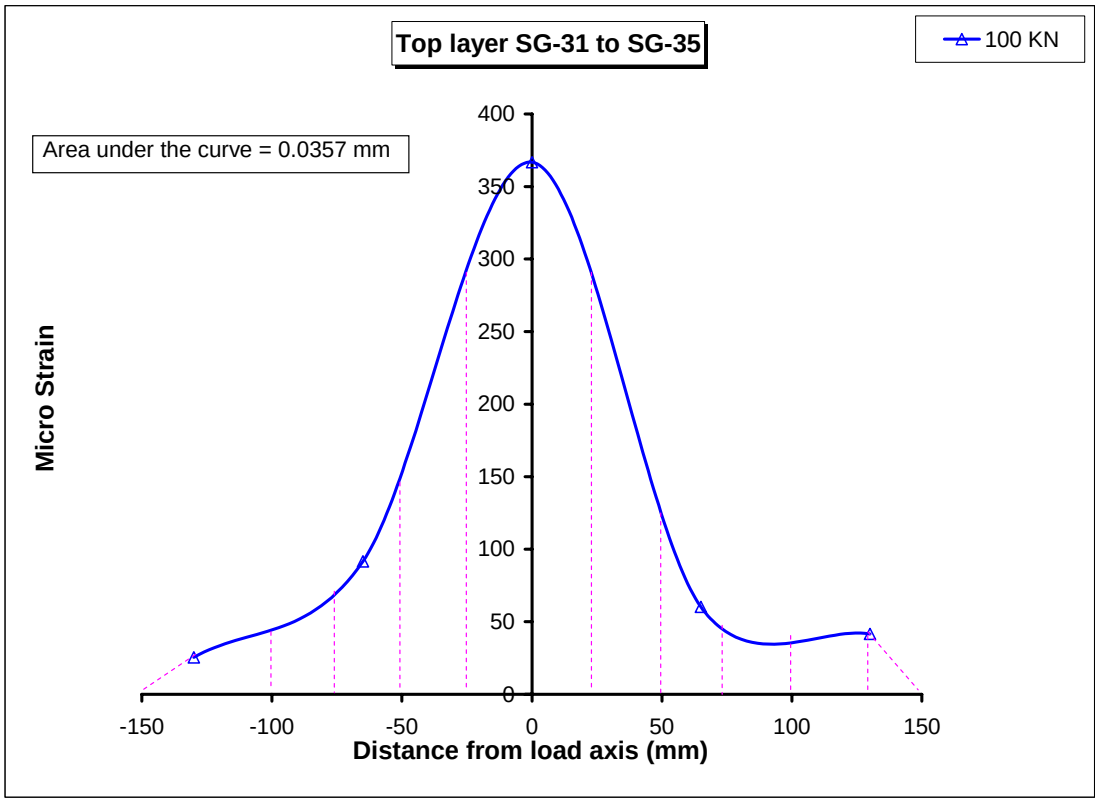


Figure A. 1 - Calculation of area under the strain-load curve based on Simpson's method for Specimen GP-04

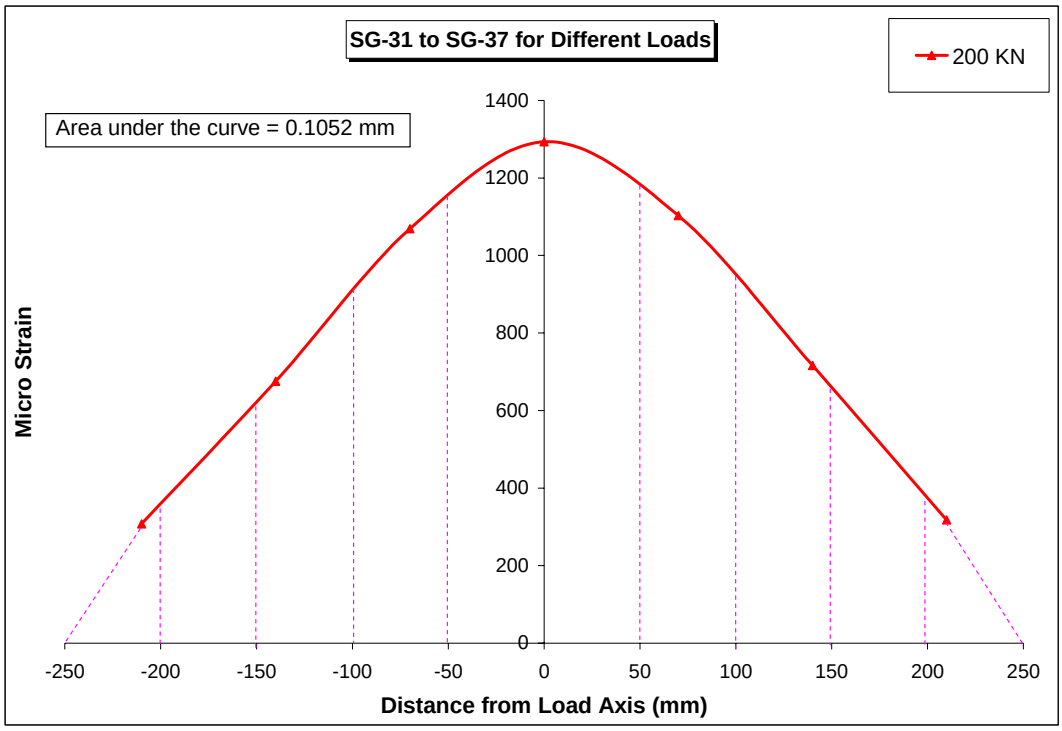


Figure A. 2 - Calculation of area under the strain-load curve based on Simpson's method for Specimen GP-08

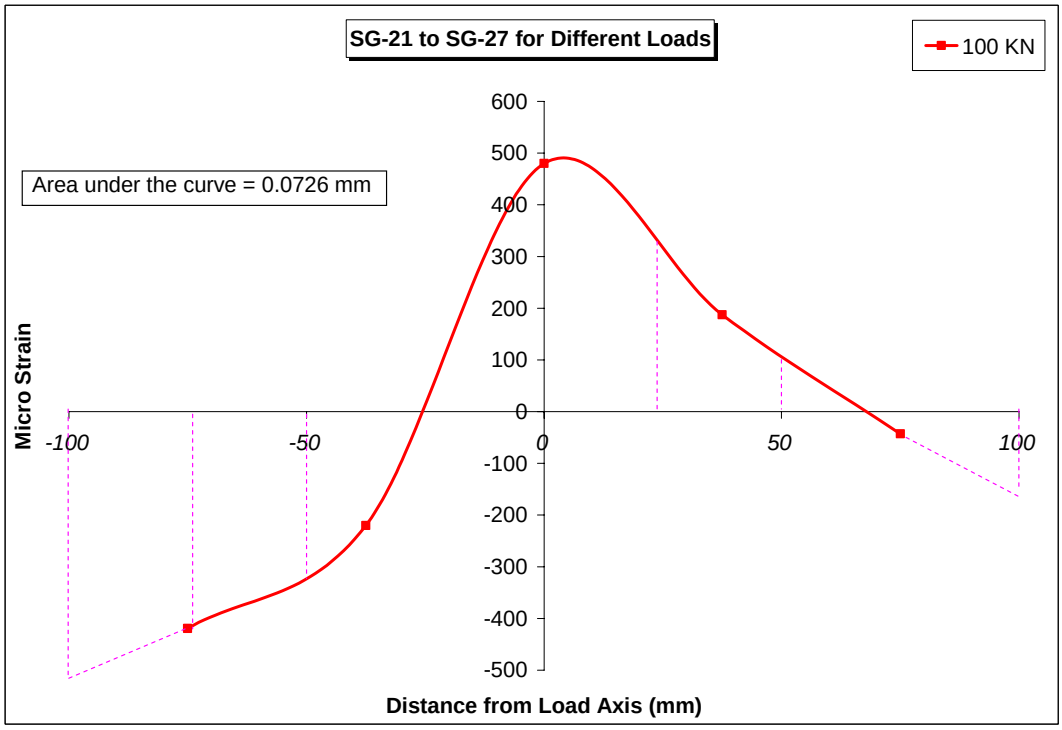


Figure A. 3 - Calculation of area under the strain-load curve based on Simpson's method for Specimen GP-12

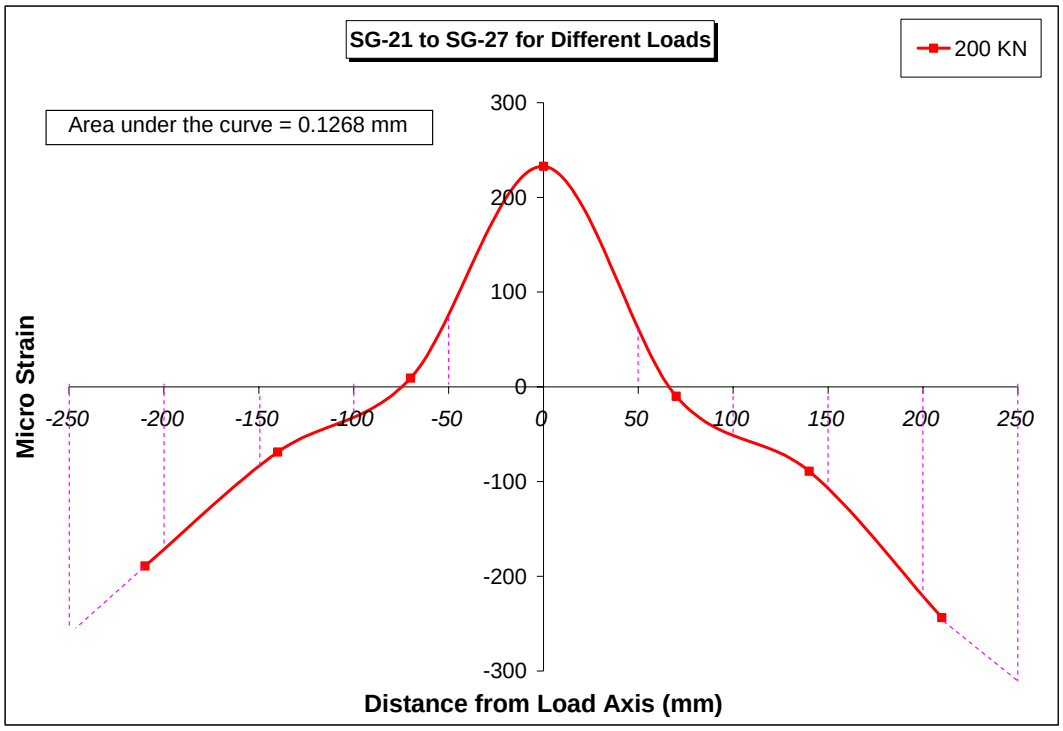


Figure A. 4 - Calculation of area under the strain-load curve based on Simpson's method for Specimen GP-09

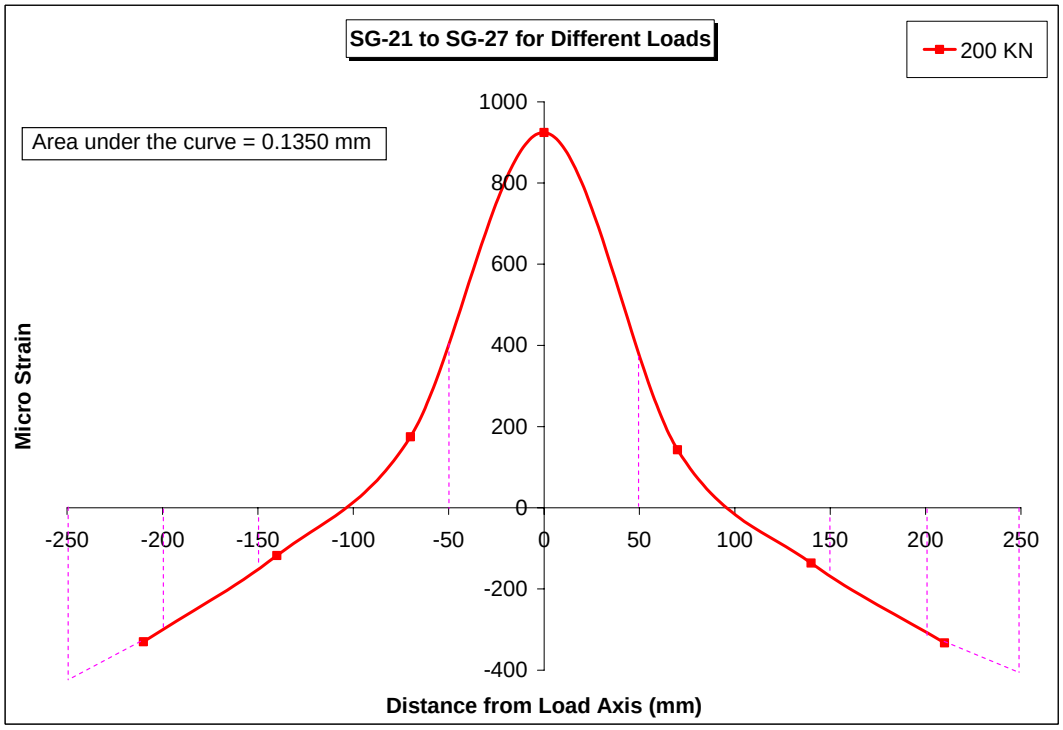


Figure A. 5 - Calculation of area under the strain-load curve based on Simpson's method for Specimen GP-10

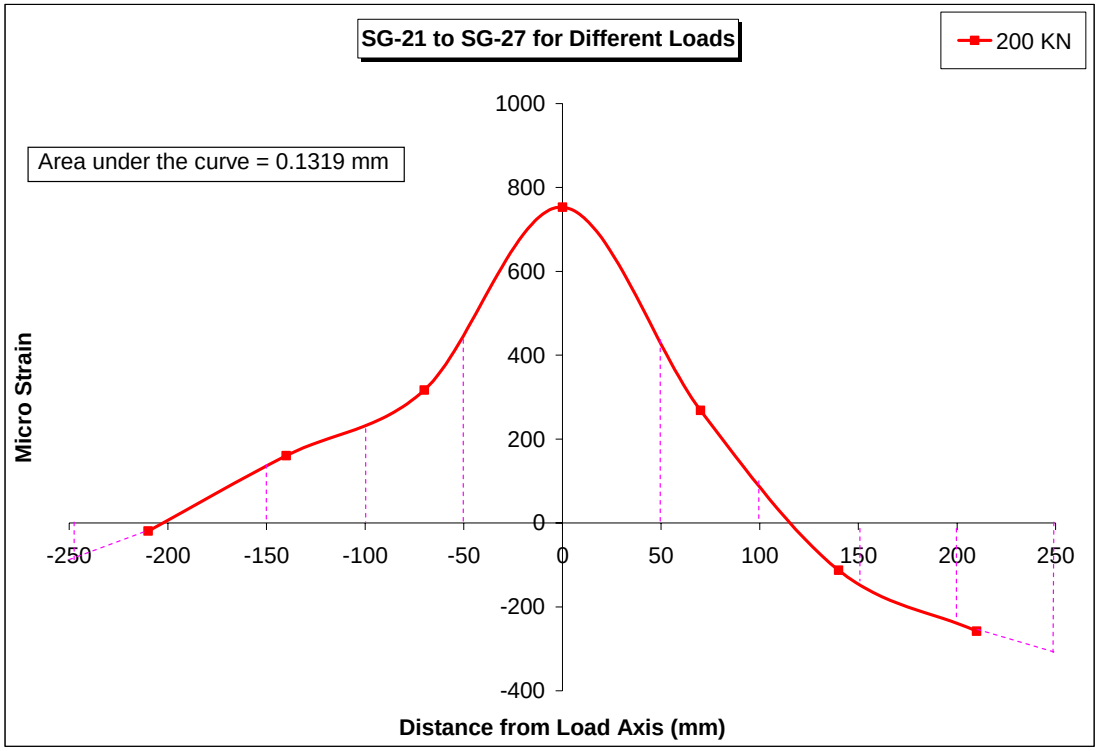


Figure A. 6 - Calculation of area under the strain-load curve based on Simpson's method for Specimen GP-11

## VITA AUCTORIS

NAME: Hassan Abbasi

PLACE OF BIRTH: Tehran, Iran

EDUCATION: Islamic Azad University, Tehran, Iran

1988-1992, B.Sc., Civil Engineering

Islamic Azad University, Tehran, Iran

1993-1995, M.A.Sc., Civil Engineering (Hydraulic Structure)

University of Windsor, Windsor, Ontario, Canada

2007-2009, M.A.Sc., Civil Engineering (Structure)